PHOTOGRANULES FOR WASTEWATER TREATMENT

from community assembly to targeted microbial functions

Lukas M. Trebuch

Propositions

1. Photosynthesis is vital for resource recovery from wastewater.
   (this thesis)

2. “Intermitted fasting” improves functionality of photogranules.
   (this thesis)

3. Unbiased science needs unconditional basic funding.

4. Protecting intellectual property hampers scientific progress.

5. Economic viability requires ecological sustainability.

6. Social science is the most misused discipline in the era of social media.

7. Life is like music: dissonance and consonance, suspense and resolution.

8. Happiness is an essential element in education.

Propositions belonging to the thesis, entitled

Photogranules for wastewater treatment: from community assembly to targeted microbial functions

Lukas M. Trebuch
Wageningen, 20 April 2022

Photogranules for wastewater treatment

From community assembly to targeted microbial functions

Lukas M. Trebuch

Thesis committee

Promotors

Prof. Dr Louise E.M. Vet
Emeritus Professor of Evolutionary Ecology
Wageningen University & Research

Prof. Dr René H. Wijffels
Professor of Bioprocess Engineering
Wageningen University & Research

Co-Promotors

Dr Tânia V. Fernandes
Senior Scientist, Aquatic Ecology
Netherlands Institute of Ecology, Wageningen

Dr Marcel G.J. Janssen
Assistant Professor, Bioprocess Engineering
Wageningen University & Research

Other members

Prof. Dr Hauke Smidt, Wageningen University & Research
Prof. Dr Jef Huisman, University of Amsterdam
Prof. Dr Anushree Malik, Indian Institute of Technology Delhi, New Delhi, India
Dr Kim Milferstedt, French National Institute for Agriculture, Food, and Environment, Narbonne, France

This research was conducted under the auspices of the Graduate School Production Ecology and Resource Conservation.

Photogranules for wastewater treatment

From community assembly to targeted microbial functions

Lukas M. Trebuch

Thesis

submitted in fulfilment of the requirements for the degree of doctor
at Wageningen University
by the authority of the Rector Magnificus,
Prof. Dr A.P.J. Mol,
in the presence of the
Thesis Committee appointed by the Academic Board
to be defended in public
on Wednesday 20 April 2022
at 4 p.m. in the Aula.

Photogranules for wastewater treatment: From community assembly to targeted microbial functions

232 pages

PhD thesis, Wageningen University, Wageningen, the Netherlands (2022)

With references, with summary in English

ISBN: 978-94-6447-085-7

DOI: https://doi.org/10.18174/562026

TABLE OF CONTENTS


LOTUS
Local Treatment
of Urban Sewage Streams
for Healthy Reuse

Chapter 1

General Introduction

1 INTRODUCTION

1.1 Global nutrient cycles and resource recovery

The sun is the main energy input of our planet and fuels life and nutrient cycles. Phototrophic processes on land and water convert inorganic C, N and P into organic molecules that are essential for all higher life forms, including humans (**figure 1**). Without the sun fuelling these processes, life as we know it would not be possible and the nutrient cycles would cease to exist. All human life relies on these global nutrient cycles, but human activities also heavily interfere in these cycles and create an imbalance in the distribution of C, N and P (Peñuelas et al., 2012).

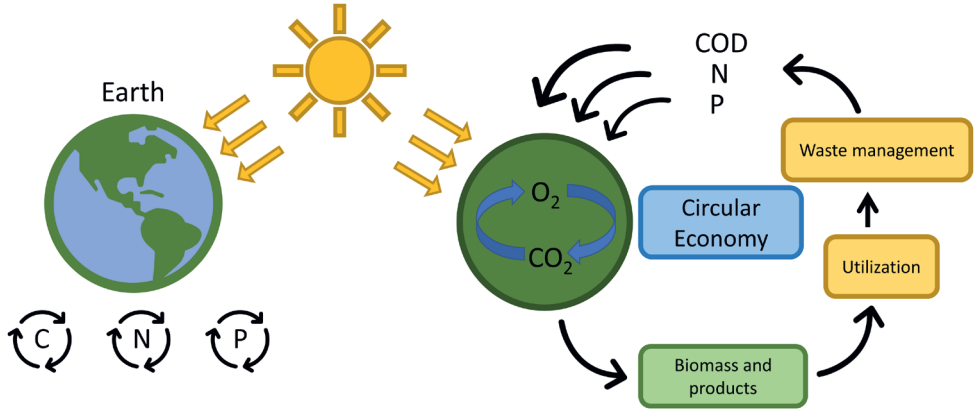

Figure 1: Sunlight driven (eco-)systems. On the left is Earth, which has the sun as the main energy input fuelling carbon, nitrogen, and phosphorus cycles. On the right is a possible biobased light-driven "Circular Economy" where the sun provides a major fraction of the metabolic energy necessary to treat wastewater, recover nutrients and produce valuable biomass. The biomass and derived products are further utilized until they come back to the waste management system as wastewater (COD, N, P).

Since the industrial revolution in 1860, massive amounts of carbon have been released from the Earth's crust into the biosphere via use of fossil oil, coal and natural gas for energy and petrochemical products. This introduced a surplus of carbon to the biosphere that contributes, in the form of carbon dioxide, to global warming and causes ocean acidification (Huber and Knutti, 2012). In addition, the industrialization and globalization of agriculture led to anthropogenic nitrogen fixation (e.g., by leguminous crops and Haber-Bosch process) equal to the total amount of nitrogen fixed naturally on land and in the oceans together (Peñuelas et al., 2012).

The situation with phosphorus is even more alarming. The worldwide application of mineral phosphorus fertilizer resulted in a tremendous phosphorus input to the

biosphere and an ecologically devastating global redistribution of phosphorus. Unlike nitrogen fertilizers, phosphorus fertilizers are not volatile and consequently very little phosphorus is redistributed from croplands to nearby natural terrestrial ecosystems (Mahowald et al., 2008; Peñuelas et al., 2012). However, excessive application of phosphorus fertilizer can result in substantial transfers of phosphorus to adjacent freshwater bodies, followed by transport to coastal waters causing eutrophication and algae blooms. Due to all these anthropogenic inputs the stoichiometry of carbon and nitrogen relative to phosphorus has changed, which alters natural and managed ecosystems around the globe (Peñuelas et al., 2013). Mitigating these anthropogenic consequences on the environment is one of the most pressing challenges we face today.

Most of the carbon, nitrogen and phosphorus from agricultural lands becomes our food (or animal feed) and ultimately ends up as faeces and urine in our wastewater. Wastewater has always been characterized as a polluted stream and wastewater treatment plants are mainly focused on removal rather than recovery of the elements present in wastewater. However, we now realize that wastewater is not just a waste stream but a valuable source of phosphorous and other elements that we need to start mining. Therefore, wastewater treatment is a good starting point to investigate technologies to increase resource use efficiency and move towards systems that can close nutrient cycles and facilitate a circular economy (**figure 1**). Similar to the sun fuelling global nutrient cycles, humans could use the same principle on a smaller scale and design light-driven biological recovery processes.

1.2 Biological wastewater treatment and biogranules

Biological wastewater treatment is performed using an array of different microorganisms that remove organic and inorganic pollutants by various anaerobic and aerobic processes. In biological treatment units, it is desired to retain dense biomass to ensure the effectiveness of treatment and increase economic feasibility. The conventional activated sludge (CAS) process, developed over 100 years ago, revolutionized wastewater treatment and is still one of the most widely applied wastewater treatment systems (Ardern and Lockett, 1914). The main principle of this system is a bioreactor operation that allows the retention of active bacterial biomass as microbial flocs within the treatment system and the easy alternation of process conditions (e.g., anaerobic, anoxic, or aerobic) to steer removal of certain compounds. In this process, organics, nitrogen and phosphorus are mainly removed through bacterial assimilation and dissimilation, including biological oxidation, nitrification-denitrification, and phosphorus accumulation (Chen et al., 2020).

The separation of cell retention and hydraulic retention has traditionally been carried out by settling biomass and recycling them to the bioreactor. To reduce footprint, technologies such as the use of immobilizing matrix, centrifugal systems, membrane filtration units have been developed. Instead of using extra equipment, microbial granulation can be applied as an alternative method to attain high treatment efficiency (Tay et al., 2006).

Biogranules are discrete well-defined cell aggregates formed by cell-to-cell attraction (Milferstedt et al., 2017a). Compared to microbial flocs, biogranules have regular, dense, and strong structure with excellent settleability, enabling high cell retention (Liu et al., 2009). The first biogranules discovered in the environmental field were used to treat industrial wastewater under anaerobic conditions converting organics to biogas (Lettinga et al., 1980). Other biogranules with distinct microbial communities and functions were discovered soon after.

In the 1990s the aerobic granular sludge (AGS) process was developed. It uses the same removal mechanisms of the activated sludge process, but with bacterial biomass that densely aggregates as biogranules (de Kreuk et al., 2005; Morgenroth et al., 1997; M. Pronk et al., 2015). Aerobic granules have the advantages of enhanced settleability of the biomass, and thus separation of active biomass and liquid, compared to an activated sludge floc. That allows the intensification of the treatment process, which reduces areal footprint and energy consumption. Nevertheless, aerobic granular sludge systems are designed to remove nutrients rather than recover them, use up to 70% of the energy consumption for mechanical aeration, and emit considerable amounts of greenhouse gasses (i.e., CO_2, N_2O) (de Sousa Rollemberg et al., 2018; M. Pronk et al., 2015).

1.3 Introducing photosynthesis in wastewater treatment

It is apparent that present wastewater treatment is not particular environmentally and economically sustainable due to high energy consumption, greenhouse gas emissions, and inefficient energy and resource recovery (Y. J. Liu et al., 2018). Ideally, a future wastewater treatment plant would be a water factory that can produce water for various reuse purposes, a resource factory for recovering valuable secondary raw materials, and a power factory enabling energy-neutral or even positive operation (Kehrein et al., 2020; Zhang et al., 2021).

In conventional wastewater treatment metabolic energy is mainly derived from organic compounds (COD) by chemoheterotrophs or from inorganic compounds (e.g. H_2, NH_3, NO_2, H_2O) by chemoautotrophs (Chen et al., 2020). Introducing phototrophic organisms in wastewater treatment would provide additional metabolic

energy from light and could thereby enhance treatment performance (**figure 2**). Simultaneously, oxygenic photosynthesis could significantly improve sustainability by reducing aeration needs and greenhouse gas emissions by internally cycling O_2 and CO_2. Further, the plethora of phototrophic organisms (200.000-800.000 algal species) could extend the portfolio of possible products and application of the produced biomass (Borowitzka et al., 2016). With photosynthesis driving the treatment process, it will be important to have bioreactors that enable efficient light penetration of the culture and light availability for phototrophs. This will require bioreactors with high surface to volume ratios.

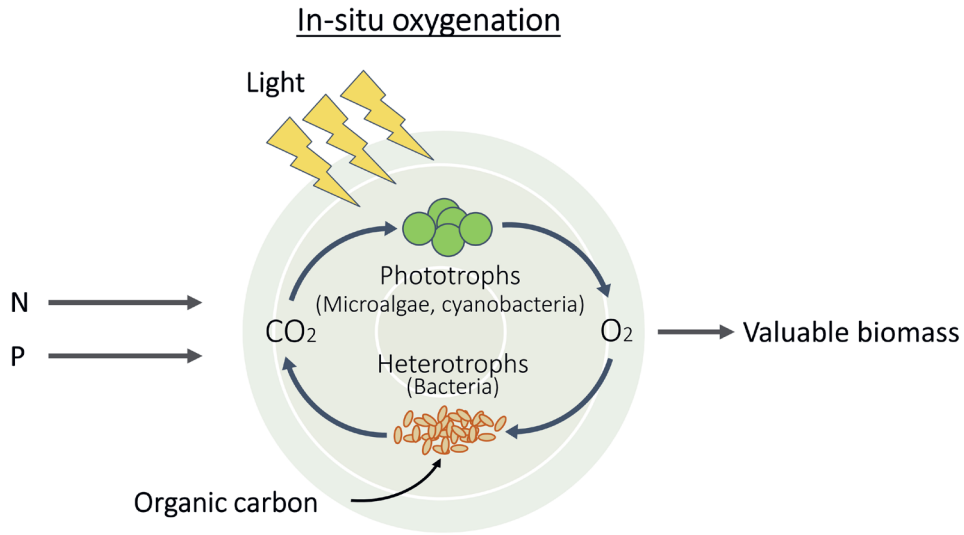

Figure 2: *In-situ* oxygenation and the oxygen and carbon dioxide cycle within communities of phototrophs (microalgae, cyanobacteria) and heterotrophs (bacteria).

Using phototrophs in large-scale wastewater treatment was explored by Oswald in the 1950s (Oswald et al., 1957). Oswald first investigated waste stabilizing ponds (WSP) and introduced in 1963 the "high-rate algal pond" (HRAP), which are shallow lagoons allowing higher light penetration than the previous deep ponds. These systems are easy to construct and maintain and use *in-situ* oxygenation by phototrophs, which excludes any mechanical aeration. However, WSP and HRAP usually have low removal rates and consequently have long retention times (days instead of hours) and a large footprint. Another drawback is that the poor separation of biomass and treated liquid often requires additional steps such as flocculation, energy-demanding filtration, or centrifugation.

A first attempt to facilitate harvesting in HRAP systems was returning settled biomass from a clarifier to the bioreactor (Gutzeit et al., 2005). In that manner well-

settling microalgal-bacterial flocs form, and it is possible to separate hydraulic retention time (HRT) from solid retention time (SRT) as it is done in the activated sludge process. The concept of microalgal-bacterial flocs was further pursued and tested at pilot-scale under various conditions (Park et al., 2015, 2011; van den Hende, 2014; Van Den Hende et al., 2011b, 2011a). Although, biomass harvesting by gravity sedimentation was achievable, the removal rates were still lower compared to conventional treatment systems while the footprint was substantially larger.

1.4 Discovery and microbial ecology of photogranulation

The formation of granular sludge is regarded as the "holy grail" in wastewater treatment as it facilitates and enhances the treatment process while simultaneously decreasing the demand for equipment and space (Beun et al., 1999; Lettinga et al., 1980; Milferstedt et al., 2017a). The same concept for intensifying the conventional activated sludge to aerobic granular sludge can be applied to phototrophic microbial communities by the generation of phototrophic microbial aggregates – the photogranules. These photogranules consist of a complex microbial community of phototrophic (cyanobacteria, eukaryotic algae) and non-phototrophic (heterotrophs, nitrifiers, denitrifiers) organisms that remove organics, nitrogen, and phosphorus via biomass assimilation.

The first photogranule was serendipitously discovered in 2011 when activated sludge that was left on a lab windowsill in a closed 20mL vial changed to a granule (Milferstedt et al., 2017b; Park and Dolan, 2019; Park and Takeuchi, 2021). This 'hydrostatic photogranulation' was later attributed to the enrichment of Oscillatoriales, an order of motile filamentous cyanobacteria, often either found in low abundances or undetectable in activated sludge (Milferstedt et al., 2017b). Interestingly, this hydrostatic photogranulation appears to be "intrinsic" to the microbial community of the photogranule as other dynamic operation conditions are absent. Conversely, other biogranule formation is strongly dependent on external drivers, such as hydrodynamic shear and washout conditions in the case of anaerobic granules or alternating environmental conditions (nutrient and oxygen rich and poor conditions) for aerobic granules (Milferstedt et al., 2017a). These 'hydrostatic photogranules' were used to seed sequencing batch reactors (SBRs) where rapid growth of new granules occurred (**figure 3**). Photogranules in SBRs have been shown to treat wastewater without external aeration (Abouhend et al., 2018; Milferstedt et al., 2017b).

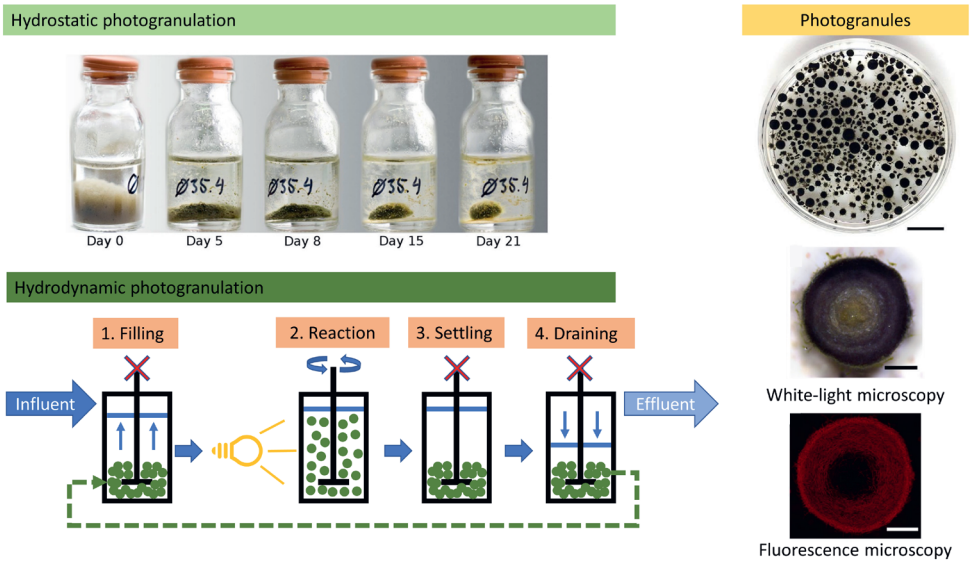

Figure 3: Photogranulation. (A) Hydrostatic photogranulation from activated sludge in closed illuminated 20mL vials demonstrated by Milferstedt et al. (2017b). The photogranulation took place over a course of 21 days. (B) Hydrodynamic photogranulation was achieved in sequencing batch reactors (SBR) inoculated with either hydrostatically produced photogranules, activated sludge, aerobic granular sludge or other mixture of microalgae and bacteria. SBRs were mixed by mechanical stirrer or aeration. (C) Images of photogranules in a Petri dish (scale bar 5.5 mm), under white-light microscopy or fluorescence microscopy (both scale bars 800 µm) presented by Milferstedt et al. (2017b).

Motile filamentous cyanobacteria of the order of Oscillatoriales have repeatedly been shown to be important for successful hydrostatic and hydrodynamic photogranulation. Oscillatoriales are known for their filamentous morphology and gliding motility. These characteristics allow Oscillatoriales to form the complex mat-like structures and exhibit the locomotive entanglement that is key for photogranulation (Milferstedt et al., 2017b). The gliding motility allows Oscillatoriales to move toward or away from light, nutrients or other organism and allows to position themselves in areas with optimized physiochemical conditions (Garcia-Pichel and Castenholz, 2001; Kruschel and Castenholz, 1998; Malin and Walsby, 1985; Pentecost, 1984; Whale and Walsby, 1984). Brehm et al. (2003) argued that a spherical arrangement would provide optimal access for light, nutrients, and other resources. Additionally, the formation of biogranules could facilitate close spatial and temporal coupling of organic matter producers and consumers, i.e. phototrophs, heterotrophs and diazotrophs, along a physiochemical gradient (Paerl and Priscu, 1998). Further, the excretion of extracellular polymeric substances (EPS) excreted by phototrophic and non-phototrophic organisms act like a glue that holds the microbial community together. Oscillatoriales and EPS excretion

can also attract bacteria that use cyanobacterial metabolites, including EPS and oxygen, further promoting agglomeration (Kuo-Dahab et al., 2018; Takeuchi et al., 2001).

In parallel, other research groups assembled photogranule-like aggregates that mostly originate from aerobic granules covered with a layer of eukaryotic algae (Arcila and Buitrón, 2016; Huang et al., 2015; Kumar and Venugopalan, 2015; L. Liu et al., 2018; Tiron et al., 2017). That was mainly achieved by illuminating SBRs optimized for aerobic granule sludge and letting a phototrophic community establish. Interestingly, the reported photogranulation principle appeared to be different to the hydrostatic one and more resembled the assembly of aerobic granules, needing hydrodynamic shear and alternating anaerobic and aerobic conditions. The focus of these studies was on the engineering aspect and often the microbial community was not assessed. However, there are some reports that in addition to eukaryotic algae, filamentous cyanobacteria were also present, which could have contributed to photogranulation (Ahmad et al., 2017; Tiron et al., 2017).

Although taxonomically the microbial community of photogranules can be very different, the same functional groups are often represented. The two main functional groups in photogranules are oxygenic photoautotrophs (cyanobacteria and eukaryotic algae) and chemoheterotrophs (Abouhend et al., 2018; Milferstedt et al., 2017b). Nitrifiers and denitrifiers are frequently reported but usually represented in lower abundance (Abouhend et al., 2018; Liu et al., 2017; Meng et al., 2019b). The observation that the functional distribution in photogranules is consistent across studies while the taxonomic distribution is not, can be attributed to the fact that most metabolic functions can be performed by multiple taxonomically different organisms (Louca et al., 2016). In complex and diverse microbial assemblages, such as photogranules, this leads to a functional redundancy that is strongly linked to the stability of functions against environmental perturbations. Hence, photogranules can exhibit similar functionality despite different community composition.

Investigating hydrostatic photogranulation is highly intriguing and could expose the principal mechanisms of spherical phototrophic aggregation. However, it is also essential to better understand photogranulation under hydrodynamic conditions. In the wastewater treatment process photogranules will experience highly fluctuating physical and chemical conditions. To date there is a poor understanding of the effect of these conditions on photogranulation, microbial community assembly and function, granule morphology, microscale functioning, and finally on the efficiency of nutrient assimilation. Therefore, it is key to elucidate the effect of wastewater characteristics and bioreactors' operation conditions on the assembly of the microbial community as well as its functions.

1.5 Photogranules for wastewater treatment

Photogranules have been shown to tightly couple *in-situ* oxygen generation through photosynthesis with oxygen-consuming processes like organic matter conversion and nitrification, to the extent that external aeration can be eliminated (Abouhend et al., 2018). Another aspect to consider is the greenhouse gases (CO_2, N_2O) that are emitted by conventional treatment systems as well as AGS. Introducing photosynthesis to biological wastewater treatment showed the potential to strongly reduce CO_2 emissions and thereby contribute to the sustainability of wastewater treatment plants.

Compared to conventional biological wastewater treatment systems, photogranules can derive metabolic energy from both light and organic carbon. As a consequence, the biomass productivity of phototrophs is increased by 2-3x in comparison to CAS or AGS (Abouhend et al., 2018; Cai et al., 2019; Huang et al., 2015). Currently, high biomass productivity is not desired in conventional treatment systems since it can have a significant impact on the operational costs due to sludge disposal (Cieślik et al., 2015). However, high biomass productivity is advantageous for resource recovery where wastewater is reclaimed and transformed into valuable biomass containing, in addition to the major elements (C, N, P) also microelements (e.g. Fe, Mo, Zn, Cu) (Kehrein et al., 2020; Silva et al., 2019; Suleiman et al., 2020). The biomass can then be utilized as biofertilizer or source for biopolymers, lipids, proteins and can be reintroduced to the economy as products.

Photogranules exhibit similar nitrogen and COD removal rates as CAS and AGS but lower removal rates for phosphorus (Abouhend et al., 2018). A functional group that has not been investigated in detail in photogranules are polyphosphate accumulating organisms (PAOs). PAOs are an integrate part of CAS and AGS and are responsible for high phosphorus removal by accumulating vast amounts of polyphosphate intracellularly. These organisms require specific conditions, alternating between nutrient rich anaerobic and nutrient poor aerobic conditions – also called a feast-famine regime (Chen et al., 2020). In non-granular form the combination of phototrophs and PAOs was previously investigated as phototrophic enhanced biological phosphorus removal (photoEBPR) (Carvalho et al., 2018; Oyserman et al., 2017). PhotoEBPR proved to be a feasible method to boost phosphorus removal by phototrophic microbial communities and would be advantageous if implemented in photogranules as well. Ideally, polyphosphate accumulation would be an integrate part of the photogranule functions next to oxygenic photosynthesis, chemoheterotrophy, nitrification and denitrification (**figure 4)**. Adding functions also increases the complexity of the

microbial community, so it is vital to assess how to accommodate and steer the desired functions within photogranules.

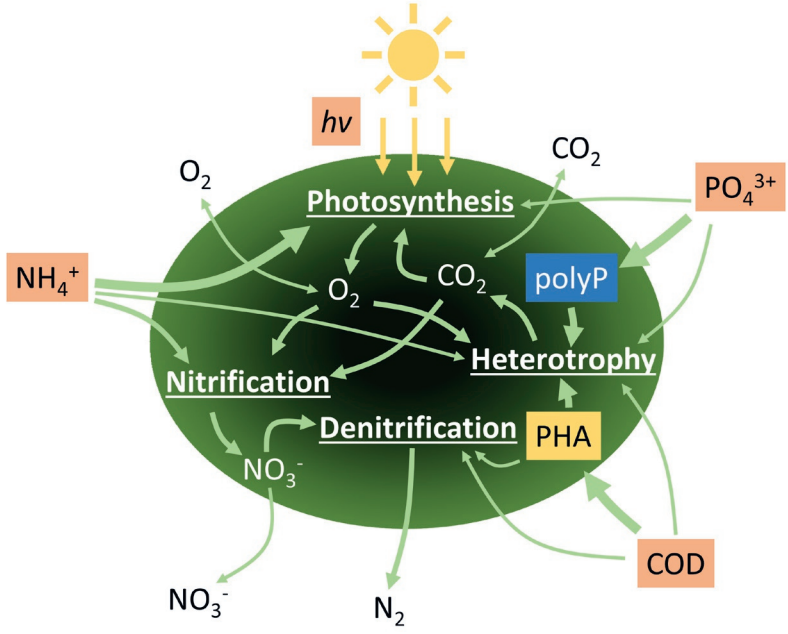

Figure 4. The desired functions in a photogranule 1) Oxygenic photosynthesis; 2) Chemoheterotrophy; 3) Polyphosphate accumulation, and optionally 4) nitrification; 5) denitrification for enhanced nitrogen removal. The main metabolic energy source for the microbial community is light (*hv*) and organic carbon substrate (COD). Polyphosphate (polyP) and polyhydroxyalkanoates (PHA) are important constituents of the metabolism of polyphosphate accumulating organisms. Biomass assimilation of ammonium (NH_4^+) and phosphate (PO_4^{3-}) by nitrifiers (nitrification) and denitrification (denitrifiers) is neglected. The thickness of the arrows indicates the magnitude of rate. The thicker the higher.

Ultimately, photogranules convert COD, N and P from wastewater into valuable biomass. The phototrophic organisms help lower the need for aeration due to *in-situ* oxygenation via photosynthesis. Additionally, photosynthesis will sequester inorganic carbon (CO_2) from heterotrophic activity and thereby lower greenhouse gas emissions. The generated photogranule biomass can be utilized as a whole or fractionated into certain constituents (e.g., carbohydrates, proteins, lipids, photopigments, polyhydroxyalkanoates, polyphosphate) for various applications (e.g., biofertilizer, biopolymers, feed, platform chemicals, biofuel). Applying photogranular treatment technology could be a great step towards more sustainable wastewater treatment and could potentially transform wastewater treatment plants into resource factories (Fernandes et al., 2017; Kehrein et al., 2020; Silva et al., 2019).

2 OUTLINE OF THIS THESIS

The overarching aim of this thesis was to advance the field of phototrophic wastewater treatment by systematically exploring the microbial community assembly and functions of photogranules. To achieve this, we designed bioreactor systems that allowed photogranulation and subsequently explored the functional potential of photogranules for wastewater treatment by changing operation conditions. We integrated various approaches and techniques to investigate microbial community composition and functions, physical structure, and microscale functionality of photogranules. Ultimately, we provided a holistic overview on the microbial ecology of photogranules and engineering of photogranular bioreactors to pave the way for more sustainable wastewater treatment.

In **chapter 2** we assembled photogranules under hydrodynamic conditions in lab-scale bioreactors operated in sequencing batch mode. We used a diverse and species-rich inoculum from various sources and followed the microbial community assembly from free-suspended cells to floccular aggregates and finally to photogranules. We specifically focused on the impact of hydraulic retention time on photogranule assembly. The change in microbial community composition was followed using molecular techniques. Additionally, extracellular polymeric substances excreted by microbes were investigated to decipher their role in the agglomeration process.

Wastewater can have various compositions and different elemental ratios. In low N:P ratio wastewaters microorganisms can face insufficient amounts of nitrogen for growth, hindering the biological treatment process. Therefore, in **chapter 3** we investigated the effect of nitrogen limitation on the treatment performance and morphology of photogranules. This gave valuable insight into the response of photogranules to nutrient stress, and to what extend treatment performance is affected.

In **chapter 4** we set out the get a better insight into the physical, chemical, and biological structure of photogranules and the metabolic functions on a microscale. This was achieved by applying microscopic and microsensor techniques and conducting incubations with isotopically labelled carbon or nitrogen substrates. We elucidated the structural role of motile filamentous cyanobacteria and EPS. Further, we investigated the effect of different light and nutrient conditions on photogranule functioning, visualized light and substrate gradients, and explored microbial activity on a microscale.

Photogranules showed high removal rates for carbon and nitrogen, but lower rates for phosphorus compared to other granular biological treatment systems. In **chapter 5** we explore the possibility of enhancing phosphorus removal by introducing

polyphosphate accumulating organisms (PAOs). We mixed photogranules with aerobic granular sludge and operated the bioreactors under a feast-famine regime with an anaerobic (dark) and aerobic (light) phase. The integration of PAOs into photogranules was followed by microscopy and molecular techniques Further, we investigated the suitability of the PG+ process under a natural diurnal cycle by introducing a 12h anaerobic phase during nighttime.

Lastly, I summarized all our findings in **chapter 6** and discuss them in detail. To support the discussion, I performed a meta-analysis on publicly available microbial community data of photogranules and used our lab-scale findings to perform a scenario analysis. The meta-analysis gave insight into the richness of microbial community composition and functions of photogranules. Further, it indicated possible key functions and traits that are necessary for photogranulation. The scenario analysis illustrated the large-scale application of photogranule technology and provided estimates for treatment performance and areal requirement. Additionally, I outlined design principles for photogranular bioreactor configuration and mode of operation at large-scale.


THE NORTH FACE

Chapter 2

Impact of hydraulic retention time on community assembly and function of photogranules for wastewater treatment

Lukas M. Trebuch[1,2], Ben O. Oyserman[3,4], Marcel Janssen [2], René H. Wijffels [2,5], Louise E. M. Vet [6], Tânia V. Fernandes [1]

[1] *Department of Aquatic Ecology, Netherlands Institute of Ecology (NIOO-KNAW), Droevendaalsesteeg 10, 6708 PB Wageningen, The Netherlands*

[2] *Bioprocess Engineering, AlgaePARC Wageningen University, P.O. Box 16, 6700 AA Wageningen, The Netherlands*

[3] *Department of Microbial Ecology, Netherlands Institute of Ecology (NIOO-KNAW), Droevendaalsesteeg 10, 6708 PB Wageningen, The Netherlands*

[4] *Bioinformatics Group, Wageningen University, Wageningen, The Netherlands*

[5] *Faculty of Biosciences and Aquaculture, Nord University, N-8049, Bodø, Norway*

[6] *Department of Terrestrial Ecology, Netherlands Institute of Ecology (NIOO-KNAW), Droevendaalsesteeg 10, 6708 PB Wageningen, The Netherlands*

Published in Water Research

https://doi.org/10.1016/j.watres.2020.115506

1 ABSTRACT

Photogranules are dense, spherical agglomerates of cyanobacteria, microalgae and non-phototrophic microorganisms that have considerable advantages in terms of harvesting and nutrient removal rates for light driven wastewater treatment processes. This ecosystem is poorly understood in terms of the microbial community structure and the response of the community to changing abiotic conditions. To get a better understanding, we investigated the effect of hydraulic retention time (HRT) on photogranule formation and community assembly over a period of 148 days. Three laboratory bioreactors were inoculated with field samples from various locations in the Netherlands and operated in sequencing batch mode. The bioreactors were operated at four different HRTs (2.00, 1.00, 0.67, 0.33 days), while retaining the same solid retention time of 7 days. A microbial community with excellent settling characteristics (95-99% separation efficiency) was established within 2 to 5 weeks. The observed nutrient uptake rates ranged from 24 to 90 mgN L^{-1} day^{-1} and from 3.1 to 5.4 mgP L^{-1} day^{-1} depending on the applied HRT. The transition from single-cell suspension culture to floccular agglomeration to granular sludge was monitored by microscopy and 16S and 18S rRNA gene amplicon sequencing. In particular, two important variables for driving aggregation and granulation, and for the structural integrity of photogranules were identified: 1. Extracellular polymeric substances (EPS) with high protein to polysaccharide ratio and 2. specific microorganisms. The key players were found to be the cyanobacteria *Limnothrix* and *Cephalothrix*, the colony forming photosynthetic eukaryotes within *Chlamydomonadaceae*, and the biofilm producing bacteria *Zoogloea* and *Thauera*. Knowing the makeup of the microbial community and the operational conditions influencing granulation and bioreactor function is crucial for successful operation of photogranular systems.

Keywords: *Microalgae and cyanobacteria; phototrophic granulation; extracellular polymeric substances; metataxonomics; microbial ecology; functional network*

GRAPHICAL ABSTRACT

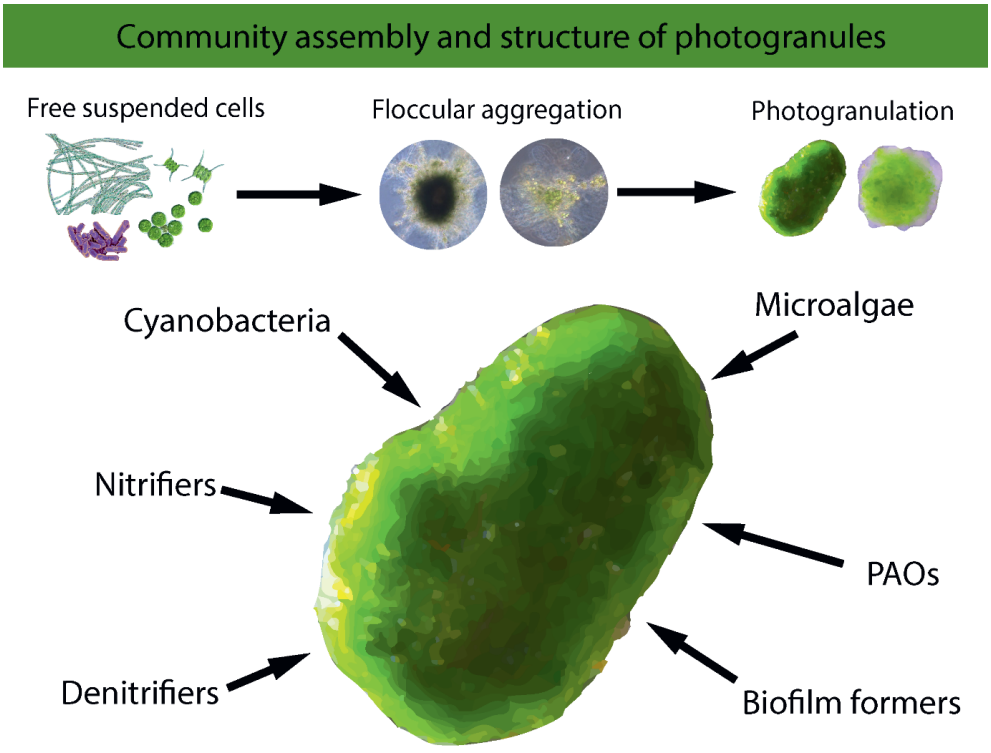

2 INTRODUCTION

Biological wastewater treatment systems are ubiquitous and essential for maintaining high water quality and prevent excess discharge of nutrients and pollutants into the environment (Henze, 2008). However, wastewater treatment also comes at a cost as it is an energy intensive process (McCarty et al., 2011) and contributes to greenhouse gas emissions (Cakir and Stenstrom, 2005). Hence, improving the efficacy and sustainability of these systems through technological innovation may have broad scale impacts on global sustainability. The incorporation of phototrophic organisms, such as microalgae and cyanobacteria, shows great potential in improving the sustainability of treatment processes by mitigating greenhouse gasses (Smith et al., 2010), closing nutrient cycles (Fernandes et al., 2015), matching wastewater N:P ratio for effective treatment by using phototrophic consortia (Fernandes et al., 2017), and providing oxygen to drive processes such as nitrification and polyphosphate accumulation (Oyserman et al., 2017). While promising, one of the current bottlenecks in the wider application of phototrophic communities in wastewater treatment is the harvesting of the biomass.

A principal operational parameter which ensures the effectiveness and economic feasibility of treatment is to retain the microbial community as dense biomass within the treatment system (Ardern and Lockett, 1914; Milferstedt et al., 2017a). This requires operational parameters which steer the microbial community to form natural and well settling aggregates. These aggregates may be described as either flocs or granules, depending on their structure, density, and settleability. In general, granules are discrete well-defined microbial aggregates formed by cell-to-cell attraction with regular dense and strong structure, and excellent settleability. Although the first granules were discovered over 50 years ago (Lettinga et al., 1980), the biological mechanisms driving granule formation and the operational parameters that select for their formation are still relatively unknown (Wilén et al., 2018). This complex microbial function is far from being fully understood and bears many ecological questions that need to be answered.

Merging granule technology with other biochemical processes such as photosynthesis holds the promise of producing well settling photoautotrophic systems in so called photogranules. In general, photogranules can be described as spherical biofilm systems of phototrophic and heterotrophic microorganism. Photogranules were already obtained from different seeding cultures: (1) hydrostatically incubated activated sludge (Abouhend et al., 2018), (2) activated granular sludge mixed with unicellular green algae (Liu et al., 2017), and have demonstrated to work at lab-scale in airlift reactors as well as in aeration-free mechanically stirred reactors (Meng et al., 2019a; Tiron et al., 2017). Photogranules are commonly cultivated in sequencing batch operation to provide cyclic

wash-out conditions, assure selection of well-settling biomass and prevent growth of individual cells in suspension. This operation strategy is similar to the one applied in aerobic granular sludge technology and assures a selection pressure for granular morphology (de Kreuk, 2006).

Motile filamentous cyanobacteria showed to be an important constituent of photogranule formation and vital under static incubation and mixed operation conditions (Abouhend et al., 2018; Milferstedt et al., 2017b). In green algae dominated photogranules, *Zoogloea* was shown to be involved in the granulation process due to EPS production (Huang et al., 2015; Zhang et al., 2018a). Few studies also addressed other functional groups such as nitrifiers (Abouhend et al., 2018; Huang et al., 2015; Tiron et al., 2015), denitrifiers (Stauch-White et al., 2017) or polyphosphate accumulating organisms (PAOs) (Cai et al., 2019) in photogranules. However, successful implementation of photogranular technology will require a deeper biological understanding of the processes and the microbial community that drive granular structure and function so that this knowledge may be parameterized both under static and hydrodynamic conditions. Integrating systems biology and community-based approaches can provide significant insight into the physiology and role of specific organisms in community function (Oyserman et al., 2016) which can help identify additional operational strategies to steer biomass characteristics towards a particular ecosystem function. Therefore, in order to fully exploit photogranule technology, a first step is linking information about the microbial ecology of phototrophic granulation with properties of the granules.

In this study we examined the effect of hydraulic retention time (HRT) on the function and assembly of a photogranular community. By using amplicon sequencing, microscopic observation, characterization of the EPS matrix and general acquisition of bioreactor performance, key organisms and factors can be identified. We compared taxonomical & functional groups correlation with chemical and physical data from the bioreactor system to identify potential biological drivers of key functional properties. This will enhance the understanding of photogranular systems and help to further improve the operational strategies.

3 MATERIALS AND METHODS

3.1 Algal-bacterial community

The bioreactors were inoculated with biomass from nutrient rich sources at equal proportions by mass. The inoculum comprised out of field samples from various locations in the Netherlands and sludge from an upflow anaerobic sludge blanket

(UASB) reactor operated 35°C and 8 days HRT at the Netherlands Institute of Ecology (NIOO-KNAW), The Netherlands. The field samples were taken in selected places with high temperature and nutrient loading. They originate from a tropical (35°C) fish breeding aquarium, a eutrophic small pond at a farm and a clarifier of the wastewater treatment plant of the paper industry PARENCO B.V. (Renkum, The Netherlands). In addition, two microalgal laboratory strains used in previous research on wastewater at NIOO-KNAW (Fernandes et al., 2015), *Chlorella sorokiniana* and *Chlorococcum* sp. from the culture collection at NIOO-KNAW were added. The final mixture of algae and bacteria was inoculated with equal proportions in terms of biomass concentration with a final density of 0.025 g L^{-1}. After 10 days of cultivation in batch biomass reached a concentration of approximately 2 g L^{-1}.

3.2 Experimental set-up

Three 1.7 L bubble column bioreactors were operated for 116 days as sequencing batch reactors with HRTs of 2.00, 1.00 and 0.67 days. From day 116 to the end of the experiment (day 148), the 2.00 d HRT bioreactor was changed to 0.67 d and the 1.00 d HRT bioreactor was changed to 0.33 d. The third bioreactor was kept at the same condition (HRT of 0.67 d). The operation procedure of each 12h (2.00, 1.00, 0.67 d HRT) or 6h (0.33 d HRT) cycle was: 30 min of settling, 15 min of decanting, 15 min of filling and 660 min (12h cycle) and 300 min (6h cycle) reaction time. After decanting, synthetic wastewater (modified BG-11 medium) was added with following composition: 472.0 mg L^{-1} $(NH_4)_2SO_4$, 56.0 mg L^{-1} K_2HPO_4, 75.0 mg L^{-1} $MgSO_4.7H_2O$, 420 mg L^{-1} sodium acetate trihydrate, 36.0 mg L^{-1} $CaCl_2.2H_2O$, 8.4 mg L^{-1} EDTA ferric sodium salt, 1.8 mg L^{-1} $Na_2EDTA.2H_2O$, 2.86 mg L^{-1} H_3BO_3, 1.81 mg L^{-1} $MnCl_2.4H_2O$, 0.44 mg L^{-1} $ZnSO_4.7H_2O$, 0.079 mg L^{-1} $CuSO_4.5H_2O$, 0.22 mg L^{-1} $Na_2MoO_4.2H_2O$, 0.05 mg L^{-1} $Co(NO_3)_2$ $6H_2O$, 0.12 mg L^{-1} Vitamin B_1 and 0.0012 mg L^{-1} Vitamin B_{12}. The final concentrations of the major constituents are: 100 mg_N L^{-1}, 10 mg_P L^{-1}, 200 mg_{COD} L^{-1}. The nutrient load per day for each HRT are summarized in **Table S1** in the supplemental material. For each bioreactor, a solid retention time of 7 days was achieved by decanting the settled biomass twice a week to lower the biomass concentration to 1 g L^{-1}. The biomass concentration within the bioreactor before harvesting the biomass was usually between 2-3 g L^{-1}.

Each glass bioreactor had an inner diameter of 0.10 m and a conical bottom part and was illuminated from one side with two warm-white LED flood lights providing an incident light intensity of 500 µmol m^{-2} s^{-1} (PAR range) at the reactor surface. Illumination followed a 12:12 (light:dark) cycle which resulted in an total light input of 0.68 mol_{ph} $reactor^{-1}$ day^{-1}, or 0.4 mol_{ph} L^{-1} day^{-1}, considering the reactor geometry. The

bioreactors were aerated with 400 mL.min^{-1} of 5% CO_2 enriched air (regulated by mass flow controllers) to ensure non-limiting inorganic carbon conditions and mixing of the culture. Temperature was controlled at 35 °C by water baths and pH was controlled at 6.7±0.1 by automatic addition of 1M HCl and 1M NaOH by pH controllers.

3.3 Analytical Methods

Daily samples for NH_4^+−N, PO_4^{3-}−P, NO_3^-−N, and NO_2^--N analysis were filtered through a 0.2 μm cellulose acetate filter (VWR) and measured in a Seal QuAAtro39 AutoAnalyzer (SEAL Analytical Ltd., Southampton, UK) according to standard protocols (APHA/AWWA/WEF, 2012). Total inorganic nitrogen is the sum of NH_4^+−N, NO_3^-−N, and NO_2^--N measured in liquid. Biomass dry weight (DW), elemental composition and sludge volume index (SVI) of the algal-bacterial biomass was determined according to standard methods (APHA/AWWA/WEF, 2012). The separation efficiency (SE) of the biomass was calculated from the biomass concentration of the total bioreactor content and effluent (**equation S1** in supplemental information). The elemental composition of homogenized freeze-dried biomass was measured. For C and N analyses a subsample (about 2mg) was folded into a tin cup and analysed with an organic elemental analyzer (Flash 2000, Interscience Breda). Cellular P was analysed by combusting a subsample (about 2mg) for 30min at 550°C in Pyrex glass tubes, followed by a digestion step with 10 mL persulfate (2.5%) for 30 min at 121°C. The digested solution was measured for PO_4^{3-} on a Seal QuAAtro39 AutoAnalyzer (SEAL Analytical Ltd., Southampton, UK). Extracellular polymeric substances (EPS) were extracted with the formamide-sodium hydroxide method according to Adav and Lee (2008). Total polysaccharides were measured with the phenol-sulfuric method (DuBois et al., 1956), and total proteins with the modified Lowry method using Modified Lowry Protein Assay Kit (ThermoFisher Scientific, USA) (Lowry et al., 1951). The results are given in polysaccharide and protein content of EPS, which are abbreviated with EPS-PS and EPS-PN. Both, EPS extractions and measurements of total polysaccharides and proteins were performed in triplicates. Microscopic observations were performed with a fluorescence microscope (Leica DMI4000 B, Germany) and a stereo microscope (Leica M2015C). Pictures were obtained with the software Cell* (Soft Imaging Systems GmbH, Germany) and Leica Application Suite (LAS version 4.7).

3.4 Statistical analysis

The acquired physical, chemical and biological data of all applied HRTs were summarized and quasi-steady state conditions were statistically compared by one factor ANOVA with Tukey's HSD as a post hoc test (**table S2**). In the case of HRT 0.67d, the dataset of two bioreactors (R1 & R3) operated at the same HRT were combined to one.

3.5 16S and 18S rRNA gene amplicon sequencing

From each reactor, biomass was sampled at nine time points. The initial inoculum, after 10 days batch phase and start of experiment (referred to as day 0), and days 11, 25, 32, 60, 82, 119 and 140 respectively. DNA extraction from each time point was conducted in triplicate. In addition, the starting inoculum was also extracted in triplicate. Specifically, 15 mL of harvested sludge was centrifuged at 5500 rpm and the supernatant discarded. The cell pellets were immediately frozen at -80 °C until further processing. DNA was extracted by using the DNeasy PowerSoil Isolation Kit (Qiagen GmbH, Hilden, Germany). The quantity and quality of DNA were spectrophotometrically determined with a NanoDrop (ThermoFisher Scientific, USA). The 75 genomic DNA samples were submitted for sequencing to Génome Québec (MacGill University, Montreal, CA). The 16S rRNA gene V3/V4 variable region was amplified using primer pair 341F (CCTACGGGNGGCWGCAG) and 805R (GACTACHVGGGTATCTAATCC) (Herlemann et al., 2011). The 18S rRNA gene V4 variable region was amplified using the primer pair 616*F (TTAAARVGYTCGTAGTYG) and 1132R (CCGTCAATTHCTTYAART) (Hugerth et al., 2014). Both sets of primers were modified to add Illumina adapter overhang nucleotides sequences to the gene-specific sequences. Sequencing was performed using an Illumina MiSeq system (Illumina MiSeq, USA) with 300-bp reads (v3 chemistry). The obtained sequences were processed with the Hydra pipeline version 1.3.3 (Hollander, 2018) implemented in Snakemake (Köster and Rahmann, 2012). Taxonomic alignment of the sequences was done to the SILVA database (release 132) using SINA (https://www.arb-silva.de). The analysis of the microbiome data was performed with the R-package *phyloseq* (version 1.26.1) (McMurdie and Holmes, 2013). All high-throughput sequencing data are deposited in the National Center for Biotechnology Information database and can be found under the accession number SAMN12373400-SAMN12373549 and under the SRA bioproject PRJNA556418.

3.6 Raw read processing

A total of 7.869.303 16S and 8.723.187 18S raw reads were generated. After quality trimming, adapter trimming and length filtering using *cutadapt* version 1.18 (Martin, 2013), the Hydra pipeline version 1.3.3 (Hollander, 2018) implemented in Snakemake (Köster and Rahmann, 2012) was used to merge paired end reads and cluster OTUs. A total of 3.748.927 16S and 2.306.332 18S contigs remained that were further processed using the R package *phyloseq* version 1.26.1 (McMurdie and Holmes, 2013). In the downstream process the 16S and 18S data set was normalized using the cumulative sums scaling (CSS) function of the R package *metagenomSeq* version 1.24.1 (Paulson et al., 2013). The community structure and the change through time of the 16S and 18S dataset were analysed by Principal Coordinate Analysis (PCoA) of a Bray-Curtis dissimilarity matrix. For clustering the 16S and 18S dataset were subsetted to the top 20 OTUs and known functional groups based on the MIDAS database (McIlroy et al., 2015) and Milferstedt et al. (2017b) (table A4 in supplemental information)

3.7 Correlation network analysis

Pearson correlation coefficient (PCC) between microbial data and functional parameter (**table S5** in supplemental materials) obtained from the reactor operations were determined with the R function *cor* in the R package *stats* version 3.5.2. A threshold of > 0.5 and <-0.5 for the PCC was used to filter OTUs only correlating strongly with functional parameters. This threshold was greater than 2 standard deviations from the mean PCC. The software Cytoscape 3 was used to analyse the correlation network and to visually represent the network (Su et al., 2014).

4 RESULTS

4.1 Photogranule formation

The development of a well settling algal-bacterial community was strongly influenced by the applied HRT. With decreasing HRT, and therefore increasing hydraulic pressure, the microbial community was driven more rapidly towards floccular aggregates. Specifically, at an HRT 0.67 d the assembly time was reduced to 11 days compared to 32 days at HRT 2.00. The hydraulic pressure dictated the SE as well, which resulted in better separation at lower HRTs. When changing the HRT at day 116 from 2.00 d to 0.67 d and from 1.00 d to 0.33 d the settling properties increased significantly, and the microbial community shifted to be dominated by photogranules.

In **Figure 1,** the separation efficiency (SE) of biomass from the liquid is displayed as a percentage (%) of the total amount of biomass in the system. As HRT decreased, the

separation efficiency of the biomass increased. Specifically, a SE higher than 90% in phase 1 was achieved for the bioreactor with an HRT of 0.67 d in 10 days. The bioreactor with an HRT of 1.00 d achieved this SE in 24 days of operation, whereas the bioreactor operated at an HRT of 2.00 d required 32 days. These results show that a lower HRT accelerated the assembly of flocs and granules by rapid selecting for well-settling biomass. The higher hydraulic pressure experienced by the microbial community at HRT 1.00 d, and below, drives a SE greater than 90%. Furthermore, in the case of HRT 0.67 d and HRT 0.33 d in phase 2 the SE increased to 99%. In **Figure 2A** the long-term effect of HRT on SE and SVI is depicted. A lower HRT drives a higher SE and lower SVI. The variability in SE and SVI was also lower with lower HRT, suggesting that low HRT increased the functional stability**.** This implies that it promotes a more stable settling and therefore improves biomass retention in the system. The increased SE was accompanied by a decrease in SVI. While the microalgal-bacterial community exhibited an SVI of >300 mL g^{-1} at the start of operation it was reduced to an average of 57±9 mL.g^{-1} when it began to show granular biomass structure.

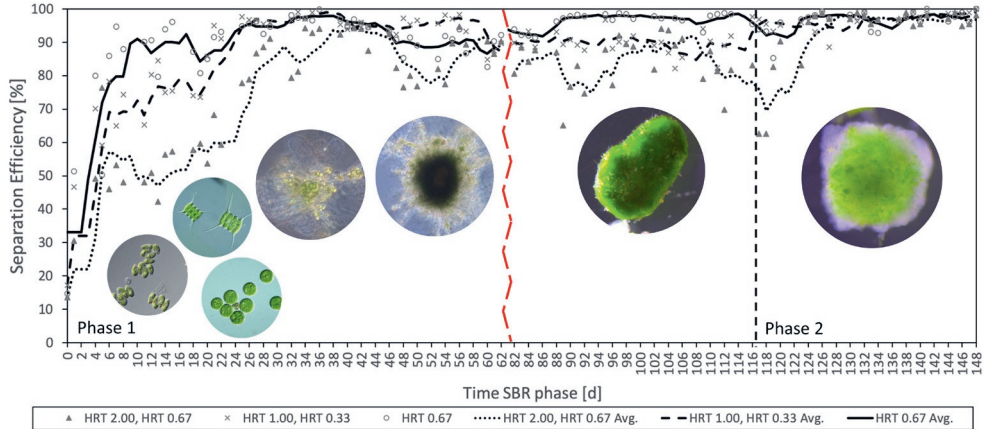

Figure 1: SE (%) of biomass of the 3 bioreactors over the course of the experiment. The first month is characterized by the assembly of the microbial community to well-settling biomass, while the following two months feature first photogranule appearance and further maturation. At day 116 (phase 2) a shift in the HRT was performed. The red dashed line at day 62 symbolizes a two-week period of not stringent monitoring. The microscopic images provided along the timeline are taken at following timepoints (from left to right): first 2 of eukaryotic green algae and motile filamentous cyanobacteria from the inoculum; next 2 at t=32 and t=60 of floccular aggregates; last 2 at t=82 and t=140 of photogranules. A scale bar is included in each picture.

The morphological changes of the photogranules during the operation were followed by microscopic observation with selected pictures shown in **Figure 1**. The inoculum consisted of free organisms such as green algae, cyanobacteria, and bacteria. Motile filamentous cyanobacteria present in the inoculum started to entangle and form early aggregates as flocs in the first weeks of operation and started to incorporate other

prokaryotes and colony-forming photosynthetic eukaryotes. After about 3 month of operation the first granular structures appeared as shown by the microscopic images of t=82 and 140 days in **Figure 1**.

It has been shown that EPS may act like a glue that promotes the spatial alignment of both algae and bacteria to agglomerates (Flemming et al., 2007). Characterisation of the EPS matrix in terms of proteins (EPS-PN) and polysaccharides (EPS-PS) showed that EPS is a substantial part of the floccular and granular biomass ranging from 8-34% (**Figure S4**). In **Figure 2B** the average EPS is depicted for the applied HRT. There is no significant difference in constituent (EPS-PN and EPS-PS), however there is a significant increase in PN/PS ratio with lower HRT. While being a substantial part from the first appearance of floccular structure there was a change from mostly EPS-PS to a majority of EPS-PN content. This is reflected in a shift from the PN/PS ratio in EPS from 1.0 to 6.6 at HRT 0.67. The makeup of EPS in the photogranules in the last month of operation at HRT 0.67 was found to be 239±42 $mg_{EPS}\ g_{VSS}^{-1}$ with a PN/PS ratio of about 6.6.

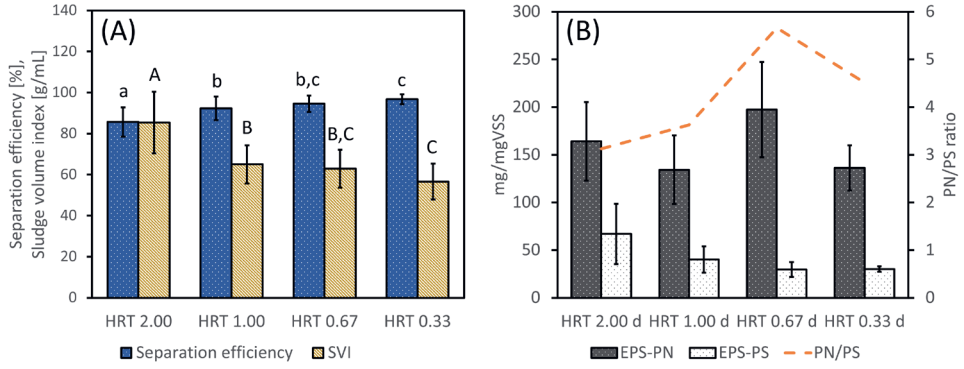

Figure 2: (A) Relation between HRT, separation efficiency (SE) and sludge volume index (SVI) over applied HRT. The standard deviation of the measured values is displayed as error bars. The letters (a, b, c, d, A, B, C, D) above the bars indicate the significant difference between observations. **(B)** The EPS composition in terms of EPS-PN, EPS-PS and PN/PS ratio (orange line) for each applied HRT.

4.2 Nutrient removal performance

The initial phase of bioreactor operation was characterized by a rapid assembly of a well-settling floccular microbial community with stable nitrogen and phosphorus removal after 2-4 weeks. In **Figure 3A** the average volumetric nutrient removal rates across the applied HRT are shown. With decreasing HRT, the volumetric removal rate for nitrogen increased significantly from 24 to 90 $mg_N\ L^{-1}\ day^{-1}$ with the maximum at HRT 0.33. After 40 days of operation nitrification started to occur in all three bioreactors, but no stable nitrification rate was obtained until the end of operation

(**Figure S1**). Since the increase in nitrogen removal could not be explained with nitrogen assimilation in the biomass, the potential denitrification was assessed. Therefore, a mass balance over nitrogen using in and out coming nitrogen of the bioreactor, the biomass productivity and the elemental composition of the biomass was performed. In that way it was shown that for HRT 0.67 denitrification accounted for 23% of the nitrogen removal and for HRT 0.33 for 26% (**Figure S7**). The volumetric removal rate of phosphorus increased with decreasing HRT from 3.1 to 5.4 mg_P L^{-1} day^{-1}, however not significantly. COD in the form of acetate was fully consumed in all applied HRTs, which translates in a volumetric removal rate of 97 to 580 mg_{COD} L^{-1} day^{-1} (**Figure S2**). With decreasing HRT, the biomass productivity increased as well (**Figure 3B**). While there is no significantly difference in biomass productivity between HRT 2.00, 1.00 and 0.67, there was a significant increase at HRT 0.33. This can be explained due to the increased COD load per day and the larger contribution of heterotrophic growth in the bioreactor (**Figure S5**).

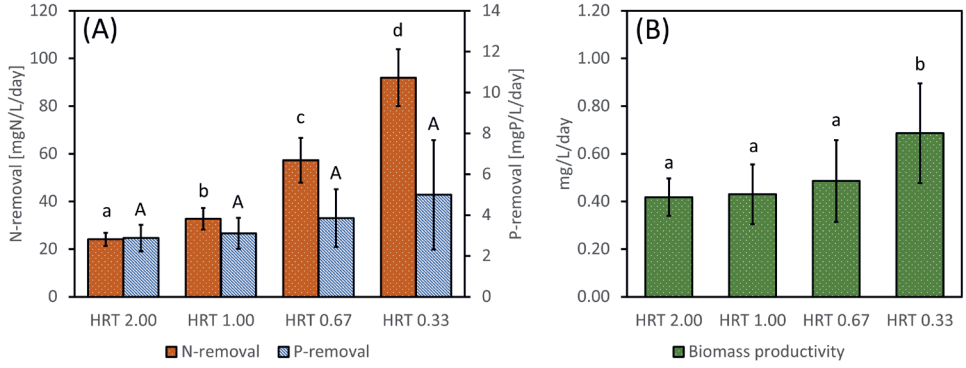

Figure 3: (A): Volumetric nutrient removal rates per mol of photons of each applied HRT. All values shown are averaged over the quasi-steady state conditions measurements. **(B)** Biomass productivity at the different HRTs applied. The error bars are the standard deviation in the observed time frame. The letters (a, b, c, d, A) above the bars indicate the significant difference between observations.

In phototrophic systems the removal rates per mol of photon supplied are important to know next to the volumetric removal rates. Considering a volumetric photon supply of 0.4 mol_{ph} L^{-1} day^{-1} the removal rate per mol of photons range from 59 to 226 mg_N mol_{ph} day^{-1} nitrogen and 7.1 to 12.2 mg_P mol_{ph} day^{-1} for phosphorus depending on the applied HRT. The biomass yield is ranging from 1.0 to 1.7 g_X mol_{ph} day^{-1}, which is higher than observed values for phototrophic growth due to the heterotrophic growth that gets an increased importance at lower HRT.

4.3 16S and 18S rRNA-Gene-Based Microbial Community Assembly

The principal coordinates analysis (PCoA) demonstrated tight clustering of triplicate samples for both the 16S and 18S data sets (**Figure 4**). Thus, all downstream analysis on relative abundance for each date was conducted using the average OTU read abundance from triplicates. The PCoA revealed a clear and recurring trajectory of the prokaryotic and eukaryotic community from planktonic organisms to the assembly of photogranules. Bioreactor 1 and 2 followed a similar trajectory, however, bioreactor 3, which was operated at the lowest initial HRT of 0.67 days, diverged from the other two bioreactors at day 32, but then re-converged reaching the same general community structure by day 140. Interestingly, all three bioreactors showed a similar 16S microbial community at day 140 regardless of the history of the community and applied HRT. The 18S community showed more dynamic and did not reach a stable community as the 16S one. In both PCoA plots a "horseshoe effect" is visible. This phenomenon is often observed in microbiome studies that sample along an environmental gradients in which multiple different niches are present and differentially represented (Morton et al., 2017). Here we show that this horseshoe effect was also observed through time as microbiomes adapt to novel conditions from their seed environment.

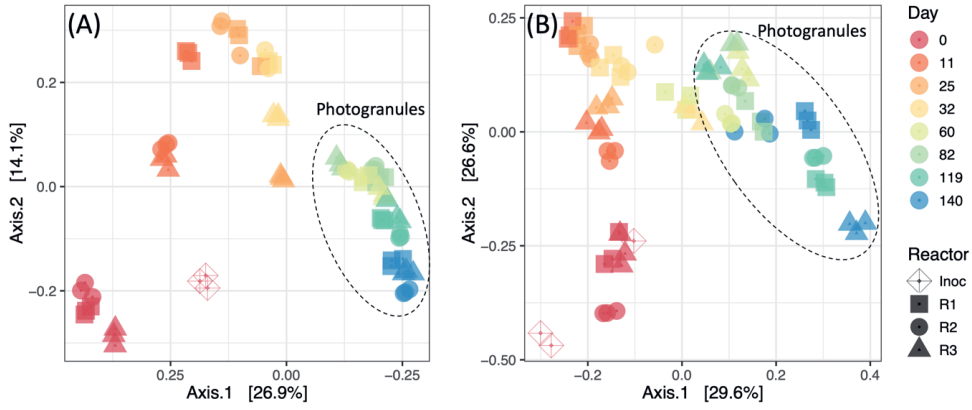

Figure 4: Principal coordinates analysis (PCoA) was performed on the 16S **(A)** and 18S **(B)** rRNA gene sequences to explore the similarities in between the set of triplicate measurements of each sampling day. This analysis demonstrates the overlap of triplicate measurements and the trajectory of the microbial community to photogranules.

4.4 Prokaryotic community (16S)

For the clustering analysis 61 OTUs were included related to functional groups in correspondence with the MIDAS database (McIlroy et al., 2017) and Milferstedt et al. (2017b) (**table S4**). In addition, any of the top 20 OTUs that were not assigned a

functional group were also included giving a final total of 54. The functional groups included: phototrophs (19 taxa), biofilm former (3 taxa), filamentous organism (13 taxa), nitrifiers (2 taxa), denitrifiers (6 taxa), polyphosphate accumulating organisms (PAOs, 9 taxa) and methanotrophs (6 taxa). The analysis revealed four distinct bacterial communities in the time series. Initially, the prokaryotic photosynthetic community was characterized by an abundance of *Rhodobacter* (OTU_16), *Oscillatoria* PCC-6304 (OTU_103), *Pseudanabaena* PCC-7429 (OTU_385), *Tychonema* CCAP_1459-11B (OTU_401), *Cyanobium* PCC-6307 (OTU_819), *Planktothricoides* SR001 (OTU_1279) and *Phormidium* ETS-05 (OTU_1374). This diverse community of cyanobacteria decreased through time and was replaced in all bioreactors by a simplified cyanobacterial community dominated by *Limnothrix* (OTU_4) (10%) and *Cephalothrix* SAG 75.79 (OTU_5) (11%). Other cyanobacterial OTUs such as *Leptolyngbya* ANT-L52.2 (OTU_291), *Leptolyngbya* PCC-6306 (OTU_2) and *Alkalinema* CENA528 (OTU_15) showed no distinct pattern over the course of the experiment and exhibit a similar abundance at the beginning and the end of the experiment.

Concomitant to the increase of the simplified photosynthetic community, the non-photosynthetic prokaryotic reference taxa for biofilm formation, *Zoogloea* (OTU_12), *Thauera* (OTU_24) and *Meiothermus* (OTU_7) increased. In all treatments *Zoogloea* became the most abundant organism at the end of the time series with 13-18% relative abundance. In contrast, *Meiothermus* showed its highest abundance (18%) at day 32 at HRT 1.00 d and then decreased in all bioreactors.

The nitrifying bacterial community was composed of only a single identified OTU, *Nitrosomonas* (OTU_68) within the *Nitrosomonadaceae* family, which saw a general increase over time from the inoculum. Several heterotrophic nitrifiers and aerobic denitrifiers were present in considerable abundance such as *Comamonas* (OTU_23), *Zoogloea* (OTU_12), *Pseudomonas* (OTU_385), *Diaphorobacter* (OTU_10), *Thauera* (OTU_24) and *Pelomonas* (OTU_202).

The functional group of PAOs showed a general increase over time except for *Gemmatimonas* (OTU_313), which initially increased at HRT 1.00 and 0.67 with a sudden decrease most likely due to washout. The most prominent representatives that increased were *Pseudomonas* (OTU_3), *Acinetobacter* (OTU_18) and the novel cyanobacterial lineage *Obscuribacterales* (OTU_80), a putative PAO enriched in a photo-EBPR system (Oyserman et al., 2017).

4.5 Eukaryotic community (18S)

In the majority of the sampling points, known photosynthetic organisms represented over 90% of the eukaryotic community based on relative abundance. Initially, the

photosynthetic fraction of the eukaryotes was dominated by only three green algae *Chlorella sorokiniana* (OTU_1) (13%), *Chlorococcum vacuolatum* (OTU_4) (32%) and *Desmodesmus sp. HSJ717* (OTU_43) (20%). Both *Chlorella sorokiniana* (OTU_1) and *Chlorococcum vacuolatum* (OTU_4) were present in the initial inoculum but showed divergent patterns through time. In all bioreactors, *Chlorella sorokiniana* (OTU_1) showed a steep increase until day 25, whereas *Chlorococcum vacuolatum* (OTU_4) decreased in relative abundance. Despite these divergent early trajectories, both populations eventually rebounded and returned to similar relative abundances as in the beginning. In contrast, *Desmodesmus sp. HSJ717* (OTU_43) generally showed a decrease in all bioreactors. In the final photosynthetic eukaryotic community, a more diverse assemblage was found. Next to *Chlorella sorokiniana* (OTU_1) (23-29%) and *Chlorococcum vacuolatum* (OTU_4) (8-19%), the community was enriched with *Scenedesmaceae sp.* A2_2 (OTU_78) (2-9%), *Chlamydomonadaceae sp.* KMMCC_FC-97 (OTU_20) (5-7%) and *Chlamydomonadales* (OTU_3) (14-16%).

The non-photosynthetic eukaryotic community was characterized by predatory eukaryotic organisms such as rotifers, ciliates, amoeba and fungi. Amongst the predatory eukaryotic community, we detected *Echinamoeba exundans* (OTU_119), *Spirotrichea* (OTU_29), *Bilateria* (OTU_69), *Vermamoeba* (OTU_56), *Ascomycota* (OTU_168) and *Basidiomycota* (OTU_30). These taxa were present in all sample points at very low levels except on day 140, when a sudden increase was observed in all three bioreactors.

4.6 Correlation network of microbial community, biomass characteristics and reactor function

A correlation network using Pearson correlation coefficient (PCC) was carried out to assess the relation between operational conditions, functional parameters, and microbial community. In **figure 5** the correlation network for all taxa, both prokaryotic and eukaryotic, show a positive correlation with biomass characteristics (EPS, CNP content, SVI) and reactor performance (SE, nutrient removal). The most connected nodes in the network are attributed to motile filamentous cyanobacteria, colony forming photosynthetic eukaryotes, biofilm producing denitrifiers and organism involved in the removal and conversion of nitrogen. SE, SVI and EPS content are strongly correlated to the cyanobacteria *Limnothrix* (OTU_4) and *Cephalothrix* SAG_75.79 (OTU_5) while EPS is correlated with *Zoogloea* (OTU_12), *Thauera* (OTU_24), *Limnothrix* (OTU_4) and *Cephalothrix* SAG_75.79 (OTU_5). The node for EPS-PS is isolated from the rest of the network and is mostly correlated with eukaryote *Desmodesmus* sp. HSJ717 (OTU_43). From the network analysis it was shown that the total nitrogen removal rate is mainly

attributed to the phototrophic eukaryotes *Chlamydomonadaceae sp. KMMCC_FC-97* (OTU_20) and *Chlamydomonadales* (OTU_3), and the non-phototrophic prokaryote *Thauera* (OTU_24). Partial nitrification is largely correlated with *Comamonas* (OTU_23), *Alicycliphilus* (OTU_9), *Pseudomonas* (OTU_3), *Nitrosomonas* (OTU_68) and *Diaphorobacter* (OTU_10), while nitrification is correlated with *Diaphorobacter* (OTU_10) and an OTU from the family *A4b* (OTU_137). In this network one taxa from the order of *Obscuribacterales* (OTU_80) is present and is the only node connected to P removal. A significant correlation of three taxa from the family *Microscillaceae* (OTU_76), *mle_1-27* (OTU_25) and the genus *Pelomonas* (OTU_202) with phosphorus content of the biomass is observed. These organisms belong to the family of *Comamonadaceae* that is often observed in wastewater treatment systems and show many putative PAOs. Interestingly, *Leptolyngbya* PCC-6306 (OTU_2) and other OTUs that were abundant throughout such as *Acidovorax* (OTU_149), *Chlorella sorokiniana* (OTU_1) and *Chlorococcum vacuolatum* (OTU_4) did not correlate with function, likely because they did not vary in relative abundance through time as they were in high abundance in the inoculant and maintained this status as abundant organisms.

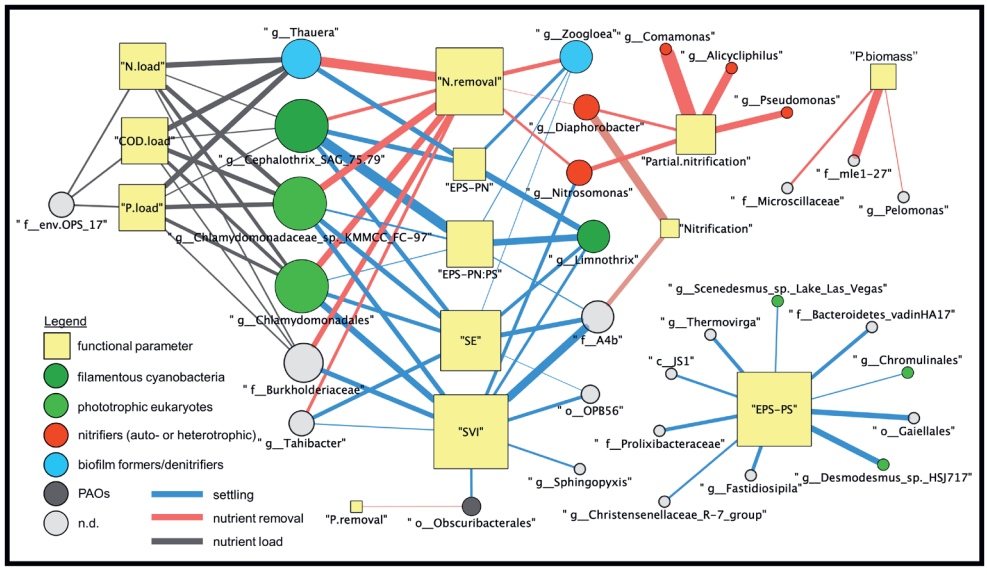

Figure 5: Network analysis of taxonomical and functional data on biomass characteristics and reactor function. The functional network consists of taxa that strongly positively correlate with the attributed function. Functions of taxa and kind of interaction is colour coded. The size of the nodes represents the connectivity of the taxa or reactor function. Edge colour indicates the kind of relation and the thickness the correlation between two nodes.

5 DISCUSSION

5.1 Photogranule formation

One of the most fundamental selection criteria for biomass in bioreactors is sedimentation. Effective settling and retention within the system is generally achieved through the formation of aggregates such as floc and granules. Organisms that do not participate in granule formation do not settle and therefore are washed out of the system. Here we show that applying lower HRT increases the rate at which granule formation is achieved. In all HRTs the EPS matrix makes a substantial part of the total photogranular biomass with no significant difference among them. The EPS obtained from photogranules at the end of the experiment showed an average EPS content of 239±42 $mg_{EPS}\ g_{VSS}^{-1}$ with a PN/PS ratio of about 6.6. This is lower than values found for aerobic granules (311 to 418 $mg_{EPS}\ g_{VSS}^{-1}$) however with a higher PN/PS ratio (3.4 to 6.2) (Adav and Lee, 2008). Our observation fall within the range of recent studies on photogranules that reported EPS values from 35.1 to 252.3 $mg_{EPS}\ g_{VSS}^{-1}$ with an PN/PS ratio from 1.2 to 6.9 (Ansari, Abouhend and Park, 2019; Cai *et al.*, 2019, Kuo-Dahab *et al.*, 2018;).

The HRT had no consistent effect on the overall EPS-PN content, but generally lead to increasing PN/PS ratio at lower HRT. With increasing PN/PS ratio the SE increases while the SVI decreases (**Figure 2A**, **Figure S4**). These findings are in agreement with previous research on aerobic granules highlighted the importance of high PN/PS ratio for successful granulation (Adav et al., 2008; Pronk et al., 2017; Seviour et al., 2012). The high EPS-PN and low EPS-PS observed is attributed to increased hydrophobicity by decreasing the negative surface charge and excess Gibbs energy of the surface (Ding et al., 2015; Wilén et al., 2018). Activated sludge with floccular structure has usually a PN/PS ratio of around 0.9 that indicates low hydrophobicity (Adav and Lee, 2008). Polysaccharides contribute to the formation of cross-network structure with cells (Seviour et al., 2009). However, a higher polysaccharide compared to protein content is associated with floccular structures with loose morphology and slime properties (Flemming et al., 2007). The increase of the PN/PS from flocs (0.7) to photogranules (7.4) is in accordance with the change in surface properties of the biomass to photogranules (**Figure S3**).

5.2 Nutrient removal of a photogranular bioreactor

The maximum removal rate of 90 $mg_N\ L^{-1}\ day^{-1}$ and 5.4 $mg_P\ L^{-1}\ day^{-1}$ was three times higher than similar photo-heterotrophic treatment systems (Liu et al., 2017; Van Den Hende et al., 2014, 2011b; Wang et al., 2015). The ammonical nitrogen removal, in

particular, was improved through time due to nitrification/denitrification which correlated with the change of the microbial community from flocs to granules. Nitrification/denitrification are generally described as an additional nitrogen removal path in the use of algal-bacterial communities (Arashiro et al., 2017; Oyserman et al., 2017; Rada-Ariza et al., 2017; Van Der Steen et al., 2015). The consensus is that the assembly of microbes to flocs and granules increases the stratification over the biomass and hence creates anoxic/anaerobic conditions in the centre, which would allow denitrifiers to convert nitrate into nitrogen gas (Adav et al., 2010).

An overall increase in volumetric nitrogen removal rate was observed with decreasing HRT from 2.00 to 0.33 days that was not proportional to the N assimilation in the biomass. This suggests that the higher ammonium and COD loading at lower HRT had a positive effect on the nitrifying/denitrifying community in the photogranules as shown by Princic *et al.*, (1998) for aerobic granules. The higher nutrient loading could lead to a deeper penetration of nutrients in the granular structure and increased denitrification (Alpkvist et al., 2006). The high abundance of *Zoogloea* and *Thauera*, both known denitrifiers, could have influenced the N removal at HRT 0.67 and 0.33 days (**Figure S7**).

The main removal mechanism for P is via assimilation in biomass that matches with the biomass productivity and P content (about 1%). Although the presence of several putative PAOs was detected by 16S analysis, only *Obscuribacteriales* correlated with P removal, a finding in agreement with Oyserman et al. (2017) which also saw the enrichment of this lineage under non-granular photosynthetic feast-famine conditions. Carvalho et al. (2018) demonstrated as well the successful implementation of photosynthetic cultures enriched in PAOs under feast famine conditions. In our study, the enrichment of PAOs was not selected for directly. Incorporating the feast famine regime that selects for PAO could increase the P removal of granular sludge while maintaining the benefits of well-settling granular sludge.

5.3 Community assembly of planktonic organisms to photogranules

The two most abundant photosynthetic prokaryotic taxa, *Limnothrix* (OTU_4), *Cephalothrix* SAG_75.79 (OTU_5), are both motile filamentous cyanobacteria from the order of *Limnotrichales* and *Nostocales*. These taxa are ubiquitous in nature but have not been reported previously to play an important role in the formation of photogranules. They show great functional and morphological similarities with the genus *Microcoleus*, a motile filamentous cyanobacteria previously found in photogranules by Milferstedt et al. (2017b) and Stauch-White et al. (2017). In their research they hypothesize that at

least one motile filamentous cyanobacteria in high abundance is necessary to form photogranules. Our results support these findings.

Our and previous reported findings confirm that these filamentous cyanobacteria have an important role in the initiation of photogranulation. Interestingly, filamentous bacteria such as *Thiothrix* in aerobic granules are generally unwanted since they lead to outgrowth and bulking sludge (de Kreuk, 2006). However, in the formation of anaerobic granular sludge the filamentous *Methanosaeta* is thought to be crucial in granulation. This was proposed as the "Spaghetti theory" by Wiegant (1988). In photogranulation a similar concept could be developed where filamentous organisms may become entangled in microscopic knots which become the nucleus (a niche) for other organisms to attach and form agglomerates that mature to granules.

With the assembly of photogranules, known biofilm producing prokaryotes such as *Zoogloea* (OTU_12), *Thauera* (OTU_24) and *Meiothermus* (OTU_7) were enriched as granule formation progressed. These organisms were previously reported as important for the assemblage of aerobic granules by Weissbrodt *et al.*, (2013), and found to be a vital part of the microbial community in aerobic granules incubated under photosynthetic conditions (Cai et al., 2019; Zhang et al., 2018a, 2018b). As known biofilm and therefore EPS producers it is very likely that that they substantially contribute to the granular matrix. However, it is not possible to state which organisms contributed to what extend to the EPS matrix.

Interestingly, we saw that the washout conditions of decreasing HRT only dictated the time for photogranule assembly, despite ending with similar microbial community structure (**Figure 4**). This suggests that while HRT might not drive differences in final community structure of a granule, it does increase the rate at which granule formation is achieved based on other functional parameters such as SE, SVI and EPS. SRT could have a larger effect on the final algal-bacterial community as Bradley et al., (2019) recently showed. Other operational choices such as settling time, feeding regime, nutrient limitation, aeration, or mechanical mixing would be interesting to test and evaluate the determining effect on the community structure of photogranules.

5.4 Network analysis of microbial community structure and reactor function – finding biological drivers of physical and chemical properties in photogranules

The network analysis showed that only a few organisms drive a wide array of functional parameters. Microbes with the highest connectivity included the cyanobacteria *Limnothrix* (OTU_4), *Cephalothrix* SAG_75.79 (OTU_5) and the

photosynthetic eukaryote *Chlamydomonadales* (OTU_3), suggesting they may be key players in granule formation and community structure. Their strong correlation with SVI, SE and PN/PS ratio indicates their structural importance in the photogranular makeup. Additionally, they are related to nitrogen removal, which could be simply explained by their high relative abundance. Interestingly, OTU 137 from the family of *A4b* showed a strong positive correlation with SVI, SE and the PN/PS ratio of EPS as well. These taxa usually make up the core microbial community of anaerobic digesters (Xia et al., 2016). Their presence could be an indicator for dense granular structures that provide an anaerobic niche despite a highly aerated system. This is especially seen in the relationship with SVI and *A4b,* which has the strongest correlation of all organisms in the microbial community.

Conversely, the network analysis also showed that one parameter or function can be influenced by many different organisms of the community in various degrees. Functions associated with the EPS matrix are influenced by various organisms. *Zoogloea* (OTU_12), which was expected to strongly correlate with EPS related functions only weakly correlates with EPS-PN. However, a strong correlation with N content in the biomass and nitrogen removal rate was observed. *Thauera* (OTU_24), another known EPS producer and prominent denitrifier, exhibits a much stronger correlation to nitrogen removal than to EPS related functions (Adav et al., 2010). Although less abundant it suggests that this taxon has a stronger influence on the functional parameters. The most prominent being SVI, SE, EPS-PS and nitrogen removal. But also, other more conserved reactor functions such as partial nitrification and nitrification are connected to many organisms of the community especially of the genus *Nitrosomonas*, *Comamonas*, *Pseudomonas, Diaphorobacter*, *Thauera* and *Pelomonas*.

As shown here, when starting with a suspended diverse microbial community and by applying the right operational criteria such as phototrophic conditions, sedimentation and hydrodynamic, a photogranular community can be formed. However, the question how to stir the microbial community of the photogranule to improve desired traits such as nitrogen or phosphorus removal. Ideally photogranule has excellent sedimentation, incorporates high nutrient removal rates and requires minimum external input such as aeration. The photogranules obtained in this study show three times higher (up to 90 $mg_N\ L^{-1}\ day^{-1}$) removal performance in comparison to other phototrophic systems but are still lower than other conventional treatment systems. For aerobic granular sludge operated at full scale maximum volumetric removal rates are reported from 170 $mg_N\ L^{-1}\ d^{-1}$ and 240 $mg_P\ L^{-1}\ d^{-1}$ (M. Pronk et al., 2015). This is 2 (for N) and 50 (for P) times higher than the volumetric removal rates obtained here. To improve the nutrient removal rate of N and P the focus could be to improve the conditions for higher

nitrification rates and Enhanced Biological Phosphorus Removal (EBPR) by PAOs. This would require additional operation strategies, which amongst others would include a sophisticated feeding strategy, for example with providing feast/famine conditions of the primary nutrient (N, P, COD) as in Oyserman et al. (2017). In this way another selection on nutrient limitation would be applied on the microbial community that would promote organisms that produce storage compounds such as EPS, lipids, polyhydroxyalkanoate, polyphosphate. Due to the density of these polymers, it might be beneficial for the overall treatment process by promoting settleability and nutrient removal but might also be interesting for later applications of the photogranular biomass. In addition, microalgae would fuel the whole process by converting photonic energy into chemical energy, potentially excluding external oxygen supply and reduce greenhouse gases such as CO_2 (Borowitzka and Moheimani, 2013).

6 CONCLUSION

Low HRTs provide cyclic wash-out conditions in the bioreactors with a strong selective pressure for well-settling biomass. Decreasing HRT improved settling, with a critical HRT threshold of 1 day. Below this threshold, settling efficiency was above 95%, but above this threshold separation efficiency stayed below 90%. Despite the differences between bioreactors in HRT, after one month of operation all three bioreactors showed a similar microbial community with floccular structure and good separation efficiencies. After three months of operation photogranules were obtained in all bioreactors. Decreased HRT provides a 'shortcut' to produce well settling biomass (Figure 1), alters reactor community structure more rapidly (Figure 4), and maintain high nutrient removal and reactor function (Figure 2 & 3). Future research should be aimed to understand additional factors related to granule formation such as SRT and nutrient feeding strategies and parametrizing them in combination with low HRT. The network analysis identified the key bacterial and eukaryotic taxa driving reactor functions. The settling properties of the granules were most linked to motile filamentous cyanobacteria (*Limnothrix*, *Cephalothrix* SAG_75.79), photosynthetic eukaryote *Chlamydomonadales* in combination with EPS producers (*Zoogloea*, *Thauera*). The nutrient removal properties were most linked to nitrifiers/denitrifiers (*Nitrosomonas*, *Comamonas*, *Thauera*, *Pseudomonas*, *Diaphorobacter* and *Pelomonas*) and putative PAOs (*Obscuribacterales*). Compared to other photogranular systems a different microbial assemblage was found but with similar functional redundancy. Therefore, it might not be about specific strains but about having (a) representative(s) from a function group with many potential strains. Further research is needed to find out if the final community structure and function is decoupled and depend mostly on the operation conditions rather than on the inoculum.

7 ACKNOWLEDGMENTS

The authors would like to thank Mauk Westerman Holstijn and Egbert Trompetter for their help in carrying out the experiment. Nico Helmsing, Gilles Wijlhuizen, for setting up the bioreactors and analysis. Suzanne Wiezer for her assistance in microscopy and taxonomy. Stefan Geisen for choosing the primers and discussion on amplicon sequencing. Mattias de Hollander and Fleur Gawehns-Bruning for their bioinformatic support. Génome Québec (MacGill University, Montreal, CA) for the 16S and 18S rRNA gene amplicon sequencing. Casper van Leeuwen for his help with the statistical analysis.

8 SUPPLEMENTAL MATERIAL

8.1 Nutrient load

Table S1: Nutrient load at each applied HRT in terms of nitrogen, phosphorus and COD.

HRT	Nitrogen	Phosphorus	COD
[day]	*[mgN L^{-1} day^{-1}]*	*[mgP L^{-1} day^{-1}]*	*[mgCOD L^{-1} day^{-1}]*
2.00	50	5	100
1.00	100	10	200
0.67	150	15	300
0.33	300	30	600

8.2 Nutrient removal

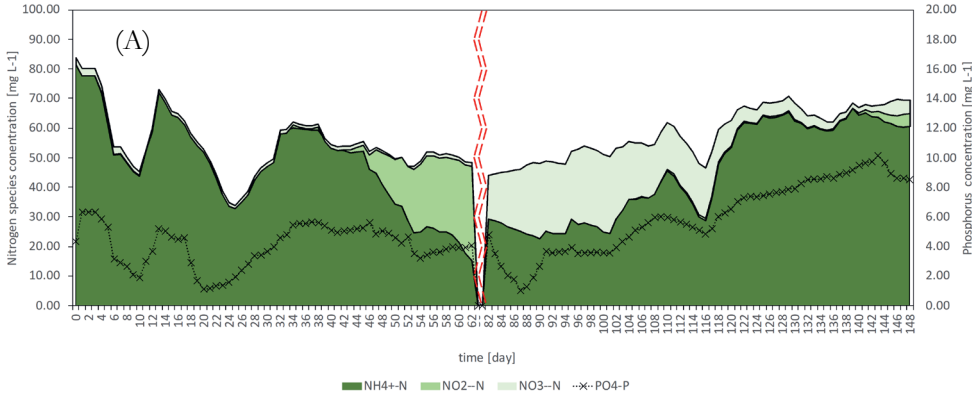

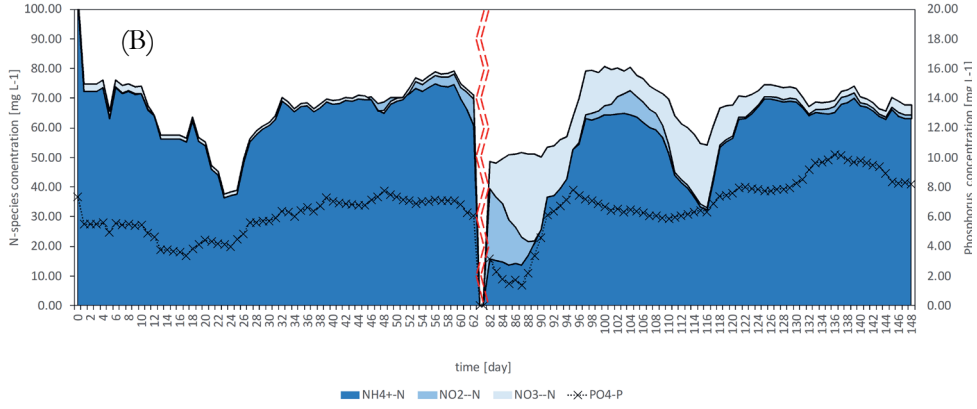

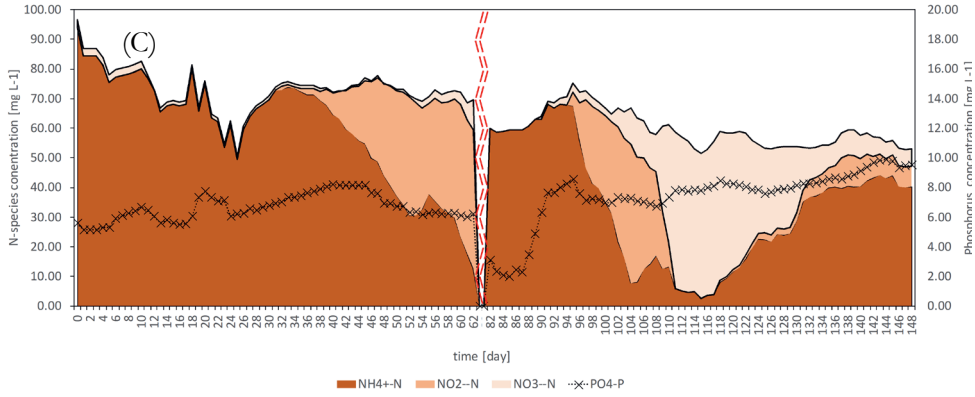

Figure S1: Evolution of NH_4^+-N, NO_2^--N, NO_3^--N concentration is depicted for the three bioreactors operated. The increases in first ammonium oxidizing bacteria (AOBs) and later in nitrite oxidizing bacteria (NOBs) led to the shift in nitrogen species from ammonium to nitrite to nitrate. The dashed line with the black crosses represents the PO_4^{3-}-P concentration. (A) for R1, (B) for R2 and (C) for R3.

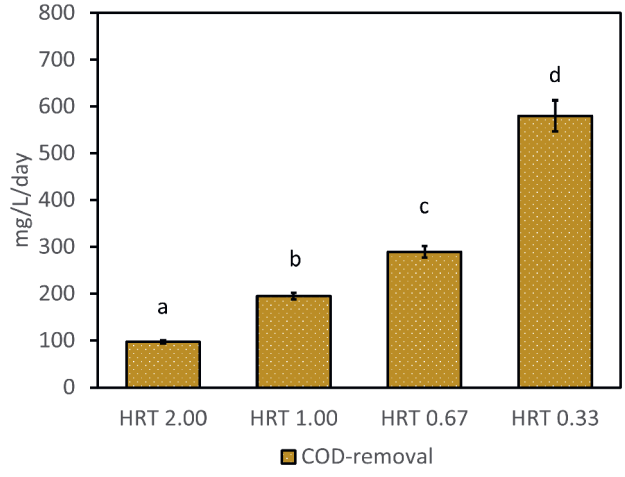

Figure S2: Volumetric COD_S (acetate) removal rate observed at different HRTs applied. The values are expressed in mg of COD. In most of the days the COD_S level in the effluent was well below 15 mg L^{-1}meaning that almost all the incoming acetate was consumed. The letter (a, b, c, d) shows the significant difference between the applied HRTs.

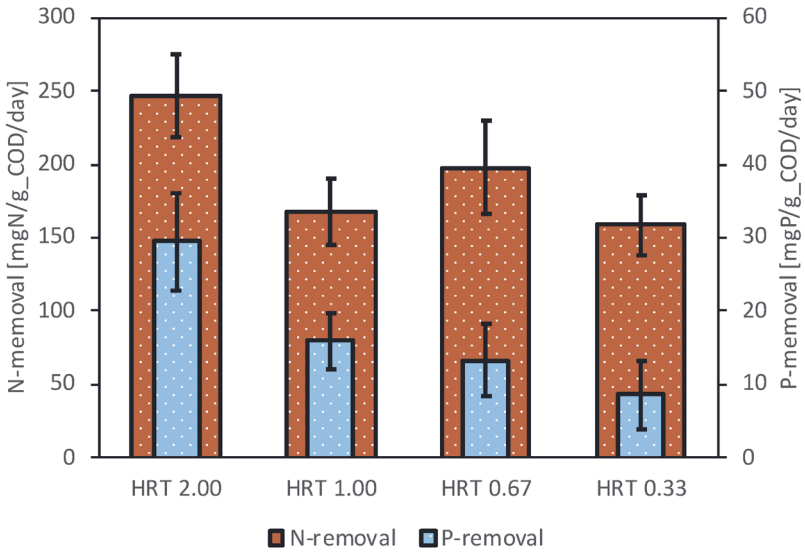

Figure S3: Removal yield per gram of COD.

Table S2: Results of statistical test performed on HRT data set on various parameters. Presented are single-factor ANOVA and as a post hoc test the Tukey's HSD.

N-removal						
ANOVA: single-factor						
Source of Variation	*SS*	*df*	*MS*	*F*	*P-value*	*F crit*
Between Groups	84705.48	3	28235.16	244.8535774	1.94E-68	2.64739085
Within Groups	24331.35	211	115.3145			
Total	109036.8	214				

Post hoc test:			q-value	3.695
Tukey-Kramer HSD	num df	4	den df	211
Comparison	*Absolute Difference*	*Critical range*	*result*	
HRT 2.00 to HRT 1.00	8.701	2.731587	*significantly different*	
HRT 2.00 to HRT 0.67	29.353	2.731587	*significantly different*	
HRT 2.00 to HRT 0.33	66.072	2.731587	*significantly different*	
HRT 1.00 to HRT 0.67	20.652	2.731587	*significantly different*	
HRT 1.00 to HRT 0.33	57.371	2.731587	*significantly different*	
HRT 0.67 to HRT 0.33	36.719	2.731587	*significantly different*	

P-removal						
ANOVA: single-factor						
Source of Variation	*SS*	*df*	*MS*	*F*	*P-value*	*F crit*
Between Groups	28.09742	3	9.3658059	2.0931245	*0.102186*	*2.647595*
Within Groups	939.657	210	4.4745574			
Total	967.7545	213				

Post hoc test:			q-value	*3.695*
Tukey-Kramer HSD	num df	4	den df	*210*
Comparison	*Absolute Difference*	*Critical range*	*result*	
HRT 2.00 to HRT 1.00	0.987	1.1400937	*not significantly different*	
HRT 2.00 to HRT 0.67	0.740	1.1400937	*not significantly different*	

HRT 2.00 to HRT 0.33	0.943	1.1400937	*not significantly different*	
HRT 1.00 to HRT 0.67	0.246	1.1400937	*not significantly different*	
HRT 1.00 to HRT 0.33	0.043	1.1400937	*not significantly different*	
HRT 0.67 to HRT 0.33	0.203	1.1400937	*not significantly different*	

Separation efficiency (SE)						
ANOVA: single-factor						
Source of Variation	SS	df	MS	F	*P-value*	*F crit*
Between Groups	3005.108	3	1001.7027	29.610302	*5.24E-16*	*2.647595*
Within Groups	7104.202	210	33.829533			
Total	10109.31	213				

Post hoc test:			q-value	*3.695*
Tukey-Kramer HSD	num df	4	den df	*210*
Comparison	*Absolute Difference*	*Critical range*	*result*	
HRT 2.00 to HRT 1.00	6.457	3.1348265	*significantly different*	
HRT 2.00 to HRT 0.67	8.787	3.1348265	*significantly different*	
HRT 2.00 to HRT 0.33	11.083	3.1348265	*significantly different*	
HRT 1.00 to HRT 0.67	2.331	3.1348265	*not significantly different*	
HRT 1.00 to HRT 0.33	4.626	3.1348265	*significantly different*	
HRT 0.67 to HRT 0.33	2.296	3.1348265	*not significantly different*	

Sludge volume index (SVI)						
ANOVA: single-factor						
Source of Variation	SS	df	MS	F	*P-value*	*F crit*
Between Groups	7843.129	3	2614.376	14.00234	*2.01E-07*	*2.718785*
Within Groups	14936.79	80	186.7099			
Total	22779.92	83				

Post hoc test:			q-value	*3.711*
Tukey-Kramer HSD	num df	4	den df	*80*
Comparison	*Absolute Difference*	*Critical range*	*result*	
HRT 2.00 to HRT 1.00	20.301	8.225889	*significantly different*	
HRT 2.00 to HRT 0.67	22.467	8.225889	*significantly different*	
HRT 2.00 to HRT 0.33	28.761	8.225889	*significantly different*	
HRT 1.00 to HRT 0.67	2.166	8.225889	*not significantly different*	
HRT 1.00 to HRT 0.33	8.460	8.225889	*significantly different*	
HRT 0.67 to HRT 0.33	6.294	8.225889	*not significantly different*	

Biomass productivity						
ANOVA: single-factor						
Source of Variation	SS	df	MS	F	*P-value*	*F crit*
Between Groups	3.441779	3	1.14726	12.39492	*9.62E-08*	*2.628968*
Within Groups	34.33934	371	0.092559			
Total	37.78112	374				

Post hoc test:			q-value	*3.695*
Tukey-Kramer HSD	num df	4	den df	*374*
Comparison	*Absolute Difference*	*Critical range*	*result*	
HRT 2.00 to HRT 1.00	0.020	0.195689	*not significantly different*	
HRT 2.00 to HRT 0.67	0.085	0.195689	*not significantly different*	
HRT 2.00 to HRT 0.33	0.357	0.195689	*significantly different*	
HRT 1.00 to HRT 0.67	0.065	0.195689	*not significantly different*	
HRT 1.00 to HRT 0.33	0.337	0.195689	*significantly different*	
HRT 0.67 to HRT 0.33	0.272	0.195689	*significantly different*	

8.3 Separation efficiency

The separation efficiency (SE) of the biomass within the bioreactor was calculated from the biomass concentration in the effluent ($C_{x,eff}$) and in the bioreactor ($C_{x,reactor}$). The value is expressed as the percentage of biomass that remains in the system during the cyclic wash-out conditions (**Equation S1**).

$$SE = (1 - \frac{C_{x,eff}}{C_{x,reactor}}) * 100 \qquad \text{Equation S1}$$

8.4 EPS quantification

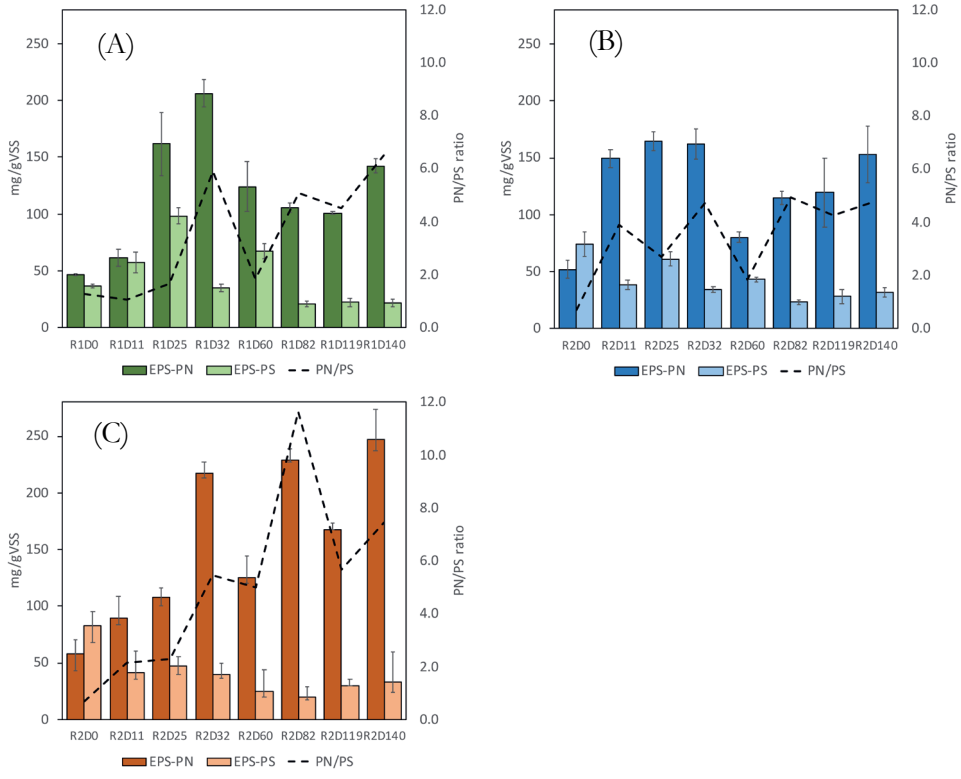

Figure S4: Extracellular polymeric substances (EPS) content of the three bioreactors (R1=A, R2=B and R3=C) at day 0, 11, 25, 32, 60, 82, 119 and 140 The EPS content is represented in two fractions: EPS-PS = total polysaccharides, EPS-PN: total proteins with the standard deviation of triplicate measurements as error bars. In addition, the PN:PS ratio is presented as a dashed line.

8.5 Biomass productivity, elemental composition and removal rates per biomass

For the maximum theoretical biomass productivity two possible growth ways were taken into account: (I) phototrophic and (II) heterotrophic. For the phototrophic growth the volumetric light availability from 0.4 mol L^{-1} day^{-1} was used with a biomass yield on light of 0.9 g_X mol_{photon}^{-1}. For heterotrophic growth the yield factor was calculated from standard stoichiometry using acetate as carbon source.

$$CH_3COO^- + 0.236\ NH_4^+ + 0.824\ O_2 \rightarrow 1.18\ CH_{1.5}O_{0.4}N_{0.2} + 0.764\ H_2O + 0.764\ HCO_3^- + 0.056\ CO_2$$

The resulting yield factor for heterotrophic biomass on acetate is 0.49 g_X $g_{acetate}^{-1}$.

The contribution of phototrophic biomass is equal in all HRTs since the same amount of light was provided. Only the heterotrophic growth is changing due to the different COD (acetate) loadings at different HRT. With decreasing HRT, the COD load increases and thus the heterotrophic biomass growth:

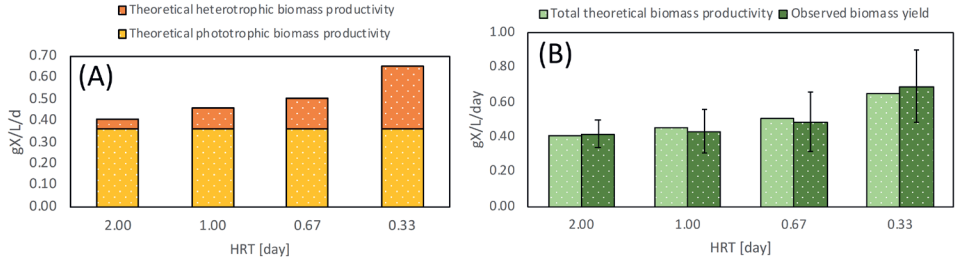

Figure S5: (A) The theoretical attribution of phototrophic and heterotrophic biomass production at different HRTs and COD loads. (B) The theoretical maximum biomass productivity is compared to the observed biomass productivity. The error bars are the standard deviation of the measurements.

Table S3: Elemental composition for the biomass in terms of carbon I, nitrogen (N) and phosphorus (P). The values are averages and standard deviations over the operation period of the respective HRT. The first 35 days of operation are excluded from this representation.

	C		N		P	
	Avg. [%]	*Std.Dev. [%]*	*Avg. [%]*	*Std.Dev. [%]*	*Avg. [%]*	*Std.Dev. [%]*
HRT 2.00	44.6	4.2	7.6	1.3	1.0	0.3
HRT 1.00	43.6	5.1	8.0	1.5	0.8	0.2
HRT 0.67	46.4	3.4	9.0	1.1	1.0	3.9
HRT 0.33	47.2	1.2	9.8	0.8	0.6	0.2

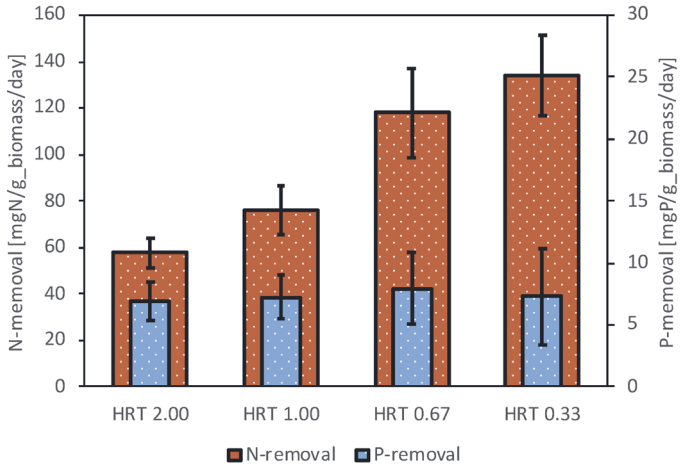

Figure S6: Nitrogen and phosphorus removal rates per biomass.

8.6 Potential denitrification

The potential denitrification in the bioreactor was calculated in two ways, both including a mass balance approach, once over nitrogen, the other over acetate. The first approach (I) included the elemental composition of the biomass (N content) (table A3), the biomass productivity and the observed nitrogen removal. The second approach (II) included the COD removal rate, the biomass productivity and standard stoichiometry for denitrification after Metcalf and Eddy (Fourth Edition 2003; p.619) with acetate as organic substrate.

$$5\,CH_3COO^- + 8\,NO_3^- \rightarrow 4\,N_2 + 10\,CO_2 + 6\,H_2O + 8\,OH^-$$

The resulting yield factor is 1.60 $mol_N.mol_{acetate}^{-1}$.

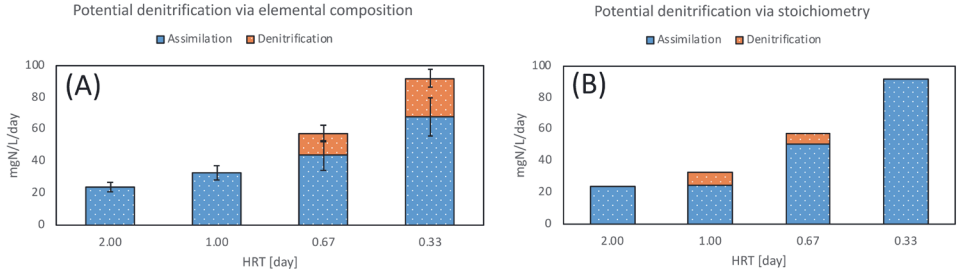

Figure S7: The potential denitrification that could have attributed to N-removal. This was calculated in two different ways: (A) empirical via the elemental composition of the biomass, and (B) theoretically via standard stoichiometry found in literature.

8.7 Considered functional groups

Table S4: Functional groups considered according to the MIDAS database (March 2013) and Milferstedt et al. (2017)

Filamentous	AOBs	NOBs	Denitrifiers	Methanotrophs	PAO
Anaerolinea	Nitrosospira	Nitrobacter	Candidatus Competibacter	Methanobacterium	Candidatus Obscuribacter
Catenibacterium	Nitrosomonas	Candidatus Brocadia	Defluviicoccus	Methanobrevibacter	Corynebacterium 1
Fodinicola	Candidatus Brocadia	Candidatus Nitrotoga	Candidatus Promineofilum	Methanoculleus	Candidatus Accumulimonas
Leptolinea		Nitrospira	Candidatus Accumulibacter	Methanolinea	Candidatus Accumulibacter
Turicibacter			Anaerolinea	Methanomassiliicoccus	Tetrasphaera
Candidatus Amarolinea			Bradyrhizobium	Methanosarcina	
Candidatus Brevefilum			Corynebacterium 1	Methanosphaerula	
Candidatus Promineofilum			Iamia	Methanospirillum	
Candidatus Sarcinathrix			Thiothrix	Methanothermobacter	
Candidatus Villogracilis			Uruburuella	WCHA1-57	
CWWC007			Haliangium	Methanosaeta	
Candidatus Defluviifilum			Skermania		
Candidatus Microthrix			Dechloromonas		
Haliscomenobacter			Sulfuritalea		
Kouleothrix			Acidovorax		
Neomegalonema			Rhodoferax		
Thiothrix			Zoogloea		
Gordonia			Thauera		
Skermania					
Candidatus Nostocoida					

8.8 Bubble plot of clustered OTUs

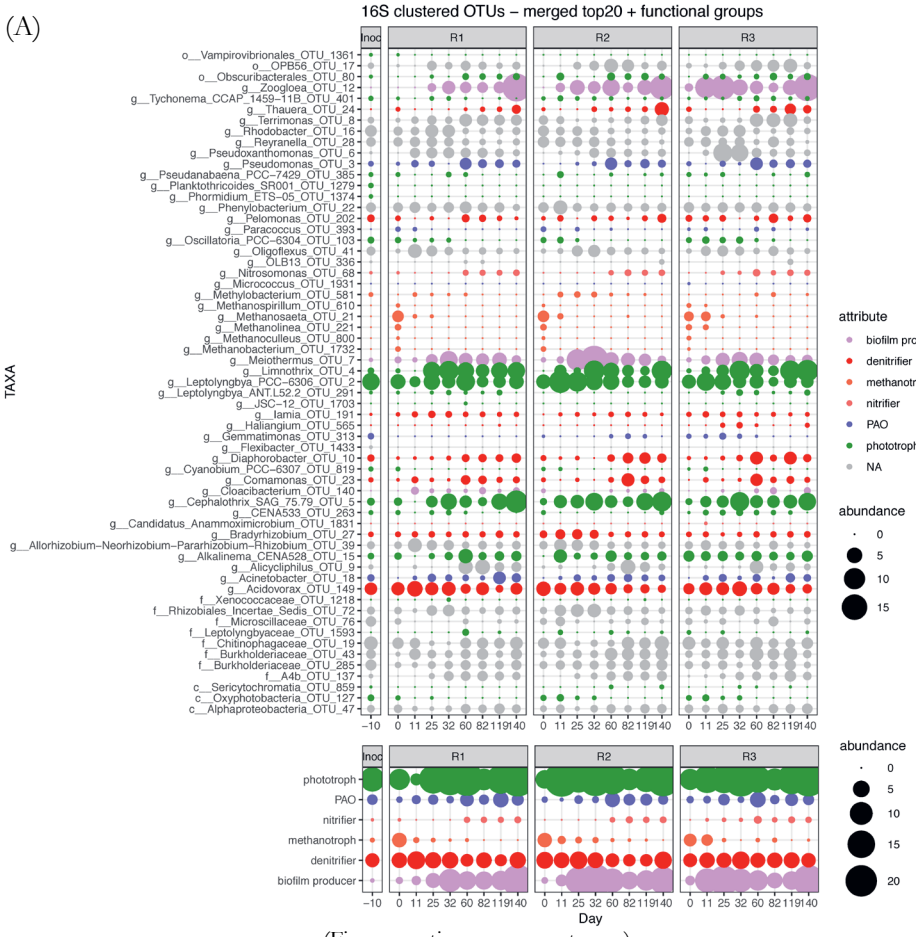

(Figure continuous on next page)

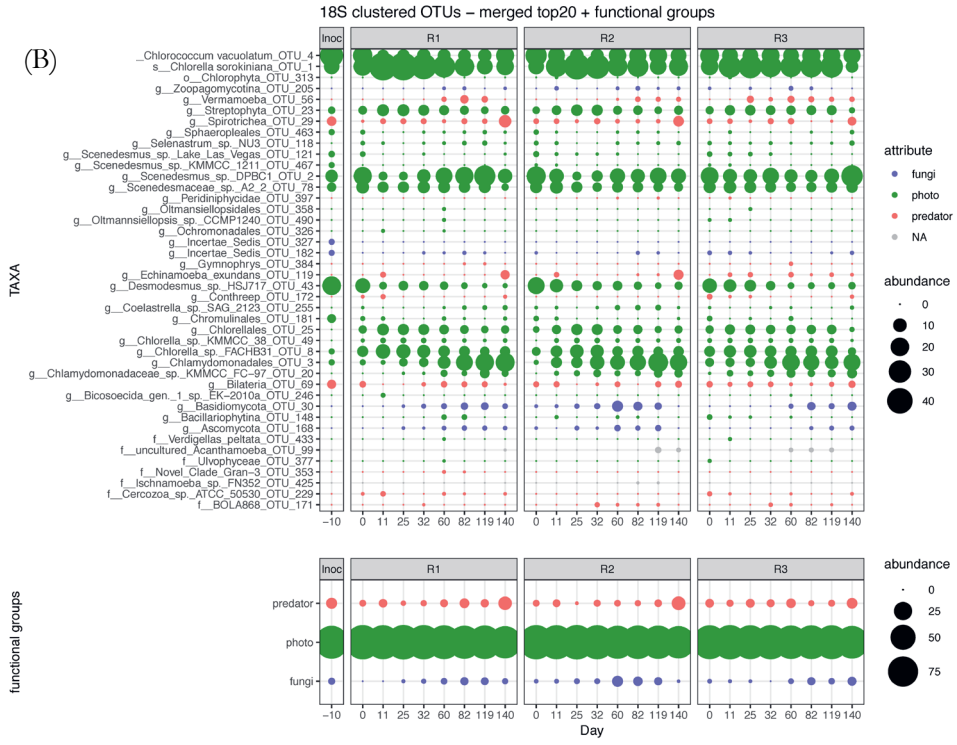

Figure S8: (A, B) Hierarchical clustering and normalized relative abundances of the top 20 16S and 18S OTUs and additional functional groups of 16S OTUs. The functional groups considered for the 16S OTUs were: photosynthetic organisms, indicator species for biofilm formation, nitrifiers and possible PAO candidates. In total there are 53 16S OTUs (top 20 OTUs + functional groups) presented in this figure. The top 20 18S OTUs were separated according to photosynthetic organisms and predators. The predatory eukaryotes include amoeba, rotifer, and fungi.

8.9 Correlation network

For the correlation network physical, chemical and biological measurements were used to find correlation in between these and the microbial community. With that key player for a specific reactor function could be identified. In **table S5** all the measurements and parameters are summarized.

Table S5: Physical, chemical and biological characteristics used for the correlation network between reactor function and microbial community. Most of the empirical data shown her is an average of three consecutive days around the sampling point the microbial community.

	R1D0	R1D11	R1D25	R1D32	R1D60	R1D82	R1D119	R1D140	R2D0	R2D11	R2D25	R2D32	R2D60	R2D82	R2D119	R2D140	R3D0	R3D11	R3D25	R3D32	R3D60	R3D82	R3D119	R3D140
HRT [day]	2.00	2.00	2.00	2.00	2.00	2.00	0.67	0.67	1.00	1.00	1.00	1.00	1.00	1.00	0.33	0.33	0.67	0.67	0.67	0.67	0.67	0.67	0.67	0.67
N-load [mg L^{-1} day^{-1}]	50.00	50.00	50.00	50.00	50.00	50.00	149.25	149.25	100.00	100.00	100.00	100.00	100.00	100.00	303.03	303.03	149.25	149.25	149.25	149.25	149.25	149.25	149.25	149.25
P-load [mg L^{-1} day^{-1}]	5.00	5.00	5.00	5.00	5.00	5.00	14.93	14.93	10.00	10.00	10.00	10.00	10.00	10.00	30.30	30.30	14.93	14.93	14.93	14.93	14.93	14.93	14.93	14.93
COD-load [mg L^{-1} day^{-1}]	100.00	100.00	100.00	100.00	100.00	100.00	298.51	298.51	200.00	200.00	200.00	200.00	200.00	200.00	606.06	606.06	298.51	298.51	298.51	298.51	298.51	298.51	298.51	298.51
SE [%]	13.59	49.77	77.79	79.40	91.47	80.62	82.63	95.44	17.22	65.21	97.63	96.60	84.78	89.88	93.22	97.50	14.69	90.20	94.84	98.06	87.75	93.88	92.80	96.14
SVI [mL g^{-1}]	347	164	103	128	69	72	92	80	368	142	98	83	63	48	64	45	343	113	97	89	62	67	54	53
Biomass prod. [g L^{-1} day^{-1}]	0.18	0.15	0.39	0.30	0.35	0.34	0.48	0.38	0.05	0.54	0.52	0.34	0.48	0.55	0.51	0.47	0.05	0.35	0.51	0.37	0.38	0.44	0.37	0.26
N-removal [mg L^{-1} day^{-1}]	11.02	16.24	30.89	19.99	24.65	27.96	49.44	53.34	9.45	43.74	45.75	24.43	34.28	51.47	93.03	122.68	4.20	45.48	57.15	39.33	42.33	59.82	64.19	70.53
P-removal [mg L^{-1} day^{-1}]	2.34	2.40	3.77	2.44	2.96	2.62	4.16	2.00	0.49	6.02	4.29	2.54	3.95	6.83	6.88	3.17	0.55	6.24	5.57	4.09	5.90	10.31	3.36	1.30
Partial Nitrification [mg L^{-1} day^{-1}]	0.00	0.00	0.00	0.00	0.31	0.00	0.00	0.02	0.00	0.00	0.00	0.00	0.04	0.24	0.01	0.01	0.00	0.00	0.00	0.03	0.47	0.00	0.01	0.06
Nitrification [mg L^{-1} day^{-1}]	0.00	0.00	0.00	0.00	0.01	0.15	0.05	0.03	0.00	0.00	0.00	0.00	0.01	0.09	0.08	0.01	0.02	0.00	0.00	0.00	0.06	0.00	0.43	0.05
P_biomass [%]	1.23	1.60	0.95	0.82	0.76	0.75	0.81	0.84	1.07	1.11	0.58	0.81	0.69	0.57	0.46	0.79	1.39	1.56	0.62	1.07	1.08	10.96	3.02	0.95
N_biomass [%]	5.41	8.65	7.51	6.48	8.66	8.67	8.73	10.55	4.70	8.53	8.33	8.23	8.70	9.36	9.00	10.60	6.78	7.62	9.20	9.08	9.33	8.98	9.61	10.40
C_biomass [%]	35.72	47.29	43.56	46.08	47.44	47.65	45.80	45.31	33.20	42.41	43.95	47.09	46.03	48.99	48.37	46.05	45.28	38.41	45.04	52.33	47.31	48.29	48.66	47.07
NtoP ratio [mol mol^{-1}]	75	76	119	145	160	164	262	139	80	98	196	151	173	222	273	151	84	63	189	13	113	11	42	129
CtoP ratio [mol mol^{-1}]	10	12	18	17	25	26	43	28	10	17	32	23	28	36	44	30	11	11	33	2	19	2	7	24
EPS_tot [mg g^{-1}]	83.01	118.94	259.76	241.28	191.55	126.14	123.35	164.07	126.00	187.64	225.52	196.26	123.48	138.38	147.65	185.00	141.00	131.37	155.47	257.44	150.25	248.92	196.91	280.38
EPS_PN [mg g^{-1}]	46.55	61.53	161.63	206.26	124.01	105.36	100.95	142.24	52.00	149.24	164.46	162.02	80.29	115.10	119.50	153.00	58.00	89.74	108.07	217.47	125.19	229.24	167.36	247.17
EPS_PS [mg g^{-1}]	36.46	57.41	98.13	35.02	67.53	20.77	22.40	21.84	74.00	38.40	61.06	34.23	43.19	23.28	28.15	32.00	83.00	41.63	47.40	39.97	25.06	19.68	29.55	33.21
PN/PS ratio	1.08	1.07	1.65	5.89	1.84	5.07	4.51	6.51	0.80	3.89	2.69	4.73	1.86	4.94	4.24	5.44	1.27	5.51	2.28	8.68	3.13	4.56	5.66	7.44

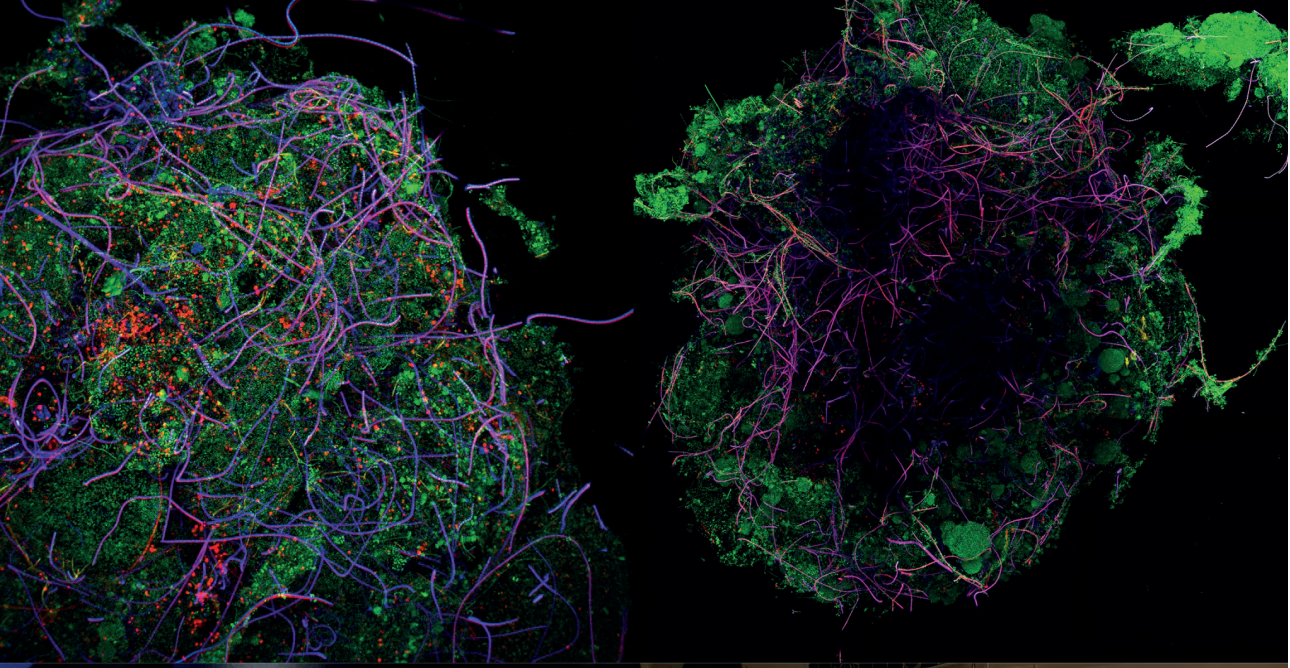

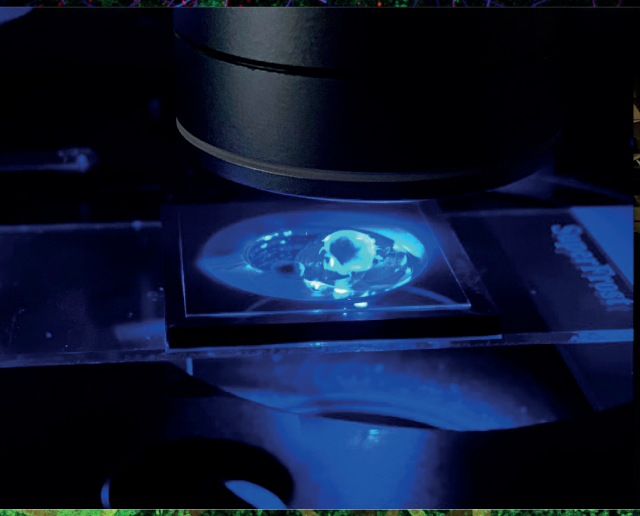

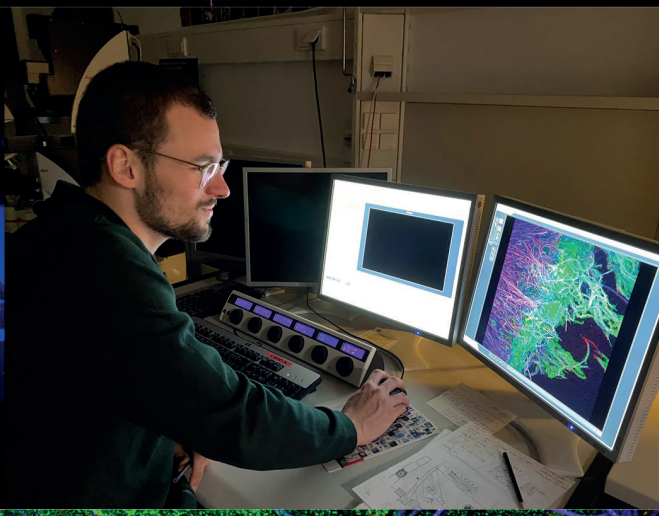

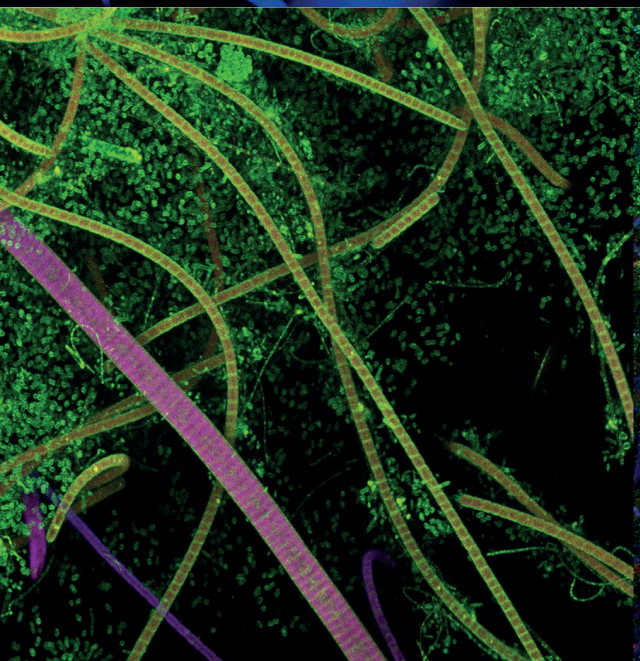

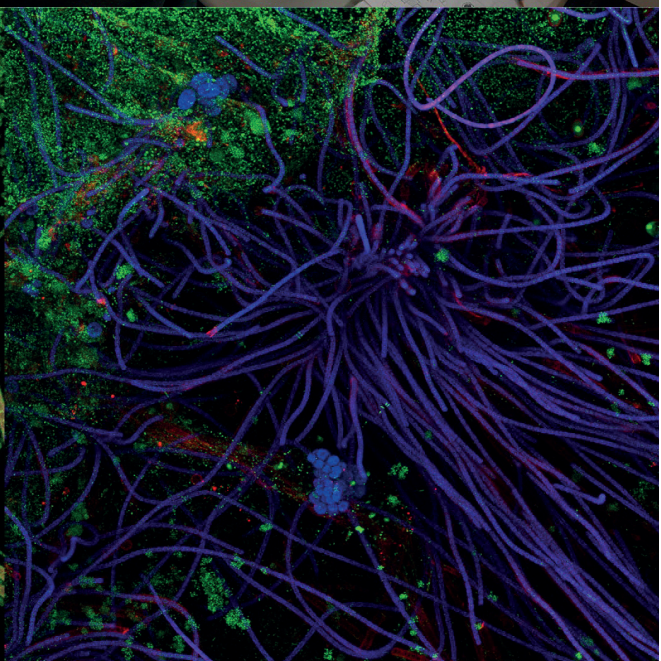

Chapter 3

How N_2-fixation can sustain wastewater treatment performance of photogranules under nitrogen limiting conditions

Lukas M. Trebuch[1,2], Kobe Schoofs[1,2], Stijn M.F. Vaessen[1,2], Thomas R. Neu[3], Marcel Janssen[2], René H. Wijffels[2,4], Louise E.M. Vet[5], Tânia V. Fernandes[1]

[1] *Department of Aquatic Ecology, Netherlands Institute of Ecology (NIOO-KNAW), Droevendaalsesteeg 10, 6708 PB Wageningen, The Netherlands*

[2] *Bioprocess Engineering, AlgaePARC Wageningen University, P.O. Box 16, 6700 AA Wageningen, The Netherlands*

[3] *Microbiology of Interfaces, Department River Ecology, Helmholtz Centre for Environmental Research - UFZ, Brueckstrasse 3A, 39114, Magdeburg, Germany*

[4] *Faculty of Biosciences and Aquaculture, Nord University, N-8049, Bodø, Norway*

[5] *Department of Terrestrial Ecology, Netherlands Institute of Ecology (NIOO-KNAW), Droevendaalsesteeg 10, 6708 PB Wageningen, The Netherlands*

1 ABSTRACT

Photogranules are dense spherical agglomerates of phototrophic and non-phototrophic microorganisms with excellent settling capacity. They are easy to harvest and efficient at phosphorus (P) and nitrogen (N) recovery. Wastewater characteristics can vary significantly, and in some municipal wastewaters the N:P ratio is as low as 5 resulting in nitrogen limiting conditions. Here we assess the microbial community, function, and morphology of photogranules under nitrogen replete (N+) and nitrogen limiting (N-) conditions in sequencing batch reactors. Photogranules subjected to low influent ammonium concentrations of 15 mgN/L were nitrogen deprived 2/3 of a batch cycle duration. Surprisingly, this nitrogen limitation had no adverse effect on biomass productivity. Moreover, phosphorus and COD removal were similar to their removal under nitrogen replete conditions. Although biomass productivity, P and COD removal performance of the two nitrogen treatments were similar, the difference in granule morphology was obvious. While N+ photogranules were dense and structurally confined, N- photogranules showed rather loose structures with occasional voids within the granule. The microbial community analysis and subsequent functional annotation revealed in both treatments a relatively high abundance of cyanobacteria, especially from non-heterocyst-forming types such as *Leptolyngbya boryana* PCC-6306 and *Cephalothrix komarekiana* SAG 75.79 as well as bacteria capable of N_2-fixation. These were higher at N- (38%) than N+ treatment (29%), showing that the microbial community of photogranules could adjust to nitrogen limitation by performing N_2-fixation while maintaining high biomass productivity, phosphorus, and COD removal.

Keywords: *Photogranules, nitrogen limitation, N_2-fixation, CLSM, metataxonomics, functional annotation, FAPROTAX*

GRAPHICAL ABSTRACT

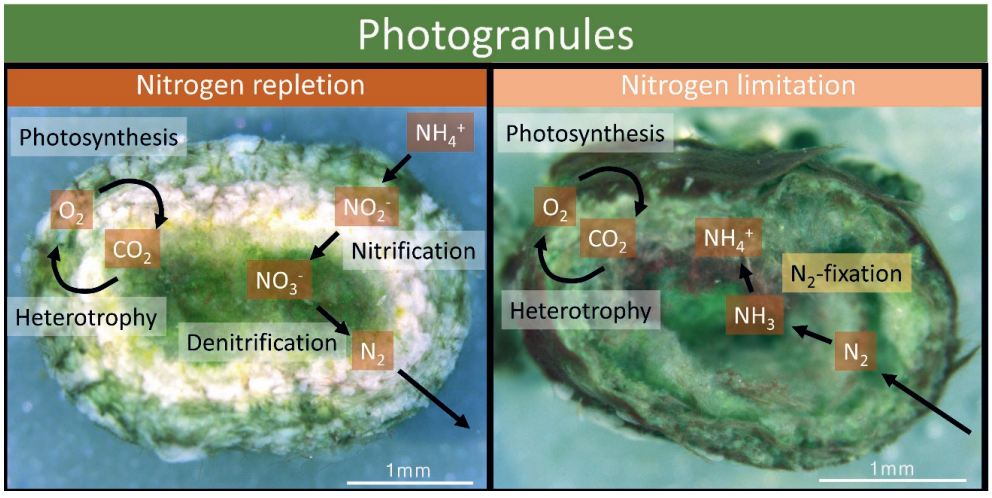

2 INTRODUCTION

Municipal wastewater characteristics can vary significantly between countries and seasons. In municipal wastewaters with minor input of industrial wastewaters the molar N:P ratio can be as low as 5 (Chen et al., 2020). This poses challenges for biological wastewater treatment since it can result in nitrogen limiting conditions adversely affecting growth of the microorganisms and thereby treatment performance.

In recent years, photogranules were suggested as alternative biological wastewater treatment with light as primary energy input (Abouhend et al., 2018; Trebuch et al., 2020). Photogranules are dense spherical biofilms, with excellent settling properties, consisting of cyanobacteria, eukaryotic algae, nitrifiers, denitrifiers and other non-phototrophic organisms. They show considerable advantages in terms of treatment capacity and ease of harvesting compared to other light driven wastewater treatment systems. Light intensity, substrate, and concentration gradients along the radius of a photogranule create different microenvironments which allow functional stratification. Due to the different microenvironments, biological processes requiring different conditions (light, aerobic, anoxic, anaerobic) could occur in the same bioreactor, thereby improving nutrient removal (Lemaire et al., 2008; Meyer et al., 2005). Generally, photogranules exhibit a phototrophic outer layer with non-phototrophic organisms in the inner layers towards the centre (Abouhend et al., 2020). This already allowed to successfully combine photoautotrophy, nitrification and simultaneous denitrification within the same bioreactor (Trebuch et al., 2020).

So far, most of the research has focussed on photogranule initiation and microbial community assembly. Little is known about the effect of varying wastewater characteristics, and so far, there are no studies on nitrogen limitation. In municipal wastewater most nitrogen is in inorganic form as ammonium (NH_4^+) and in the process of biological wastewater treatment it is incorporated either into microbial biomass or converted via nitrification/denitrification to nitrate (NO_3^-) and further to di-nitrogen (N_2). In the global nitrogen cycle, N_2 is subsequently fixed and reduced to ammonium (NH_4^+) again by nitrogen fixing bacteria, cyanobacteria or archaea known as diazotrophs. The main enzyme involved in the N_2-fixation process is nitrogenase. Many cyanobacteria are crucial for nitrogen cycling in aquatic ecosystems (Fani et al., 2000).

Cyanobacteria can be unicellular or filamentous with heterocyst-forming and non-heterocyst forming variants of which many show nitrogenase activities (Flores et al., 2015). Since oxygen, which co-evolved with photosynthesis, is the main antagonist of nitrogenase, cyanobacteria developed strategies to protect nitrogenase against oxygen. Some cyanobacteria develop specialized cells called heterocysts, which show no

photosynthetic but only have nitrogen fixing activity. In this manner they shield nitrogenase from oxygen and can fix nitrogen during light periods. Unicellular and non-heterocyst-forming cyanobacteria do not have specialized cells to perform N_2-fixation. Therefore, N_2-fixation can only happen temporally separated (e.g. during dark periods) or spatially separated (e.g. in dark zones of a biofilm) from photosynthesis (Flores et al., 2015).

Non-heterocyst-forming motile filamentous cyanobacteria of Subsection III genre of Cyanobacteria based on Bergey's bacterial taxonomy (Castenholz et al., 2015) are commonly found in photogranules and proofed to be key for photogranule assembly (Milferstedt et al., 2017b; Trebuch et al., 2020). Some representatives of Subsection III showing nitrogenase activity and present in photogranules include *Microcoleus* sp., *Leptolygnbya boryana*, *Plectonema boryanum*, *Cephalothrix komarekiana* (Flores et al., 2015; Rippka and Waterbury, 1977; Severin et al., 2010; Stanier et al., 1979). When subjected to nitrogen limitation during wastewater treatment these cyanobacteria could switch to N_2-fixation during dark periods or dark zones within the photogranule, to overcome nitrogen limitation.

In previous research on photogranules nitrogen concentrations used in the experiments were high (100 mgN/L) (Trebuch et al., 2020) compared to nitrogen concentration found in several municipal wastewater (15-20 mgN/L) leading to nitrogen limiting conditions (Chen et al., 2020). In this study, we set out to investigate the effect of nitrogen limitation on photogranules by evaluating their biological and physical characteristics and their treatment performance.

3 MATERIALS AND METHOD

3.1 Bioreactor setup and operation

Photogranules obtained from previous research (Trebuch et al., 2020) were cultivated in six bubble columns with a diameter of 10 cm and a working volume of 1.6 L (**figure S1**). Bioreactors were operated in sequencing batch mode for 105 days with a settling time of 5 minutes per cycle, a hydraulic retention time (HRT) of 0.67 days and operating cycles of 12 hours. Day:night cycles of 12 hours were used in such a way that every operating cycle was subjected to 6 hours of light and 6 hours of darkness. A sludge retention time (SRT) of 7 days was achieved by actively removing 114 ml of the mixed liquor at the end of each cycle.

Three replicate bioreactors were operated at an influent nitrogen concentration of 100 mg/L (N+) compared to 15 mg/L (N-) for the other three replicate bioreactors. Synthetic wastewater (modified BG-11 medium) was used with following composition:

382.0 mg L^{-1} NH_4Cl (N+) or 57.3 mg L^{-1} NH_4Cl (N-), 56.0 mg L^{-1} K_2HPO_4, 75.0 mg L^{-1} $MgSO_4$ x $7H_2O$, 420 mg L^{-1} sodium acetate trihydrate, 36.0 mg L^{-1} $CaCl_2$ x $2H_2O$, 8.4 mg L^{-1} EDTA ferric sodium salt, 1.8 mg L^{-1} Na_2EDTA x $2H_2O$, 2.86 mg L^{-1} H_3BO_3, 1.81 mg L^{-1} $MnCl_2$ x $4H_2O$, 0.44 mg L^{-1} $ZnSO_4$ x $7H_2O$, 0.079 mg L^{-1} $CuSO_4$ x $5H_2O$, 0.22 mg L^{-1} Na_2MoO_4 x $2H_2O$, 0.05 mg L^{-1} $Co(NO_3)_2$ x $6H_2O$, 0.12 mg L^{-1}. This results in a synthetic wastewater of 100 mg N L^{-1} (N+) or 15 mg N L^{-1} (N-), 10 mg P L^{-1}, and 200 mg COD L^{-1}. The N:P ratio is 22 for the N+ and 3 for the N- treatment.

Warm-white light was provided by LED lamps from one side with a light intensity at the inner surface facing the lamps of the bioreactor of 500 µmol/m^2/s. The spectrum of the LED lamps used can be found in the supplemental materials (**figure S2**). The bubble columns were aerated with pressurized air enriched with 5% (v/v) CO_2 at 0.5 L/min using mass flow controllers (SLA5800 Series, Brooks Instrument LLC). Temperature was kept constant at 35°C with an external water bath connected to a glass heat exchanger submerged in the bioreactor. The pH was automatically controlled at 6.7 ± 0.1 by the addition of 1 M of HCl or 1 M of NaOH.

3.2 Analytical methods

Daily samples for NH_4^+−N, PO_4^{3-}−P, NO_3^-−N, and NO_2^-−N analysis were filtered through a 0.2 µm polyethersulfrone syringe filter (VWR), stored at -20°C and measured in a Seal QuAAtro39 AutoAnalyzer (SEAL Analytical Ltd., Southampton, UK) according to standard protocols (APHA/AWWA/WEF, 2012). Total inorganic nitrogen was considered as the sum of NH_4^+−N, NO_3^-−N, and NO_2^-−N measured in liquid. COD analysis was performed using the LCK914 COD cuvette tests (Hach Lange, Germany). Additionally, on day 54, 75, 82, 91 and 105, when bioreactors were in steady state, individual 12-hour cycles were analysed for nutrients (N, P and COD) as described before. Biomass dry weight (DW), elemental composition, and sludge volume index (SVI) of the photogranular biomass was determined according to standard methods (APHA/AWWA/WEF, 2012). The separation efficiency (SE) of the biomass was calculated from the biomass concentration of the total bioreactor content and effluent (**equation S1**). The elemental composition of the homogenized freeze-dried biomass was measured. For C and N analyses an aliquot (about 2mg) was folded into a tin cup and analysed in an organic elemental analyser (Flash 2000, Interscience Breda). Cellular P was analysed by combusting an aliquot (about 2 mg) for 30 min at 550°C in Pyrex glass tubes, followed by a digestion step with 10 mL persulfate (2.5%) for 30 min at 121°C. The digested solution was measured for PO_4^{3-}−P on the Seal AutoAnalyzer.

Extracellular polymeric substances (EPS) were extracted with the formamide-sodium hydroxide method according to Adav and Lee (2008). Total polysaccharides were measured with the phenol-sulfuric method (DuBois et al., 1956), and total proteins with the modified Lowry method using Modified Lowry Protein Assay Kit (ThermoFisher Scientific, USA) (Lowry et al., 1951). The results are given in polysaccharide and protein content of EPS, which are abbreviated with EPS-PS and EPS-PN. Both, the EPS extractions and the measurements of total polysaccharides and proteins were performed in triplicates.

3.3 Morphology of photogranules

To elucidate the morphology of the photogranules, microscopic observations were performed with a fluorescence microscope (Leica Microsystems Ltd, DMI4000 B, Germany) and a stereo zoom microscope (Leica Microsystems Ltd, M205C, Germany). Images were analysed with the software Cell* (Soft Imaging Systems GmbH, Germany) and Leica Application Suite (Leica Microsystems Ltd, LAS version 4.7, Germany).

Next to this, confocal laser scanning microscopy (CLSM) (Leica TCS SP5X, Germany) was used to assess 3-dimensional structure of the granules. The system was equipped with an upright microscope and a white laser was controlled by the LAS-AF 2.4.1 software. For recording image data stacks a 25x NA 0.95 and 63x NA 1.2 water immersion lens was used. Photogranules with sizes between 1-4 mm were collected on day 54, 82 and 105 and either directly observed fresh or fixed in 5% Paraformaldehyde in 10x PBS and stored at 4°C until analysis. Samples were mounted in cover well chambers having the appropriate spacers. The granules were stained inside the chambers, which were then filled up with water and covered with a high-quality coverslip. Surface images were taken from whole granules, whereas cross-section images were obtained from photogranules cut in half. Glycoconjugates were detected by means of fluorescence lectin-binding analysis (FLBA) according to Staudt et al. (2004) and Zippel & Neu (2011). In order to identify a suitable lectin, a photogranule screening with all commercially available lectins was performed (Neu and Kuhlicke, 2017). From the lectins shortlisted, the BAN lectin conjugated with fluorescein or Alexa-568 was selected for staining glycoconjugates. The BAN lectin derived from banana (*Musa paradisiaca*) has a single-carbohydrate binding specificity for D-Mannose and D-Glucose (Singh et al., 2005) **(table S1**). For counterstaining the fluorochrome Syto9 or Syto64 was used to visualize nucleic acids. The autofluorescence of photosynthetic pigments from cyanobacteria and eukaryotic algae were employed to identify the phototrophic organisms. Settings for recording image data stacks sequentially were: Excitation: A) 480 nm and 635 nm (simultaneous) and 565 nm (sequential); Emission: 500-550 nm

(Syto9), 585-650 nm (BAN-A568, phycobilins), 650-720 nm (Chl A) and B) Excitation 490 nm, 570 nm and 635 nm (simultaneously); Emission: 505-560 nm (BAN-fluo), 580-620 nm (phycobilins), 650-720 nm (Chl A). Image datasets were analysed with the imaging software Fiji (Schindelin et al., 2012). Individual image data stacks from tile scans were stitched together using Photoshop (version CS6).

3.4 Biomass yield and nutrient removal on light and COD

All bioreactor system received the same photon flux of 0.34 mol_{ph}/L/d (r_{ph}) and COD loading of 0.299 g/L/d (r_{COD}). The r_{ph} was calculated from averaged light measurements conducted over the entire bioreactor surface (0.528 $mol_{ph}/A_{reactor}$/d) divided over the bioreactor volume (1.6 L). With r_{ph} and r_{COD} the biomass productivity (**equation 1-3**) could be estimated and compared to measured values. The measured biomass yield on light or COD was calculated from the measured biomass productivity and the estimated biomass productivity of phototrophs and heterotrophs (**equation 4-5**). For calculation, a biomass yield on light Y_{Xph} of 0.7 g/mol_{ph} (assuming 25 mol_{ph} for 1 mol_{O2}) (Boelee et al., 2012) and a biomass yield on acetate (COD) Y_{XCOD} of 0.49 g/g was used (Chen et al., 2020). For simplification, the total sum for biomass productivity was accounted of both, phototrophs, and heterotrophs. Similar calculations were used to obtain nutrient removal rates on light (**equation S2-5**).

$$r_{X_{hetero}} = Y_{\frac{X}{COD}} * r_{COD} \qquad \text{equation 1}$$

$$r_{X_{photo}} = Y_{\frac{X}{ph}} * r_{ph} \qquad \text{equation 2}$$

$$r_X = r_{X_{photo}} + r_{X_{hetero}} \qquad \text{equation 3}$$

$$Y_{\frac{X}{ph},measured} = \frac{r_{X_{measured}} - r_{X_{hetero}}}{r_{ph}} \qquad \text{equation 4}$$

$$Y_{\frac{X}{COD},measured} = \frac{r_{X_{measured}} - r_{X_{photo}}}{r_{COD}} \qquad \text{equation 5}$$

3.5 Nitrogen and phosphorus mass balance

For both nitrogen and phosphorus, the same calculations were applied. Here the calculations are given for nitrogen as an example: The nitrogen loading per treatment (Q_N with unit g/L/d) was compared to the nitrogen removed (R_N with unit g/L/d

calculated from the influent and effluent concentration) and assimilated into the biomass ($r_X * x_N$). The biomass assimilated is assessed from the observed biomass productivity ($_X$ in g/L/d) and multiplied by the nitrogen content of the biomass (x_N in g_N/g_X). Thereby, the nitrogen balance was assessed (**equation 6-7**). The equations of the phosphorus balance can be found in the supplemental material (**equation S6-7**).

$$N_{balance,removal} = Q_N - R_N \quad \text{equation 6}$$

$$N_{balance,assimilated} = Q_N - r_X * x_N \quad \text{equation 7}$$

3.6 16S and 18S rRNA gene amplicon sequencing

From each bioreactor, biomass was sampled at 3 time points: the initial inoculum (referred to as day 0), day 54 (middle of experimental run) and the final day 105. DNA extraction from each time point was conducted in triplicate. Specifically, 15 mL of harvested sludge was centrifuged at 5500 rpm and the supernatant discarded. The cell pellets were immediately stored at -80 °C until further processing. DNA was extracted using the DNeasy PowerSoil Pro Isolation Kit (Qiagen GmbH, Hilden, Germany). The quantity and quality of DNA were spectrophotometrically determined with a NanoDrop (ThermoFisher Scientific, USA). The 42 genomic DNA samples were sequenced at Génome Québec (MacGill University, Montreal, CA). The 16S rRNA gene V3/V4 variable region was amplified using primer pair 341F (CCTACGGGNGGCWGCAG) and 805R (GACTACHVGGGTATCTAATCC) (Herlemann et al., 2011). The 18S rRNA gene V4 variable region was amplified using the primer pair 616*F (TTAAARVGYTCGTAGTYG) and 1132R (CCGTCAATTHCTTYAART) (Hugerth et al., 2014). Both sets of primers were modified to add Illumina adapter overhang nucleotides sequences to the gene-specific sequences. Sequencing was performed using an Illumina MiSeq system (Illumina MiSeq, USA) with 300-bp reads (v3 chemistry). After adapter trimming using *cutadapt* version 1.18 (Martin, 2013), the R package *DADA2* (Callahan et al., 2016) was used to quality filter, merge paired end reads, generate amplicon sequencing variants (ASVs) and do taxonomic alignment of the sequences to the SILVA database (release 138) (https://www.arb-silva.de). The 16S and 18S data set was normalized using the cumulative sums scaling (CSS) function of the R package *metagenomSeq* version 1.24.1 (Paulson et al., 2013). The analysis of the microbiome data was performed with the R-package *phyloseq* (version 1.26.1) (McMurdie and Holmes, 2013) and the R-package *ampvis2* (version 2.7.11) (Andersen et al., 2018).

3.7 Annotation of functional predictions

The python script FAPROTAX (Louca et al., 2016) was used to perform functional annotation of the microbial community. The FAPROTAX database was extended by functional groups such as polyphosphate accumulating organisms (PAO) and glycogen accumulating organisms (GAO) found in the MiDAS field guide version 3.7 (Nierychlo et al., 2020). Additionally, N_2-fixing cyanobacteria were added that were not yet included in the FAPROTAX database (Bergman et al., 1997; Berrendero et al., 2016; Brocke et al., 2018; Lyimo and Hamisi, 2009; Severin et al., 2010; Stanier et al., 1979; Stewart and Lex, 1970). Only the taxa found from the prokaryotic community (16S rRNA sequences) were used to predict functions.

4 RESULTS

The aim of this study was to investigate the N, P and COD removal capacity of photogranules under nitrogen replete and nitrogen limited conditions. For this purpose, a combination of morphological (microscopic, particle size distribution, EPS composition) and microbiological (16S and 18S rRNA gene amplicon sequencing with functional annotation) parameters were analysed in order to record the dynamics and changes of the system. Two different influent concentrations for nitrogen were chosen: 100 mg_N/L (N+) and 15 mg_N/L (N-), which resulted in a daily volumetric loading rate of 149 mg_N/L/day (N+) and 22.4 mg_N/L/day. From our previous study the average volumetric nitrogen removal rate under non-limiting conditions was 54 mg_N/L/day (Trebuch et al., 2020). Hence, the conditions chosen for this experiment resulted in volumetric loading rates which were 3x higher for the N+ treatment and 2.5x lower for the N- treatment compared to the average observed volumetric nitrogen removal rate from the previous study.

4.1 Biomass productivity and composition of photogranules under nitrogen replete and limiting conditions

Under both nitrogen treatments similar average biomass productivities of 0.36±0.05 g/L/d (N+) and 0.40±0.06 g/L/d (N-) were observed (**figure 1A**). Light and organic carbon were the primary energy input for the system, and we assessed how much the phototrophic and heterotrophic metabolism contributed to the overall biomass productivity. During the experiment, all COD as acetate was consumed and all bioreactors received the same amount of light. The theoretical biomass productivity was calculated as 0.38 g/L/d (0.15 g/L/d by heterotrophic and 0.23 g/L/d by phototrophic metabolism) (**equation 1-3**). This value lies in between the average biomass productivities of N+ and N-.

When calculating with a fixed yield on acetate the remaining biomass fraction can be attributed to phototrophy. This resulted in a phototrophic contribution to biomass productivity of 59% (N+) and 63% (N-) and biomass yields on light of 0.64 g/mol_{ph} (N+) and 0.76 g/mol_{ph} (N-). When calculating with a fixed phototrophic biomass productivity of 0.23 g/L/d, the yield on acetate changes to 0.45 g/g (N+) and 0.57 g/g (N-). With this variable contribution of heterotrophy to biomass productivity, the phototrophic contribution changes to 63% (N+) and 57% (N-). In both scenarios with either fixed heterotrophic or phototrophic yield, the photoautotrophic metabolism accounted for more than half of the biomass productivity (nutrient assimilation) and thereby contributed significantly to the energy budget.

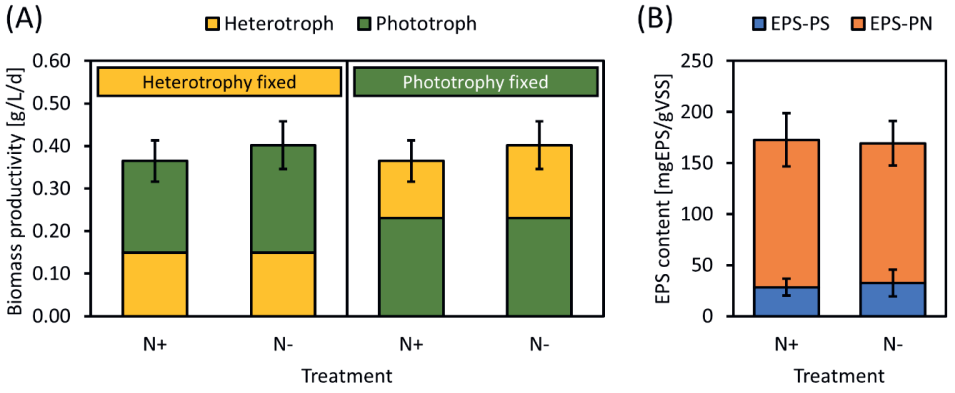

Figure 1: Average biomass productivity and EPS content of photogranules under N+ and N- treatment from day 54 to day 104. **(A)** The biomass productivity is subdivided into the theoretical calculation of biomass yield on COD (heterotroph) and light (phototroph). The left panel shows biomass productivity with a fixed theoretical yield on COD and thereby heterotrophy. The right panel shows biomass productivity with a fixed theoretical yield on light and thereby phototrophy. **(B)** EPS is given as fraction of proteinaceous EPS compounds (EPS-PN) and polysaccharides (EPS-PS).

Interestingly, the average EPS and the fraction of proteins (EPS-PN) and polysaccharides (EPS-PS) of photogranule biomass under both treatments were not different either (**figure 1B**). The average EPS composition under the N+ treatment was 144±26 $mg_{EPS\text{-}PN}/g_{VSS}$ and 28±8 $mg_{EPS\text{-}PS}/g_{VSS}$ and under N- treatment was 137±22 $mg_{EPS\text{-}PN}/g_{VSS}$ and 33±13 $mg_{EPS\text{-}PS}/g_{VSS}$. In both treatments EPS made up 17% of the total biomass. The average CNP composition of the photogranule biomass from day 54 to 105 was similar between treatments (**table 1**).

Table 1: Elemental composition of photogranule biomass under nitrogen replete (N+) and nitrogen limiting (N-) conditions. The average and standard deviation of the phosphorus, nitrogen, and carbon content of 105 days of reactor operation are given for each treatment (n=27).

	P [%w/w]		N [%w/w]		C [%w/w]	
	Avg.	Std.	Avg.	Std.	Avg.	Std.
N+	1.36	*0.09*	9.71	*0.31*	43.90	*0.56*
N-	1.22	*0.03*	9.80	*0.27*	45.05	*0.35*

4.2 Treatment performance of photogranules under nitrogen replete and limiting conditions

Under nitrogen replete conditions the photogranular bioreactors showed average volumetric removal rates of 52.4±3.5 mg_N/L/day and 5.0±0.7 mg_P/L/day, as measured over the last 50 days of operation (**figure 2A,B**). When comparing the nitrogen removed by the system compared to the nitrogen assimilated into the biomass a mismatch of 27-28% was observed. This was attributed to nitrification/denitrification occurring in the photogranule. All three bioreactors of the N+ treatment showed full nitrification after 40 days of operation and had stable nitrification rates throughout the rest of the experiment (**figure S3 and S5**). When looking at one 12 h cycle, 6 h light followed by 6 h dark, a difference in nitrogen removal rates and nitrification rates was observed (**figure 2C**). In the first 6 hours (light phase) an average ammonium removal rate of 7.1±0.5 mg_N/L/h and a nitrification rate of 4.2±1.0 mg_N/L/h was obtained. In the subsequent 6 hours of darkness the average ammonium removal rate decreased to 5.8±0.4 mg_N/L/h while a similar nitrification rate of 4.3±0.4 mg_N/L/h to the one in the light phase was obtained.

In the N- treatment full ammonium removal was observed already 4 hours into the 12-hour cycle (**figure 2D**). Nitrite and nitrate were absent in the effluent of the bioreactor and when additionally monitored during the 12h cycle. This suggests that ammonium was readily used and assimilated by the microbial community, although cryptic nitrification and denitrification cannot be excluded completely. This limited photogranules of nitrogen for about 2/3 of the time. Surprisingly, under nitrogen limiting conditions (full nitrogen removal) similar nitrogen assimilation rates (44.9±6.6 mgN/L/day) and phosphorus removal rates (4.7±0.7 mgP/L/day) were obtained when compared to nitrogen replete conditions.

When looking at the nitrogen mass balance it was observed that the nitrogen assimilated into biomass was 2x higher compared to the nitrogen removed. This suggests that about twice as much nitrogen ended up in biomass than supplied via the

influent. The explanation for this mismatch can be found in part of the microbial community (cyanobacteria and non-phototrophic bacteria) that can perform N_2-fixation under nitrogen limitation. This process would supply nitrogen as ammonium from nitrogen gas (N_2) available in access via the incoming gas (pressurized air enriched with 5%v/v CO_2) used for aeration. In that manner the N- photogranules could sustain growth especially when ammonium was depleted.

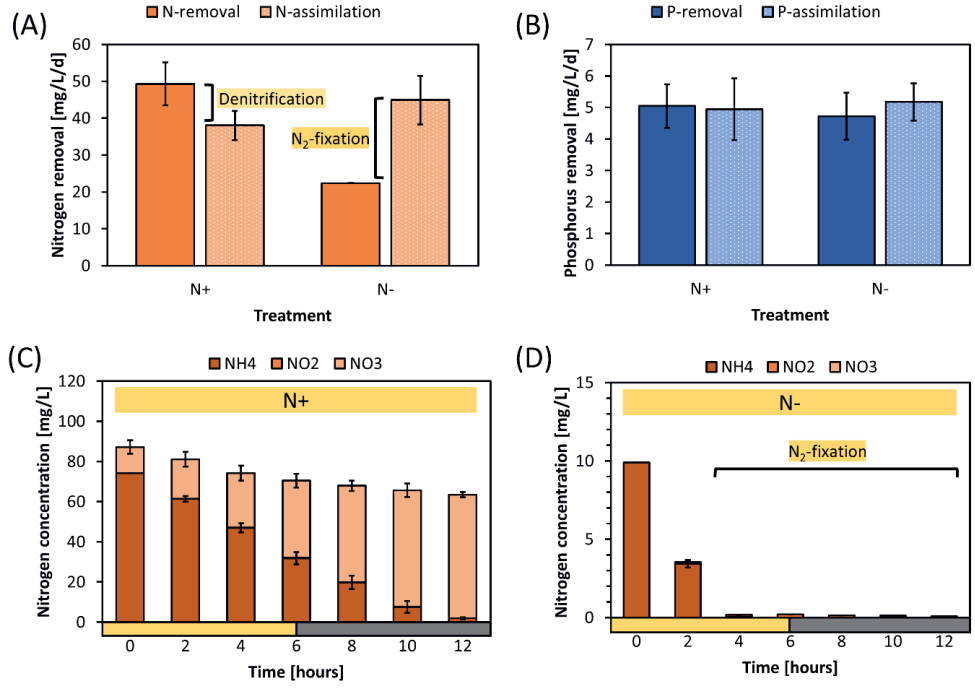

Figure 2: Reactor performance for nitrogen and phosphorus of the two nitrogen treatments (N+/N-). **(A)** Nitrogen removal and assimilation rates of both treatments. **(B)** Phosphorus removal and assimilation rates of both treatments. The results in panel A and B are averaged over triplicate bioreactor operation and steady-state operation from day 54 to 105. Bottom graphs show nitrogen development in a 12-hour cycle with 6 hours of light (yellow bar) and 6 hours of darkness (grey bar) of the N+ treatment **(C)** and N- treatment **(D)**. The values for ammonium (NH_4-N), nitrite (NO_2-N) and nitrate (NO_3-N) are averages of 5 cycles (days 54, 75, 82, 91 and 105). After 4 hours into the cycle under the N- treatment no ammonium, nitrite or nitrate is present, and N_2-fixation is likely to occur.

4.3 Morphological changes under nitrogen limitation

Although the performance of the different nitrogen treatments was similar, there was a clear difference in granule morphology. While N+ photogranules were dense and structurally confined (**figure 3A**) the N- photogranules showed rather loose structures with occasional voids within the granule (**figure 3B**). In both granular morphotypes, motile filamentous cyanobacteria were an essential structural feature that form a network where other organisms could embed themselves.

The N+ photogranules showed a prominent and dense shell of 400-500 µm thickness highly abundant in non-phototrophic organisms (green) next to phototrophs (blue, pink) (**figure 3C**). The non-phototrophic organisms in the shell comprise of nitrifiers and heterotrophic bacteria (e.g., denitrifier). Between the shell and the centre, a zone emerged that showed filamentous cyanobacteria radially aligning from surface to centre. The centre itself exhibited dense structures of jumbled filaments with non-phototrophic organisms in between. The surface of the N+ photogranules consisted mainly of cyanobacteria (pink) and eukaryotic algae (blue), but were also coated with colonies of non-phototrophic organisms (green) (**figure 3E,F**). These non-phototrophic organisms were also visible as white spots on the surface or in the interior of the N+ photogranule in macroscopic images (**figure 3A)**.

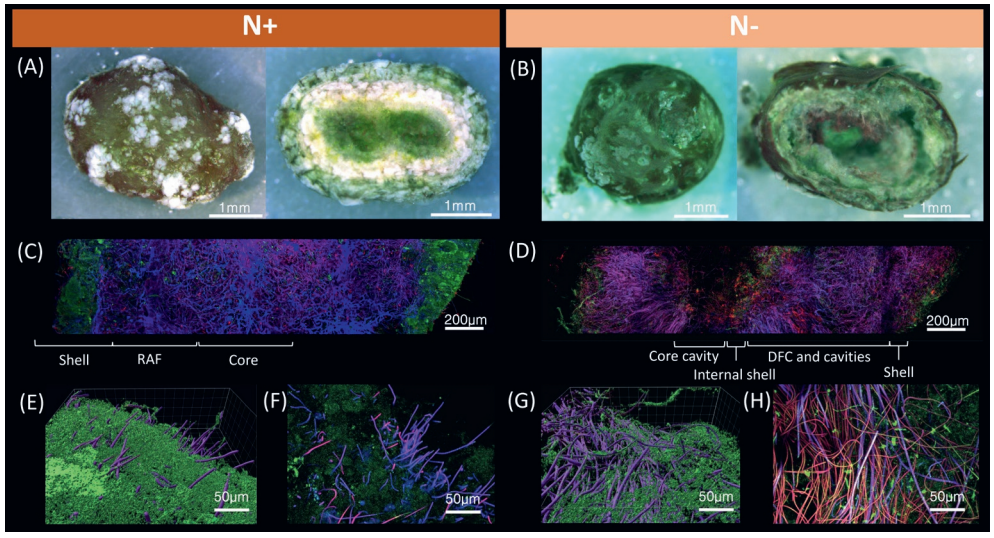

Figure 3: Macroscopic (A, B) and microscopic images (C-H) of photogranules cultivated under high nitrogen (N+) and limited nitrogen (N-). At the top, whole granule (left) and cross section of the same (right) under N+ **(A)** and N- **(B)** visualized by stereo microscopy. In the RBG false coloured images from CLSM four different components can be distinguished: filamentous cyanobacteria (purple), eukaryotic microalgae (blue), phototrophic and non-phototrophic bacteria (green), and glycoconjugates (red). In the middle CLSM image of photogranule cross section with different zones indicated under N+ **(C)** and N- **(D)**. Shell = dense bacterial shell close to the surface of the photogranule. RAF = radially aligned filamentous cyanobacteria. Centre = the centre of the photogranule, DFC = dense filamentous clutters, Centre cavity = hollow space in close to the centre of the photogranule. At the bottom CLSM images of the surface of photogranules represented in three dimensions (left, **E**) and the same CLSM image from the surface as maximum intensity projection from a top view (right, **F**) under N+. The equivalent images are shown for N- three dimensional (left, **G**) and as maximum intensity projection from a top view (right, **H**).

The N- photogranules had phototrophs, mainly cyanobacteria, throughout most of its structure and frequently developed voids within (**figure 3B**). The voids are visible as dark and less intense areas in the CLSM image in **figure 3D** and are possible indications for channels that connect surface and centre. The N- photogranules showed only a thin

and poorly developed non-phototrophic shell and the surface was mostly defined by cyanobacteria (**figure 3D,G,H**). In the voids found in the centre area non-phototrophic organisms formed a thin layer, which was termed the internal shell. Although, the general structure appeared to be less confined compared to the N+ photogranules, the N- photogranules still formed spheroid aggregates with excellent settling properties (SVI < 60 mL/g).

4.4 Microbial community composition under two nitrogen treatments

The microbial community of photogranules under both nitrogen treatments was comprised of several motile filamentous non-heterocyst-forming cyanobacteria, eukaryotic algae, nitrifying and denitrifying bacteria, one type of fungi and a low abundance of predatory organisms. Since the samples taken on day 54 and 105 showed good replication for each treatment, we present the microbial community as an average of the replicate bioreactors and the two sampling points. In **figure 4A** the prokaryotic community under N+ and N- treatment is depicted. The dominant cyanobacteria in the N+ treatment was *Alkalinema pantanalense* CENA 528 (16 %), while in the N- treatment *Cephalothrix komarekiana* SAG 75.79 (16%) had the highest abundance. In both treatments the cyanobacteria *Leptolyngbya boryana* PCC-6306 was present at abundances of 16% (N+) and 10% (N-) and *Limnothrix* sp. with abundances of 1.4 % (N+) and 1.0% (N-). The most prominent chemoheterotroph and denitrifier in the N+ treatment was *Zoogloea* sp. (10 %) compared to *Thauera* sp. (19 %) in the N- treatment. The nitrifiers *Nitrosomonas* sp., *Nitrobacter* sp. and *Nitrospira* sp. that made up 2% of the prokaryotic community under nitrogen repleted conditions, were only present below 0.04% under nitrogen limitation. This is in accordance with the absent nitrification activities observed in the N- treatment.

The eukaryotic community mainly consisted of eukaryotic algae with 45% under N+ and 54% under N- (**figure 4B**). Under nitrogen replete conditions *Chlorella* sp. was dominant with 37%, followed by *Chlorococcum* sp. 4% and *Botryosphaerella* sp. with 3%. Under nitrogen limitation *Chlorella* sp. decreased in abundance to 27%, *Chlorococcum* sp. significantly increased to 26% and *Botryosphaerella* sp. decreased to 1%. Next to eukaryotic algae, the fungi *Trichosporon* sp. with 36% was found under N+ conditions but was absent under N- conditions. Nitrogen limitation led to an increase from 3% to 21% in predatory eukaryotes such as rotifers, ciliates, and amoeba. The main representatives were *Colpodidium* sp., *Gymnophrys* sp. and *Vermamoeba* sp.

Generally, nitrogen limitation resulted in a slightly less diverse microbial community according to the alpha diversity index of Shannon and Simpson (**figure 4C**). Nitrogen

limitation added another selection criterion for the microbial community upon which it must adapt to. The core microbial community of both N+ and N- photogranules consisted of about 70 organisms of which around 66% were shared (**figure 4D**). This shared core community consisting of cyanobacteria such as *Cephalothrix komarekiana* SAG 75.79, *Alkalinema pantanalense* CENA 528, *Leptolyngbya boryana* PCC-6306 and *Limnothrix* sp., nitrifiers *Nitrosomonas* sp., *Nitrobacter* sp. and *Nitrospira* sp., and heterotrophic bacteria/denitrifiers *Thauera* sp. as well as *Zoogloea* sp.. All these taxa together made up 85% of the total abundance of all organisms in both treatments and are thereby responsible for the main functional contribution to the system.

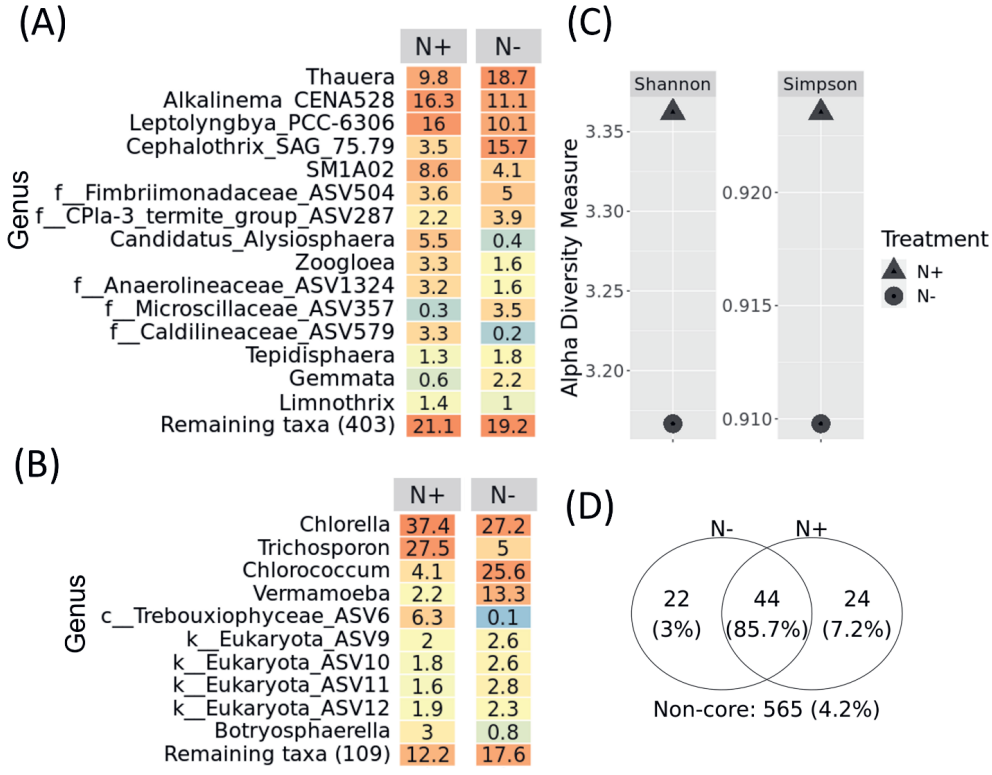

Figure 4: Microbial community analysis of N+ and N- treatment. The 16S and 18S rRNA gene amplicon sequencing data was averaged over the triplicate bioreactors and sampling day 54 and 105 when bioreactors were in steady state. **(A)** top 15 ASVs of the 16S rRNA dataset at genus level. **(B)** top 15 ASVs of the 18S rRNA dataset at genus level. **(C)** Alpha diversity according to Shannon and Simpson. **(D)** Venn diagram of shared ASVs from both treatments. More information on the microbial community can be found in the supplemental materials (**figure S6-S7**).

4.5 Functional abundance found under different nitrogen treatments

To gain insight into functional abundances in both treatments, FAPROTAX was used to annotate metabolic functions to the prokaryotic community (**table 2**). With this approach about 40% of all taxa could be attributed to a certain function. Most of the annotated functions are related to the core community that represents 85% of total prokaryotes, which are cyanobacteria, nitrifiers and denitrifiers. This approach highlighted the functional potential of the two microbial communities but does not necessarily show the actual functions carried out.

Table 2: Functional distribution between N+ and N- treatment are represented as relative abundance (%). The functional data was obtained by FAPROTAX, which was extended using the MiDAS field guide version 3.7. If a functional group had too many representatives only the most abundant taxa are specified. Multiple functions can be assigned to one organism and therefore the grand total of all functions per treatment can exceed 100%. In addition, there are taxa that are not assigned to any function and are summed up in the category "other".

Function	N+	N-	#Genera (Taxa)	Representatives (selected)
photoautotrophy	47%	50%	5 (62)	*Cephalothrix* SAG 75.79; *Alkalinema* CENA528; *Leptolyngbya* PCC-6306; *Limnothrix* sp.;
photoheterotrophy	0%	1%	1 (1)	*Candidatus* Obscuribacter
phototrophy	47%	50%	6 (63)	--
chemoheterotrophy	22%	31%	50 (115)	*Zoogloea* sp.; *Thauera* sp.
PAOs	1%	1%	1 (1)	*Candidatus* Obscuribacter
nitrification	2%	0%	3 (3)	*Nitrosomonas* sp.; *Nitrospira* sp.; *Nitrobacter* sp.
denitrification	16%	27%	2 (5)	*Zoogloea* sp.; *Thauera* sp.
nitrogen fixation	29%	38%	9 (9)	*Leptolyngbya* PCC-6306, *Cephalothrix* SAG 75.79; *Bradyrhizobium* sp.; *Azospira* sp.; *Methylocystis* sp.
fermentation	0%	1%	6 (13)	*Cellulosimicrobium* sp.; *Desulfobulbus* sp.; *Romboutsia* sp.; *Opitutus* sp.; *Verrucomicrobium* sp.
other	27%	16%	102 (482)	--

About half of the functional abundance was attributed to phototrophy with 47% under N+ and 50% under N- conditions. This included five genera performing photoautotrophy and one taxon performing photoheterotrophy all of which were cyanobacteria described in **table 2**. Next to photoautotrophy, chemoheterotrophy was the second most prominent energy metabolism. Under nitrogen limitation chemoheterotrophy was enriched from 22% to 31% due to the enrichment of *Thauera* sp. in the prokaryotic community.

N_2-fixation showed a significant increase from 29% to 38% under nitrogen limitation. That is especially attributed to the enrichment of *Leptolyngbya boryana* PCC-6306 and *Cephalothrix komarekiana* SAG 75.79. Both are non-heterocyst forming cyanobacteria that can perform N_2-fixation under nitrogen limitation, even during the light period by shielding the nitrogen sensitive nitrogenase from their photosynthetic activity either in space or time (Flores et al., 2015; Rippka and Waterbury, 1977). In addition, there were *Bradyrhizobium* sp., *Azospira* sp. and *Methylocystis* sp. also known to perform N_2-fixation. However, these bacteria were generally in low abundance (<1%) and are not expected to contribute significantly. The finding of nitrogen fixing organisms supports the observation that under nitrogen limitation, N_2-fixation can maintain photogranule treatment performance with respect to biomass productivity as well as phosphorus and COD removal.

Nitrification decreased from 2% to 0.04% under nitrogen limitation and had an insignificant contribution to nitrogen removal. Surprisingly, denitrification increased from 16% to 27%, which is related to the increase in *Thauera* sp. under nitrogen limitation. However, all common denitrifier are ordinary heterotrophs and under N- conditions *Thauera* sp. is not expected to perform denitrification.

5 DISCUSSION

5.1 Different nitrogen removal mechanisms under N+ and N- conditions

The two nitrogen treatments significantly affected the nitrogen removal mechanisms in N+ and N- photogranules. Due to the high concentration of ammonium under N+ conditions the diffusion into the N+ photogranules was deeper and thereby a higher ammonium uptake and conversion was expected with depth (Picioreanu et al., 1998). De Kreuk et al. (2005) and Baeten et al. (2018) showed that in aerobic granules the penetration depth increases with increased nitrogen concentration. Further, they indicated that granule sizes of 1.25-1.5 mm were optimal for stratifying microbial processes which facilitate simultaneous nitrification in the surface aerobic zone and denitrification in the centre anoxic zone. When looking at the morphology of N+ photogranules a clear stratification from the surface dominated by phototrophs and a defined outer layer of about 500 µm was characteristic. This outer layer was highly abundant in both phototrophs and non-phototrophic organisms (nitrifiers, denitrifiers). In the dense and jumbled centre cyanobacteria and denitrifiers can be identified (**figure 3**). The ammonium penetrating the photogranule is available for uptake by phototrophs (about 50-60%) and heterotrophs (about 30%) or for conversion by nitrifiers and subsequent denitrifiers (about 27%).

The nitrifying community consisting of *Nitrosomonas* sp., *Nitrobacter* sp. and *Nitrospira* sp. established themselves well within the microbial community of the photogranules and reached stable nitrification rates after day 40 (**figure S3 and S5**). Due to nitrogen replete condition and excess of O_2 and CO_2, the nitrifiers fully convert ammonium to nitrate with an average rate of 4.2±1.0 mg_N/L/h. This rate is lower than maximum rates of 12-14 mg_N/L/h obtained in aerobic granules (de Kreuk et al., 2007), but comparable to algal-bacterial consortia with 3.7-7.7 mg_N/L/h (Karya et al., 2013). A fraction of about 27%, of the produced nitrate was further denitrified and converted to N_2 by *Thauera* sp. and *Zoogloea* sp. (**figure 2A**). This fraction is lower compared to activated sludge or aerobic granular sludge systems where 60-80% of nitrogen is denitrified (Chen et al., 2020).

Under N- conditions the nitrogen concentration was low and the penetration depth into the photogranule was limited. Therefore, the nitrogen uptake changed from diffusion to surface dependent uptake as only the organisms in the top layer of the photogranule would be supplied with sufficient nitrogen (M Pronk et al., 2015). Although ammonium was fully depleted after 4 hours the N- photogranules still sustained phosphorus and COD removal as under N+ conditions. Assuming the remaining 8 hours were fully nitrogen depleted, biological N_2-fixation would need to supply 2.5-3.0 mg_N/L/h of nitrogen to sustain the productivity observed. This required an N_2-fixation rate about 4x lower than the rates achieved by cyanobacteria under optimal conditions, and seems a realistic rate to supply photogranules with nitrogen (Bothe et al., 2010). Further details on the calculation can be found in the supplemental material (**equation S8**).

5.2 Closer look at the N_2-fixing microbial community

The functional annotation revealed that in both nitrogen treatments a significant fraction of the microbial community, both cyanobacteria and other diazotrophs, could perform N_2-fixation (**table 2**). Especially, cyanobacteria show a widespread presence of the nitrogenase-encoding genes since this enzyme originated very early in evolution similar to cyanobacteria (Fani et al., 2000). This accounts also for non-heterocyst-forming motile filamentous cyanobacteria (Subsection III) crucial for photogranule formation (Milferstedt et al., 2017b). *Leptolyngbya boryana* (formally known as *Plectonema boryanum)* or *Cephalothrix komarekiana* SAG 75.79 (formerly known as *Phormidium tergestinum* or *Oscillatoria tenuis*) are both capable of N_2-fixation (Stanier et al., 1979; Stewart and Lex, 1970). Generally, non-heterocyst-forming cyanobacteria prefer anoxic or micro-oxic conditions for N_2-fixation, but they also have been shown to fix nitrogen under aerobic conditions by shielding the oxygen sensitive nitrogenase from their

photosynthetic activity (internal O_2 production) either temporally or spatially (Flores et al., 2015; Klipp et al., 2005).

The bioreactor used in this study were mixed with compressed air enriched with 5%v/v CO_2 during light and dark periods. This assured constant O_2 and CO_2, but also N_2 supply to the photogranules. Due to the constant supply with O_2 the bulk liquid in the bioreactors were not anoxic during dark periods (**figure S8**). Therefore, N_2-fixation must have occurred especially in the depths of the photogranules or in the dark periods where photosynthesis is absent and nitrogenase was protected from internally produced and externally introduced oxygen. In some non-heterocyst-forming N_2-fixing cyanobacterial mats spatial separation of oxygenic photosynthesis in the top layer of the mat and N_2-fixation further into the mat during light periods was observed (Paerl et al., 1995, 1991). The cyanobacterial mat continued to fix N_2 during the night including in the upper layers and in the presence of oxygen, but absence of photosynthetic activity. This affirms that N_2-fixation is possible both during light and dark periods even under aerobic conditions.

5.3 Morphological change under nitrogen limitation

Under N- conditions the photogranules were physically stable but changed their morphology significantly in relation to N+ conditions (**figure 3**). The low nitrogen concentrations resulted in more irregularly shaped photogranules with hollow structures such as channels and voids within. Similar observation were made by Yin et al. (2019) in aerobic granules under nitrogen deficiency where nitrogen uptake switched from diffusion to surface dependent uptake and resulted in irregular morphologies.

A common strategy of microorganism to compete for and assure contact with nutrients is to maximize the surface area. Irregular structures on the surface of the granule or voids and channels can help microorganism to maximize their surface area compared to volume (Gonzalez-Gil and Holliger, 2014). This is a common phenomenon also observed in phototrophic biofilms such as cyanobacterial mats that create (filamentous) outgrowth and channel systems to assure substrate supply (Grewe and Pulz, 2012).

For N_2-fixation, the same arguments can be used. Most likely the hollow structures in the interior of the photogranule facilitated the transport of N_2 to and NH_4^- away from the nitrogen fixing community (Berrendero et al., 2016). When looking at cyanobacterial mats in aquatic ecosystems these strategies can be found as well (Severin et al., 2010). Especially, during the light periods when N_2-fixation occurred inside the photogranule the transport of substrates from the bulk fluid to the centre must be assured. The hollow structure in the N- photogranules would facilitate this exchange.

5.4 Possible metabolic activities during a 12-hour cycle under nitrogen limitation

During a 12-hour cycle the photogranules experienced a 6-hours light phase and 6-hours dark phase (**figure 2D**). In the beginning of the cycle of the N- treatment, ammonium, phosphate, and acetate were readily available. In the first 4 hours of the light period, ammonium and acetate were present until full consumption. This period was marked by phototrophic (light, ammonium, phosphate, and inorganic carbon consumption) and heterotrophic (ammonium, phosphate, and organic carbon consumption) activity. Next to that, N_2-fixing cyanobacteria and diazotrophic bacteria could assimilate CO_2 (cyanobacteria) and acetate (diazotrophic bacteria) to internally store carbon as glycogen necessary for N_2-fixation (Flores et al., 2015). Some filamentous cyanobacteria that were spatially restricting N_2-fixation to the interior of the photogranule might be active as well (Hagemann et al., 2010). This would allow N_2-fixation when the cyanobacteria are metabolically most active in the light period. N_2-fixation might be already happening from the very beginning of the cycle depending on the availability of ammonium in the centre of the photogranule. Finally, this would be relevant once ammonium was fully depleted during the second half of the light period.

The remaining 6 hours of the batch cycle were not illuminated. During this dark period N_2-fixation can continue in the centre but could also occur in upper layers under aerobic conditions when photosynthetic activity was absent. Part of the phototrophs and heterotrophs were using the internal carbon pool for maintenance. Since ammonium was fully depleted N_2-fixation was the primary metabolism in this phase. Both N_2-fixing cyanobacteria and diazotrophic bacteria degraded and respired the internal glycogen pool to acquire N_2 and form NH_3. The nitrogen could further be stored as a nitrogen reserve material such as cyanophycin (in cyanobacteria) or excreted into the bulk fluid where it would be available of other organisms (H. Li et al., 2001; Vitousek et al., 2002).

5.5 Relevance of N_2-fixation in photogranule wastewater treatment and effect of short-term nitrogen limitation

Generally, it seems unusual to include biological N_2-fixation in the context of wastewater treatment as removal or recovery is the prime objective. However, wastewater treatment systems can experience variable influent conditions and the microbial community can at times suffer from nitrogen limitation particularly in wastewaters with low N:P ratios. This can especially occur as treatment systems are mostly operated close to 100% removal. As been found in this study, N_2-fixation can be very relevant in photogranule wastewater treatment where even long-term nitrogen

limitation did not adversely affect biomass productivity, phosphorus, and COD removal.

The overall microbial community composition of the N+ and N- treatment only differed minimally and 85% of the total abundance of prokaryotic taxa were shared (**figure 4**). The major difference between the two treatments was the relative abundance of specific N_2-fixing cyanobacteria, nitrifiers and denitrifiers. Under nitrogen limitation the microbial community adapted to the conditions by an increase in the N_2-fixing cyanobacteria *Cephalothrix komarekiana* SAG 75.79, a near absence of nitrifiers (<0.05%) and a shift in the heterotrophic (denitrifying) community from *Zoogloea* sp. to *Thauera* sp. was observed. Still the functional analysis revealed a significant N_2-fixing potential in both treatments with 29% (N+) and 38% (N-). This illustrates the native N_2-fixing capabilities of photogranules due to motile filamentous non-heterocyst-forming cyanobacteria (Subsection III), which make up a large fraction of the microbial community. Further, it suggests that the cyanobacteria present in photogranules could switch their metabolism upon nitrogen limitation promptly to N_2-fixation even on a short time-scale as observed in naturally occurring cyanobacterial mats (Severin et al., 2010).

The absence of a lag phase after inoculation affirms that the microbial community quickly adapted to nitrogen limiting conditions even on short timescale within days maybe even hours. The organisms capable of N_2-fixation are native to photogranules and could be readily switch their metabolism upon nitrogen limitation in order to buffer short-term (or long-term) nitrogen limiting events. The knowledge that most of the cyanobacteria relevant for photogranules can perform N_2-fixation if required, can be of high relevance both for ecological and engineering purposes.

6 CONCLUSION

Under both nitrogen treatments phototrophs accounted for 59% (N+) and 63% (N-) of the overall biomass productivity and consequently contributed substantially to nutrient assimilation. N+ photogranules exhibit full nitrification, while denitrification contributed to 27% of the nitrogen removal. Under nitrogen limitation the native microbial community of photogranules adapted and sustained treatment performance in terms of phosphorus and COD removal by means of N_2-fixation. Especially the highly abundant non-heterocyst-forming cyanobacteria *Leptolyngbya boryana* PCC-6306 and *Cephalothrix komarekiana* SAG 75.79 showed to be both relevant for photogranule structure and N_2-fixation. As a result of nitrogen limitation, the N- photogranules exhibited a different morphology and appeared less confined compared to N+ photogranules. N- photogranules increased their specific surface by forming voids and channels possibly to facilitate surface dependent uptake of nitrogen at low concentrations and N_2-fixation. Despite, these morphological changes the N- photogranules still showed excellent settling properties and proved to offer similar treatment capacity as N+ photogranules. Overall, the microbial community composition and functional array only differed slightly between N+ and N-. This suggests that photogranules could switch their metabolism upon nitrogen limitation to sustain biomass productivity and treatment performance even on short timescale.

7 ACKNOWLEDGEMENTS

The authors would like to thank Ute Kuhlicke from UFZ Magdeburg for her excellent support with confocal laser scanning microscopy and Nico Helmsing for his support with bioreactor operation and chemical analysis.

8 SUPPLEMENTAL MATERIAL

8.1 Bioreactor setup

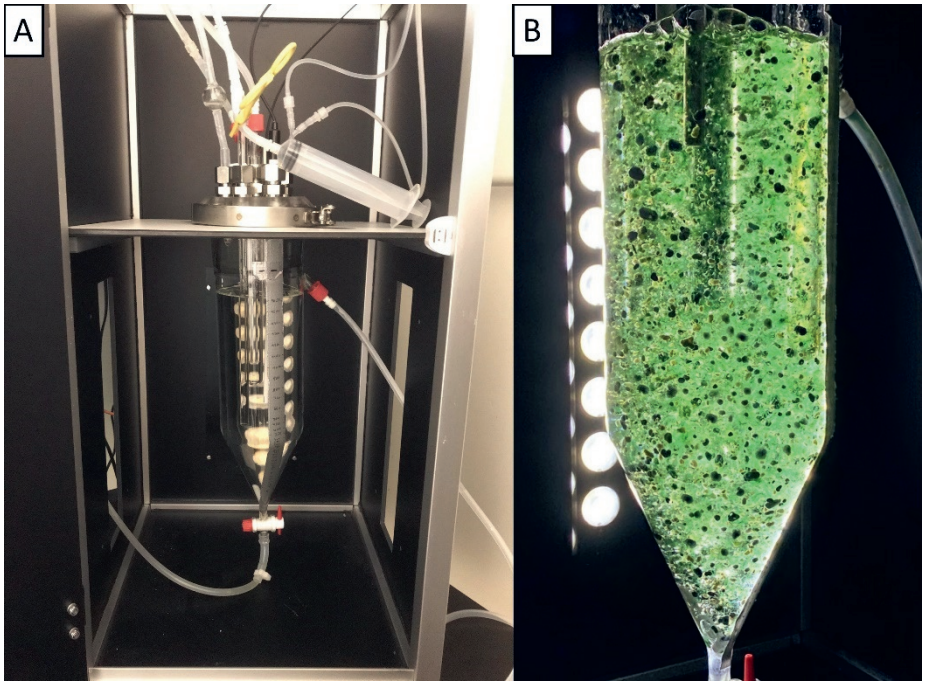

Figure S1: One of the six bubble column bioreactor setup used during the experiment. A) Empty reactor setup with aeration port at the bottom, overflow port at the side and other ports on top. LED light source is at the back of the bioreactor. B) Close up of one N+ bioreactor

8.2 Information on LED light spectrum

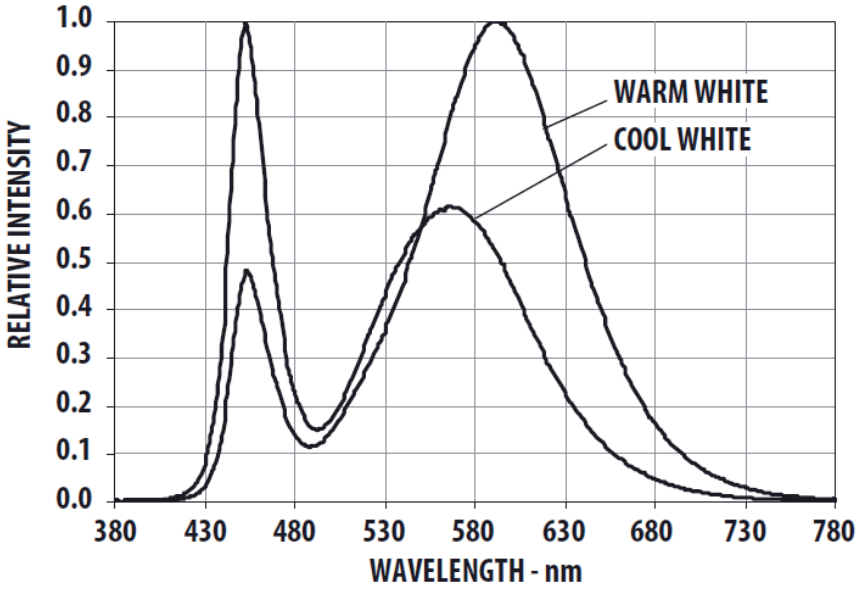

Figure S2: Light spectrum of LED lamps represented as relative intensity vs. wavelength as provided by the manufacturer (Avago Technology, USA). The warm white LED lamps were used for the experiment.

8.3 Lectin used for glycoconjugate visualization

Table S1: Detailed information on the BAN lectin used to stain glycoconjugates

Lectin	Origin	Label	Specificity	Carbohydrate linkage type	Reference
BAN	*Musa paradisiaca*	FITC	D-Mannose and D-Glucose	1–2, 1–3, and 1–6 linked mannosides/glucosides	(Singh et al., 2005)

8.4 Separation efficiency

The separation efficiency (SE) was used to assess how well the biomass separates from the liquid. SE is calculated as the proportion of biomass concentration (mg/L) of the mixed bioreactor content and the effluent (**equation S1**).

$$SE = 1 - \frac{C_{x,effluent}}{C_{x,reactor}} \qquad \text{equation S1}$$

8.5 Nutrient removal rate on light and COD

Similar to the biomass yield on light or COD, the removal rate of nitrogen (N) and phosphorus (P) on light, $Y_{\frac{N}{ph},measured}$ or $Y_{\frac{P}{ph},measured}$, ($g/mol_{ph}$) and COD, $Y_{\frac{N}{COD},measured}$ or $Y_{\frac{P}{COD},measured}$, ($g/g_{COD}$) was calculated (**equation S2-S5**). The removal rate of nitrogen (R_N) and phosphorus (R_P) (g/L/d) was used for that.

$$Y_{\frac{N}{ph},measured} = \frac{R_N}{r_{ph}} \qquad \text{equation S2}$$

$$Y_{\frac{N}{COD},measured} = \frac{R_N}{r_{COD}} \qquad \text{equation S3}$$

$$Y_{\frac{P}{ph},measured} = \frac{R_P}{r_{ph}} \qquad \text{equation S4}$$

$$Y_{\frac{P}{COD},measured} = \frac{R_P}{r_{COD}} \qquad \text{equation S5}$$

8.6 Phosphorus mass balance

The phosphorus mass balance was calculated in a similar way as the nitrogen mass balance (**equation S6-S7**). The phosphorus loading (Q_P with unit mg/L/d) was compared to the phosphorus removed ($R_P$with unit g/L/d calculated from the influent and effluent concentration) and assimilated into the biomass ($r_X * x_P$). The biomass assimilated is assessed from the observed biomass productivity (r_X in g/L/d) and multiplied by the phosphorus content of the biomass (x_P in g_P/g_X).

$$P_{balance,removal} = Q_P - R_P \qquad \text{equation S6}$$

$$P_{balance,assimilated} = Q_P - r_X * x_P \qquad \text{equation S7}$$

8.7 Nitrogen evolution in N+ treatment

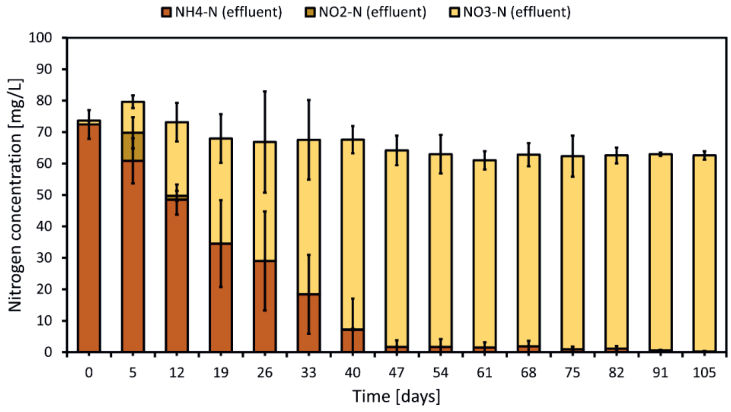

Figure S3: Effluent concentration of ammonium (NH_4-N), nitrite (NO_2-N) and nitrate (NO_3-N) of the N+ treatment averaged of biological replicates (n=3). The error bars represent the standard deviation. The influent concentration of the N+ treatment is 100 mgN/L as ammonium.

8.8 Biomass concentration and productivity

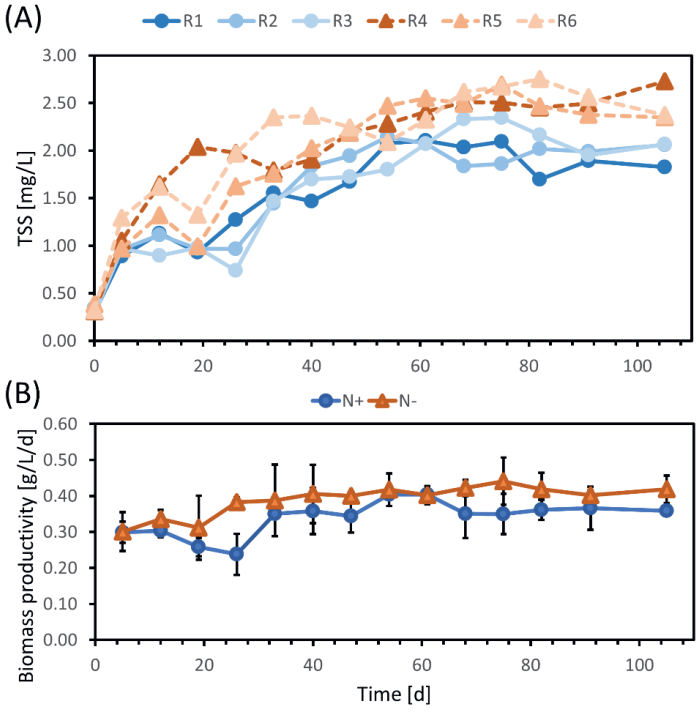

Figure S4: Biomass concentration and biomass productivity of N+ and N- treatment. (A) Biomass concentration of individual replicates of N+ (R1 -R3) and N- (R4-R6) treatment. (B) Averaged biomass productivity of N+ and N- treatment over replicates (n=3). Error bars represent standard deviations.

8.9 Nutrient removal under N+ and N- treatment

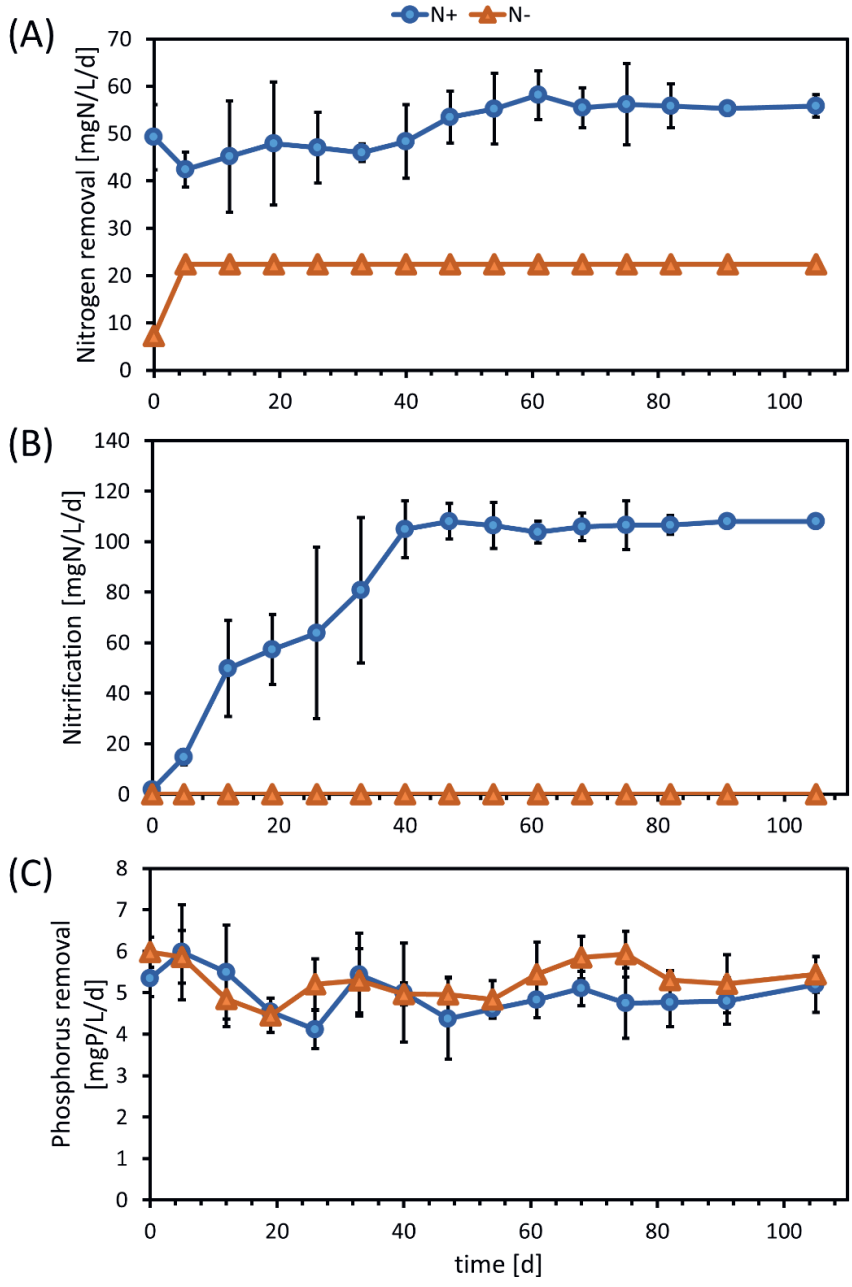

Figure S5: Nitrogen and phosphorus removal of N+ and N- treatment. (A) Averaged nitrogen removal of N+ and N- treatment over replicates (n=3). (B) Averaged nitrification rate of N+ and N- treatment over replicates (n=3). (C) Averaged phosphorus removal of N+ and N- treatment over replicates (n=3).

8.10 Microbial community composition

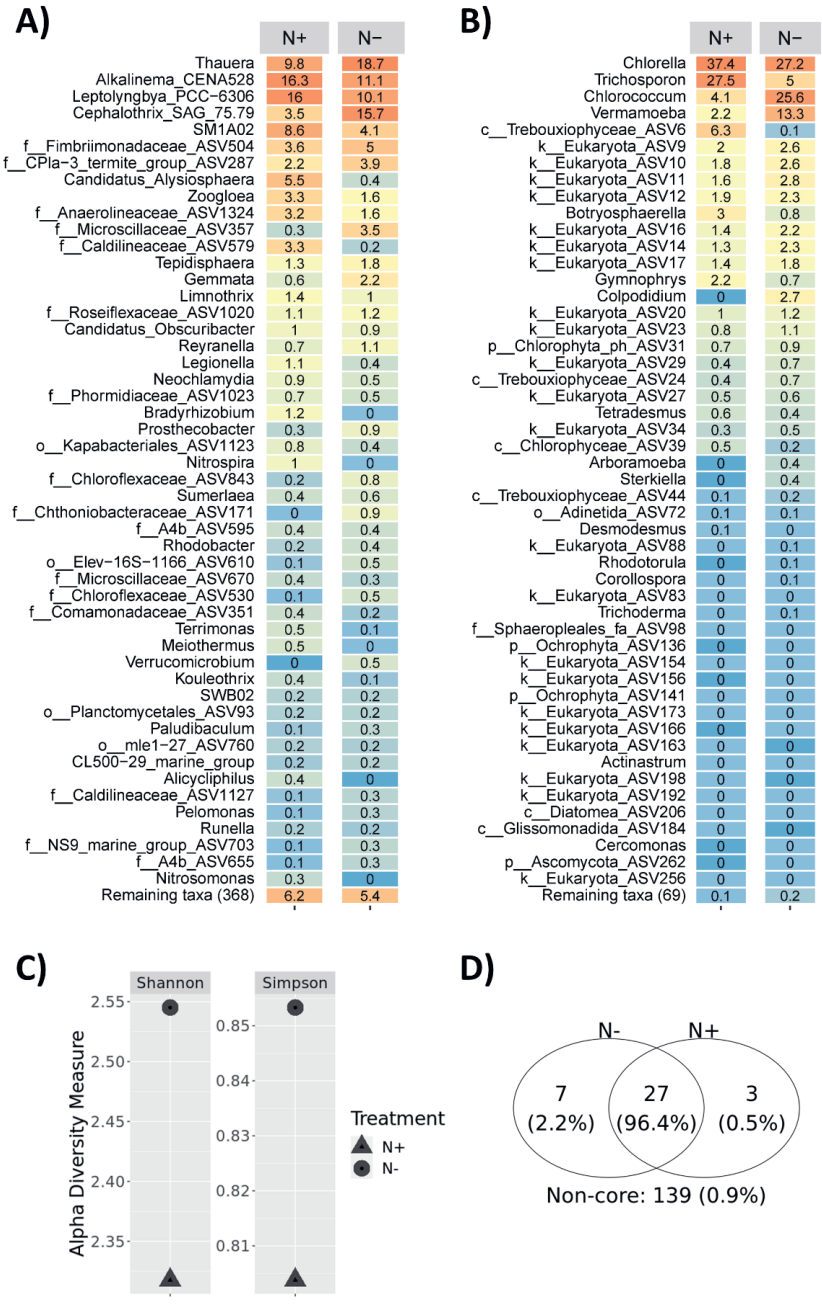

Figure S6: Microbial community composition of photogranules under nitrogen replete (N+) and nitrogen limitation (N-). A) the top 50 ASVs of the 16S dataset. B) the top 50 ASVs of the 18S dataset. C) Alpha diversity according to Shannon and Simpson of the 18S dataset. D) Venn diagram of the core microbiome of the 18S dataset and the overlap between N+ and N- photogranules.

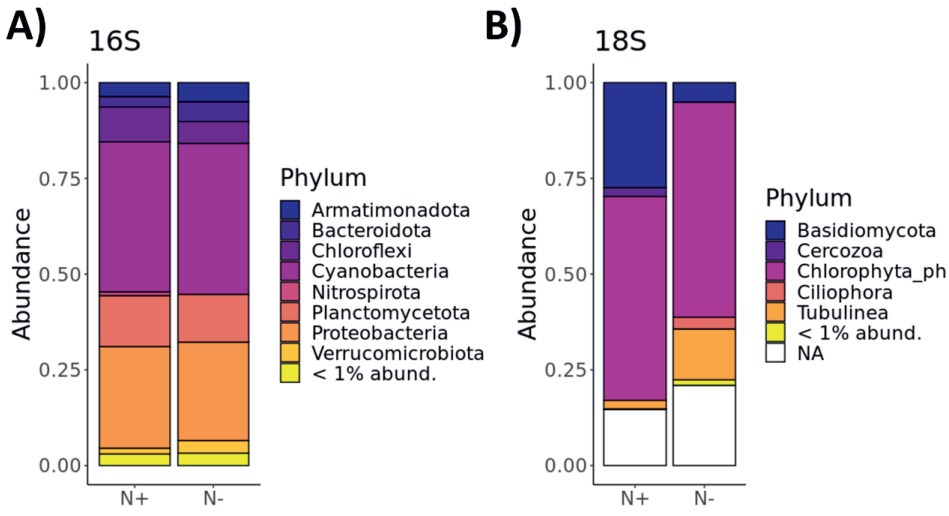

Figure S7: Microbial community composition at phylum level of A) the 16S and B) 18S dataset. All ASVs with abundances lower than 1% are grouped together and displayed as "< 1% abundance" and "NA" are ASVs that are not assigned at phylum level.

8.11 Dissolved oxygen concentration under N- treatment

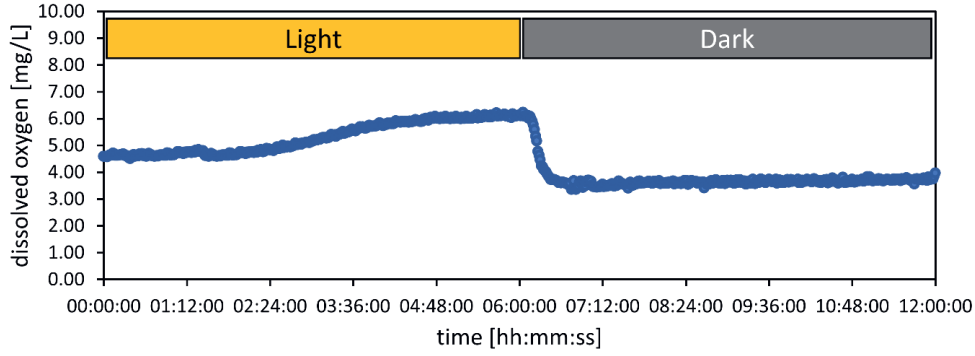

Figure S8: Dissolved oxygen concentration of N- treatment during one 12hour cycle with 6 hours light and 6 hours dark.

8.12 Theoretical N_2-fixation rate vs. N_2-fixation rate observed in nature

Bothe et al. (2010) reported a maximum N_2-fixation rate ($R_{N_2\_fix}$) of 0.3mg_N/h/$mg_{chlorophyll\text{-}a}$ for cyanobacteria under optimal conditions. Assuming an average chlorophyll-a content in photogranules ($Chl\_a_{photogranule}$) of 20±2 mg/g_{VSS} (Trebuch et al., 2020) and a biomass concentration of 2.0 g/L (C_X) in the bioreactor, a maximum volumetric N_2-fixation rate of 11 mg_N/L/h could be achieved. A rate of 2.5-3.0 mg_N/L/is required, which is about 4x lower than reported in (calculated from) natural observations.

$$R_{N_2\_fix} = Chl\_a_{photogranule} \times C_X \qquad \text{equation S8}$$

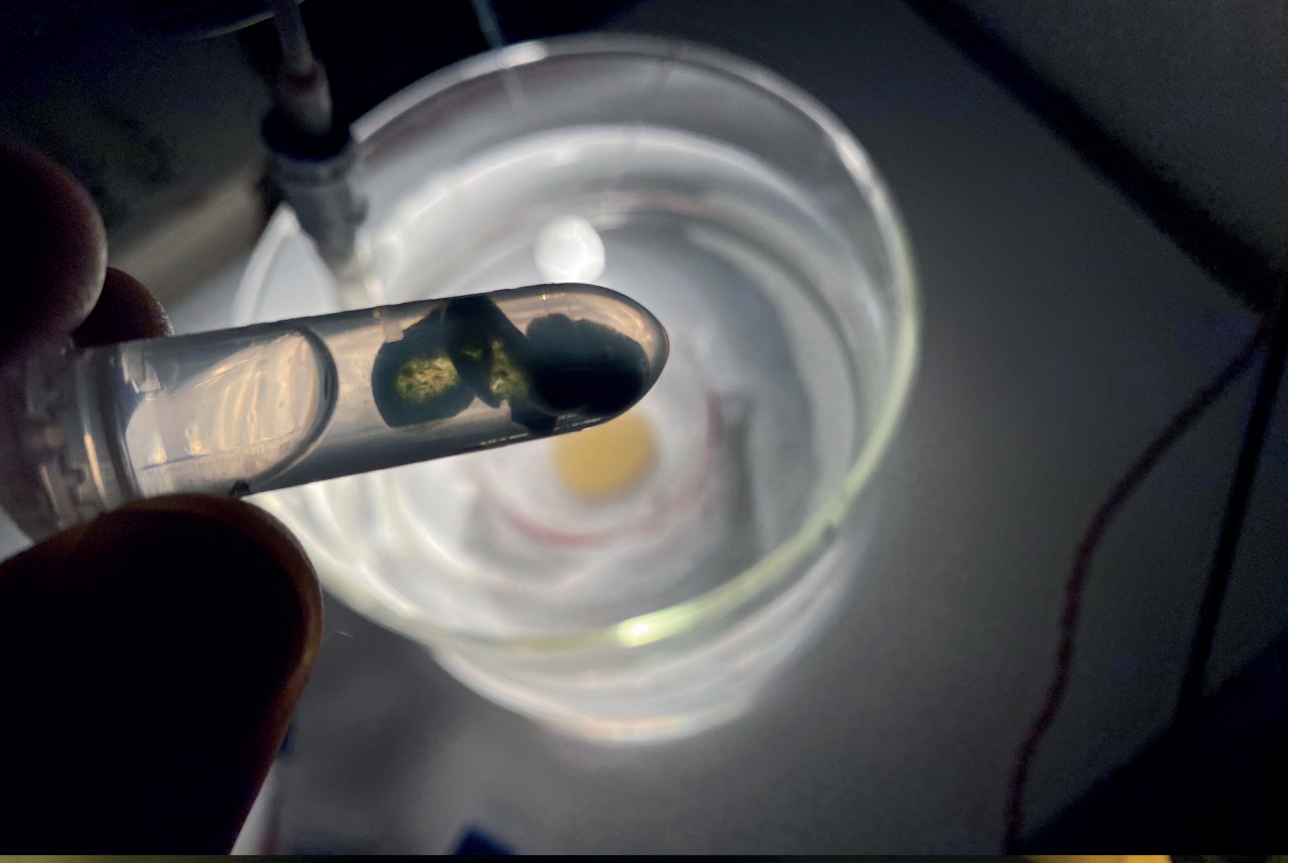

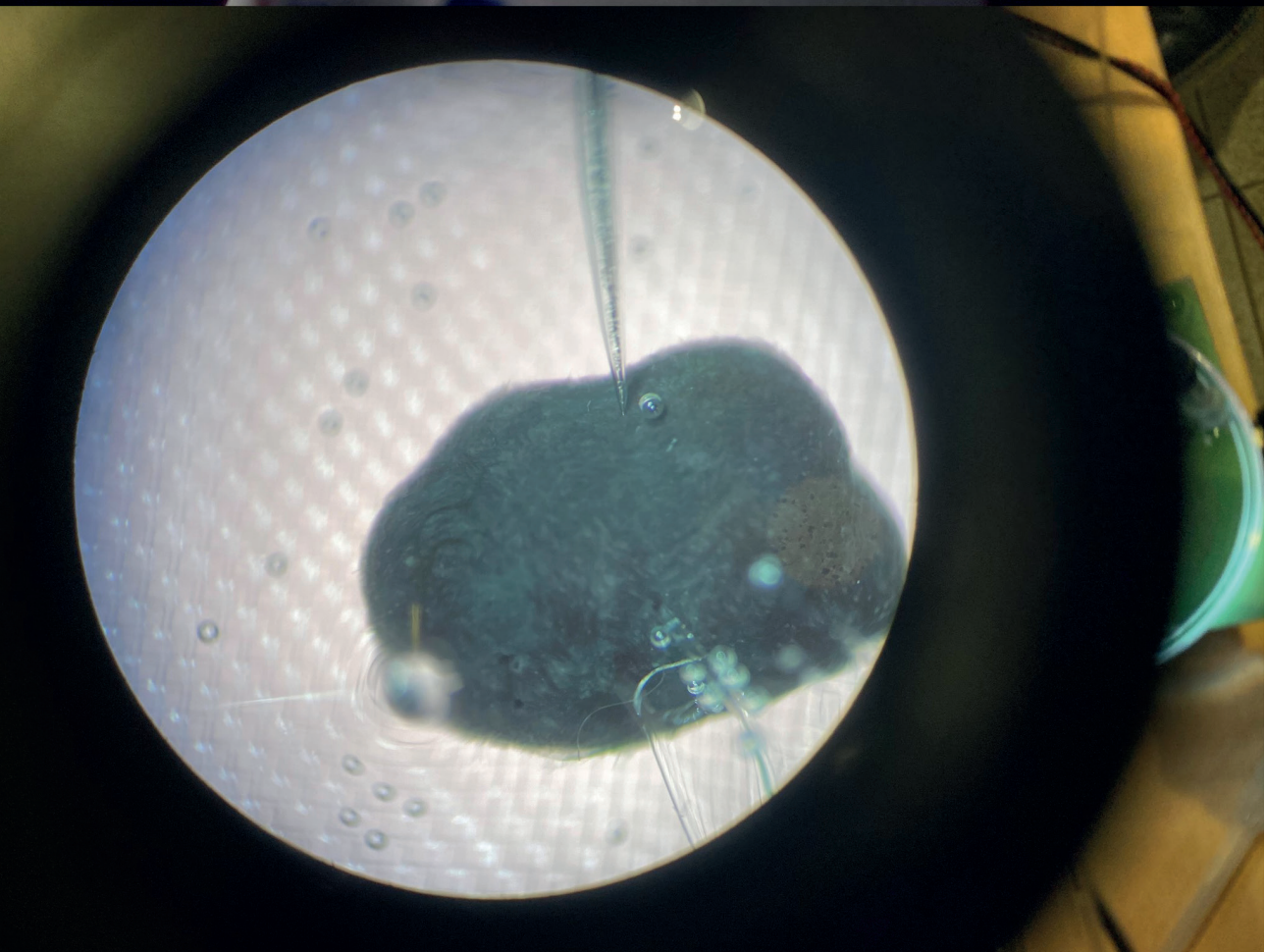

Chapter 4

High resolution functional analyses and community structure of photogranules

Lukas M. Trebuch[1,2,*], Olivia Bourceau[3*], Stijn M.F. Vaessen[1,2], Thomas R. Neu[4], Marcel Janssen[2], Dirk de Beer[3], Louise E.M. Vet[5], René H. Wijffels[2,4], Tânia V. Fernandes[1]

[1] *Department of Aquatic Ecology, Netherlands Institute of Ecology (NIOO-KNAW), Droevendaalsesteeg 10, 6708 PB Wageningen, The Netherlands*

[2] *Bioprocess Engineering, AlgaePARC Wageningen University, P.O. Box 16, 6700 AA Wageningen, The Netherlands*

[3] *Max-Plank-Institute for Marine Microbiology, Microsensor Research group, Celsiusstrasse 1, 28359 Bremen, Germany*

[4] *Microbiology of Interfaces, Department River Ecology, Helmholtz Centre for Environmental Research - UFZ, Brueckstrasse 3A, 39114, Magdeburg, Germany*

[4] *Faculty of Biosciences and Aquaculture, Nord University, N-8049, Bodø, Norway*

[5] *Department of Terrestrial Ecology, Netherlands Institute of Ecology (NIOO-KNAW), Droevendaalsesteeg 10, 6708 PB Wageningen, The Netherlands*

** Contributed equally to this work*

1 ABSTRACT

Photogranules form phototrophic ecosystems with great potential for "aeration-free" wastewater treatment. Their microbial community is a complex mixture of phototrophic and heterotrophic microorganisms that form dark-green spheroid aggregates (up to 5mm in diameter). Photogranules from a sequencing batch reactor were investigated by fluorescence microscopy, metataxonomic analyses and microsensors to determine the light, carbon, and nitrogen budgets. The photogranules were physically robust with rubbery appearance and stratified, with phototrophs present especially in the outer 500 μm and with an anoxic centre. Distributions of light, photosynthesis, respiration, nitrification, and denitrification were determined by microsensors (O_2, NO_3^-, light), and conversion rates by ^{14}C and ^{15}N tracer studies. The microbial community consisted of 47% phototrophs (cyanobacteria, eukaryotic algae), 5% nitrifiers, and 43% heterotrophs. Filamentous cyanobacteria formed a network that provided rigidity to the photogranule and a scaffold in which other organisms were embedded. Light was rapidly attenuated by Chlorophyll-a and an array of other pigments. Photosynthetic activity was restricted to the outer 500 μm and was relatively insensitive to the oxygen and nutrient (ammonium, phosphate, acetate) concentrations tested. Nitrification was observed predominantly in the outer 500 μm, while denitrification potentially extended further into the photogranule centre. Nitrification/denitrification, and photosynthesis/respiration were internally coupled, leading to C-, O- and N-cycling. Our results illustrate the structure of photogranules and the conversion processes occurring within. We demonstrated high conversion rates (light, carbon, nitrogen) as well as good stability of photogranules. Our findings foster a deeper fundamental understanding of photogranule assembly and function and will aid engineering decisions in photogranular wastewater treatment in the future.

Keywords: *Wastewater, microalgae and bacteria, microsensor, stable isotopes, CLSM*

GRAPHICAL ABSTRACT

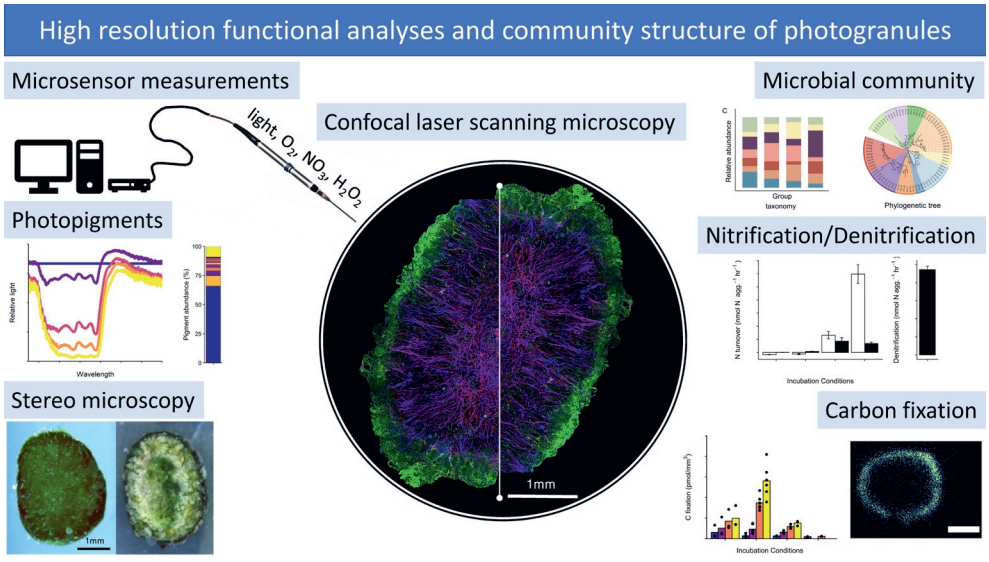

2 INTRODUCTION

Spherical aggregates of microorganisms, called biogranules, are revolutionizing wastewater treatment processes. Manipulating conditions in wastewater treatment reactors allows the creation of an artificial ecosystem that continuously selects for desired functional traits in its microbial community. These functions include conversion processes to purify water and self-aggregation of the microbial biomass. Self-aggregation, i.e., forming biogranules, facilitates functional stratification (aerobic and anaerobic zones) and facilitates biomass harvesting because dense microbial aggregates rapidly settle at the bottom of reactors once mixing is stopped. Generally, biogranules are formed in reactors where the liquid residence time is shorter than the doubling time of the microorganisms, as it generates selective pressure to biomass retention and suspended cells are washed out (Beeftink and van den Heuvel, 1987).

Phototrophic spherical aggregates, called photogranules, were first described by Brehm et al. (2003). They observed spherical aggregation of filamentous cyanobacteria, diatoms and heterotrophic bacteria when culturing phototrophic mats from the North Sea. This discovery was made 20 years after anaerobic granulation in wastewater treatment systems was first observed (Lettinga et al., 1980). Since then, additional examples of phototrophic spherical aggregates in nature have been reported. For example, cryoconites are spherical microbial communities of cyanobacteria and heterotrophic bacteria found in the ice of glaciers (Langford et al., 2010). Other examples include the green and the pink "berries" found in salt marshes. The green berries are formed through a symbiotic relationship of cyanobacteria and diatoms, while the pink berries are microbial communities of sulphur-oxidizing purple sulphur bacteria and sulphur-reducing bacteria (Wilbanks et al., 2017, 2014).

Recently, photogranules were proposed as a promising wastewater treatment process to remove and recover nitrogen, phosphorus and carbon from wastewater (Abouhend et al., 2018; Trebuch et al., 2020; Zhang et al., 2021). They exhibit excellent settling properties, and their *in-situ* photosynthetic oxygen production is particularly advantageous because it can fuel oxygen-demanding microbial processes such as nitrification and respiration. This will allow closure of the O_2, and CO_2 cycle within the treatment process and move towards "aeration-free" wastewater treatment. In recent years, photogranules have been subject to investigations of their microbial community assembly and impact on reactor function (Ansari et al., 2019; Gikonyo et al., 2021; Ji et al., 2021, 2020; Trebuch et al., 2020).

In phototrophic biofilms in nature, as in photogranules, concentration gradients of various dissolved chemical species (e.g., oxygen, substrates) are formed due to

diffusional limitation. Similarly, light intensity gradients are formed by light absorption and scattering (Wolf et al., 2007). These intersecting gradients create a varied environment that can support the simultaneous growth of diverse microorganisms filling different niches, such as photoautotrophs, chemoautotrophs, and heterotrophs, exhibiting aerobic, anoxic, and anaerobic metabolisms (Flemming et al., 2016). Complex interactions between these microbial groups take place, some of which are symbiotic while others are competitive. For example, heterotrophs may grow on extracellular organic compounds excreted by phototrophs. The latter, in turn, may fix the inorganic CO_2 produced in heterotrophic growth. Aerobic chemoautotrophs, such as nitrifiers, may benefit from photosynthesis-enhanced oxygen levels while simultaneously competing with phototrophs for inorganic carbon and nitrogen.

We studied the physical and biological stratification and functioning of photogranules by microscopic imaging, applying bioinformatic tools, microsensors and labelling with stable isotopes. The findings provide valuable insight into the spatial and temporal distribution of functional activity (photosynthesis, nitrification, and denitrification) within photogranules and their dependency on external factors (light, nutrients). Further, the results can be used to support engineering decisions in photogranular wastewater treatment.

3 MATERIALS AND METHOD

3.1 Cultivation and sample preparation

Photogranules were obtained from bioreactors as described previously (Trebuch et al., 2020) (**figure S1**). The bioreactors were bubble columns with a diameter of 10 cm, a height of 38 cm and a bottom cone of 10 cm. The working volume was 1.6 L, which resulted in a liquid level at a height of 28 cm from the bottom of the cone. Mixing was achieved by gassing with air enriched with 5%v/v CO_2 at a rate of 500 mL/min. Temperature was controlled at 35 °C and pH was kept at 6.8±0.1. Bioreactors were operated in sequencing batch mode with a settling time of 5 minutes, a hydraulic retention time (HRT) of 0.67 days, and an operating cycle of 12 hours. Day:night cycles of 12 hours were superimposed on the sequencing batch cycle such that each batch cycle was subjected to 6 hours light and 6 hours darkness. A sludge retention time (SRT) of 7 days was achieved by actively removing 114 ml of the mixed liquor at the end of every batch cycle. The influent contained 100 mg N/L (7.14 mmolN/L) as ammonium, 10 mg P/L (0.32 mmol P/L) and 200 mg COD/L (3.15 mmol/L of sodium acetate). Photogranules were sampled from the mixed phase of the bioreactor and were either directly analysed or fixed in paraformaldehyde (PFA) in 5% phosphate buffered saline (PBS) for later analysis. Photogranule size ranged from 0.4 to 5 mm with an average diameter of 2.6 mm. Photogranules with sizes ranging from 2 to 4 mm were used for analysis. This size range was representative for the system and sample preparation was feasible for all analyses.

3.2 White light microscopy and confocal laser scanning microscopy (CLSM)

A stereo microscope (Leica M205C, Germany) was used to visualize whole and sectioned photogranules under white light. Images were obtained with the Leica Application Suite (LAS version 4.13, Germany). The 3-dimensional structure of the granules was examined by multi-channel CLSM (Leica TCS SP5X, Germany). The system with an upright microscope and a super continuum light source was controlled by the LAS-AF 2.4.1 software. Image data stacks were recorded with 25x NA 0.95 and 63x NA 1.2 water immersion lenses. Samples were mounted in a cover well chamber with matching spacers. For this purpose, the photogranules were cut in half and stained inside the chamber, which was then filled up with water and closed with a high-quality coverslip. For identifying a suitable lectin, a screening with all commercially available lectins was performed. Glycoconjugates were detected by fluorescence lectin-binding analysis (FLBA), according to Staudt et al. (2004) and Zippel & Neu (2011). After testing

several lectins, the BAN lectin labelled with Alexa-568 was selected for imaging. BAN is a lectin derived from banana (*Musa paradisiaca*), which has single-carbohydrate binding specificity for D-Mannose and D-Glucose (Singh et al., 2005). The fluorochrome Syto9 was used as a counterstain to visualize nucleic acids. Cyanobacteria and eukaryotic algae were identified based on their pigments. The settings for recording image data stacks sequentially were as follows: Excitation: 480, 635 nm and 565 nm, emission: 500-550 nm (Syto9), 585-650 nm (BAN-A568, phycobilins), 650-720 nm (Chl A). Images were processed with the imaging software Fiji (Schindelin et al., 2012) and individual image data stacks were stitched together using Photoshop (version CS6).

3.3 16S and 18S rRNA gene amplicon sequencing

DNA samples were taken to assess the microbial community. Specifically, 15 mL of harvested photogranules were centrifuged at 5500 rpm and the supernatant discarded. The cell pellets were immediately frozen at -80 °C until further processing. DNA was extracted in triplicate by using the DNeasy PowerSoil Pro Isolation Kit (Qiagen GmbH, Hilden, Germany). The quantity and quality of DNA were spectrophotometrically determined with a NanoDrop One (ThermoFisher Scientific, USA). The DNA samples were submitted for sequencing to Génome Québec (MacGill University, Montreal, CA). The 16S rRNA gene V3/V4 variable region was amplified using primer pair 341F (CCTACGGGNGGCWGCAG) and 805R (GACTACHVGGGTATCTAATCC) (Herlemann et al., 2011). The 18S rRNA gene V4 variable region was amplified using the primer pair 616*F (TTAAARVGYTCGTAGTYG) and 1132R (CCGTCAATTHCTTYAART) (Hugerth et al., 2014). Both sets of primers were modified to add Illumina adapter overhang nucleotides sequences to the gene-specific sequences. Sequencing was performed using an Illumina MiSeq system (Illumina MiSeq, USA) with 300-bp reads (v3 chemistry). Primers were removed from the raw sequences using *cutadapt* (version 1.18) (Martin, 2013). The obtained sequences were processed further with DADA2 (Callahan et al., 2016). Taxonomic alignment of the sequences was done to the SILVA database (release 138) using SINA (https://www.arb-silva.de). The 16S and 18S data set was normalized using the cumulative sums scaling (CSS) function of the R package *metagenomSeq* version 1.24.1 (Paulson et al., 2013). The analysis of the microbiome data was performed with the R-package *phyloseq* (version 1.26.1) (McMurdie and Holmes, 2013).

3.4 Microsensor measurements

Photogranules were pinned with glass needles to a nylon mesh fitted over a small petri dish (**figure S2**). The petri dish was submerged in tap water (**table S1**), and amended with acetate, medium stocks, and nitrate as indicated. Oxygen concentration

was determined using a Clark-type oxygen microsensor (Revsbech, 1989) fitted to a motorized micromanipulator and two-point calibrated in oxygen-saturated water and basic sodium ascorbate (oxygen-free baseline). Nitrate concentrations were determined using a nitrate LIX membrane sensor manufactured in house (Max Planck Institute for Marine Microbiology, Bremen, Germany), calibrated in a nitrate dilution series (de Beer et al., 1997).

Using the oxygen and nitrate profiles generated from the microsensor measurements, the net consumption/production of reactants was calculated by calculating the flux at each depth, then multiplying by the surface area of the photogranule at that depth, assuming a perfect sphere.

$$Production\ \left[\frac{nmol}{h}\right] = D * \frac{dC\ [nmol]}{dx\ [\mu m]} * 4 * pi * r^2 \qquad \text{equation 1}$$

3.5 ^{14}C carbon fixation incubations

Photogranules were incubated without headspace in 6 mL glass vials at pH 6.5 in tap water amended with either 3 mmol or 10 mmol DIC, and amended with 8 mmol ammonium, 3 mmol phosphate, and/or 3 mmol acetate as indicated. Additionally, photogranules were provided with ~60 kBq ^{14}C bicarbonate. Vials were constantly rotated and incubated for six hours at room temperature in the dark (nitrification experiment) or in the light (photosynthesis, ~250 µmol/m^2/s). Incubations were performed simultaneously. Incubations were stopped by removing 600 µL supernatant and replacing it with a 20% paraformaldehyde solution, to a final concentration of 2% PFA. Photogranules used for control (blanks) were killed first in paraformaldehyde and then exposed to the tracer for 6 hours.

The photogranules were washed twice in 10 mM carbonate buffer to remove unreacted carbonate tracer and embedded by immersing in OCT tissue freezing medium (Leica) overnight, then frozen in 1 ml plastic cups at -20°C and sectioned in 20 µm thick slices in a cryomicrotome. The slices were caught on polylysine slides, and the radioactivity distribution was imaged in a radio-imager (BioSpaceLab, Paris), until 1.000.000 counts were obtained. Blanks were counted for 12 hours, as 1.000.000 counts could not be obtained in a reasonable time.

3.6 ^{15}N nitrogen incubations

Photogranules were incubated in 6 mL gas-tight glass vials in tap water amended with 3 mmol DIC and either 1 mmol ^{15}N ammonium or 1 mmol ^{15}N nitrate and incubated without headspace at room temperature in the dark or light as indicated. Two photogranules were placed in each vial, one small and one large. Four separate vials were prepared per condition, and the photogranules in one vial per group were killed at 4 separate time points (~0, 2, 4.5, and 5.5 hrs incubation). Photogranules were killed with a 1:1 w/v ZnCl solution. Timepoint 0 was used as the blank.

After killing the photogranule, a 2 mL helium headspace was created in each vial. The vials were shaken vigorously and allowed to equilibrate for 5 days. Subsequently, 150 µL of headspace was injected into an IR-MS and analysed for ^{15}N-N_2. Injections were calibrated against a series of ambient air injections, allowing calculation of the excess ^{15}N nitrogen content. Excess ^{15}N was calculated as ($^{29}N_2$ + (2 * $^{30}N_2$)). Rates of denitrification were calculated by fitting a linear equation to the excess ^{15}N production (Holtappels et al., 2011).

NO_x, the sum of nitrate and nitrite, was converted to NO with acidic vanadium chloride and measured with a CLD 60 Chemiluminescence NO/NO_x analyser (Braman and Hendrix, 1989). NO_x content was calibrated against a dilution series of nitrate. The rate of nitrification was then determined by fitting a linear equation to the sum of the excess ^{15}N at each time point and the nitrate concentration.

4 RESULTS

4.1 Physical structure of photogranules

The photogranules exhibited a defined physical and biological structure (**figure 1A, 1E**). Filamentous cyanobacteria (phycobilin and Chl A autofluorescence) with gliding motility formed a complex network, which functioned as a support structure to myriads of other prokaryotic and eukaryotic microorganisms (**figure 1B**). Microscopic observations of photogranule cross sections revealed physical and biological stratification from surface to centre. A dense shell of both phototrophic and non-phototrophic organisms (stained by SYTO9) formed at the outer 300-500 µm of the granule (**figure 1A- 1D**). Below this shell was a zone of radially aligned filamentous (RAF) cyanobacteria followed by a dense and jumbled centre. Eukaryotic algae (Chl-a autofluorescence) occurred in microcolonies throughout the photogranule from surface to centre. Glycoconjugates (visualized by lectin staining) surrounded the filamentous cyanobacteria throughout the entire photogranule (**figure S3**). Glycoconjugates are evidence for excretion of extracellular polymeric substances (EPS) by phototrophic and

non-phototrophic organisms and can contribute to the physical structure of the photogranule. The BAN lectin used in this study visualizes glycoconjugates with D-glucose and D-mannose as monosaccharide building blocks.

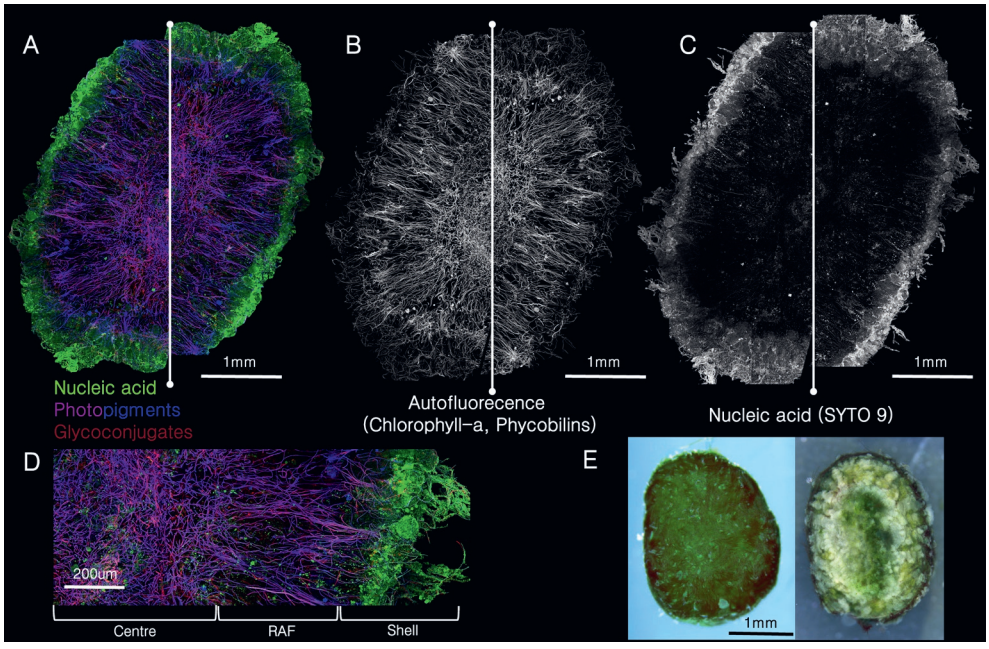

Figure 1: Microscopy photographs of photogranules A) CLSM image of a photogranule cross section showing nucleic acids assigned to phototrophic and non-phototrophic bacteria (green), photopigments (blue, purple) and glycoconjugates (red) **B)** The same cross-section showing only the autofluorescencent signal of the photopigments chlorophyll-a and phycobilin **C)** and the nucleic acid signal (SYTO 9). **D)** Closeup of the CLSM cross section from the centre to the surface of the photogranule. The cross section can be divided into 3 distinct zones: 1) the centre, 2) radially aligned filaments (RAF) and 3) the shell. **E)** A stereo microscope image of a photogranule of about 4 mm in diameter under white light. The left image shows the whole photogranule and the right images the cross-section of the same photogranule. In the RBG false coloured images from CLSM four different components can be distinguished: filamentous cyanobacteria (purple), eukaryotic microalgae (blue), phototrophic and non-phototrophic bacteria (green), and glycoconjugates (red). In panels A, B, and C, the CLSM images are made of 14 individual images stitched together and are mirrored across the white vertical line to illustrate a whole photogranule. Due to limitations of the CLSM technique only half of the photogranule could be captured and for representation purposes the image was mirrored indicated by the white vertical line. For reference of size a scale bar was added to each image.

4.2 Microbial community composition

The microbial community consists of both phototrophic organisms, including motile filamentous cyanobacteria and eukaryotic algae, and non-phototrophic organisms (**figure 2A**). The 16S dataset is dominated by amplicon sequencing variants (ASV) attributed to phototrophic organisms from the Phylum of *Cyanobacteria* (37%) and non-phototrophic organisms from the Class *Proteabacteria* (28%). The two most highly abundant ASV are the cyanobacteria *Leptolyngbya boryana PCC-6306* (ASV899) with 15% rel. abundance and *Alkalinema pantanalense CENA528* (ASV765) with 13% rel. abundance. Next to the phototrophic community, nitrifiers and denitrifiers are present. The nitrifiers *Nitrosomonas* sp., *Nitrobacter* sp. and *Nitrospira* sp. make up about 5%, while the aerobic chemoheterotrophs and denitrifiers *Thauera* sp. and *Zoogloea* sp. make up 15% to the prokaryotic community. Strictly anaerobic prokaryotes from the Family *Anaerolineaceae* and *Caldilineaceae* make up together 5% suggesting that part of the photogranule is anaerobic. The 18S dataset was dominated by ASVs attributed to eukaryotic microalgae (58%), fungi (18%) and protists (2%) (**figure 2B**). The eukaryotic algae present are *Chlorella* sp. (39%), *Chlorococcum* sp. (13%), *Botryoshaerella* sp. (1%) and *Tetradesmus* sp. (1%). The fungi present is *Trichosporon* sp. (18%).

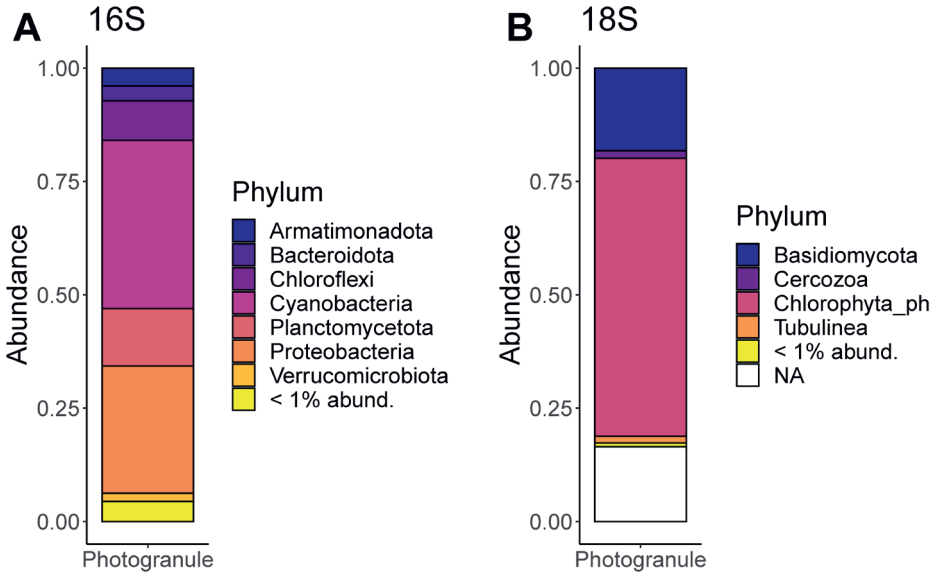

Figure 2: Microbial community composition obtained by 16S and 18S rRNA gene amplicon sequencing. The relative abundance is given on Phylum level. All ASVs with abundances lower than 1% are grouped together and displayed as "< 1% abundance" in the two bar plots. "NA" are ASVs that are not assigned at phylum level. **A)** 16S dataset and **B)** 18S dataset.

4.3 Light and photopigments

The photogranules effectively absorbed light across the visible light spectrum (**figure 3A**). Within 600 µm depth 90% of the surface light was completely absorbed. Chlorophyll-a and beta-carotene made up the majority of pigments in the photogranule (**figure 3B**). A limited number of other pigments also contributed to light attenuation. Few pigments had absorption peaks in the 530-650 nm range despite significant light attenuation in these regions (**figure S4**). Chlorophyll-a does have some limited absorption in this region, though substantially less so than near its peaks at 400-450 and 650-700 nm. The water-soluble fraction of pigments such as phycobiliproteins (e.g., phycocyanin and phycoerythrin) were not assessed. Phycobiliproteins are essential pigments of cyanobacteria. Considering the high abundance of cyanobacteria in the microbial community of photogranules it is believed that these pigments also played a vital role in the light absorption process. Interestingly, there was an increase of light intensity in the range of 700-800 nm especially in the 100 and 200 µm depth when compared to the reference light intensity at depth 0µm (**figure 3A**), possibly indicating fluorescence by photopigments (Grigoryeva and Liss, 2020; Kühl and Fenchel, 2000).

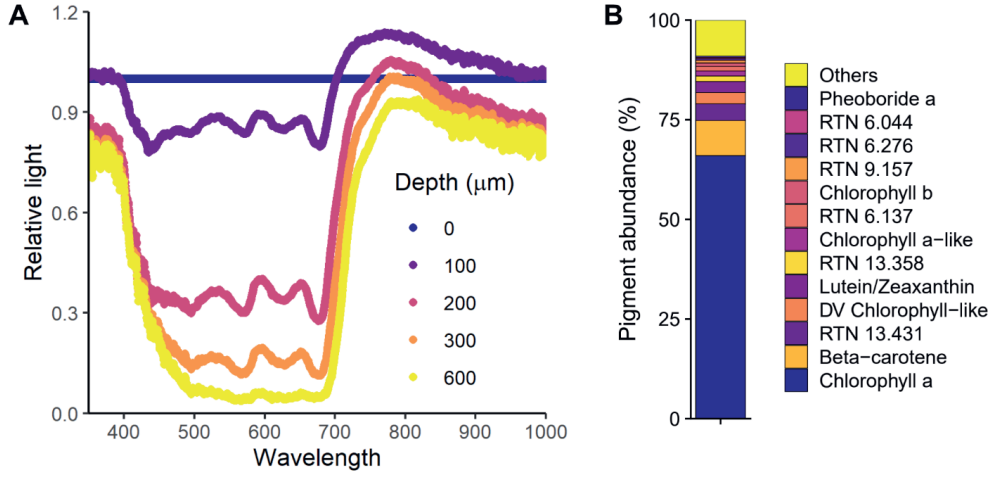

Figure 3: Light availability and pigments found in photogranules. A) The light relative to the photogranule surface, measured with a light microsensor, is plotted for 7 different depths. Surface illumination is approximately 250 µmol/m²/s E. Light is rapidly and broadly absorbed across the visible light spectrum. **B)** The relative abundance of pigments presents at least 1% of the total ethanol-acetone extractable pigmented material detected by UPLC in at least one of 6 samples.

4.4 Photosynthesis and carbon fixation

Photogranules had a high potential for both oxygen production by photosynthesis and oxygen consumption (**figure 4A**). In the presence of acetate, oxygen consumption surpassed oxygen production, leading to anoxia throughout the majority of the photogranule's depth. In the absence of acetate, the photogranule was saturated with oxygen throughout its interior (**figure 4A**). This led to a maximum oxygen production of 738 nmol-O_2/photogranule/h when summing up the oxygen production rate along the depth (**equation 1**). Despite the decrease in oxygen accumulation in the presence of acetate, photosynthesis remained active, resulting in substantial carbon fixation comparable to levels in the absence of acetate (**figure 4D**). This indicates that oxygen is rapidly cycled in the photogranule, and that during periods of acetate exposure, respiration is likely oxygen-limited, even in the light. In contrast, the interior of the photogranule appears light-limited, as the majority of the light-driven carbon fixation in the photogranule occurs in the outer edges (**figure 4C, D**). This is in line with the rapid light attenuation observed in photogranules (**figure 3A**). Considering a photogranule with a diameter of 4 mm a maximum carbon fixation rate of 383 nmol-C/photogranule/h was calculated (**equation S1**).

Carbon fixation in the photogranule was relatively insensitive to short-term changes in nutrient concentration (**figure 4D**). Carbon fixation was similar in all photogranules incubated in untreated tap water, in tap water with 3 mM acetate, in tap water with 8 mM ammonium, in tap water with 3 mM phosphate, as well as in tap water with both 8 mM ammonium and 3 mM phosphate. This would suggest that the rate of carbon fixation, and therefore photosynthesis, should not change over the normal course of the reactor batch cycle. Nevertheless, the rate of aerobic respiration and other oxygen-consuming processes, as nitrification, likely changes substantially, as oxygen becomes available or is removed.

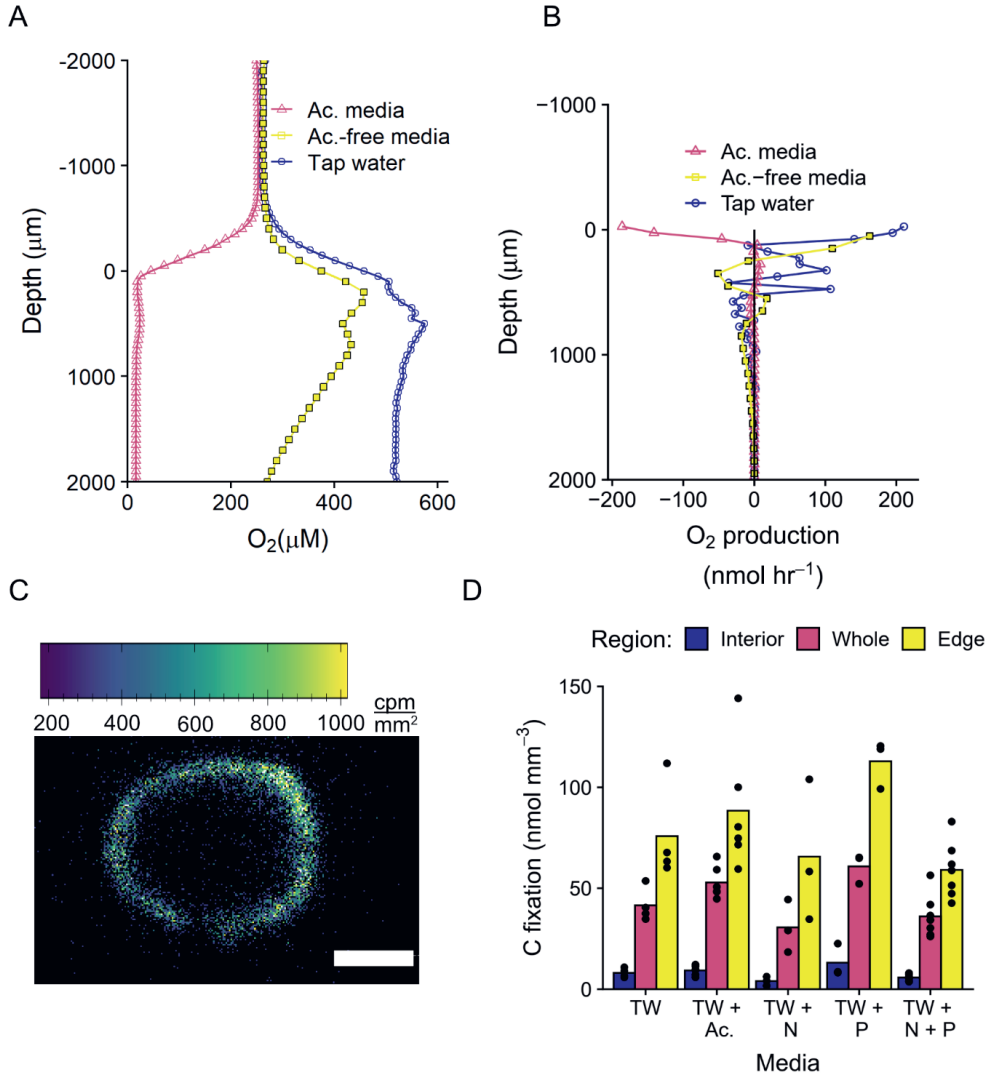

Figure 4: Photosynthesis. **A)** Oxygen profiles were measured in the same photogranule under three different conditions: untreated tap water (blue circles), growth media without acetate (yellow squares), and growth media with acetate (pink triangles). **B)** The total oxygen production at each depth of the photogranule, calculated from the profiles in figure A, assuming a spherical aggregate 4 mm in diameter. **C)** A representative microradiograph image of the distribution of ^{14}C from carbon fixation in a photogranule (incubated with acetate). White scale bar is 1 mm. **D)** Carbon fixation in photogranules incubated in the light in untreated tap water (TW), tap water amended with 3 mM acetate (TW + Ac.), tap water amended with 8 mM NH_4^+ (TW+N), tap water amended with 3 mM PO_4^{3-}, and tap water amended with both 8 mM NH_4^+ and 3 mM PO_4^{3-}. Carbon fixation was measured by incubating photogranules with ^{14}C-CO_2 then determining ^{14}C fixation with a microradiograph. The carbon fixation was visually segregated by region: the interior of the photogranule (blue), the entire photogranule (purple) and the outer edge of the photogranule (yellow). The black dots represent measurements of individual photogranules. These light-exposed incubations were carried out simultaneously to incubations in the dark, which are displayed in figure 4A.

4.5 Nitrification/denitrification and carbon fixation

Autotrophic nitrification occurred largely in the outer edges (0-500μm) of the photogranule in dark incubations with ^{14}C-labeled carbonate, with or without ammonium and the nitrification inhibitor ATU (**figure 5A**). Carbon fixation was highest in the incubations containing ammonium (0.9 nmol mm^{-3}) although there was still detectable carbon fixation in the incubations without ammonium and with ATU. The slightly higher level of carbon fixation (0.4 nmol mm^{-3}) in photogranules incubated in untreated tap water compared to the photogranules incubated with ATU (0.3 nmol mm^{-3}) suggests that the photogranules may have stored some residual ammonium or used the low concentrations of ammonium (<0.03 mg/L or <2.14 μmol/L) available in the tap water (**table S1**). The higher level of carbon fixation in photogranules incubated with ATU compared to dead photogranules (Blank, 0.06 nmol mm^{-3}), indicates there is significant anaplerotic carbon fixation in the photogranule (0.2 nmol mm^{-3}).

Microsensor profiles of nitrate concentrations in the light and dark confirm the distribution of nitrification predicted by the dark carbon-fixation distribution (**figure 5B, C**). While the absolute concentration of nitrate peaks in the photogranule centre (**figure 5B**), the rate of nitrate production, calculated from the same profiles, has two peaks at the outer edge. The first peak corresponds to a dip in oxygen concentration observed in multiple other photogranules as well (**figure 5B, C**). The rate of nitrate consumption peaks in between the two nitrification peaks, rather than at the photogranule centre. The photogranule centre contributes little to the overall N cycling in the photogranule, partly due to its low volume relative to the outer edge (**figure 5C**). Summing up the nitrate production rates at each depth an overall nitrate production rate of 93.7 nmol/photogranule/h (with NH_4^+) and 25.1 nmol/photogranule/h (without NH_4^+) was observed.

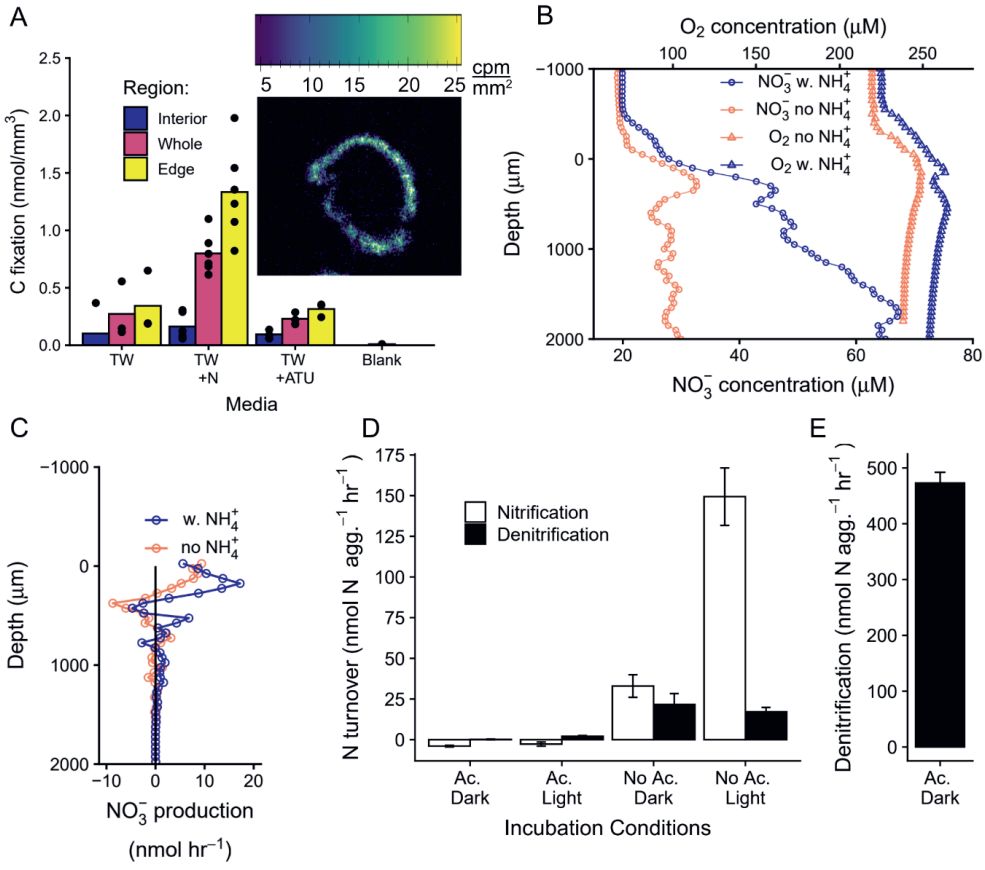

Figure 5: Nitrogen cycling. A) Carbon fixation in photogranules incubated in the dark in untreated tap water (TW), tap water amended with 8 mM NH_4^+ (TW + N), tap water amended with 8 mM NH_4^+ and the nitrification inhibitor ATU (TW + ATU), and in photogranules killed with paraformaldehyde before tracer addition (Blank). Carbon fixation was measured by incubating photogranules with ^{14}C-CO_2 then determining ^{14}C fixation by microradiography. The carbon fixation was visually segregated by region: the background of the image (blue), the interior of the photogranule (purple), the entire photogranule (orange) and the outer edge of the photogranule (yellow). **B)** The average of three microprofiles of nitrate (circles) and oxygen (triangles) concentrations in the same photogranule incubated in the light first without NH_4^+ (orange) then with 100 μM NH_4^+ (blue) after reaching steady state. **C)** The rate of nitrate production at each depth calculated from the profiles in panel B, in nmol/hr, assuming a spherical photogranule with a radius of 1800 μm. Positive values indicate zones of production, while negative values indicate zones of consumption. **D)** Nitrification (white bars) and denitrification (black bars) in photogranules incubated with 1 mM ^{15}N-labeled ammonium, either in the dark or the light, and with or without the addition of 3 mM acetate. Rates are a linear fit of the production of nitrate or ^{15}N-N_2 in 4 separate vials stopped at different points. Nitrification represents rate of production of extracellular nitrate plus the production of ^{15}N-N_2. Denitrification denotes the production of ^{15}N-N_2. Error bars indicate the standard error of the slope. **E)** The rate of denitrification in photogranules incubated with ^{15}N-NO_3^- with acetate in the dark. The error bar represents the standard error of the slope.

Nitrogen cycling in the photogranules was either oxygen or carbon-limited, depending on the incubation conditions (**figure 5D, E**). In the presence of acetate there was no nitrification when photogranules were incubated with ^{15}N-ammonium in the dark (**figure 5D**), due to an absence of oxygen. Some nitrification in the presence of acetate must occur in the light, as indicated by elevated denitrification (black bar, **figure 5D**), although net nitrate was consumed from the background concentration of 10 μM (white bar, **figure 5D**). In the absence of acetate, nitrification was much higher, especially when incubated in the light (max. 150 nmol-N/photogranule/h) (**figure 5D**). Interestingly, denitrification was also higher in the absence of acetate, although the photogranules were always oxic in the absence of acetate, and there should be little free organic carbon. This indicates that there is significant carbon recycling within the photogranules, and that denitrification is tolerant to oxygen. Nonetheless, denitrification was clearly carbon-limited or depressed by oxygen in the absence of acetate, as indicated by the much higher rate of denitrification in photogranules incubated with ^{15}N-nitrate in the dark, with acetate (max. 480 nmol-N/photogranule/h) (**figure 5E**).

5 DISCUSSION

5.1 Physical, biological, and structural features of photogranules

The structural analysis (**figure 1**) revealed the spatial distribution of cyanobacteria, eukaryotic algae, non-phototrophic organisms (nitrifiers, denitrifiers) and glycoconjugates within a photogranule. Motile filamentous cyanobacteria and excreted extracellular polymeric substances (EPS) formed the structural "backbone" of the photogranule. Motile filamentous cyanobacteria (*Alkalinema pantanalense*, *Leptolyngbya boryana*, *Cephalothrix komarekiana* and *Limnothrix* sp.) generated a complex network of filaments that provided structural rigidity similar to the one observed in cyanobacterial mats (Stal, 1995; Tamulonis and Kaandorp, 2014). EPS can give additional structural support to the photogranule as it has been shown to be essential for the proliferation of microbial communities within biofilms (Wingender et al., 1999). The lectin stain revealed that a large fraction of polysaccharide in the EPS was attributed to D-glucose and D-mannose. The glucose constituents were likely produced by filamentous cyanobacteria, as it is the dominating monosaccharide in the polysaccharide fraction of their EPS structure (P. Li et al., 2001; Nicolaus et al., 1999; Zippel and Neu, 2011). Both glucose- (especially α(1-4)glucans) and mannose-containing polysaccharides have been shown to play a key role in biofilm cohesion in both aerobic granules and phototrophic microbial mats (McSwain et al., 2005; Rossi and De Philippis, 2015). The lectin-specific

BAN glycoconjugates reported will show only part of the total glycoconjugates present. Consequently it is anticipated that there are other types of glycoconjugates as well as other matrix compounds present such as extracellular proteins and eDNA (Neu and Lawrence, 2017).

The importance of filamentous cyanobacteria in photogranule formation was highlighted previously (Abouhend et al., 2020; Milferstedt et al., 2017b; Trebuch et al., 2020). It was proposed that initially, filamentous, and motile cyanobacteria form a nucleus of filaments (a bundle) that can harbour other organisms. When growing this structure becomes more and more physically and biologically stratified and finally results in a photogranule. While young and small photogranules (<0.5mm) do not have a defined structure, photogranules grown to sizes of several millimetres show a clear stratification. For example, Abouhend et al. (2020) observed photogranule sizes of >2.5mm in which cyanobacteria became less abundant in the centre and formed a distinct layer of about 1.25+/-0.14mm close to the surface.

In our study we found that independent of photogranule size, the filamentous cyanobacteria were present in the entirety of the photogranule. However, they showed different arrangements of the filaments from surface to centre. While the cyanobacteria filaments were densely packed and jumbled at the surface and centre, in the area in between, they aligned themselves radially. One explanation for this phenomenon is the competition for space within the photogranule, as radially arranging the filaments would facilitate movement between regions with higher exposure to light (phototaxis) and higher levels of other substrates (chemotaxis) (Stal, 1995). This is especially important considering the thick shell of non-phototrophic organisms in the first 500 μm of the photogranule that the cyanobacteria need to "pierce" through and compete with in order to remain at the surface of the photogranule. Such radial movement of cyanobacteria (*Cephalotrix* sp. formerly known as *Phormidium* sp.) was previously observed in microbial spheres derived from subcultures of microbial mats composed of cyanobacteria, diatoms and heterotrophic bacteria originating from the North Sea (Brehm et al., 2003). Their movement was shown to be triggered by light and substrates.

5.2 Functional stratification in photogranules

Many aspects of photogranules parallel cyanobacterial mats, cryoconite, and other phototrophic biofilms occurring in nature. In natural systems, as well as in photogranules, physical and biological stratification occurs according to the availability and gradients of light and nutrients (Wolf et al., 2007). The photogranule surface was exposed to the highest light and substrate levels resulting in the highest photosynthetic and nitrifying activities. Inner parts of the photogranule harboured anoxic zones that

allowed anaerobic processes such as denitrification to occur. Most of the microbial activity was still confined to the outer 500 μm of the photogranule. In that region phototrophs (cyanobacteria and eukaryotic algae) attenuated about 90% of all incoming light and showed the highest photosynthetic activity at around 400-500 μm (max. 100 nmol/h). The photopigments absorbed well in the visible light spectrum between 450-700nm. However, outside this range the light was only attenuated by up to 20% at a depth of 600 μm. Especially at the longer wavelengths there was still light energy in the depth of the photogranule that remained unused. This part of the light spectrum could be utilized by microorganisms with photopigments absorbing in this range such as green or purple (non-)sulphur bacteria having bacteriochlorophylls with maximum infrared absorption up to 1040 nm (George et al., 2020). These organisms can be observed in microbial mats with anoxic zones and sufficient sulphide levels (de Beer et al., 2017). However, not in our photogranules as no sulphide was added to the medium, and thus no anaerobic sulphate reducing bacteria were present to reduce sulphate to sulphide (confirmed with sulphide microsensor).

In addition to the high concentration of cyanobacteria in the outer part of the photogranule there was also a large population of non-phototrophic organisms, including nitrifiers (*Nitrosomonas* sp., *Nitrobacter* sp. and *Nitrospira* sp.) and chemoheterotrophic bacteria/denitrifiers (*Thauera* sp. and *Zoogloea* sp.). This high density of microbes supported high oxygen production/consumption and nitrate production, as well as carbon fixation (**figures 4 and 5**). Towards the centre only marginal nitrification and denitrification was observed. The nitrate accumulation observed in the microsensor profile (**figure 4B**) was not caused by increased nitrification rates at lower depth but mostly due to the reducing rate of denitrification towards the centre. This was confirmed by ^{14}C incubation studies specifically targeting nitrification that showed most of the nitrifying activity is indeed in the outer edge of the photogranule.

Although the centre of the photogranule seems to be relatively inactive it may harbour other functions. These functions could include substrate storage (e.g. as lipids, starch or EPS), fermentative processes or decomposition of dead organic constituents, which all lead to photogranule internal nutrient cycling. The centre is mostly anoxic to anaerobic and provides an opportunity for anaerobic respiration. Anaerobic prokaryotes such as *Anaerolineaceae* and *Caldilineaceae* and the fungi *Trichosporon* sp. found in the photogranule can ferment carbohydrates and mineralize organic phosphorus and nitrogen, comprised in EPS or necrotic biomass, to H_2, alcohols (e.g. butanol, ethanol), ketones (e.g. acetone), PO_4^{3-}, NH_4^-, which in turn can be reused within the photogranule again (Middelhoven, 2004; Yamada et al., 2006; Zhang et al., 2017). Cyanobacteria are

adapted to anoxic conditions as well and can ferment six-carbon sugars (e.g. glucose) to e.g. lactate or ethanol (Stal, 1997). This internal nutrient cycling increases in significance the larger the photogranule become and it might allow various metabolic processes to occur despite external substrate limitation.

Interestingly, photosynthesis and carbon fixation rates were relatively insensitive to the nutrient conditions tested. This suggests that photosynthetic activity can remain stable over the course of the light period during a sequencing batch cycle independent of the change in concentration and availability of ammonium, nitrate, phosphate, and acetate. The primary process of photosynthesis is carbon fixation in form of carbohydrates which can be stored as polysaccharides. Under nitrogen limitation carbohydrates are still commonly accumulated and (short-term) phosphorus limitation can be overcome by taking recourse to internal storage of phosphorus (e.g. polyphosphate) (Solovchenko et al., 2019). Under both conditions, photosynthetic activity can be sustained. Municipal wastewater characteristics can vary throughout day and season and thus photogranules are subjected to a highly fluctuating environment within the treatment system. Showing robustness to these changing conditions is key to maintaining treatment performance.

5.3 Nutrient removal and microbial activity during a sequencing batch cycle

The photogranules were cultivated in sequencing batch reactors with distinct phases of reaction (700 min), settling (5 min), effluent withdrawal and influent addition (together 15 min). Two batch cycles with a length of 12 hours were conducted per day. One cycle had 6 hours of light followed by 6 hours of darkness and the second cycle 6 hours of darkness followed by 6 hours of light. Here we want to illustrate the conditions and microbial activities of photogranules occurring in the first batch cycle (**figure 6**). At the beginning of a batch, nutrients such as ammonium (NH_4^+), phosphate (PO_4^{3-}) and acetate were available in high concentration. In this phase the photogranules could maintain high photosynthetic, heterotrophic, nitrification and denitrification activities, which resulted in ammonium, phosphate, acetate and carbon dioxide consumption and oxygen, nitrate, and di-nitrogen (N_2) production. Ammonium is both assimilated into biomass and consumed by nitrification, while phosphate is only assimilated into biomass. In the dark phase the phototrophs switched from photosynthesis to respiration on internally stored photosynthates. Nitrification continued until all ammonium was converted to nitrate. Since all acetate was already consumed, denitrification must have been fuelled by intracellularly stored carbon (e.g. as

polyhydroxyalkanoates) (Alzate Marin et al., 2016) or internally recycled carbon by decomposition of organic matter (Nielsen and Sloth, 1994).

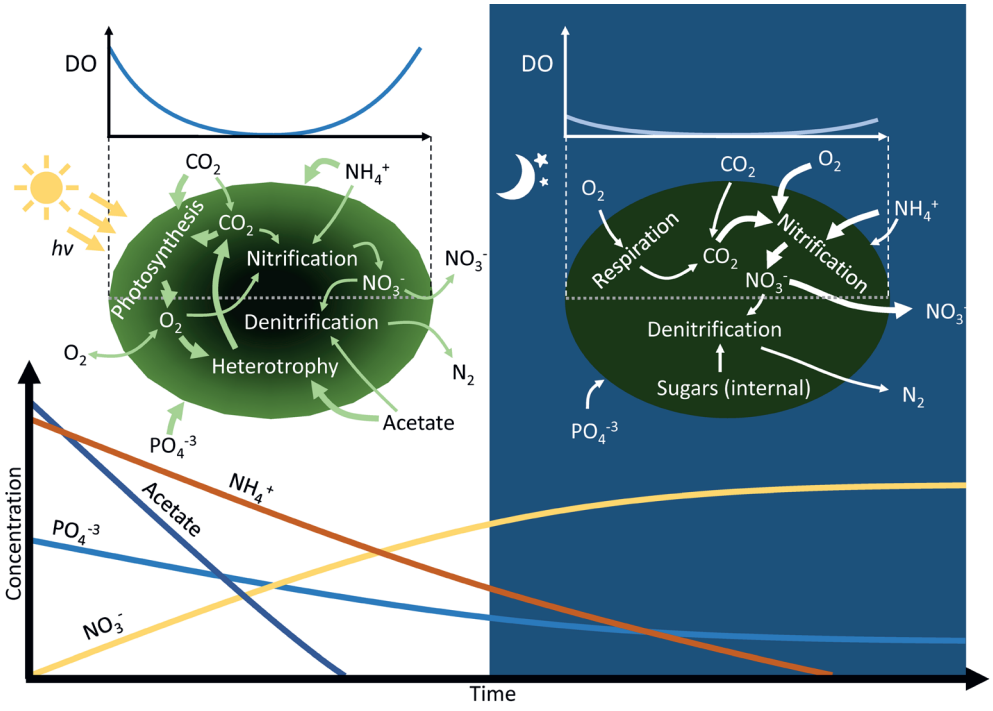

Figure 6. Schematic representation of the conditions and main metabolic processes occurring during a sequencing batch cycle in a photogranule. One cycle has 6 hours light followed by 6 hours darkness. On the left side the "light metabolism" of the photogranule characterized by photosynthesis, heterotrophy, nitrification and dentification is represented. On the right the "dark metabolism" of the photogranule is shown which is dominated by photorespiration, nitrification and to a lower extend with denitrification activities. The line thickness of the arrow indicates the magnitude of the conversion rate (the thicker the higher). Phosphate (PO_4^{3-}) is the only constituent that is not attributed to a certain metabolism in this drawing. As phosphate is essential for all organisms it is here generally attributed to biomass accumulation by the entirety of the photogranule. Ammonium (NH_4^+) is both attributed to nitrification (thinner arrow during light, thicker arrow during darkness) and generally for biomass assimilation (thicker arrow during light, thinner arrow during darkness). The dissolved oxygen (DO) concentration over the cross-section of the photogranule is depicted on top of the two photogranules. This schematic representation is based on the microsensor measurements, ^{14}C and ^{15}N incubations and nutrient data from the bulk liquid in the bioreactor (figure S5 and S6).

Phototrophs made up the majority of the microbial community with 37% of prokaryotes as cyanobacteria and 73% of eukaryotes as green algae and thereby largely determined the overall removal activity. During the light period phototrophs were growing and significantly contributing to nitrogen and phosphorus removal by incorporating these elements into their biomass. As phosphorus is generally removed (by all organisms) via biomass assimilation, the removal rate decreased significantly

during the dark phase when phototrophs undertake cellular maintenance (Borowitzka et al., 2016).

The nitrifying organisms found in photogranules were from the genera *Nitrosomonas*, *Nitrobacter* and *Nitrospira* with *Nitrospira* as the dominant genus. The general low abundance of nitrifying organisms (1 %) can be explained by the competition with phototrophs for carbon dioxide and ammonium (Van Der Steen et al., 2015). This was emphasized by the ^{14}C incubation that showed a 50-100x lower inorganic carbon fixation by nitrification compared to photosynthesis (**figure 4 and 5**). Still nitrification activity was substantial and overall the observed rates during bioreactor operation were 3x lower compared to aerobic granules, but comparable to microalgal-nitrifier consortia grown in floccular biomass (de Kreuk et al., 2007; Karya et al., 2013).

Due to high nitrification activity and respiration of acetate in the beginning of the sequencing batch cycle, oxygen was consumed at a higher rate than produced by phototrophs (**figure 2**). This led to oxygen limitation and most of the photogranules became anoxic. These conditions facilitated simultaneous nitrification and denitrification within the photogranule, which primarily occurred in the first 500 μm of the photogranules. Consequently, in the early stage of the batch cycle the nitrification/denitrification process was oxygen limited. However, along the batch cycle, there was a switch from oxygen-limited nitrification to carbon-limited denitrification towards the end of the cycle when acetate was fully consumed by chemoheterotrophs/denitrifiers i.e., *Thauera* sp. *Zoogloea* sp. after approximately 4 hours into the cycle (**figure S6**).

The ^{15}N incubations showed that denitrification can occur also during aerobic conditions both in presence and absence of acetate. Thus, denitrification was likely performed in part by aerobic denitrifier *Thauera* sp. (Wang and He, 2020). Further, the incubations showed that even in the absence of acetate the internally cycled organic carbon (e.g., organic carbon from phototrophs, or internally stored and recycled carbon) can sustain denitrification (**figure 5D**). Compared to the maximum denitrification rate with addition of acetate in the dark, the denitrification rate sustained on internally cycled carbon was about 25x lower (**figure 5E**). Nevertheless, these rates were sufficient to keep removing nitrogen from the bioreactor in the dark period.

5.4 From fundamental insight to application

The fundamental knowledge of how photogranules are structured and function will ultimately allow engineers to create novel ecosystem for wastewater treatment. In our study we investigated an active phototrophic, nitrifying, and denitrifying community

that exhibited high nitrogen and carbon removal/conversion rates and showed internally linked processes (exchange of oxygen, nitrogen, and carbon dioxide).

Introducing a phototrophic community in the wastewater treatment process will ultimately allow closure of the CO_2 and O_2 cycle of the conventional activated sludge process. In this case, an external supply of oxygen would be unnecessary as oxygen would be produced through photosynthesis and CO_2 would be supplied by the heterotrophic conversion of organic matter. However, it is unclear if phototrophic oxygen production and heterotrophic CO_2 production would be sufficient to sustain high treatment capacities over time. The overall oxygen production and oxygen consumption was calculated to be 13.61 mmol/L/d and 13.07 mmol/L/d, respectively (**equation S2-S5**). This led to a net oxygen production of the microbial community. However, in the beginning of the batch cycle when acetate was still present, the photogranule was oxygen limited, i.e., photosynthesis could not supply heterotrophic respiration and nitrification with sufficient oxygen to achieve maximal rates (**figure 4A**). This was also apparent from the hourly oxygen production rate of 1.13 mmol/L/h and oxygen consumption rate of 1.36 mmol/L/h in the first 4 hours of the cycle (considering full removal of acetate after 4 hours into the cycle and high nitrification activity). After acetate was fully consumed, photosynthesis would likely become carbon limited without external CO_2 supply. To optimize oxygen demand versus oxygen production in a system without external oxygen or CO_2 supply the light supply and specific acetate load can be altered. This will be especially important when wastewater characteristics (N, P, COD) or light conditions change.

Light supply can either be manipulated by changing the ratio between system volume and illuminated surface or by adjusting the specific light input per photogranule by manipulating the solid retention time (SRT) of the system. By lowering SRT and thereby lowering the biomass in the treatment system the specific light input per photogranule could be increased (considering a constant light input). The load of acetate and other wastewater constituents can be manipulated by changing the hydraulic retention time (HRT) at which the treatment system is operated. To decrease the acetate load, the HRT must be increased and by decreasing HRT the acetate load can be increased. If these steering mechanisms are inefficient other options such as intermitted sparging with compressed air and CO_2 could support photosynthesis or oxygen requiring processes (Brockmann et al., 2021).

As stated before, most activity was in the edge (outer 500 μm) of the photogranule due to light penetration and nutrient diffusion limitation. The photogranules (2-4mm) investigated in this study thereby showed a considerable "inactive" zone, which reduced the overall conversion rate of an individual photogranule. Smaller sizes would optimize

for conversion rate per individual photogranules and could consequently increase the maximal conversion rate of a photogranule treatment system if optimal light and substrate conditions are given. In previous studies on aerobic granules an ideal size of 1.25-1.5 mm was determined (Baeten et al., 2018; de Kreuk et al., 2005). The same was theoretically done for photogranules by Abouhend et al. (2020) that found a range of 0.5-1.7 mm as optimal. The size of the photogranule is dependent on growth kinetics that are mainly determined by the light and organic carbon load of the system. As an engineering tool the control of the solid retention time (SRT) ultimately determines the size of the photogranule as it provides an upper ceiling of the age of a photogranule. A shorter SRT would result in smaller granules and higher photogranule specific conversion rates but might be detrimental for some slow growing organisms (e.g. nitrifiers) and compromise settleability of the photogranule if granule sizes become too small (<0.5mm) (Bradley et al., 2019). Therefore, granule size must be carefully evaluated with all these different aspects in mind.

6 CONCLUSIONS

Photogranules were dominated by motile filamentous cyanobacteria forming a complex interwoven structure in which other organisms embedded themselves. EPS showed to be an important structural feature and indicated glycoconjugates with D-glucose and D-mannose as monosaccharides. Most of the microbial activity was confined to the outer 500 μm of the photogranule. This region supported high rates of oxygen production (738 nmol-O_2/photogranule/h), carbon fixation (383 nmol-C/photogranule/h), nitrification (150 nmol-N/photogranule/h) and denitrification (480 nmol-N/photogranule/h). The phototrophic community efficiently absorbed light across the visible light spectrum with an array of pigments (e.g. chlorophyll-a and beta-carotene). At a depth of 600 μm about 90% of the incoming light was absorbed. An active nitrifying and denitrifying community were present in photogranules that increased overall nitrogen removal. Simultaneous nitrification and denitrification were observed in the presence of acetate. The centre of the photogranule was relatively inactive and showed only marginable nitrification and denitrification rates. The main processes occurring in this part could be attributed to internal nutrient cycling. In this way denitrifying activities observed in the absence of acetate could be sustained by internally cycled carbon.

7 ACKNOWLEDGEMENTS

The authors would like to thank Ute Kuhlicke from UFZ Magdeburg for her excellent support with confocal laser scanning microscopy.

8 SUPPLEMENTAL MATERIAL

8.1 Photogranules

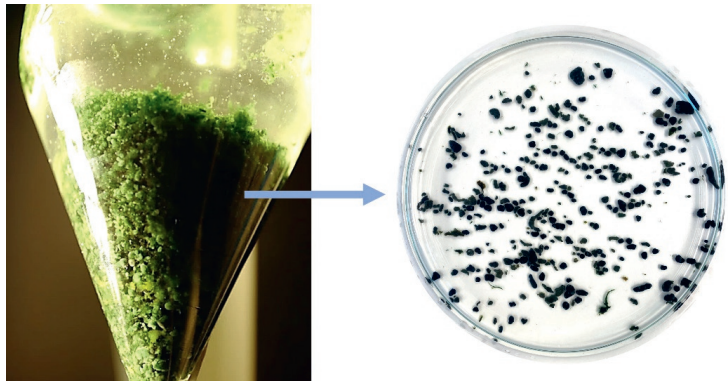

Figure S1. Examples of photogranules that were used in this study: settled in the bubble column bioreactor (left) and in a petri dish (right).

8.2 Microsensor measurements

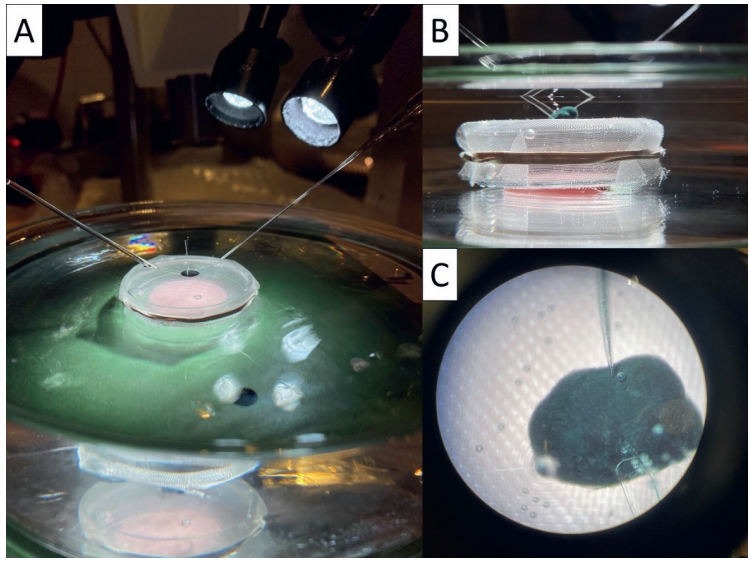

Figure S2. Microsensor setup to investigate light, oxygen, and nitrate profiles in photogranules. The photogranule was placed on a nylon net suspended on a small glass petri dish and pinned down by thin glass needles. The small petri dish was placed into a larger glass petri dish and submerged in liquid. Air was blown over the liquid surface by means of an air pump to mix the liquid. A halogen light source was used to illuminate the photogranule. (A) Image of the small petri dish within the larger petri dish. (B) Side view of the setup. (C) Image taken through a stereo microscope showing the microsensor penetrating the photogranule.

8.3 Tap water quality

Table S1. Chemical analysis of the tap water of NIOO-KNAW used for experiments. The analysis was performed by the lab of the water supply company VITENS b.v.

Vitens Laboratorium
Snekertrekweg 61
8912 AA Leeuwarden
relatiebeheer@vitens.nl

Pb. Wageningseberg
Reinwater Uitgaand

Periode : **JAN - MRT 2020**

Analysenaam	Eenheid	Gemiddelde	Minimum	Maximum	Aantal	Min.Wet	Max.Wet
Temperatuur in situ	°C	11	10.5	11.6	14		25
Zuurstof	mg/l	7.2	6.9	7.6	14	2.0	
Troebeling	FTE	0.12	<0.1	0.24	14		1.0
Zuurgraad (pH)	pH	7.92	7.82	8.04	14	7.00	9.50
Verzadigingsindex (SI) *		-0.26	-0.26	-0.26	1	-0.20	
Totaal Anorganisch Koolstof berekend							
Corrosie-index							
Theoretisch afzetbaar CalciumCarbonaat 90°	mmol/l	0.10	0.09	0.11	14		
Geleidingsvermogen bij 20 °C (EGV)	mS/m	16.9	16.0	17.5	14		125
Koolstofdioxide	mg/l	2.1	1.6	2.7	14		
Koolstofdioxide agressief	mg/l	<1	<1	1.4	14		
Waterstofcarbonaat	mg/l	92	91	94	14	60	
Chloride *	mg/l	6	6	6	1		150
Sulfaat	mg SO4 / l	8	8	8	1		150
Natrium (Na), na aanzuren	mg/l	5.29	5.29	5.29	1		150
Kalium (K), na aanzuren	mg/l	0.53	0.53	0.53	1		
Silicaat	mg Si / l	5.60	5.60	5.60	1		
Calcium (Ca), na aanzuren	mg/l	29.5	28.8	30.4	14		
Magnesium (Mg), na aanzuren	mg/l	2.20	2.14	2.32	14		
Totale Hardheid ****	mmol/l	0.83	0.81	0.85	14	1.00	
Totale Hardheid ****	°D	4.6	4.5	4.8	14	5.6	
Ammonium	mg NH4 / l	<0.03	<0.03	<0.03	3		0.20
Nitriet	mg NO2 / l	<0.01	<0.01	<0.01	3		0.10
Nitraat	mg NO3 / l	<1.0	<1.0	<1.0	1		50.0
Fosfaat-ortho	mg PO4 / l	0.06	0.06	0.06	1		
IJzer (Fe), na aanzuren	mg/l	0.014	0.013	0.014	3		0.200
Mangaan (Mn), na aanzuren	mg/l	<0.005	<0.005	<0.005	3		0.050
Aluminium (Al), na aanzuren	µg/l	<2	<2	<2	1		30.0
Antimoon (Sb), na aanzuren	µg/l	<1	<1	<1	1		5.0
Arseen (As), na aanzuren	µg/l	2.77	2.77	2.77	1		10.0
Barium (Ba), na aanzuren	µg/l	4.35	4.35	4.35	1		
Boor (B), na aanzuren	µg/l	<10.0	<10.0	<10.0	1		500
Cadmium (Cd), na aanzuren	µg/l	<0.10	<0.10	<0.10	1		5.00
Chroom (Cr), na aanzuren	µg/l	<0.5	<0.5	<0.5	1		50.0
Koper (Cu), na aanzuren	µg/l	5.36	5.36	5.36	1		2000
Kwik (Hg), na aanzuren	µg/l	<0.02	<0.02	<0.02	1		1.00
Lood (Pb), na aanzuren	µg/l	<0.5	<0.5	<0.5	1		10.0
Nikkel (Ni), na aanzuren	µg/l	<1.0	<1.0	<1.0	1		20.0
Seleen (Se), na aanzuren	µg/l	<0.5	<0.5	<0.5	1		10.0
Zink (Zn), na aanzuren	µg/l	4.77	4.77	4.77	1		3000
Cyanide, totaal	µg/l	<2	<2	<2	1		50
Fluoride	mg/l	0.06	0.06	0.06	1		1.0
Kleurintensiteit (455 nm)	mg Pt/Co/l	<3	<3	<3	1		20
UV-extinctie	1 / m	1.4	1.4	1.4	1		
Totaal Organisch Koolstof (TOC)	mg/l	<0.5	<0.5	<0.5	1		
Koloniegetal 22 °C **	kve/ml	<1	<1	1	14		100
Coliformen 37° C ***	kve/100 ml	0	0	0	14		0
Escherichia coli 37 °C ***	kve/100 ml	0	0	0	14		0
Enterococcen	kve/100ml						
Clostridium perfringens ***	kve/100 ml	0	0	0	1		0
Aeromonas 30 °C	kve/100 ml	<10	<10	<10	1		1000
Legionella, Matrix A Procedure 8,9,10	kve/l	<100	<100	<100	1		100

* *De norm is vastgesteld als rekenkundig jaargemiddelde.*
** *Het gemiddelde van Koloniegetal 22 °C is berekend als een geometrisch gemiddelde, ook de norm is een geometrisch jaargemiddelde.*
*** *Het gemiddelde van de Coliformen 37° C ,Escherichia coli 37 °C,Enterococcen en Clostridium perfringens wordt als mediaan weergegeven.*
**** *Normwaarde geldt uitsluitend bij toepassing van ontharding.*

8.4 Confocal laser scanning microscopy

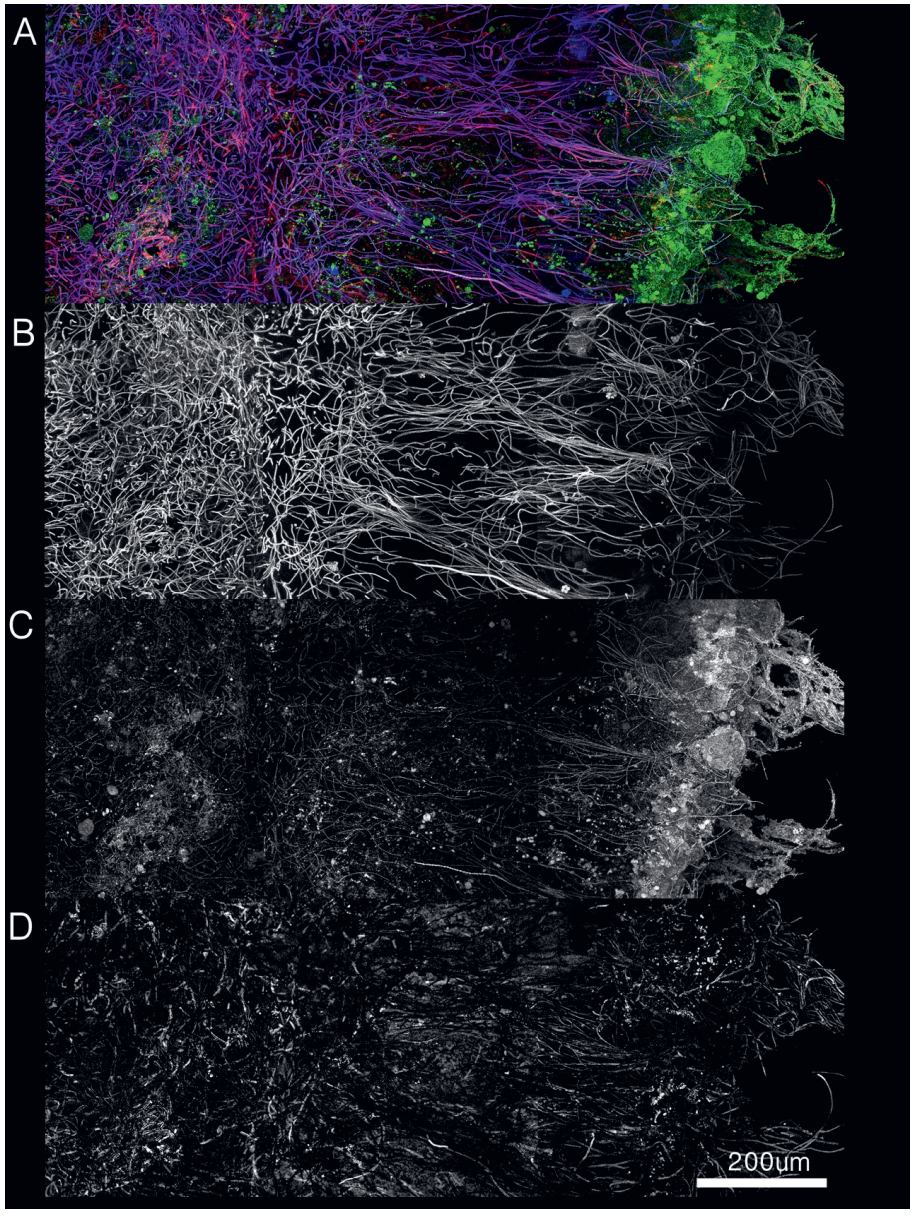

Figure S3: Magnification of the cross section shown in figure 1D. This figure should highlight some structural features e.g. the glycoconjugates, which are difficult to make out in the zoomed-out version of the same cross section. **A)** CLSM image of a photogranule cross section showing nucleic acids (green), photopigments (blue, purple) and glycoconjugates (red). **B)** The same cross section only showing the blue channel which corresponds to chlorophyll-a. **C)** The same cross section only showing the green channel which corresponds to nucleic acids stained with SYBR green. **D)** The same cross section showing the blue channel subtracted from the red channel. This corresponds to the glycoconjugates stained with the BAN lectin.

8.5 Microbial community composition

Please see table on the next page

Table S2. ASV and taxonomy table of the 16S rRNA amplicon sequencing dataset. The 20 most abundant ASV are selected and presented in relative abundance with their respective taxonomic annotation. "NA" indicates that an ASV is no assign to a specific taxonomic level.

ASV ID	Relative abundance	Kingdom	Phylum	Class	Order	Family	Genus	Species
ASV899	14.99%	Bacteria	Cyanobacteria	Cyanobacteriia	Leptolyngbyales	Leptolyngbyaceae	*Leptolyngbya*_PCC-6306	*NA*
ASV765	13.28%	Bacteria	Cyanobacteria	Cyanobacteriia	Leptolyngbyales	Leptolyngbyaceae	*Alkalinema*_CENA528	*NA*
ASV561	11.99%	Bacteria	Proteobacteria	Gammaproteobacteria	Burkholderiales	Rhodocyclaceae	*Thauera*	*aminoaromatica*
ASV113	5.75%	Bacteria	Planctomycetota	Phycisphaerae	Phycisphaerales	Phycisphaeraceae	*SM1A02*	*NA*
ASV581	4.47%	Bacteria	Cyanobacteria	Cyanobacteriia	Cyanobacteriales	Phormidiaceae	*Cephalothrix*_SAG_75.79	*komarekiana*
ASV1261	4.39%	Bacteria	Proteobacteria	Alphaproteobacteria	Tistrellales	Geminicoccaceae	*Candidatus*_Alysiosphaera	*NA*
ASV504	3.78%	Bacteria	Armatimonadota	Fimbriimonadia	Fimbriimonadales	Fimbriimonadaceae	*NA*	*NA*
ASV1324	3.03%	Bacteria	Chloroflexi	Anaerolineae	Anaerolineales	Anaerolineaceae	*NA*	*NA*
ASV579	2.60%	Bacteria	Chloroflexi	Anaerolineae	Caldilineales	Caldilineaceae	*NA*	*NA*
ASV378	2.10%	Bacteria	Cyanobacteria	Cyanobacteriia	Limnotrichales	Limnotrichaceae	*Limnothrix*	*NA*
ASV1092	2.04%	Bacteria	Proteobacteria	Gammaproteobacteria	Burkholderiales	Rhodocyclaceae	*Zoogloea*	*NA*
ASV1048	2.00%	Bacteria	Planctomycetota	Phycisphaerae	Tepidisphaerales	Tepidisphaeraceae	*Tepidisphaera*	*NA*
ASV287	1.84%	Bacteria	Planctomycetota	Phycisphaerae	Tepidisphaerales	CPla-3_termite_group	*NA*	*NA*
ASV779	1.41%	Bacteria	Planctomycetota	Phycisphaerae	Phycisphaerales	Phycisphaeraceae	SM1A02	*NA*
ASV1020	1.35%	Bacteria	Chloroflexi	Chloroflexia	Chloroflexales	Roseiflexaceae	*NA*	*NA*
ASV380	1.04%	Bacteria	Proteobacteria	Gammaproteobacteria	Legionellales	Legionellaceae	*Legionella*	*dumoffii*
ASV647	1.02%	Bacteria	Cyanobacteria	Vampirivibrionia	Obscuribacterales	Obscuribacteraceae	*Candidatus_Obscuribacter*	*NA*
ASV737	1.00%	Bacteria	Nitrospirota	Nitrospiria	Nitrospirales	Nitrospiraceae	*Nitrospira*	*NA*
ASV125	0.98%	Bacteria	Proteobacteria	Alphaproteobacteria	Rhizobiales	Xanthobacteraceae	*Bradyrhizobium*	*NA*
ASV889	0.87%	Bacteria	Proteobacteria	Gammaproteobacteria	Burkholderiales	Rhodocyclaceae	*Zoogloea*	*resiniphila*
Phototrophs	**35.87%**							
Denitrifiers	**14.91%**							
Nitrifiers	**1.00%**							
Anaerobs	**5.64%**		**Sum**	**79.96%**				

Table S3. ASV and taxonomy table of the 18S rRNA sequencing dataset. The 20 most abundant ASV are selected and presented in relative abundance with their respective taxonomic annotation. "NA" indicates that an ASV is no assign to a specific taxonomic level.

ASV ID	Relative abundance	Kingdom	Phylum	Class	Order	Family	Genus
ASV1	33.86%	Eukaryota	Chlorophyta_ph	Trebouxiophyceae	Chlorellales	Chlorellales_fa	Chlorella
ASV3	18.15%	Eukaryota	Basidiomycota	Tremellomycetes	Trichosporonales	Trichosporonaceae	*Trichosporon*
ASV2	12.67%	Eukaryota	Chlorophyta_ph	Chlorophyceae	Chlamydomonadales	Chlamydomonadales	*Chlorococcum*
ASV6	4.97%	Eukaryota	Chlorophyta_ph	Trebouxiophyceae	*NA*	*NA*	*NA*
ASV13	2.44%	Eukaryota	Chlorophyta_ph	Trebouxiophyceae	Chlorellales	Chlorellales	*Chlorella*
ASV9	2.14%	Eukaryota	*NA*	*NA*	*NA*	*NA*	*NA*
ASV10	2.01%	Eukaryota	*NA*	*NA*	*NA*	*NA*	*NA*
ASV12	1.91%	Eukaryota	*NA*	*NA*	*NA*	*NA*	*NA*
ASV11	1.81%	Eukaryota	*NA*	*NA*	*NA*	*NA*	*NA*
ASV18	1.56%	Eukaryota	Cercozoa	Incertae_Sedis	Incertae_Sedis_or	Incertae_Sedis	*Gymnophrys*
ASV14	1.53%	Eukaryota	*NA*	*NA*	*NA*	*NA*	*NA*
ASV17	1.50%	Eukaryota	*NA*	*NA*	*NA*	*NA*	*NA*
ASV16	1.49%	Eukaryota	*NA*	*NA*	*NA*	*NA*	*NA*
ASV21	1.19%	Eukaryota	Chlorophyta_ph	Chlorophyceae	Sphaeropleales	Sphaeropleales	*Botryosphaerella*
ASV24	1.13%	Eukaryota	Chlorophyta_ph	Trebouxiophyceae	*NA*	*NA*	*NA*
ASV20	1.04%	Eukaryota	*NA*	*NA*	*NA*	*NA*	*NA*
ASV26	1.00%	Eukaryota	Chlorophyta_ph	Chlorophyceae	Sphaeropleales	Sphaeropleales	*Tetradesmus*
ASV23	0.90%	Eukaryota	*NA*	*NA*	*NA*	*NA*	*NA*
ASV8	0.87%	Eukaryota	Tubulinea	Arcellinida	Echinamoebida	Echinamoebida	*Vermamoeba*
ASV28	0.79%	Eukaryota	Chlorophyta_ph	Chlorophyceae	Chlamydomonadales	Chlamydomonadales	*Chlorococcum*
Algae	**58.06%**						
Fungi	**18.15%**						
Protist	**2.44%**		**Sum**	**92.97%**			

8.6 Photopigment quantification

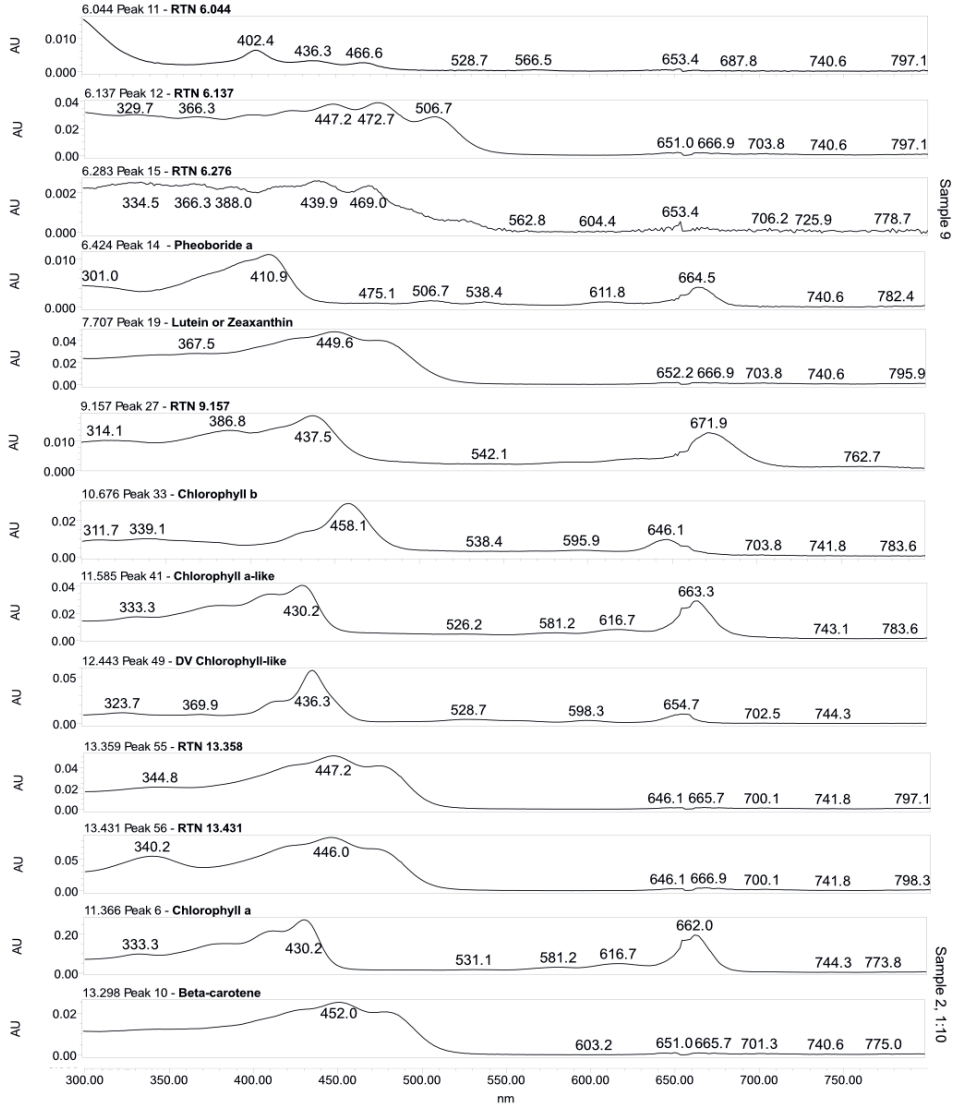

Figure S4: Pigments extracted from photogranules which were at least 1% of the total acetone-ethanol extractable pigmented material in one of 6 photogranules.

8.7 Calculations on carbon fixation rate

The measured carbon fixation rates from the ^{14}C incubations were used to calculate the total carbon fixation rate of an entire photogranule ($R_{C-fix,photogranule,total}$) in nmol N/photogranule/h. The carbon fixation rate of the "whole" photogranule

($R_{C-fix,photogranule}$) given in nmol N/mm³/h was multiplied by the volume of the photogranule (**equation S1**). In that particular the diameter of the photogranule investigated was 4 mm which resulted in a volume of 33.5 mm³.

$$R_{C-fix,photogranule,total} = R_{C-fix,photogranule} \times V_{photogranule} \quad \text{equation S1}$$

8.8 Nutrient uptake during a 12h sequencing batch

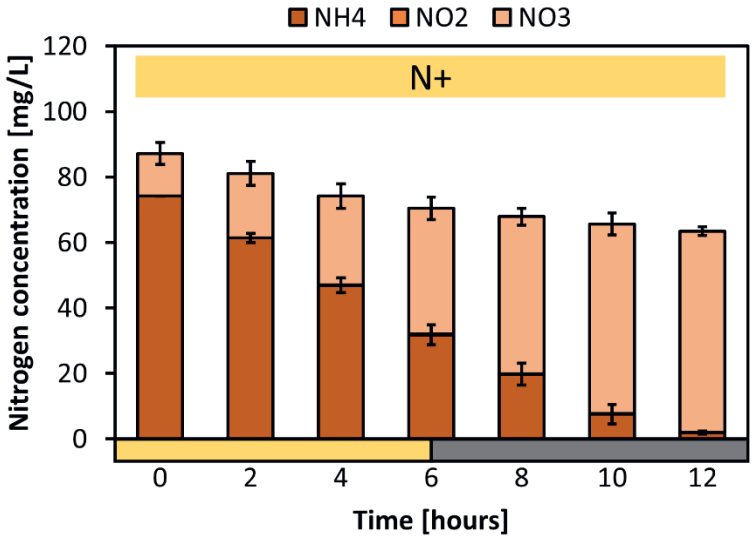

Figure S5: Nitrogen evolution over the course of a sequencing batch cycle with 6 hours light followed by 6 hours darkness. The nitrogen species depicted are ammonium (NH_4^+), nitrite (NO_2^-) and nitrate (NO_3^-). The values presented are averaged over 5 timepoints over a period of 50 days. The error bars represent the standard deviation.

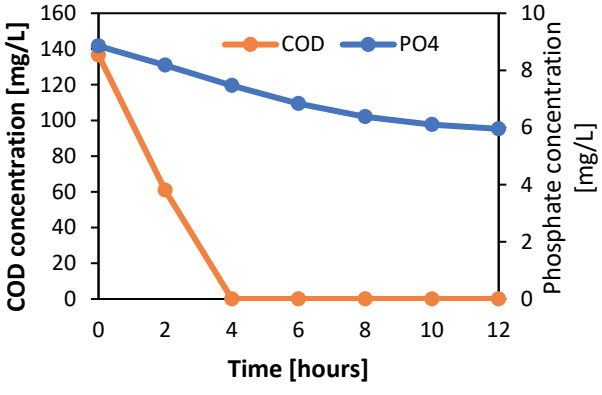

Figure S6: COD and phosphate concentration over the course of a 12-hour sequencing batch cycle. The values presented are averaged over 5 timepoints over a period of 50 days. The error bars represent the standard deviation.

8.9 Calculating overall oxygen production and consumption

The bioreactor received a total photon flux of 0.34 mol_{ph}/L/d ($I_{ph.V}$). This was calculated from averaged light measurements conducted over the entire reactor surface (0.528 $mol_{ph}/A_{reactor}$/d) divided over the reactor volume (1.6 L). When all incoming light is converted by photosynthesis to oxygen an oxygen production rate (OPR) of 13.61 mmol/L/d is obtained assuming photosynthesis to run at half of the maximal efficiency (0.04 mol-O_2/mol-photon) (Janssen, 2016):

$$OPR = I_{ph.V} * 0.04 \qquad \text{equation S2}$$

The oxygen uptake rate (OUR) is calculated according to the acetate load (R_{HAc}) and nitrification rate ($R_{NH4_{nitrification}}$) (Boelee et al., 2012; Liu and Wang, 2012):

$$5CH_3COO^- + 1NH_4^+ + 5O_2 \rightarrow C_5H_7O_2N + 3H_2O + 5CO_2 + 5OH^- \qquad \text{equation S3}$$

$$NH_4^+ + 0.0298NH_4^+ + 1.851O_2 + 0.1192CO_2 + 0.0298HCO_3^- \rightarrow 0.0298C_5H_7NO_2 + NO_3^- + 0.9702\,H_2O + H^+ \qquad \text{equation S4}$$

$$OUR = R_{HAc} + R_{NH4_{nitrification}} * 1.851 \qquad \text{equation S5}$$

Chapter 5

Enhancing phosphorus removal of photogranules by incorporating polyphosphate accumulating organisms

Lukas M. Trebuch[1,2], Jasper Sohier[1,2], Mario Pronk[3,4], Marcel Janssen[2], Louise E.M. Vet[6], René H. Wijffels[2,5], Tânia V. Fernandes[1]

[1] Department of Aquatic Ecology, Netherlands Institute of Ecology (NIOO-KNAW), Droevendaalsesteeg 10, 6708 PB Wageningen, The Netherlands

[2] Bioprocess Engineering, AlgaePARC Wageningen University, P.O. Box 16, 6700 AA Wageningen, The Netherlands

[3] Department of Biotechnology, Delft University of Technology, Van der Maasweg 9, Delft, 2629 HZ, The Netherlands

[4] Royal HaskoningDHV, Laan1914 35, Amersfoort, 3800 AL, The Netherlands

[5] Faculty of Biosciences and Aquaculture, Nord University, N-8049, Bodø, Norway

[6] Department of Terrestrial Ecology, Netherlands Institute of Ecology (NIOO-KNAW), Droevendaalsesteeg 10, 6708 PB Wageningen, The Netherlands

1 ABSTRACT

Photogranules are a novel wastewater treatment technology that can utilize the sun's energy to treat water with lower energy input and have great potential for nutrient recovery applications. The microbial community of photogranules consists of phototrophs (microalgae, cyanobacteria) and non-phototrophic microorganisms (nitrifiers, denitrifiers) that form dark-green spheroid agglomerates. Photogranules have been proven to efficiently remove nitrogen and carbon but show lower conversion rates for phosphorus compared to established treatment systems, such as aerobic granular sludge. In this study we successfully introduced polyphosphate accumulating organisms (PAOs — *Candidatus* Accumulibacter phosphatis, *Tetrashaera* ssp.) to an established photogranular culture. We operated photobioreactors in sequencing batch mode with six cycles per day and alternating anaerobic (dark) and aerobic (light) phases. We were able to increase phosphorus removal/recovery by 6 times from 5.4 to 30 mg/L/d while maintaining similar nitrogen and carbon removal compared to photogranules without PAOs. To maintain PAOs activity, alternating anaerobic feast and aerobic famine conditions were required. In future applications, where aerobic conditions are dependent on *in-situ* oxygenation via photosynthesis, the process will rely on sunlight availability. Therefore, we investigated the feasibility of the process under diurnal cycles with a 12h anaerobic phase during nighttime and six short cycles during the 12h daytime. The 12h anaerobic phase had no adverse effect on the PAOs and phototrophs. Due to the extension of one anaerobic phase to 12h the six aerobic phases were shortened by 47% and consequently decreased the light hours per day. This resulted in a decrease of phototrophs, which reduced nitrogen removal and biomass productivity up to 30%. Finally, we discuss and suggest strategies to apply PAO-enriched photogranules at large-scale.

Keywords: *Wastewater, microalgal-bacterial granules, enhanced biological phosphorus removal (EBPR), photoEBPR, microbial ecology, AGS*

GRAPHICAL ABSTRACT

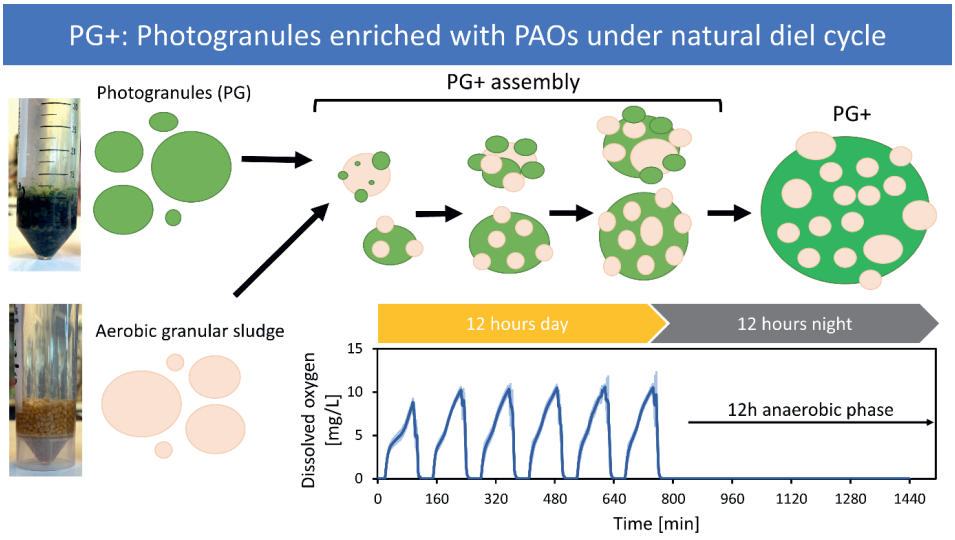

2 INTRODUCTION

Wastewater treatment must become more sustainable by applying technologies that recover energy and nutrients as well as removing pollutants. Recently, the commercialization of well-settling aerobic granular sludge (AGS) as NEREDA® has transformed biological wastewater treatment by increasing treatment capacity while decreasing the aerial footprint of the treatment plant, and saving on energy costs (M. Pronk et al., 2015) Still, AGS requires a substantial amount of mechanical aeration (consuming up to 50% of the total energy costs) and emits greenhouse gases such as CO_2 and N_2O (Brockmann et al., 2021; de Sousa Rollemberg et al., 2018; M. Pronk et al., 2015). Additionally, AGS systems are designed to convert nitrogen into N_2 rather than recovering it in the form of biomass.

An alternative to mechanical aeration is *in-situ* oxygenation via photosynthesis. In recent years, photogranules have become a promising candidate to close the CO_2 and O_2 cycles in treatment systems and thereby lower, or eliminate, the need for external aeration. The microbial community of photogranules consists of phototrophs (microalgae, cyanobacteria) and other non-phototrophic microorganisms (nitrifiers, denitrifiers) that form dark green spheroid agglomerates – the photogranule. The principal of photogranular wastewater treatment is to minimize external O_2 supply via *in-situ* oxygenation by photosynthesis and sequester CO_2 produced internally via phototrophs (Abouhend et al., 2018). Photogranule based treatment systems will be characterized by a larger footprint as the photosynthetic production of oxygen is limited by the sunlight exposed area of the treatment unit (Boelee et al., 2012). Photogranules can efficiently remove carbon and nitrogen removal but show lower phosphorus conversion rates than other established biological treatment systems (M. Pronk et al., 2015; Trebuch et al., 2020).

Enhanced biological phosphorus removal (EBPR) is a widely used strategy in conventional activated sludge (CAS) or AGS systems to increase phosphorus removal. The main contributors to phosphorus removal are polyphosphate accumulating organisms (PAOs) that can accumulate vast amounts of intracellular polyphosphate (up to 0.38 mgP/mgVSS) (Chen et al., 2020). PAOs exhibit a specialized metabolism that allows them to thrive in conditions with fluctuating nutrient levels. These organisms take up volatile fatty acids (e.g. acetate, propionate) during anaerobic conditions and store them as polyhydroxyalkanoates (PHA) (Chen et al., 2020). At the same time, polyphosphate is used as an energy source for carbon uptake and ortho-phosphate is released into the bulk liquid. Under aerobic conditions, PHA is consumed for energy and growth while nitrogen (e.g., ammonium) and phosphate is taken up. Both anaerobic

feast (COD rich) and aerobic famine (COD poor) conditions are essential for good EBPR functioning.

The combination of phototrophs and PAOs has previously been investigated in non-granular systems as photoEBPR with promising results, showing improved phosphorus removal compared to other phototrophic systems (Carvalho et al., 2021, 2018; Mohamed et al., 2021; Oyserman et al., 2017). Due to the presence of phototrophs, in some studies all required oxygen for the EBPR process could be produced *in-situ* via photosynthesis, abolishing the need for mechanical aeration (Mohamed et al., 2021; Oyserman et al., 2017). The metabolic functions within the photoEBPR process are 1) photosynthesis, 2) polyphosphate accumulation, 3) chemoheterotrophy (COD removal), 4) nitrification and 5) denitrification. Combining all functions together in one reactor system can be difficult as competition for nutrients and inhibition (e.g., by product accumulation) can adversely affect microorganisms. Competition between phototrophs, nitrifiers and PAOs for nutrients often led to suboptimal removal rates and a decrease in PAO abundance (Carvalho et al., 2018; Mohamed et al., 2021). Additionally, nitrite-oxidizing bacteria have been shown to be sensitive to light and compete with phototrophs for CO_2 (Wang et al., 2015), while PAOs are sensitive to high nitrite and oxygen concentration (Chen et al., 2020).

Granules exhibit physical and chemical gradients (e.g. light, nutrients), which facilitate stratification and spatial heterogeneity of microbial communities (Flemming and Wingender, 2010). This allows for niche differentiation and the coexistence of diverse organisms even those that feed on the same substrate, or produce metabolites that negatively affect each other (Louca et al., 2018). In the context of photoEBPR this could provide niches for all organisms helpful to wastewater treatment (phototrophs, PAOs, nitrifiers and denitrifiers) and allow them to coexist in the same reactor while expressing high conversion rates. A few studies already investigated the combination of phototrophs and AGS performing EBPR (Cai et al., 2019; Huang et al., 2015; Ji et al., 2020; Meng et al., 2019b). However, reactor operation was often not optimized for the combination of phototrophs and PAOs resulting in unstable operation and impaired removal rates compared to other AGS systems (de Graaff et al., 2020; de Kreuk et al., 2005; M. Pronk et al., 2015). Therefore, it is vital to explore strategies to effectively incorporate PAOs into photogranules, optimize operation conditions for high conversion rates and get a deeper insight into their microbial community assembly and function.

Additionally, an important aspect of light-driven processes is its dependency on the natural diel cycle of the sun. When considering a photoEBPR system with *in-situ* oxygenation, this would lead to an extended anaerobic phase during the night. At night

phototrophs would do maintenance and respire photosynthate (e.g carbohydrates) stored during the light period (Borowitzka et al., 2016). So far there are no reports on the (long-term) effect of an extended anaerobic phase on PAO performance and it is unknown if operating a photoEBPR system under a natural diel cycle is feasible. In this study, we integrated PAOs from AGS into an established PG microbial community and analysed microbial community assembly and functioning. Additionally, we investigated an operation scheme that would allow the photoEBPR process to run under natural light conditions (diel cycle) with 12h light and 12h darkness.

3 MATERIALS AND METHOD

3.1 Inoculation strategy and adaptation phase

Two different types of biomasses were used for inoculation: 1) Photogranules (PG) and 2) aerobic granular sludge (AGS) performing EBPR. PG were obtained from previous research (Trebuch et al., 2020). AGS originated from the research of de Graaff et al. (2020). Both types of granules were adapted to the experimental conditions for 28 days prior to the start of the actual experiment. This adaptation phase was carried out to assure that the microbial community was well adapted to the nutrient load, salinity, pH, and temperature used during the experimental phase.

During the experimental phase three bioreactors were operated in parallel with different inocula. 1) The first bioreactor, termed PG1, received homogenized photogranules and intact AGS in equal weight proportions (homogenization by a Miccra D9 Homogeniser; Miccra GmbH, Heitersheim, Germany). 2) The second bioreactor, termed PG2, received both intact photogranules and AGS in equal weight proportions. 3) The third bioreactor was operated with intact AGS, which served as a benchmark for phosphorus removal via EBPR.

3.2 Bioreactor set-up and operation

Three glass bubble column bioreactors with a diameter of 10cm, a total height of 28 cm and a working volume of 1.6L were used (**figure S1**). All three bioreactors were operated as sequencing batch reactors (SBRs) employing six cycles per day. During the co-cultivation phase of photogranules and AGS, one cycle consisted of anaerobic influent feeding (5min) and reaction (70min), aerobic reaction (150min), settling (5min), effluent removal (3min), and nitrogen sparging (7min). The co-cultivation phase lasted for 56 days.

Mixing of the bioreactor content was achieved via gassing with nitrogen (N_2) during the anaerobic phase and with air during the aerobic phase both enriched with 5%w/w

CO_2. In both phases a gas flowrate of 0.5L/min was maintained via mass flow controllers. Prior to feeding, the bioreactor content was sparged with N_2 gas for 7 min to remove residual O_2 and to ensure anaerobic conditions. The bioreactor temperature was kept at 20±0.5ºC and the pH was kept at 7.25 ± 0.1 by addition of 1M HCl or 1M NaOH. Bioreactor PG1 and PG2 were illuminated during the aerobic phase with three warm white LED panels each. The light sources were placed at three sides of the bioreactor, with 90° between panel 1 and 2, 90° between panel 2 and 3 and 180° between panel 3 and 1. The average incident light intensity measured over the whole bioreactor surface was 170 μmol/m^2/s, with a total light input of 0.43 mol/L/day (15h light per day). The detailed spectrum of the LED light source can be found in the supplemental materials (**figure S2**).

Synthetic wastewater was prepared by mixing tap water with 10 mL/L of stock A and 10 mL/L of stock B. Stock A consisted of 42.80 g/L sodium acetate trihydrate, 1.09 g/L KH_2PO_4 and 4.20 g/L K_2HPO_4. Stock B consisted of 6.84 g/L NH_4Cl, 7.50 g/L $MgSO_4.7H_2O$, 3.60 g/L $CaCl_2.2H_2O$, 3.50 g/L KCl and 100mL/L of trace element solution prepared according to Vishniac and Santer (1957) with 2.2 g/L of $ZnSO_4.7H_2O$ instead of 22 g/L. The concentrations of major constituents of the final synthetic wastewater were: 18 mg/L of nitrogen, 10 mg/L phosphorus and 200 mg/L of COD.

After 6 weeks (day 14 – 56) of stable C, N and P removal, the efficiencies of all bioreactors one of the anaerobic phases was extended to 12 hours (720min) while maintaining an aerobic phase of 80 min. The other five cycles had equal anaerobic phases of 40 min and aerobic phases of 80 min. The length of the light period in PG1 and PG2 was adjusted to the aerobic phases and was therefore shorter. The overall light input was reduced from 15 h/day to 8 h/day and thereby to 0.23 mol/L/day. The extension of the anaerobic phase was done gradually over one week. It was first extended from 60 to 180 min, with subsequent extension to 350, 530 and 690 min, until finally to 720min. The bioreactors were operated for an additional 3 weeks with a 12-hour anaerobic phase.

Throughout the whole experiment a hydraulic retention time (HRT) of 0.33 days was applied. The solids retention time (SRT) was maintained at 14 days by daily removal of 114mL of mixed liquor. The nutrient load was 55 mg/L/d of nitrogen, 30 mg/L/d of phosphorus, and 600 mg/L/d of COD.

3.3 Analytical methods

During the experiment, liquid samples were taken from the influent and the effluent of the bioreactors to study the nutrient removal. In addition, a liquid sample was taken

at the end of the anaerobic phase. Once a week, one or two cycles were sampled in 5- or 10-min intervals to gain more insight in conversion kinetics. All liquid samples were filtered through 0.2 μm syringe filters (PES membrane, VWR) and analysed for ammonium (NH_4^+-N), nitrite (NO_2^--N), nitrate (NO_3^--N), and phosphate (PO_4^{3+}-P) with a Skalar SAN^{++} autoanalyzer (Skalar Analytical B.V., Breda, The Netherlands) according to standard methods (APHA/AWWA/WEF, 2012). Acetate was measured by high-performance liquid chromatography (HPLC) with a Hi-Plex H anion exchange column, with a particle size of 8 μm, a length of 300 mm and an inner diameter of 7.7 mm (Agilent Technologies, Santa Clara, US). The column temperature was 50 °C, the eluent was 100% 0.01 M Sulfuric acid, and the flow was 0.6 mL/min. A UV detector was used to detect the acetate and was set to 210 nm. For rapid testing of the liquid samples for PO_4^{3+}-P the PhosVer 3 kit (Hach, Loveland, US) was used. Total suspended solids (TSS), volatile suspended solids (VSS), and sludge volume index (SVI) were assessed according to standard methods (APHA/AWWA/WEF, 2012).

3.4 Biomass characteristics and morphology

The elemental composition of homogenized freeze-dried biomass was measured. For C and N analyses an aliquot (about 2mg) was folded into a tin cup and analysed in an organic elemental analyser (Flash 2000, Interscience Breda). Cellular P was analysed by combusting an aliquot (about 2mg) for 30min at 550°C in Pyrex glass tubes, followed by a digestion step with 10 mL persulfate (2.5%) for 30 min at 121°C. The digested solution was measured for PO_4^{3-}-P on the Skalar SAN^{++} autoanalyzer (Skalar Analytical B.V., Breda, The Netherlands).

Chlorophyll was extracted with ethanol (100%) from biomass samples from PG1 and PG2 according to the protocol of Cuaresma Franco et al. (2012). Per analysis, three times 5 mL of mixed liquor from the end of the aerobic phase was transferred into a 15 mL light-blocking centrifuge tube (VWR) and subsequently centrifuged at 5000 RPM for 10 minutes. The supernatant was discarded, and the pellet was stored in a freezer at –18 °C until the extraction was performed. The full extraction protocol can be found in the supplemental materials. To improve the extraction of chlorophyll from the pellet, a metal ball (1mm) was added to each tube to allow for additional disruption of the pellet during vortexing and sonication steps. After the chlorophyll was extracted from the pellets, the concentrations of chlorophyll *a* and *b* were measured in spectrophotometrically using a quartz cuvette with a pathway of 1 cm. The absorbance at 652 nm and 665 nm was measured to quantify chlorophyll *a* and *b*. For optimal readings, the absorbance at 665 had to range between 0.2 and 0.8 and extracts were

diluted accordingly. The final concentrations of chlorophyll *a* and *b* in the extracts were calculated using Equations 1-3, based on Lichtenthaler (1987) (supplemental materials).

Biomass samples were observed via a Leica M205C stereomicroscope (Leica Camera AG) to assess granule morphology, and the integration of photogranules and AGS. Images were taken using the Leica Application Suite v4.13. Additionally, biomass samples or individual granules were fixed in 4% formaldehyde diluted in 1x PBS and stored at 4 °C for future analyses. Photogranule size was determined by analysing multiple microscopic images per sample (with a total of at least 400 particles) using ImageJ (Milferstedt et al., 2017b; Schindelin et al., 2012).

3.5 Microbial community assessment and functional annotation

From each timepoint samples were taken to assess the microbial community. DNA extraction from each time point was conducted in triplicate. Specifically, 15 mL of harvested sludge was centrifuged at 5500 rpm and the supernatant discarded. The cell pellets were immediately frozen at -80 °C until further processing. DNA was extracted using the DNeasy PowerSoil Pro Isolation Kit (Qiagen GmbH, Hilden, Germany). The quantity and quality of DNA were spectrophotometrically determined with a NanoDrop One (ThermoFisher Scientific, USA). The DNA samples were submitted for sequencing to Génome Québec (MacGill University, Montreal, CA). The 16S rRNA gene V3/V4 variable region was amplified using primer pair 341F (CCTACGGGNGGCWGCAG) and 805R (GACTACHVGGGTATCTAATCC) (Herlemann et al., 2011). The 18S rRNA gene V4 variable region was amplified using the primer pair 616*F (TTAAARVGYTCGTAGTYG) and 1132R (CCGTCAATTHCTTYAART) (Hugerth et al., 2014). Both sets of primers were modified to add Illumina adapter overhang nucleotide sequences to the gene-specific sequences. Sequencing was performed using an Illumina MiSeq system (Illumina MiSeq, USA) with 300-bp reads (v3 chemistry). The obtained sequences were processed with DADA2 (Callahan et al., 2016). Taxonomic alignment of the sequences was done against the SILVA database (release 138) using SINA (https://www.arb-silva.de). The 16S and 18S dataset was normalized using the cumulative sums scaling (CSS) function of the R package *metagenomSeq* version 1.24.1 (Paulson et al., 2013). The analysis of the microbiome data was performed with the R-package phyloseq (version 1.26.1) (McMurdie and Holmes, 2013) and ampvis2 (version 2.7.4) (Andersen et al., 2018). The community structure and the change through time of the 16S and 18S dataset were analysed by Principal Coordinate Analysis (PCoA) using weighted UniFrac distance (Lozupone et al., 2011).

The 16S dataset was annotated with functions using the tool FAPROTAX (Louca et al., 2016). The default database of FAPROTAX was extended with taxa functionally annotated within the MiDAS database (version 4.8.1) (Nierychlo et al., 2020). It is important to note that several functions can be annotated to one single taxon and consequently sum of the functional distribution can exceed 100%. A complete list of all functions considered can be found in the supplemental materials.

4 RESULTS

4.1 Assembly of PG+: photogranules enriched in polyphosphate accumulating organisms

In this study we successfully combined photogranules (PG) with aerobic granular sludge (AGS) to form PG enriched with PAOs, named PG+. PG+ were operated as a phototrophic - enhanced biological phosphorus removal (photoEBPR) system. To investigate the assembly of PG+, two different inoculation strategies were tested: 1) PG were mechanically homogenized and co-cultivated with intact AGS (referred to as PG1). 2) Both PG and AGS were kept intact and co-cultivated (referred to as PG2). The co-cultivation phase lasted for 56 days and the assembly of the PG+ was followed via microscopic observations (**figure 1**).

The first PG+ appeared in both PG1 and PG2 after one week of cultivation. They arose among intact native PG (in PG2) and AGS. Within 2-3 weeks of operation, the bioreactors were completely dominated by PG+. Most PG+ were in the range of 0.8 - 1.4mm in diameter with a maximum of 1.8mm. The morphology of PG+ was generally characterized by an interwoven network of cyanobacteria with cauliflower shaped aggregates of PAOs in between (white areas on surface) (**figure 1**). While the PG+ morphology of PG1 and PG2 was similar, two modes of assembly could be identified depending on the size and morphology of the initial PG and AGS. These modes were postulated to be important within the life cycle of PG+ as well.

In the first mode of assembly, especially in the PG1 treatment, AGS were colonized by the homogenized microbial community of PG and were gradually overgrown by phototrophic organisms (**figure 1 upper path**). Over time, the phototrophs covered the whole surface and formed a thick mat with PAO colonies protruding the surface. This eventually resulted in the typical PG+ morphology. The second mode of assembly was PG being colonized by small to medium sized AGS (**figure 1 lower path**). Over time, the AGS were incorporated into the PG and finally formed mature PG+ similar to the ones obtained via the first mode of assembly. The incorporation process of AGS might have been facilitated by motile filamentous cyanobacteria that can contribute to

the catchment of small particles (i.e., micro colonies of AGS) and entangle them within the PG+ structure by locomotion.

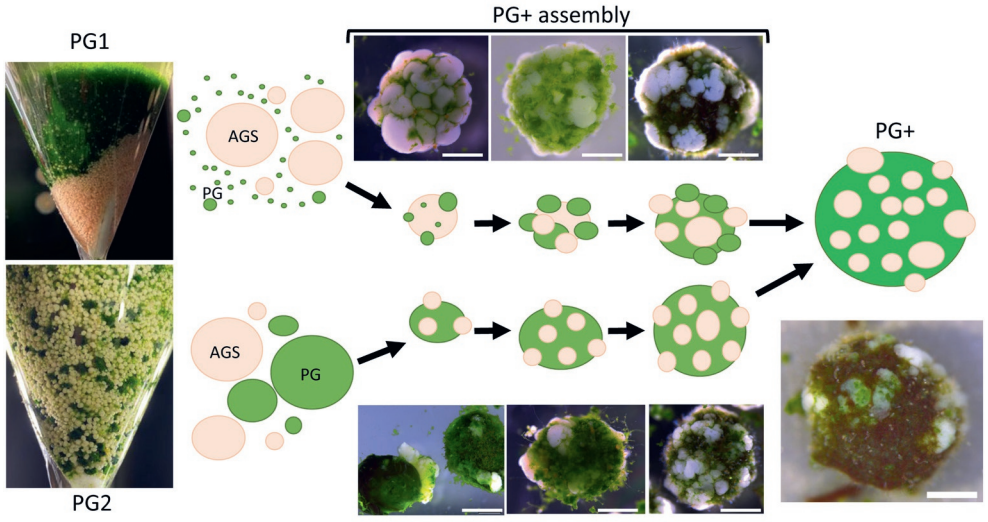

Figure 1: Schematic representation of PG+ assembly. Photogranules (PG) and aerobic granular sludge (AGS) were co-cultivated for 56 days and the incorporation of both types of granules into the hybrid granule PG+ were followed via microscopy. The white bar in the microscopic images is a scalebar of 500µm. Two different starting inoculants were used: PG1) Homogenized PG and intact AGS. PG2) Intact PG and intact AGS. Two main modes of PG+ assembly were postulated: 1) AGS are gradually overgrown by the microbial community of homogenized photogranules or small PG attaching to the surface of the AGS (upper path). 2) Both PG and AGS are intact, and the surface of the PG are gradually colonized with small sized AGS (lower path).

Both modes described above were found to occur in both systems (PG1 and PG2) in various degrees. The initial size of the PG and AGS determined which mode was dominant. In PG1 the first mode was predominant in the start-up phase, since homogenized PGs easily settled on AGS and there were no intact large PGs which AGS could colonize. After some time, both modes became important as PG+ grew larger in size. In PG2 both modes were present at the same time and both small PG colonized AGS or small AGS colonized PG.

4.2 Bioreactor performance of PG+ and AGS

During the co-cultivation phase, all three bioreactors (PG1, PG2, AGS) were operated with 6 cycles per day with 70min of anaerobic (dark) and 150 min of aerobic (light) phase. Despite the different inoculation strategies of PG1 and PG2 their performance during steady state was similar, reaching full removal of nitrogen, phosphorus, and COD already after one week of operation (53±1 mgN/L, 29.9±0.5 mgP/L and 600 mgCOD/L/d) (**figure S9**). Phosphorus release and reuptake dynamics

were similar in all three bioreactors with maximum release concentrations of about 60 mgP/L (**figure 2A-C**), while AGS showed the highest specific phosphorus release with 25 mgP/gVSS compared to 10 and 12 mgP/gVSS for PG1 and PG2. The acetate was quickly consumed in all three bioreactors at similar rates. Ammonium concentrations were relatively stable during the anaerobic phase and ammonium was primarily consumed during the aerobic phase. All three bioreactors showed excellent settling properties with average SVI values from day 10 to day 56 of 49±3 mL/g (PG1), 52±3 mL/g (PG2) and 42±3 mL/g (AGS) (**figure S5**), and average effluent concentrations of 24±15 mgTSS/L (PG1), 67±72 mgTSS/L (PG2) and 15±3 mgTSS/L (AGS) (**figure S4**).

The main differences between PG+ and AGS were the nitrogen removal, nitrification dynamics, biomass productivity, phosphorus content of the biomass specific phosphorus release and oxygen dynamics (**figure 2A- F**). Both PG1 and PG2 showed full nitrogen removal, while AGS only achieved 50-60% removal. This is mainly due to the low nitrification capacity (possibly limited by oxygen) and lower biomass productivity of AGS compared to PG1 and PG2 (**figure 2D**). The phototrophs in PG1 and PG2 could make use of light energy and consequently had double the biomass productivity. This was also evident in the 2-3x higher biomass concentration, 5.9±0.5 gVSS/L in PG1 and 5.2±0.5 gVSS/L in PG2, compared to 2.2±0.2 gVSS/L in AGS (**figure S3**). Due to the difference in biomass concentration despite similar bioreactor performance, the specific removal rates for COD and P observed for PG1 and PG2 were also 2-3x lower compared to in AGS (**figure S10-14**). The phosphorus content in the biomass of AGS was more than double (12.3 %w/w) compared to in PG1 and PG2 (4.6 %w/w) (**figure 2D**). Overall PG+ showed 4-5x higher phosphorus recovery potential than native PG, which exhibited about 1 %w/w of phosphorus in their biomass.

AGS showed nitrification activity of maximumly 5 mgN/L/d (3.3 mgN/gVSS/d), which helped with ammonium removal but not with overall nitrogen removal. Denitrification may have occurred but was not investigated in this study. The dissolved oxygen (DO) concentration during the aerobic (light) phase increased for both PG1 and PG2 in a similar fashion and reached a maximum concentration of about 12 mg/L at the end of the phase. For AGS the DO increased over the course of the aerobic phase and peaked at around 6 mg/L. This was a clear difference due to the *in-situ* oxygenation via phototrophs in PG1 and PG2. In all three bioreactors the DO rose further once all phosphorus was taken up, suggesting reduced respiration by PAOs and other heterotrophs.

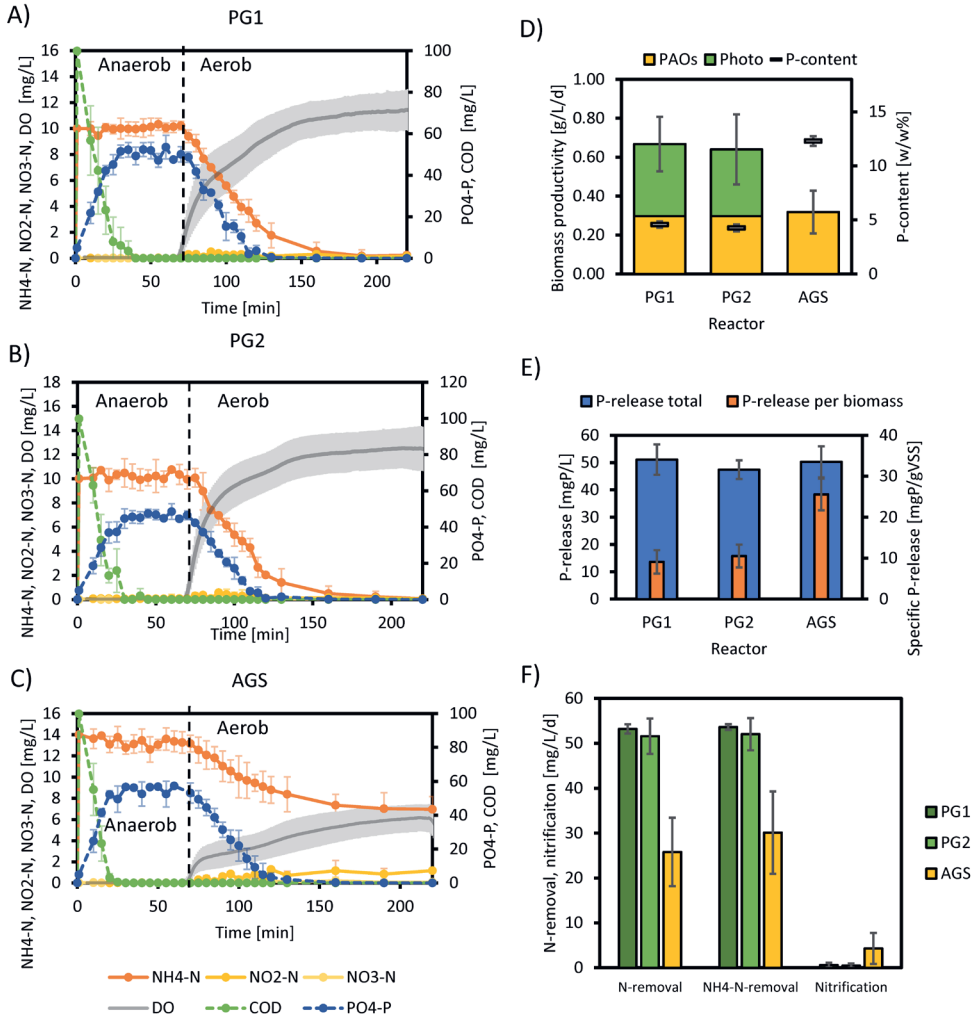

Figure 2: Bioreactor performance of PG1, PG2 and AGS during the co-cultivation phase from day 0 to day 56. In panel A, B and C the dynamics of ammonium (NH4-N), nitrite (NO2-N), nitrate (NO3-N), phosphate (PO4-P), COD and dissolved oxygen (DO) during one sequencing batch cycle are shown for PG1 **(A)**, PG2 **(B)** and AGS **(C)**. One sequencing batch cycle consisted of a 70 min anaerobic phase and a 150 min aerobic phase. The values represented are averages of 8 cycles. **D)** Average biomass productivity of PG1, PG2 and AGS with corresponding elemental phosphorus content of the biomass. The biomass productivity of PG1 and PG2 is divided into phototrophic and PAO biomass productivity based on theoretical calculations. **E)** Total phosphorus release and specific phosphorus release shown for PG1, PG2 and AGS. **F)** Average total inorganic nitrogen (TIN), ammonium (NH4-N) removal and nitrification rates of PG1, PG2 and AGS. The error bars in all figures represent the standard deviation of measurements.

4.3 The effect of a 12h anaerobic phase on PG+ and AGS systems

To test the PG+ performance under natural light conditions, we extended one of the anaerobic cycles to 12h, thus simulating the night in a diurnal cycle. We applied six feast-famine cycles in the remaining 12 hours. To summarize, one cycle of a 720 min anaerobic (dark) and a 80 min aerobic (light) phase, and five cycles of a 40 min anaerobic (dark) and a 80 min aerobic (light) phase were used.

The overall light input decreased by 47 % from 0.43 mol/L/d during the co-cultivation phase to 0.23 mol/L/d because the inclusion of the 12h anaerobic (dark) phase required shortening of the aerobic (light) phases to preserve the feast-famine regime throughout the rest of the cycle. The reduction of the light input resulted in an equivalent decrease in phototrophic biomass productivity and a decrease in the biomass concentration over time (**figure S3**). Thereby the overall nitrogen assimilation also decreased (**figure 3D**). In PG1 and PG2 the overall nitrogen removal was reduced by 12-16%, even though both bioreactors demonstrated full removal during the co-cultivation phase. Ammonium was mainly consumed during the aerobic phase and concentrations were stable for the 12-hour anaerobic phase. Similar to AGS, PG1 established an active nitrifying community which contributed to full ammoniacal nitrogen removal. The nitrifying activity was low and comparable to the one of AGS, with 5 mg/L/d turned over. PG2 had only marginable conversion of ammonium into nitrite or nitrate and thereby did not show full ammoniacal nitrogen removal. Generally, AGS was not affected by the change in operation conditions and maintained similar biomass productivity, biomass concentration and specific removal rates to that seen during the co-cultivation phase (**figure 3**, **figure S10-14**). As before, AGS did not show full ammonium removal.

The maximum DO concentration in all three bioreactor was lower than during the co-cultivation phase due to the shortened aerobic (light) phase (**figure 3**). PG1 and PG2 reached maximum DO concentrations of about 10 mg/L, while AGS only went up to around 2 mg/L. As previously observed, the DO increased more rapidly once all phosphorus was taken up completely (**figure 3A-C**). The DO profile was identical for the 5 short cycles but lower for the aerobic (light) phase immediately after the 12h anaerobic phase (**figure 3G**). This could be attributed to a lower activity of phototrophs (producing O_2), directly after the 12h anaerobic phase.

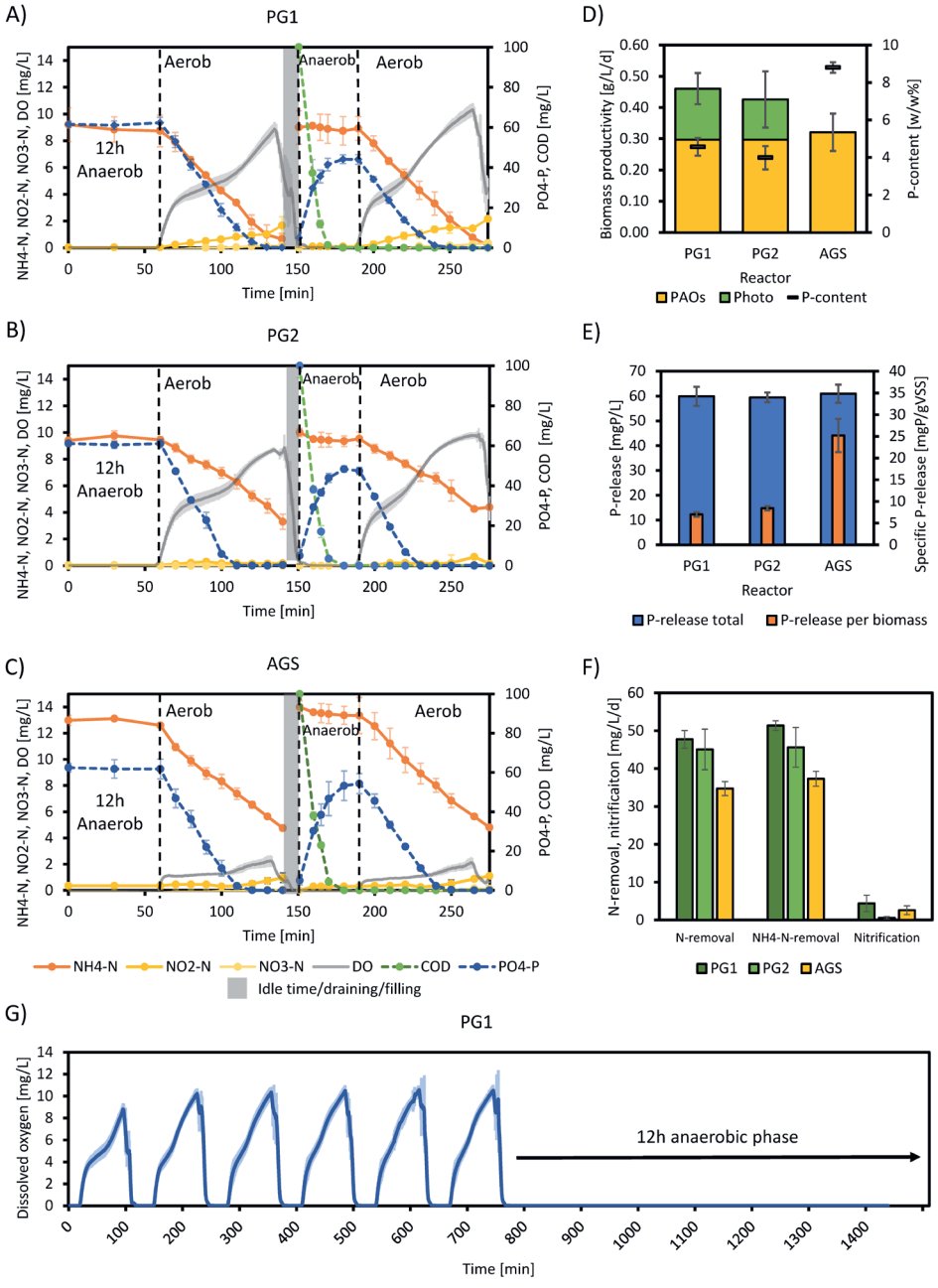

Figure 3: caption see next page

Figure 3: Bioreactor performance of PG1, PG2 and AGS during the 12h anaerobic phase from day 56 to day 80. In panel A, B and C the dynamics of ammonium (NH_4-N), nitrite (NO_2-N), nitrate (NO_3-N), phosphate (PO_4-P), COD and dissolved oxygen (DO) during one sequencing batch cycle are shown for PG1 **(A)**, PG2 **(B)** and AGS **(C)**. Five sequencing batch cycles consisted of a 40 min anaerobic phase and an 80 min aerobic phase, while one cycle had a 720 min (12h) anaerobic phase and a 120 min aerobic phase. The graphs shown are from the last 60min of the 12h anaerobic phase and the subsequent cycle consisting of a 40min anaerobic phase and a 120 min aerobic phase. The grey area between aerobic and anaerobic phase indicates draining and filling of the bioreactor. The values represented are averages of 4 cycles. **D)** Average biomass productivity of PG1, PG2 and AGS with corresponding elemental phosphorus content of the biomass. The biomass productivity of PG1 and PG2 is divided into phototrophic and PAO biomass productivity based on theoretical calculations. **E)** Total phosphorus release and phosphorus release per amount of biomass shown for PG1, PG2 and AGS. **F)** Average total inorganic nitrogen (TIN), ammonium (NH_4-N) removal and nitrification rates of PG1, PG2 and AGS. The error bars in all figures represent the standard deviation of measurements. **G)** Average DO concentration over 24h from day 56 to day 80.

Phosphorus release and reuptake dynamics were almost identical for all three bioreactors and comparable to the co-cultivation phase. Interestingly, the release during the 12-hour anaerobic phase (max. 62 mg/L of phosphorus) was higher than in the subsequent 40 min anaerobic phases (max. 54 mg/L of phosphorus) (**figure 3A-C**). Still the total phosphorus removal was complete in all three bioreactors. The specific phosphorus release of AGS stayed almost equal releasing 24 mgP/gVSS compared to 25 mgP/gVSS during the co-cultivation phase. The specific phosphorus release rate for PG1 and PG2 was lower, releasing 7 and 8 mgP/gVSS compared to 10 and 12 mgP/gVSS during the co-cultivation phase (**figure 2E and figure 3E**). The SVI of PG1 and PG2 increased slightly to 52±5 mL/g and 55±4 mL/g, while the SVI of AGS decreased to 36±1 mL/g (**figure S5**). Average biomass concentrations in the effluent of all three bioreactors were similar at about 20 mg/L (**figure S4**).

4.4 Microbial community analysis and functional annotation

During the co-cultivation phase and the extension of the anaerobic phase to 12 hours, chlorophyll-a and chlorophyll-b were measured as an indication of the fraction of phototrophic biomass **(figure 4)**. PG1 and PG2 had different starting chlorophyll concentrations (PG1 = 23 mg/gVSS and PG2 = 18 mg/gVSS) but converged at the end of the co-cultivation phase to about 28 mg/gVSS. Chlorophyll content of PG1 stabilized in the last 4 weeks of the co-cultivation phase (week 6-9), while in PG2 the chlorophyll content continued to increase until week 9. The extension of one anaerobic phase to 12 hours had a strong effect on the phototrophic community. The light input was reduced by 47% and that led to a decrease of the phototrophic biomass fraction of 40-50% during the last 3 weeks of operation.

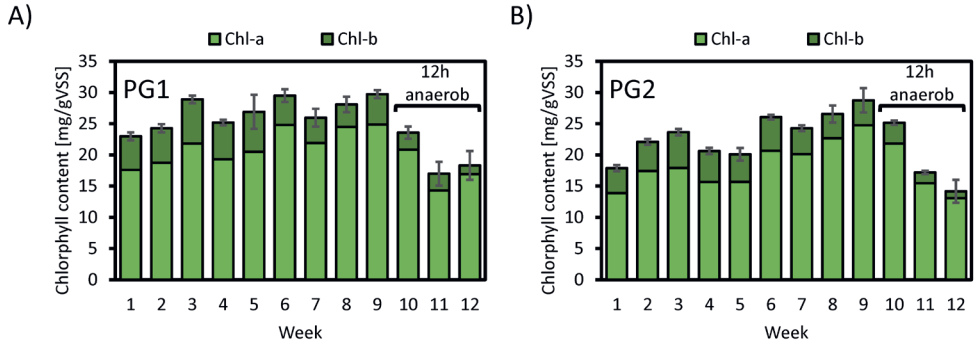

Figure 4: Chlorophyll-a and chlorophyll-b content per amount of biomass (VSS) for PG1 (A) and PG2 (B). The average chlorophyll-a and chlorophyll-b content is displayed per week of operation. In the last 3 weeks the bioreactor operation was changed to a 12h anaerobic (dark) phase.

The microbial community of PG, PG1, PG2 and AGS was analysed both with 16S and 18S rRNA gene amplicon sequencing. When looking from the inoculum to the end of the experiment the prokaryotic community converged for PG1 and PG2 in the last three sampling points, showing the strong selective effect of operating the bioreactors as photoEBPR (**figure 5**). The photogranular inoculum consisted of a diverse prokaryotic community of several cyanobacteria (e.g. *Cephalothrix komarekiana* SAG_75.79, *Alkalinema pantanalense* CENA528, *Leptolyngbya boryanum* PCC-6306, *Pseudanabaena biceps* PCC-7429) and chemoheterotrophic organisms (e.g. *Thauera* sp., *Zoogloea* sp., *Prosthecobacter* sp. and *Shinella* sp.) (**figure S16**). At the end of the co-cultivation phase (day 53) and 12-hour anaerobic phase the community was simplified (day 67 and 79) (**figure S15**). *Alkalinema pantanalense* CENA528 became the dominant filamentous cyanobacteria and most abundant prokaryotic organism in PG1 and PG2, while the abundance of chemoheterotrophs *Thauera* sp. and *Zoogloea* sp. were below 1%. *Candidatus* Accumulibacter sp. *and Tetrasphaera* sp. became the dominant PAOs making up about 52% in AGS and 7-15% in PG1 and PG2 after enrichment. Other PAOs such as *Dechloromonas* sp. and *Halobacter* sp. were also present in all three bioreactors but in low abundance (1-3%). Nitrifiers (*Candidatus* nitrotoga and *Nitrosomonas* sp.) were abundant in small amounts (below 1%) in all three bioreactors, with AGS and PG1 as the only two bioreactors showing nitrifying activity.

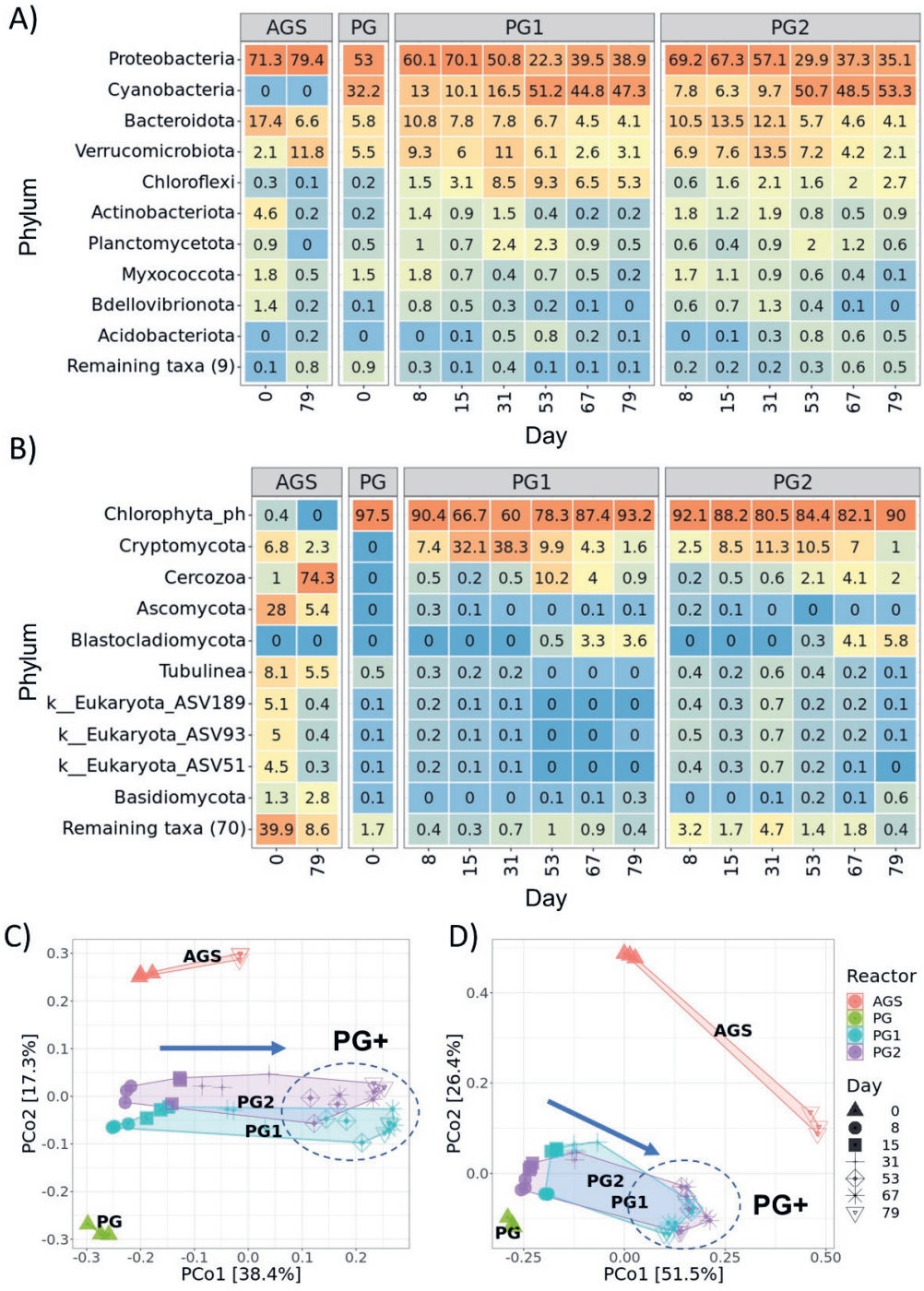

Figure 5: caption see next page

Figure 5: Microbial community composition of PG, PG1, PG2 and AGS assessed with 16S rRNA gene **(A)** and 18S rRNA gene **(B)** amplicon sequencing displayed from the inoculum (day 0), co-cultivation phase (day 8-53) and 12h anaerobic phase (day 67 and 79). The abundance of the top 10 phyla is presented as the average of biological replicates. The remaining phyla are summarized as "remaining taxa". Most phyla from the 18S dataset were unclassified and ASVs are presented instead. A principal coordinate analysis (PCoA) using weighted UniFrac distance of the raw data is shown (without averaging biological replicates) for 16S **(C)** and 18S **(D)**.

The eukaryotic community in PG1 and PG2 was characterized by green algae (*Botryosphaerella* sp., *Chlorella* sp., *Chlorococcum* sp. and *Desmodesmus* sp.) (**figure 5B**). Similar to the prokaryotic community the eukaryotic algal community started off more diverse and converged to a simplified community, with *Chlorella* sp. and *Desmodesmus* sp. as dominant green algae at the end of the co-cultivation phase (**figure 5D,F**). Next to eukaryotic algae, other organisms such as amoeba, rotifers and fungi were detected in PG1 and PG2 (2-11%). The eukaryotic community of AGS was characterized by only amoeba, rotifers and fungi, and an absence of eukaryotic algae.

The functional annotation of the 16S dataset revealed different distributions of functions for AGS, PG, PG+ and PG+ (12h). AGS was strongly dominated by PAO (54%), nitrification (1%) and denitrification (55%) while PG was characterized by photosynthesis (48%), chemoheterotrophy (52%), nitrification (0.2%) and denitrification (7%) (**figure 6**). The hybrid granule PG+ showed photosynthesis (58%), PAO (10%), chemoheterotrophy (36%), nitrification (1%) and denitrification (10%). When extending one anaerobic phase to 12 hours in PG+(12h) photosynthesis was reduced by 4% and glycogen accumulating organisms (GAO) activity started to appear with 21% of organisms performing glycogen accumulation.

The reduction in total chlorophyll is not in line with the reduction observed in the phototrophic community obtained by 16S and 18S rRNA gene amplicon sequencing and functional annotation. While total chlorophyll measurements indicated a reduction by 40-50%, according to functional annotation the phototrophic community only reduced by 4%. Since the 18S dataset was not included in the functional annotation this excludes the eukaryotic phototrophs. Still a strong decrease in the phototrophic community cannot be seen in either the 16S or 18S dataset (**figure 5 A,B**).

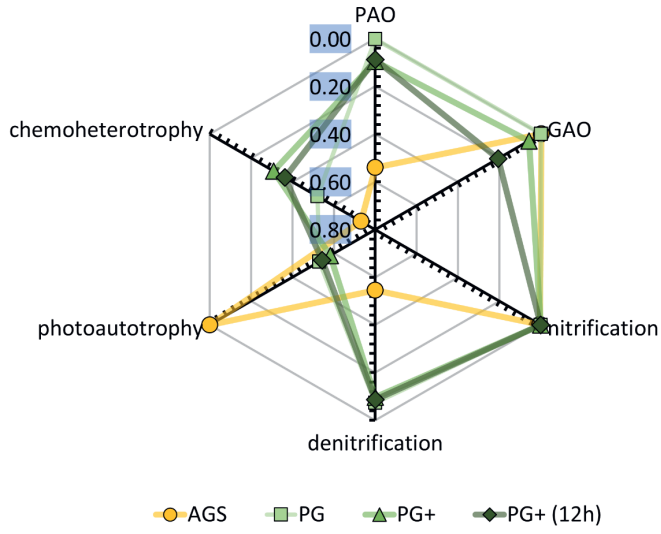

Function	Nr. Taxa (Nr. Genus)	Representatives
PAO	46 (6)	*Tetrasphaera*, *Candidatus Accumulibacter*, *Dechloromonas*
GAO	39 (3)	*Candidatus Competibacter*, *Candidatus Contendobacter*
Nitrification	5 (3)	*Candidatus Nitrotoga*, *Nitrosomonas*, *Nitrosomonadaceae oc32*
Denitrification	62 (7)	*Candidatus Accumulibacter*, *Thauera*, *Zoogloea*
Phototrophy	56 (7)	*Cephalothrix* SAG_75.79, *Alkalinema* CENA528, *Leptolyngbya* PCC-6306, *Pseudanabaena* PCC-7429
Chemoheterotrophy	248 (68)	*Candidatus Accumulibacter*, *Thauera*, *Zoogloea*

Figure 6: Radar plot of functional attribution of 16S rRNA gene sequences found in AGS, PG, PG+ and PG+ with a 12-hour anaerobic phase (PG+(12h)). The functions were assigned using FAPROTAX. The default database of FAPROTAX was extended by functional annotations provided by MiDAS. Functions are assigned according to taxonomy, where one taxon can have multiple functions. Therefore, the functional annotation can exceed 1.0 (or 100%). For visualization reasons the axis of the plot is inverted, where the 0-point is at the edge and the maximum value in the centre. In the table below the functions considered, the number of attributed taxa and the most prominent representatives are listed.

5 DISCUSSION

5.1 PG+ assembly and granule morphology

Biofilm structures such as granules are largely determined by substrate concentration gradients at the biofilm-liquid interface, the detachment forces working on the biofilm (hydrodynamic shear), the biomass yield and extracellular polymeric substance (EPS) production (Loosdrecht et al., 1997). The key for AGS formation was the introduction of an anaerobic feeding phase followed by an aerobic reaction phase. In this operation scheme, PAOs and GAOs incorporate COD anaerobically as storage polymers (PHA) and grow on these aerobically. That yields a lower aerobic growth rate compared to heterotrophic bacteria, but results in dense and sturdy biofilms (de Kreuk and van Loosdrecht, 2004). The granulation further relies to some extent on hydrodynamic conditions in sequencing batch reactors or plug flow reactors, where shear force can determine granule morphology (Nancharaiah and Kiran Kumar Reddy, 2018).

Photogranule formation was proven to work differently and is not necessarily dependent on specific operation schemes. Motile filamentous cyanobacteria govern photogranulation by the generation of extracellular polymeric substances (EPS) and locomotive entanglement (Milferstedt et al., 2017b; Trebuch et al., 2020). This has been shown to work both in hydrodynamic conditions in sequencing batch reactors and also in static incubations, confirming that external drivers such as hydrodynamic shear, washout, and fluctuating chemical conditions are not necessary for photogranulation (Gikonyo et al., 2021; Milferstedt et al., 2017b).

PG+ assembled rapidly from a diverse and species rich inoculum of PG and AGS and showed full treatment capacity 1-2 weeks after inoculation. The interplay of filamentous cyanobacteria (i.e., *Alkalinema pantanalense* CENA528) forming a complex network and AGS (i.e., PAOs) forming cauliflower shaped agglomerates were crucial for PG+ assembly. On one hand, the filamentous cyanobacteria formed mat-like structures in photogranules that served as a harbour for other organisms to embed themselves in (Milferstedt et al., 2017b). On the other hand, the motility of filamentous cyanobacteria could actively capture and incorporate microbial communities such as AGS into the photogranule structure. This locomotive entanglement of particles (e.g. sand grains) by cyanobacteria was previously observed in natural occurring photogranules, such as cryoconites or microbialites (Brehm et al., 2003; Takeuchi et al., 2001). Further, the cauliflower-shaped agglomerates of AGS provided the phototrophic organisms a rugged surface to attach to. The early attachment of the PG microbial community on AGS occurred especially in cracks and crevices. These assembly mechanisms manifested in the two identified PG+ assembly modes described in

figure 1. Smaller homogenized PGs colonized the surface of larger AGS (**figure 1**, upper path) or AGS were incorporated by locomotive entanglement of intact PG (**figure 1**, lower path). The particle size ratio of PG (intact or homogenized) to AGS might be relevant in determining which assembly pathway predominates.

5.2 PG+ functions and functional redundancy

The desired functional groups in PG+ are: 1) oxygenic photosynthesis, 2) polyphosphate accumulation, 3) chemoheterotrophy (COD removal), with 4) nitrification and 5) denitrification as optional functions to enhance overall nitrogen removal. Representatives of these functions were presented above (**figure 5&6)**. In complex and diverse microbial communities, each function or metabolism can often be performed by multiple taxonomically distinct organisms (Konopka, 2009; Louca et al., 2016). Due to the specific and selective operation conditions (feast-famine) the microbial community was simplified (**figure S15**) but still had at least 5 taxa per function that were capable of the same metabolism. This established a functional redundancy that is important for the resilience of the microbial community (and functions) to biotic and abiotic influences (environmental perturbations).

Although the microbial community composition in the beginning of the co-cultivation phase was still fluctuating (**figure 5**) the bioreactor performance was stable (**figure S2**) confirming functional redundancy in the PG+ system. Functional stability during taxonomic fluctuations is a commonly observed phenomenon in ecosystems and biological wastewater treatment systems (Wang et al., 2011). Another example for functional redundancy is the taxonomic change in the functional group of chemoheterotrophs and denitrifiers during the assembly from PG to PG+. *Thauera* and *Zoogloea* are prominent representatives of these functional groups in photogranules (Trebuch et al., 2020). In PG+ they were outcompeted by PAOs (and GAOs) that consumed all acetate during the anaerobic phase leaving no organic carbon substrate in the bulk liquid for *Thauera*, *Zoogloea* to grow during the aerobic phase. Besides the very specific polyphosphate metabolism of PAOs, they are also chemoheterotrophs and denitrifiers that can replace and take over the functions of *Thauera* and *Zoogloea*.

The high activity of polyphosphate cycling in AGS and PG+ suggests that the actual abundance of PAOs might be higher than determined by 16S rRNA gene amplicon sequencing (**figure 5&S15**). The relative abundance might differ from actual biomass fractions due to DNA extraction biases, primer biases, and variation in cell size and 16S/18S rRNA gene copy number between species (Albertsen et al., 2015). This issue of underrepresentation was especially evident for PAOs when investigating microbial communities in conventional wastewater treatment systems (Stokholm-Bjerregaard et

al., 2017). Other techniques, such as staining PAOs with fluorescence *in-situ* hybridization (FISH) probes for quantification (Weissbrodt et al., 2013) or a recently suggested *de-novo* proteomics approach (Kleikamp et al., 2021) possibly would show a higher enrichment of PAOs in AGS and PG+.

5.3 PG+ wastewater treatment performance

Compared to previous photogranules and non-granular photoEBPR systems (Abouhend et al., 2018; Ji et al., 2020; Mohamed et al., 2021), COD and nitrogen removal were improved by 2-3x in PG+, expect for PG where similar N removal was found (Trebuch et al., 2020). P removal was enhanced by 3-6x due to integration of PAOs into the PG+. The overall removal capacity and removal kinetics for phosphorus and COD of PG+ were consistent with other lab-scale operated AGS systems while showing higher rates of nitrogen assimilation into biomass (de Graaff et al., 2020; de Kreuk et al., 2005). The introduction of photosynthesis led to a two-fold increase in biomass productivity and nitrogen removal in PG+, while maintaining the same COD removal and phosphorus dynamics as AGS. Generating metabolic energy from light also simultaneously produced oxygen for heterotrophic activities. *In-situ* oxygenation via photosynthesis increases the association of phototrophs and heterotrophs via the exchange of O_2 and CO_2 (Ouazaite et al., 2020) and can reduce or even remove the need for mechanical aeration (Brockmann et al., 2021).

PG+ achieved full removal of COD, N and P before the end of the cycles, indicating that a larger removal capacity is surely attainable. COD was already fully consumed after 20min into the anaerobic feeding phase (total 70 min) (**figure 2 and 3**), while P reuptake was completed 60min into the aerobic phase (total of 150min) and N was completely removed after 100min. The early N and P depletion during the aerobic phase possibly hindered phototrophs from functioning at maximum capacity and nitrifiers from fully establishing. Further, PAOs would be able to cope with higher COD and P loads, as demonstrated in previous studies (de Graaff et al., 2020; de Kreuk et al., 2005). This suggests that the nutrient load in general can be increased. Increasing COD and P load would lead to an increased enrichment of PAOs and ease competition for P. Additionally, an increased N load could facilitate simultaneous nitrification and denitrification, which can occur in the aerobic and anoxic zones of granules with sizes of >1.5mm (de Kreuk et al., 2005; M. Pronk et al., 2015).

Combining phototrophs and PAOs in photoEBPR systems can also have adverse effects. Cai et al. (2019) observed an increase in nitrogen removal due to the growth of phototrophs, but phosphorus removal by PAOs appeared to be hindered and consequently lowered. A similar observation was reported previously by Huang et al.

(2015). They concluded that light and phototrophs inhibited nitrite oxidizing bacteria (NOB) and nitrite accumulation in the bioreactor led to inhibition of PAOs, which are sensitive to elevated nitrite concentrations (Pijuan et al., 2010). Nitrification is frequently observed in photogranules (Abouhend et al., 2018; Tiron et al., 2015; Trebuch et al., 2020), but did not fully establish in PG+. This can be attributed to competition for CO_2 and ammonium (Guerrero and Jones, 1996; Risgaard-Petersen et al., 2004), which was rapidly consumed in the PG+ systems. However, at elevated ammonium concentrations nitrite accumulation could become an issue and should be investigated in more detail.

5.4 How to fit the PG+ process into a natural diurnal cycle

Light is a primary energy input for PG+ and will majorly constrain the treatment capacity of the system. As the substitution of natural sunlight by artificial illumination was proven not to be a sustainable and economically feasible, it is not considered here (Blanken et al., 2013). High sunlight input throughput the year therefore will be crucial for the efficiency of the PG+ process. This favourable condition can be found predominantly in lower latitude countries with higher light input year-round (Slegers et al., 2013).

Phototrophic processes, and their respective rates, are highly depended on light availability. Consequently, in a light-driven wastewater treatment system operated under natural light conditions all daylight should be used as efficiently as possible. When operating a PG+ system as sequencing batch reactor the culture must be temporarily shaded in the daytime during the anaerobic phases and consequently valuable light energy remains unused. This was seen in the decrease of phototrophs and nitrogen removal in PG+ when accommodating 6 short cycles within the 12h daytime and having a 12h anaerobic phase (**figure 2-4**). Instead of operating in a time-based manner in one reactor vessel (sequencing batch reactor with defined phases in-time) it could be more advantageous to design the process in-space. Recently, the AGS process was performed continuously as plug-flow, with defined reactor compartments for each phase (Li et al., 2021; Sun et al., 2019). From these studies valuable insights can be gained about how to operate a PG+ system at large scale. A plug-flow system would allow the treatment process to run continuously and have an aerobic compartment illuminated throughout the entire day, utilizing all light energy. About 3/8 of the reactor volume would be in darkness (anaerobic) and 5/8 in light (aerobic). It is important that the continuous system is designed and operated in a way that photogranule formation and functioning at high rates are still facilitated. Additionally, a control system must be in place to steer dissolved oxygen (DO) concentration in the aerobic phases according to the light conditions, photosynthetic activity, and oxygen requirements by heterotrophs. Low DO

will slow down PAO and nitrification activity, while high DO (above 100% saturation) could negatively affect both phototrophs and PAOs (Borowitzka et al., 2016; Chen et al., 2020).

Although a 12-hour anaerobic phase had no negative effect on phosphorus cycling of PAOs, there was a proliferation of GAOs towards the end of the 3 weeks experimental phase. PAOs and GAOs have a similar metabolism and compete anaerobically for the organic carbon source (acetate in this study). While GAO can proliferate in the same feast-famine conditions as PAOs they do not have the benefit of using polyphosphate as an intermediate energy storage, and con only use glycogen (Chen et al., 2020). This results in strongly decreased phosphorus removal in GAO dominated systems (Lopez-Vazquez et al., 2009). While phosphorus removal was not affected in the 3 weeks of operating at a 12-hour anaerobic phase, the proliferation of GAOs should be investigated in more detail and for extended operation period in future studies.

5.5 Advantages and shortcomings of a PG+ wastewater treatment system

The advantage of including phototrophic, chemoautotrophic (nitrifiers) and heterotrophic (PAOs, denitrifiers) processes in one system is that overall biomass productivity, and thereby biomass assimilation of nutrients, was increased. Generating metabolic energy from both light and organic carbon substrates increased biomass yield 2-3x in PG and PG+ compared to AGS (Abouhend et al., 2018; Ansari et al., 2019; Trebuch et al., 2020). Currently, high biomass productivity is not desired in conventional treatment systems since it can have a significant impact on the operational costs, due to sludge disposal (Cieślik et al., 2015). However, using the produced biomass as a resource could transform wastewater treatment systems into valuable resource recovery facilities, where besides the major elements (C, N, P) microelements (e.g. Fe, Mo, Zn, Cu) are also reclaimed and transformed (Kehrein et al., 2020; Silva et al., 2019; Suleiman et al., 2020). The whole biomass could be used either as fertilizer (C, N, P and microelements) or fractionated for extracellular polymeric substances (EPS) or polyhydroxyalkanoates (PHA) for biopolymer production (Kehrein et al., 2020). Including phototrophs into the treatment system can potentially extend the product range of the biomass by e.g. photopigments, lipids, proteins and antioxidants (Borowitzka, 2013).

PG+ rapidly assembled from PG and AGS and showed resilience to a 12h-anaerobic phase. This suggests that the PG+ process can be quickly established and is suitable to be operate under a natural diel cycle. A hurdle for PG+ application, as for all light driven

processes (e.g., phototrophic microalgal production), is the design of a full-scale system. Photobioreactors need a high surface to volume ratio to harness light. Common designs are closed tubular systems or shallow (20-40cm deep) open raceway ponds (Borowitzka and Moheimani, 2013). Consequently, light-driven wastewater treatment will have larger areal footprints compared to conventional wastewater treatment techniques, such as conventional activated sludge or AGS (Boelee et al., 2012). Nevertheless, the disadvantage of the PG+ system having a larger areal requirement will be outweighed by its advantages. Implementing PG+ systems will enable wastewater treatment to become more sustainable by using the sun's energy, lowering, or eradicating mechanical aeration and producing valuable biomass for nutrient recovery.

Transitioning to light-driven technologies (i.e., PG+) will require us to rethink wastewater treatment systems and ideally align resource (e.g., water, nutrients) consumption and recovery to the diurnal cycle of the sun. Constraining use and discharge of (waste-)water predominantly to the light periods of the day could be an effective tool to increase resource use efficiency and reduce our ecological footprint. This might be necessary to accommodate the needs of an ever-growing population and ensure a sustainable future.

6 CONCLUSION

In this study we successfully integrated PAOs into native PGs and thereby created a hybrid granule named PG+ performing photoEBPR. PG+ significantly improved phosphorus recovery by 3-6x compared to native PG, photogranules and other microalgae-based technologies. Phototrophs additionally generated metabolic energy from light and thereby more than doubled biomass productivity of PG+ compared to AGS. This creates the opportunity for resource recovery application by valorising the generated biomass and obtaining e.g., biofertilizer, biopolymers, lipids, or proteins. Further, the generation of oxygen *in-situ* by phototrophs gives us the ability to reduce or even remove mechanical aeration in the treatment process. Operating the PG+ system under a diurnal cycle of 12h (light) and 12h (dark) resulted in an 12h anaerobic phase, which had no adverse effect on PAO or phototrophic activity. The anaerobic phases during the daytime resulted in lower overall light availability and consequently reduced phototrophic growth. This affected overall biomass productivity and nitrogen removal. Therefore, bioreactor operation in sequencing batch mode must be reconsidered and a continuous operation mode should be established with separate anaerobic (dark) and aerobic (light) compartments. This will allow photogranules to maximally utilize the light input during daytime. We provided valuable insight into how to obtain photogranules performing EBPR and the feasibility of operating such a system under a natural diel cycle at lab-scale. Further efforts towards the implementation and application of this process at larger scale need to be made.

7 ACKNOWLEDGEMENTS

The authors would like to thank Winifred Noorlander, who kindly provided the AGS inoculum and Nico Helmsing, for his excellent support with bioreactor operation and chemical analysis. Further we want to thank Ben Oyserman and Sido Altenburg for their useful and lively discussions on PAOs metabolism with phototrophic growth, and the introduction to the operation of EBPR reactors during a collaborative project (Wild Card project).

8 SUPPLEMENTAL MATERIAL

8.1 Bioreactor setup

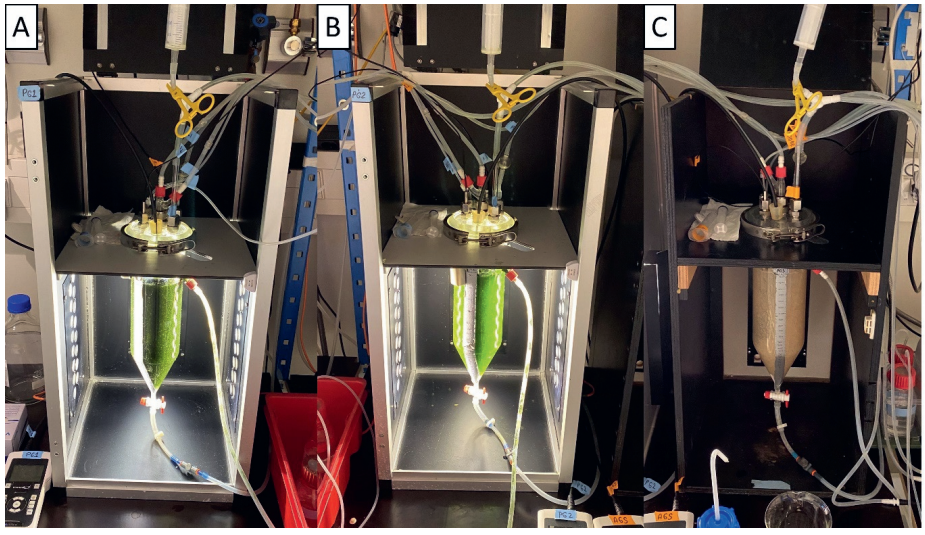

Figure S1: Bubble column bioreactor setup for A) PG1, B) PG2 and C) AGS.

8.2 Information on LED light spectrum

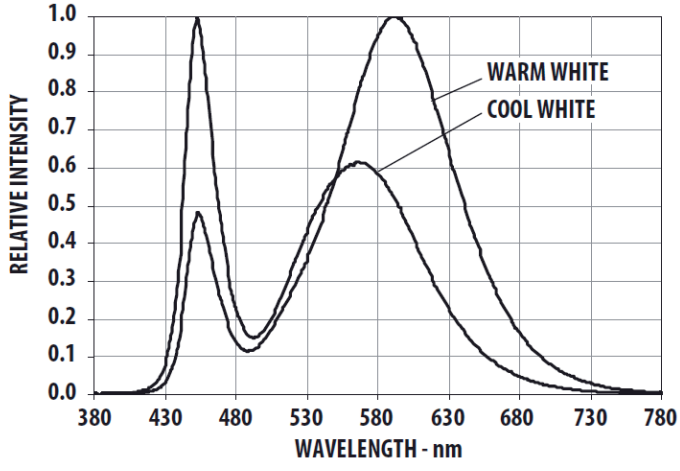

Figure S2: Light spectrum of LED lamps represented as relative intensity vs. wavelength as provided by the manufacturer (Avago Technology, USA). The warm white LED lamps were used for the experiment.

8.3 Chlorophyll-a and chlorophyll-b extraction and determination

Extraction protocol:

1. Transfer 5ml of biomass sample into a 15 mL light-blocking centrifuge tube
2. Centrifuge at 4400rpm at 4ºC for 8 min
3. Discard supernatant and add 5ml of ethanol 100% and metal ball bearing to the pellet
4. Vortex vigorously and put centrifuge tube in an ultrasound bath for 5 min to disrupt the pellet
5. Incubate the biomass suspension at 60ºC for 50min
6. Incubate the biomass suspension at 4ºC for 15 min
7. Centrifuge the biomass suspension at 4400rpm for 8 min
8. Add more ethanol if the pellet is not white after centrifugation and repeat the extraction
9. Measure chlorophyll content in a spectrophotometer at 652nm and 665nm in a quartz cuvette (blank done with ethanol)

Chlorophyll-a and chlorophyll-b were determined from absorbance at 652nm and 665nm according to the Equations 1-3 after Lichtenthaler (1987):

$$Chl_a = (16.72 \cdot A_{665} - 9.16 \cdot A_{652}) \quad (1)$$

$$Chl_b = (34.09 \cdot A_{652} - 15.28 \cdot A_{665}) \quad (2)$$

$$Chl_{tot} = Chl_a + Chl_b \quad (3)$$

With Chl_a = concentration of chlorophyll *a* in µg mL^{-1}

Chl_b = concentration of chlorophyll *b* in µg mL^{-1}

A_{665} = absorbance at 665 nm

A_{652} = absorbance at 652 nm

8.4 Biomass concentration, sludge volume index and nutrient load

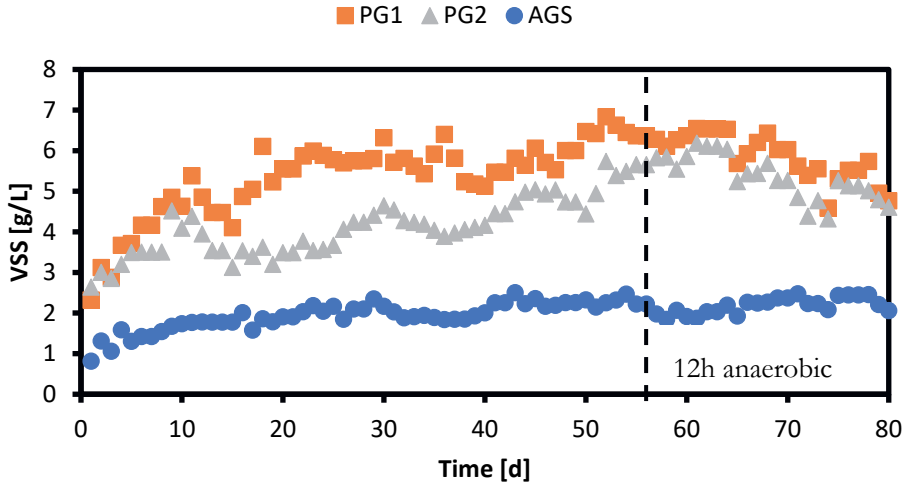

Figure S3: Biomass concentration represented as TSS and VSS in the bioreactor systems over time.

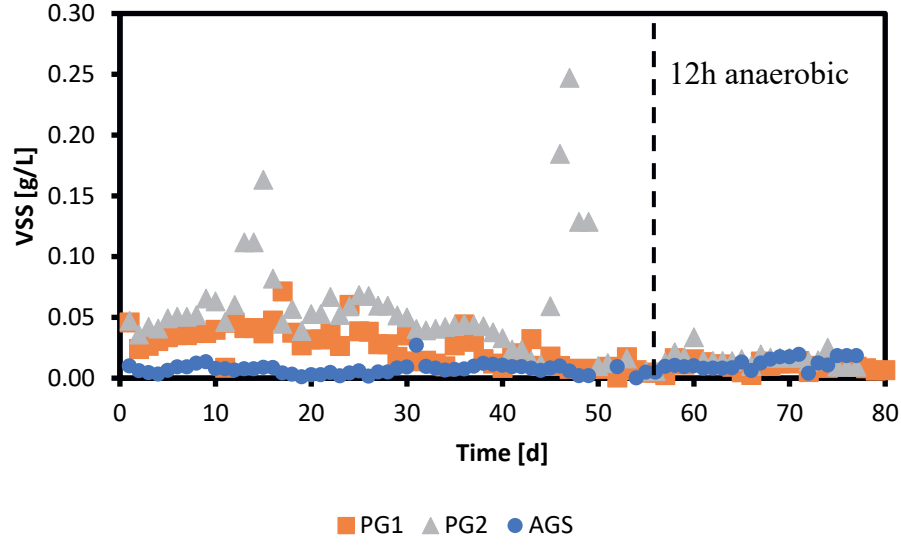

Figure S4: Biomass concentration represented as TSS and VSS in the effluent of the bioreactor systems in time.

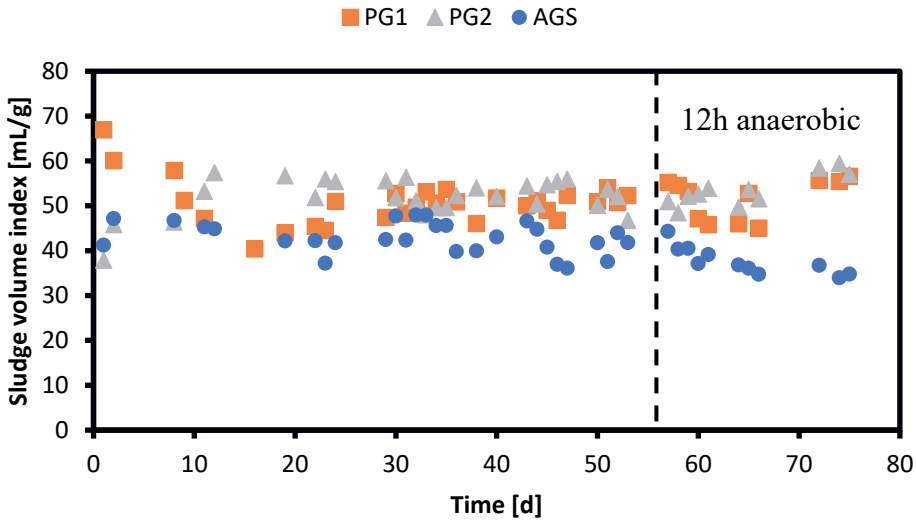

Figure S5: Sludge volume index of the bioreactor systems.

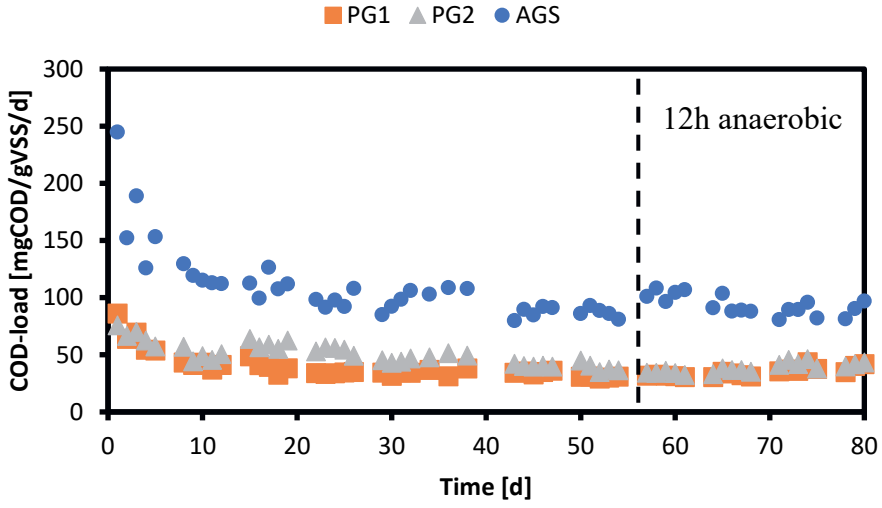

Figure S6: COD-load over time

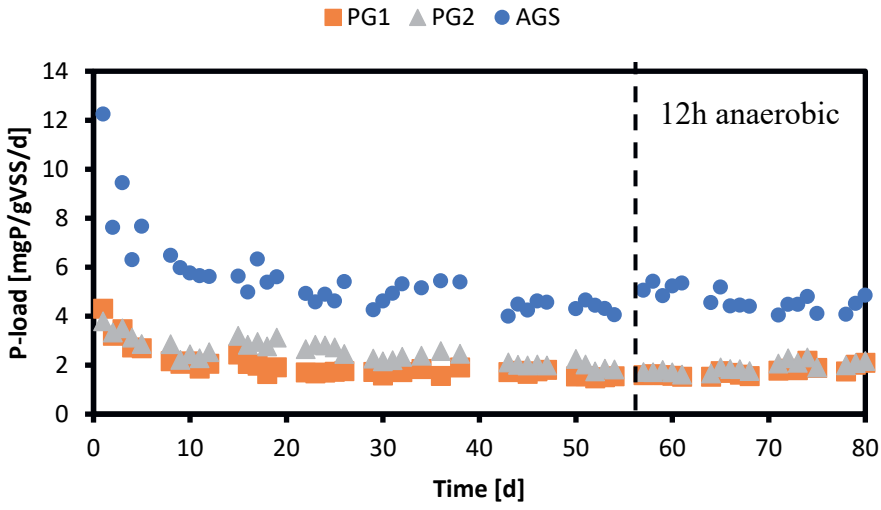

Figure S7: P-load over time.

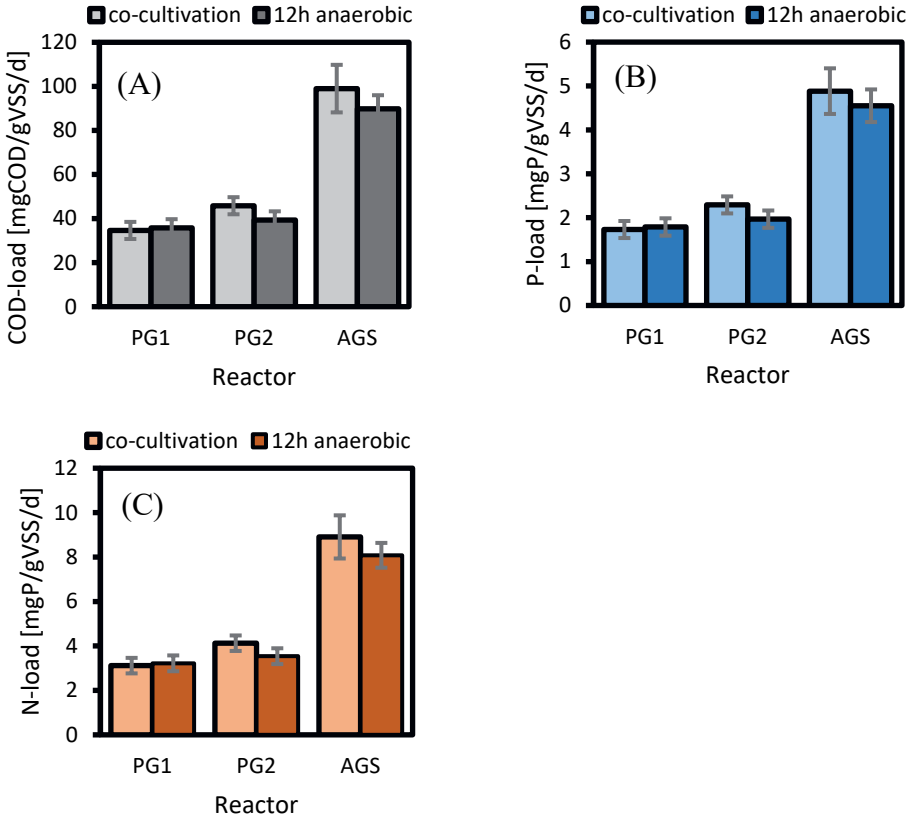

Figure S8: Averaged COD-load (A), P-load (B) and N-load (C) from the co-cultivation phase (day 10-56) and 12h anaerobic phase (day 56-80). The error bars represent the standard deviation.

8.5 Nutrient removal

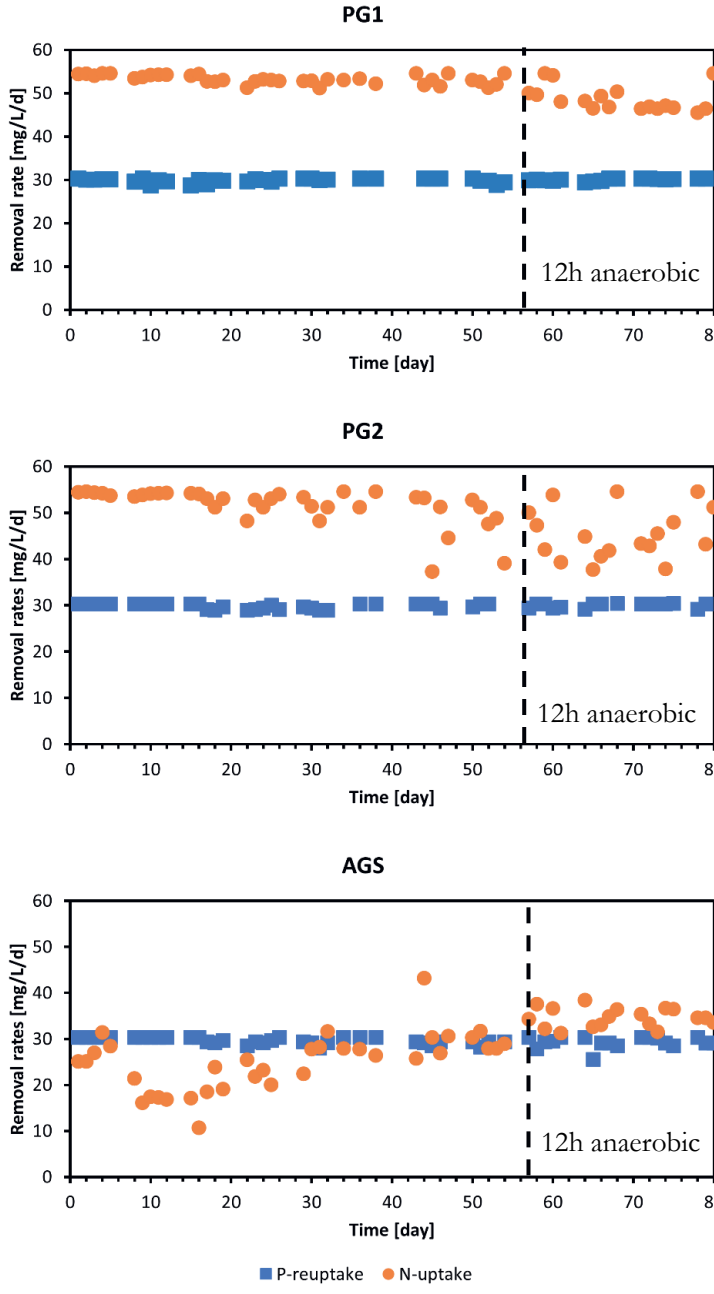

Figure S9: Nitrogen and phosphorus removal rates of PG1, PG2 and AGS.

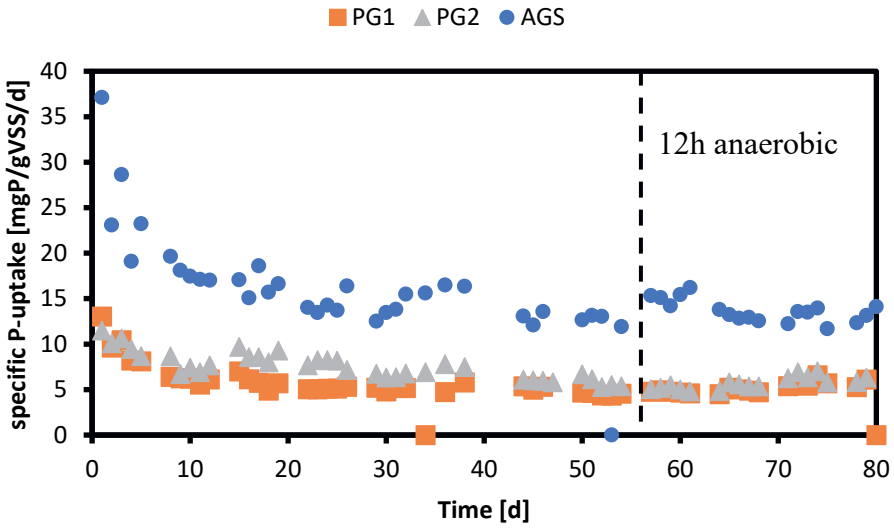

Figure S10: Specific P-uptake over time.

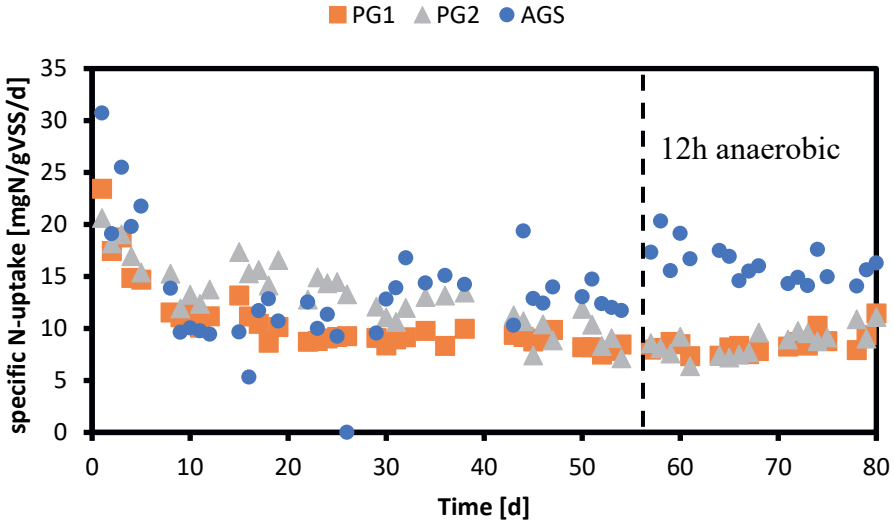

Figure S11: Specific N-uptake over time.

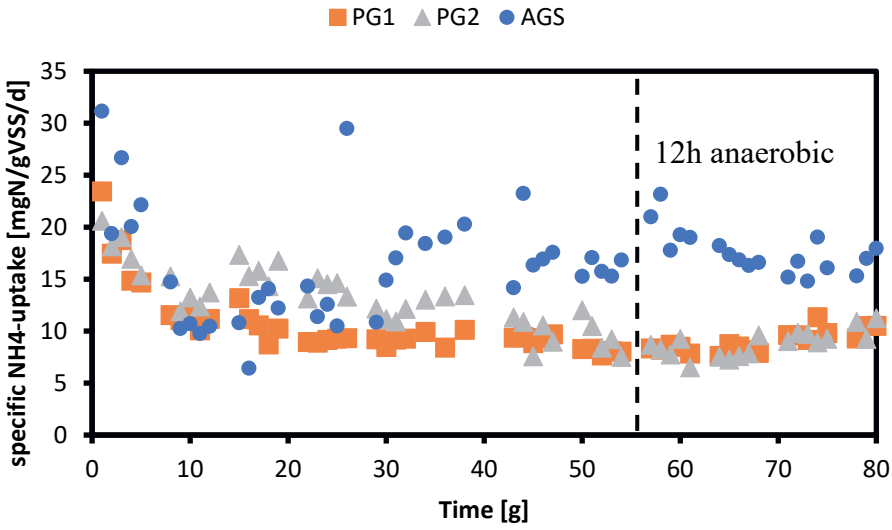

Figure S12: Specific NH4-uptake over time.

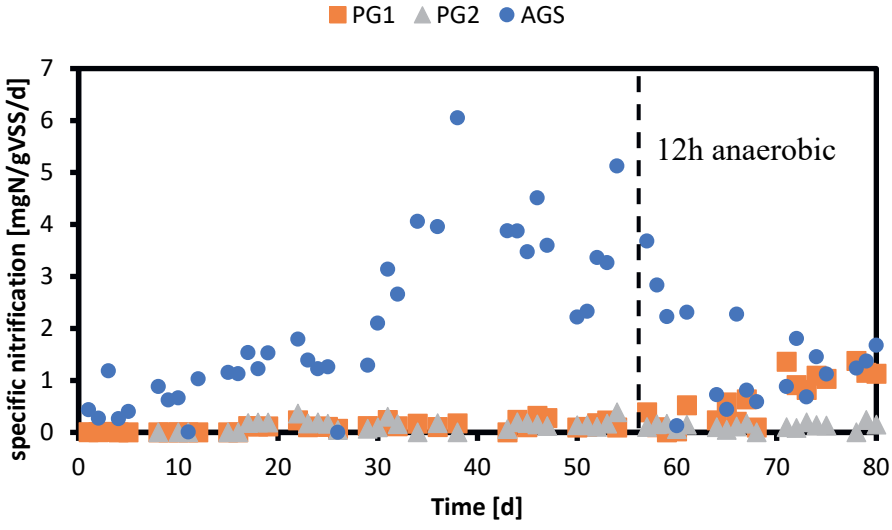

Figure S13: Specific nitrification over time.

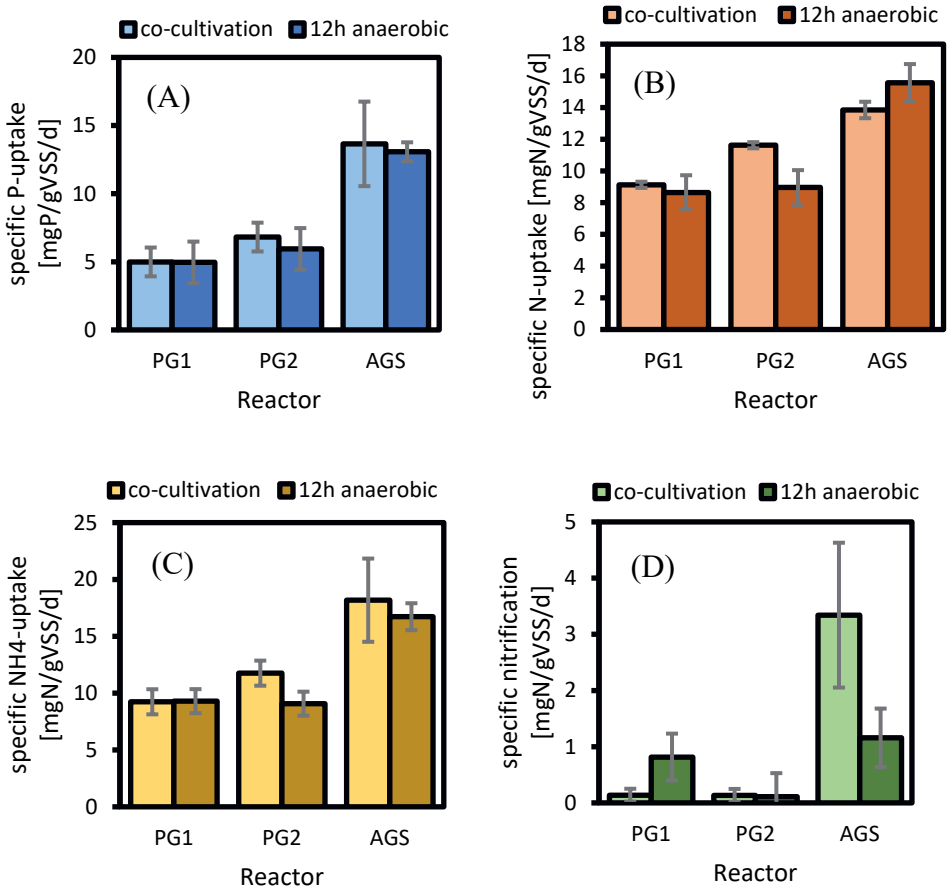

Figure S14: Average specific P-uptake (A), N-uptake (B), NH4-uptake (C) and nitrification (D) from the co-cultivation phase (day 10-56) and 12h anaerobic phase (day 56-80). The error bars represent the standard deviation.

8.6 Microbial community analysis

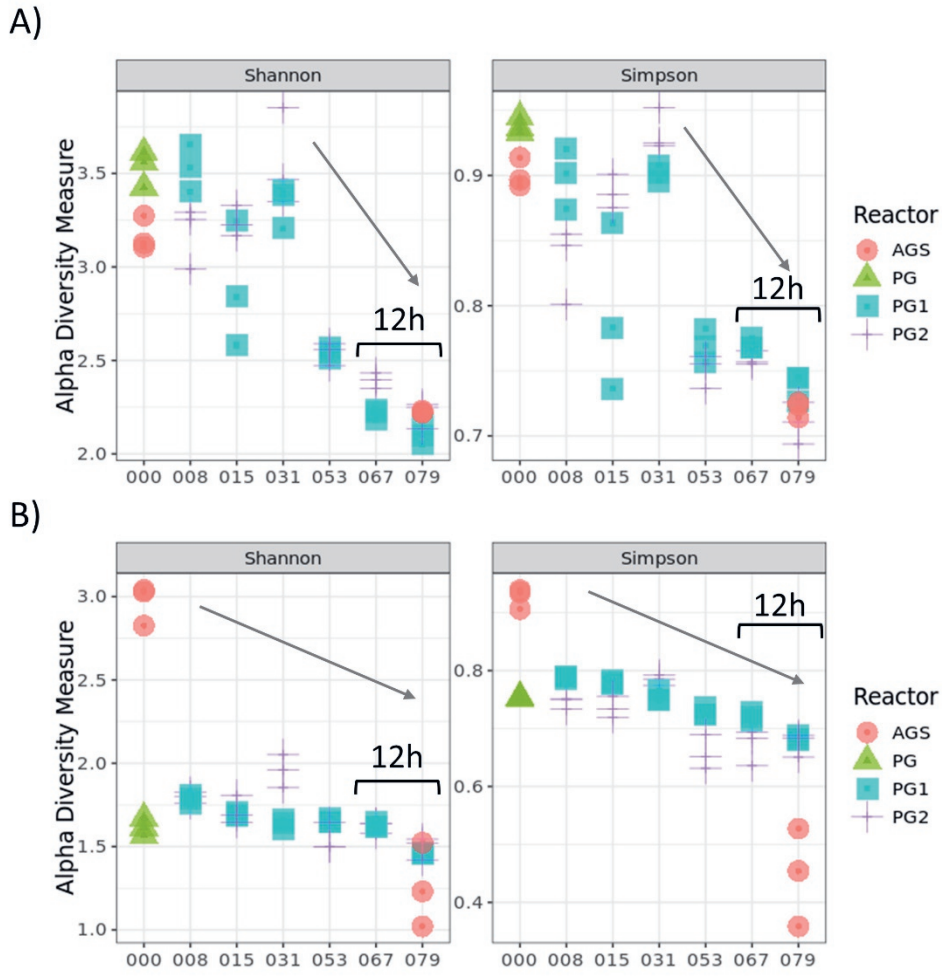

Figure S15: Alpha diversity according to Shannon and Simpson of the microbial community of PG, PG1, PG2 and AGS assessed with 16S (A) and 18S (B) rRNA gene amplicon sequencing. The inoculum (day 0), co-cultivation phase (day 8-53) and 12h anaerobic phase (day 67 and 79) is displayed.

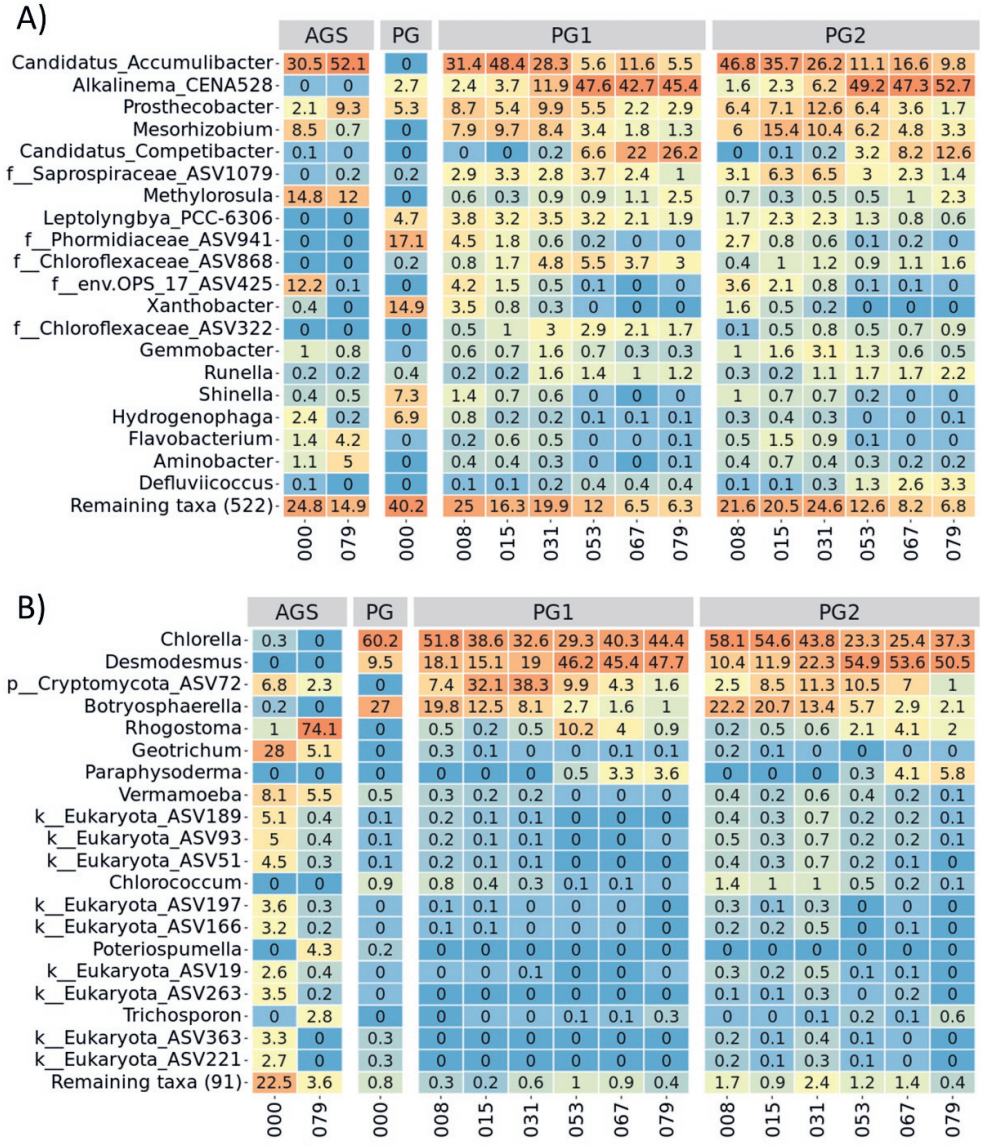

Figure S16: Microbial community composition of PG, PG1, PG2 and AGS assessed with 16S (A) and 18S (B) rRNA gene amplicon sequencing displayed from the inoculum (day 0), co-cultivation phase (day 8-53) and 12h anaerobic phase (day 67 and 79). The abundance is presented from the top 20 genera as the average of biological replicates. The remaining genera are summarized as "remaining taxa".


6.0
5.0
4.0L
3.0

Chapter 6

General Discussion

GENERAL DISCUSSION

Wastewater treatment plants are in dire need for more sustainable treatment processes and must become resource recovery facilities rather than end-of-pipe treatment facilities (Kehrein et al., 2020). As our demand for food and chemical products is ever increasing, we need to develop ways to recover valuable elements (C, N, P, microelements) from our waste streams. One way of doing this is to use the sun's energy. Especially lower latitude countries, which have high light availability throughout the year, have the prerequisites for phototrophic systems to be a suitable solution for treating wastewater. In addition, in these countries more than half of the world's population still does not even have access to proper water sanitation systems (UNICEF, 2020).

Photogranules have shown to be efficient in removing C, N and P and are easy to harvest from the treated wastewater due to their granular morphology. This thesis deals with the assembly of such photogranules (**chapter 2**), their function under nitrogen deficiency (**chapter 3**), providing detailed insights on their functionality (**chapter 4**) and finally how to increase phosphorus recovery by introducing polyphosphate accumulating organisms (**chapter 5**) (**figure 1**). One of the keys to photogranule assembly and functioning was operating the bioreactor in sequencing batch mode with alternating day:night periods and a strong selection for sedimentation after each sequencing batch cycle (**chapter 2-4**). In this manner well settling microalgal-bacterial aggregates with granular morphology were generated. To improve phosphorus assimilation the selection pressure was extended with a feast-famine regime together with co-cultivation of polyphosphate accumulating organisms (PAOs) (**chapter 5**).

The knowledge gathered throughout this thesis can be used to improve current wastewater treatment systems, upscale photogranular technology, and highlight the importance of the microbial community structure, function, and traits of photogranules. This can help to elucidate the future of photogranule wastewater treatment in general and illustrate advantages and possible hurdles along the way.

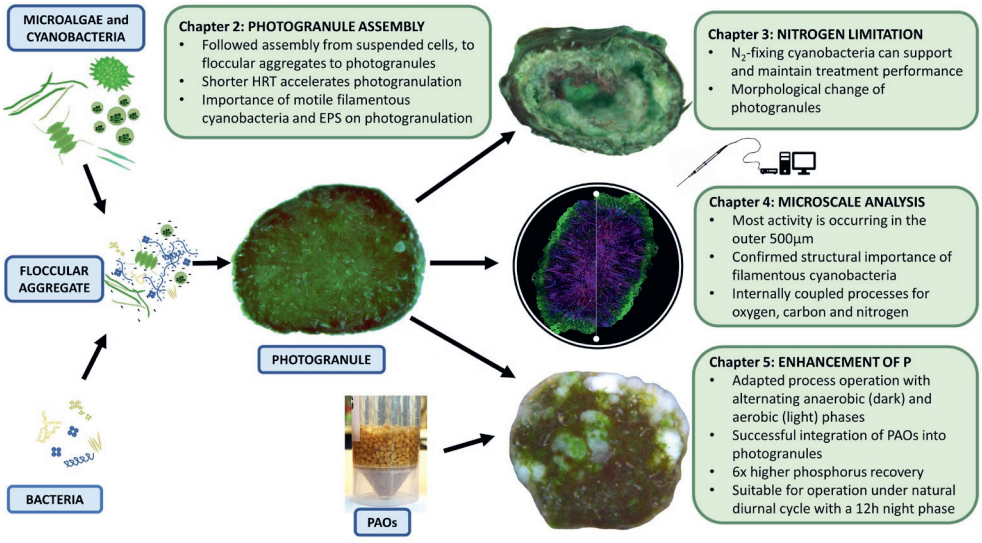

Figure 1: Summary of the experimental chapters of this thesis with the main findings highlighted.

1 PHOTOGRANULE ASSEMBLY, MICROBIAL COMMUNITY, AND FUNCTION

What are photogranules? So far, there is no clear definition of what attributes a microbial aggregate must have to be called a photogranule. Besides, within the scientific community one finds different names for the same morphological appearance, such as: oxygenic photogranule, microalgal-bacterial granules, algal-bacterial aerobic granules, or activated algae granules. Usually, when we talk about a photogranule it is a spheroid microbial aggregate of which all, or a fraction, of the microbes can perform photosynthesis (cyanobacteria and microalgae). Other metabolic functions can occur as well, from chemoheterotrophy to N_2-fixation, nitrification, denitrification, or polyphosphate accumulation (**chapter 2-5**). Despite having similar morphological appearances, photogranules can perform different functions under various conditions and they appear to be metabolically versatile. To get a better understanding on photogranule assembly, microbial community structure, and metabolic functions, I will explore in the following sections naturally occurring photogranules and perform an in-depth analysis of the microbial community assessed in other studies using photogranules for wastewater treatment.

1.1 Photogranule assembly in nature and artificial environments

Spherical phototrophic aggregates, or naturally occurring photogranules, are observed in a wide range of habitats, including hot springs (Hanada et al., 1995), salt marshes (Wilbanks et al., 2017, 2014), high-altitude lakes (Soejima et al., 2009), glacier surfaces (Takeuchi et al., 2001), freshwater lakes (Fang et al., 2014), and marine waters (Berrendero et al., 2008; Sihvonen et al., 2007) (**table 1, figure 2**). These spherical aggregates are dominated by different phototrophic communities. However, the cause for photogranulation is elusive and might be triggered by multiple external and internal stimuli, and specific functional traits within the microbial community.

Table 1: Spherical phototrophic aggregates, or naturally occurring photogranules, found in different habitats with their dominant phototrophic organisms.

Habitat	Dominant phototroph	Study
Hot spring	Filamentous anoxygenic photosynthetic bacteria	*Hanada et al. (1995)*
Salt marshes	Sulphate-oxidizing purple sulphur bacteria and sulphate-reducing bacteria	*Wilbanks et al. (2014, 2017)*
High-altitude lakes	Filamentous eukaryotic algae	*Soejima et al. (2009)*
Glacier surfaces	Filamentous non-heterocyst forming cyanobacteria	*Takeuchi et al. (2001)*
Freshwater lakes	Unicellular cyanobacteria	*Fang et al. (2014); Sand-Jensen (2014)*
Marine waters	Branched filamentous heterocystous cyanobacteria or filamentous non-heterocyst forming cyanobacteria	*Berrendero et al. (2008); Sihvonen et al. (2007); Brehm et al. (2003)*

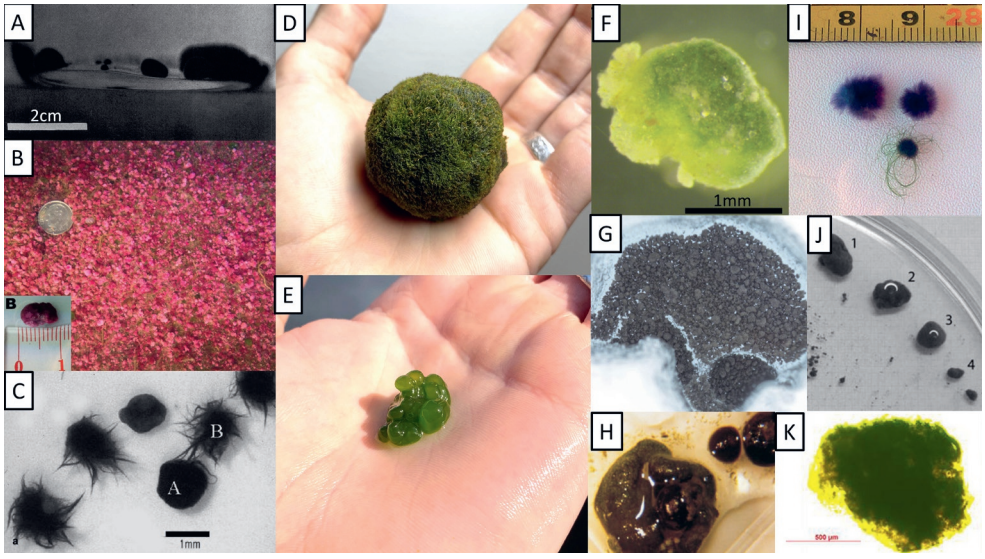

Figure 2: Photogranules found in nature in diverse habitats. A) Hot springs (Hanada et al., 1995), **B)** "Pink berry" in salt marshes (Wilbanks et al., 2014), **C)** Marine waters with filamentous non-heterocyst forming cyanobacteria (Brehm et al., 2003), **D)** High altitude lakes (Soejima et al., 2009). Picture taken by Lukas M. Trebuch, **E)** Freshwater lakes (Sand-Jensen, 2014). Picture taken by Lukas M. Trebuch, **F)** "Green berry" in salt marshes (Wilbanks et al., 2017), **G)** Glacier surface as cryoconites (Park and Takeuchi, 2021), **H)** Marine waters with branched filamentous heterocystous cyanobacteria (Berrendero et al., 2008), **I)** Fresh water lakes (Volkova et al., 2020), **J)** Glacier surface as cryoconites (Irvine-Fynn et al., 2010), **K)** Freshwater lake (Fang et al., 2014).

Photogranules for wastewater treatment were shown to be characterized by motile filamentous non-heterocyst forming cyanobacteria (**chapter 2-5**) and are frequently compared to cryoconites from glacial surfaces (Park and Takeuchi, 2021). As in cryoconites, motile filamentous cyanobacteria have shown to be important for photogranule assembly. These cyanobacteria are able to position themselves precisely within their environment according to light and chemical gradients (Garcia-Pichel and Castenholz, 2001; Kruschel and Castenholz, 1998; Malin and Walsby, 1985; Pentecost, 1984; Whale and Walsby, 1984). This allows them to efficiently use available resources (light, nutrients), avoid harmful environments (chemical, predators) and move to areas with optimized physicochemical conditions. This ability was illustrated by Häder (1984, 1987) by projecting a photographic negative onto a Petri dish containing a culture of photophobic filamentous cyanobacteria (**figure 3**). The cyanobacteria avoided lighter areas and resided in the darker areas producing a photographic positive. Further, the aggregation of filamentous cyanobacteria allows them to sense stimuli over a larger distance and respond collectively and more efficiently than individual filaments (Castenholz, 1968). An example is the thermophilic filamentous cyanobacteria *Oscillatoria terebrisformis*, which forms spherical aggregates from dispersed filaments within minutes (Castenholz, 1967) (**figure 4**).

Figure 3: Häderä's algograph experiment. A photographic negative is projected onto a Petri dish containing a culture of photophobic filamentous cyanobacteria (*Phormidium uncinatum*). The trichomes cover the lighter areas of the projection while avoiding the darker areas producing a photographic positive. Petri dish is 10 cm wide Courtesy of Donat-Peter Häder (Häder, 1984, 1987). The caption was adapted from Tamulonis et al. (2011).

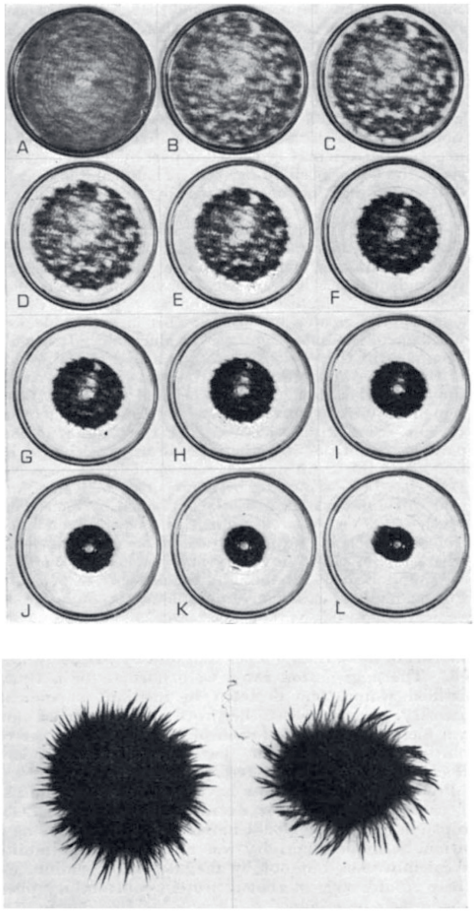

Figure 4: The aggregation of thermophilic *Oscillatoria terebrisformis* at 47 °C and 1000 lumen/ft2 in a glass Petri plate with a radius of 4-5 cm, containing 20 mL of culture medium. (A) Immediately after dispersal; (B) 10sec after dispersal; (C) 20 sec; (D) 30 sec; (E) 40 sec; (F) 50 sec; (G) 60 sec; (H) 70 sec; (I) 90 sec; (J) 180 sec; (K) 4 min; and (L) 30 min. (M-N) Two aggregated masses of *O. terebrisformis* in unagitated liquid culture medium with typical streamers of roped trichomes extending from the peripheries. The diameter of each mass is approximately 2 cm. The figure and caption was adapted from CASTENHOLZ (1967)

Brehm et al. (2003) argued that a spherical arrangement would provide a better organization for access to light, nutrients, and other resources due to the higher specific surface area compared to planar microbial mats. Additionally, the formation of spherical aggregates could facilitate close spatial and temporal coupling of organic matter producers and consumers, i.e. phototrophs, heterotrophs and diazotrophs, along a physiochemical gradient (Paerl and Priscu, 1998). This is highlighted in naturally occurring photogranules, cryoconites, in nutrient poor glacier surfaces. The formation of cryoconites provides a means for cyanobacteria to keep nutrients and associated

heterotrophic bacteria close (Takeuchi et al., 2001; Togashi et al., 2015). In *Phormidium*-dominated photogranules it was shown that a signal molecule released by heterotrophic bacteria largely determined photogranule formation (Brehm et al., 2003). Microorganisms in the interior of the photogranule are protected from grazing and unfavourable environmental conditions. Additionally, slow growing organisms are able to occupy a specific ecological niche within the photogranule.

Photogranules for wastewater treatment have been assembled under hydrostatic (i.e., in illuminated, sealed, and not-agitated vessels) or hydrodynamic conditions (i.e., photobioreactor operated in sequencing batch mode). The factors discussed above, essential in natural occurring spherical aggregates, are considered to drive the hydrostatic formation of photogranules when other environmental driving forces (i.e hydrodynamic shear) are absent (Milferstedt et al., 2017b; Park and Takeuchi, 2021). The "intrinsic" striving of the microbial community for photogranulation without dynamic operational conditions is unique in wastewater treatment engineering and biogranule formation. In contrast, other granule formation is strongly dependent on external drivers such as hydrodynamic shear, washout conditions in the case of anaerobic granules or alternating environmental conditions (nutrient and oxygen rich and poor conditions) for aerobic granules (Lettinga et al., 1980; Milferstedt et al., 2017a; Morgenroth et al., 1997).

The key organisms in hydrostatic photogranule formation were identified as filamentous cyanobacteria from the order Oscillatoriales, which are highly abundant both in photogranules generated in lab conditions and in naturally occurring cryoconites (Park and Takeuchi, 2021). Oscillatoriales are motile unbranched filamentous non-heterocyst forming cyanobacteria that make up the subsection III genre of Cyanobacteria based on Bergey's bacterial taxonomy (Castenholz et al., 2015). They were also found to predominate the microbial community of the hydrodynamically formed photogranules generated within this thesis (**Chapter 2-5**) and other studies (Abouhend et al., 2018; Gikonyo et al., 2021; Ji et al., 2020). In **Chapter 4** we illustrated that Oscillatoriales formed a complex and interwoven spheroidic network in which other organisms can embed themselves in. Extracellular polymeric substances (EPS) excreted by Oscillatoriales (filamentous cyanobacteria) and other non-phototrophic organisms possibly acted like a glue to cohere all microbes. In **Chapter 5**, we enriched photogranules with polyphosphate accumulating organisms (PAOs) from aerobic granular sludge (AGS) and assembled hybrid granules, termed PG+. PAOs were shown to be one of the main driver for granulation in AGS systems due to their ability to form dense cauliflower-shaped agglomerates (Weissbrodt et al., 2013). This agglomeration

property was also observed in PG+. During assembly Oscillatoriales started to colonize and entangle PAO granules and consolidated them into PG+.

The microbial community composition of photogranules can vary greatly and failed photogranulation is reported even when Oscillatoriales were predominating (Park and Takeuchi, 2021). Recently, Gikonyo et al. (2021) investigated hydrodynamic photogranulation and concluded that there must be a goldilocks principle where light, kinetic and biochemical energy form a zone of photogranulation. Successful photogranulation was shown under low light and moderate shear stress, while high light and shear did not support photogranule formation despite the same inoculum. With increasing reports on photogranulation it appears that there might be different photogranule assembly mechanisms as there are a multitude of phototrophic microbial communities that actually can form biogranules (Park and Takeuchi, 2021). Ji and Liu (2021) recently argued that there might be two main types of photogranules: 1) cyanobacteria-dominated photogranules and 2) eukaryotic microalgae-dominated photogranules. While cyanobacteria-dominated photogranules developed during hydrostatic incubations, both types can also be found in hydrodynamic cultivation. However, in almost all photogranules cyanobacteria and eukaryotic algae co-occur. However, the principles shaping the taxonomical structure of photogranules, and the assembly mechanisms governing photogranulation are still poorly understood.

1.2 Meta-analysis of microbial community structure

Currently there are only limited sequencing data available to give an in-depth insight into community structure and functioning. To get an overview of the taxonomic diversity and the functional distribution of the microbial community of photogranules, I collected publicly available 16S/18S rRNA gene amplicon sequencing data of six studies on photogranules. The studies range from hydrostatically formed photogranules (Milferstedt et al., 2017b; Stauch-White et al., 2017) to hydrodynamically formed photogranules in lab-scale sequencing batch reactors (Fan et al., 2021a, 2021b; Ji et al., 2021; Shen et al., 2021). I processed the raw reads of these studies in the same manner as our own sequencing data (see materials and methods) and was able to compare the results of these six studies to ours.

The inoculum used to generate photogranules came from conventional activated sludge (CAS) (Milferstedt et al., 2017b; Stauch-White et al., 2017), from aerobic granular sludge (AGS) (Fan et al., 2021a, 2021b; Ji et al., 2021; Shen et al., 2021), or from various sources (**chapter 2 and 5**). The operation conditions were not uniform and ranged from hydrostatic incubations to sequencing batch reactors fed with either real wastewater or synthetic medium (of various CNP ratios) and operated with and without the addition

of air (oxygen). Light, temperature and pH conditions were not uniform either. Despite different inocula and cultivation conditions, all studies reported the successful generation of photogranules.

On average hydrostatically formed photogranules showed higher taxonomic diversity (alpha diversity according to Shannon) compared to photogranules formed in SBRs (**figure 5**). That was particularly seen in studies focusing on "Aqua. WWT" (Fan et al., 2021a), "Light-effect" (Fan et al., 2021b), "Temp.-effect" (Ji et al., 2021), "Cold storage" (Shen et al., 2021) and "N-limit." (**Chapter 3**). In these studies, particular "stress" conditions such as inhibiting wastewater compounds, light, temperature (including cold storage), and nitrogen deprivation could have led to a simplified and less diverse microbial community.

To assess the differences in the overall microbial community between studies, I performed a principal coordinate analysis on both the 16S and 18S dataset (PCoA). Most of the studies starting with activated sludge or aerobic granular sludge as inoculum clustered and appeared to be similar in their core microbial community. That was also true for the 16S data points related to the assembly of the PG+ ("Enhance P.") where we introduced PAOs from AGS (**chapter 5**). However, the data points related to the established PG+ (highlighted in figure 5B) are clearly dissimilar, probably due to the higher abundance of PAOs in relation to the other photogranules. Interestingly, our studies on "Impact of HRT" (**Chapter 2**) and "N-limit." (**Chapter 3**) were shown to have a different microbial community than the other studies. That difference can likely be attributed to the different inocula. We used a large diversity of field samples from natural aquatic ecosystems to concentrated wastewater sludges while the other studies used only activated sludge or aerobic granular sludge from municipal wastewater treatment plants. Additionally, particular stress conditions (nitrogen limitation) could have altered the microbial community. The same accounts for "Temp.-effect" where increasing temperature might have shaped a different microbial community, shifting it away from the core community.

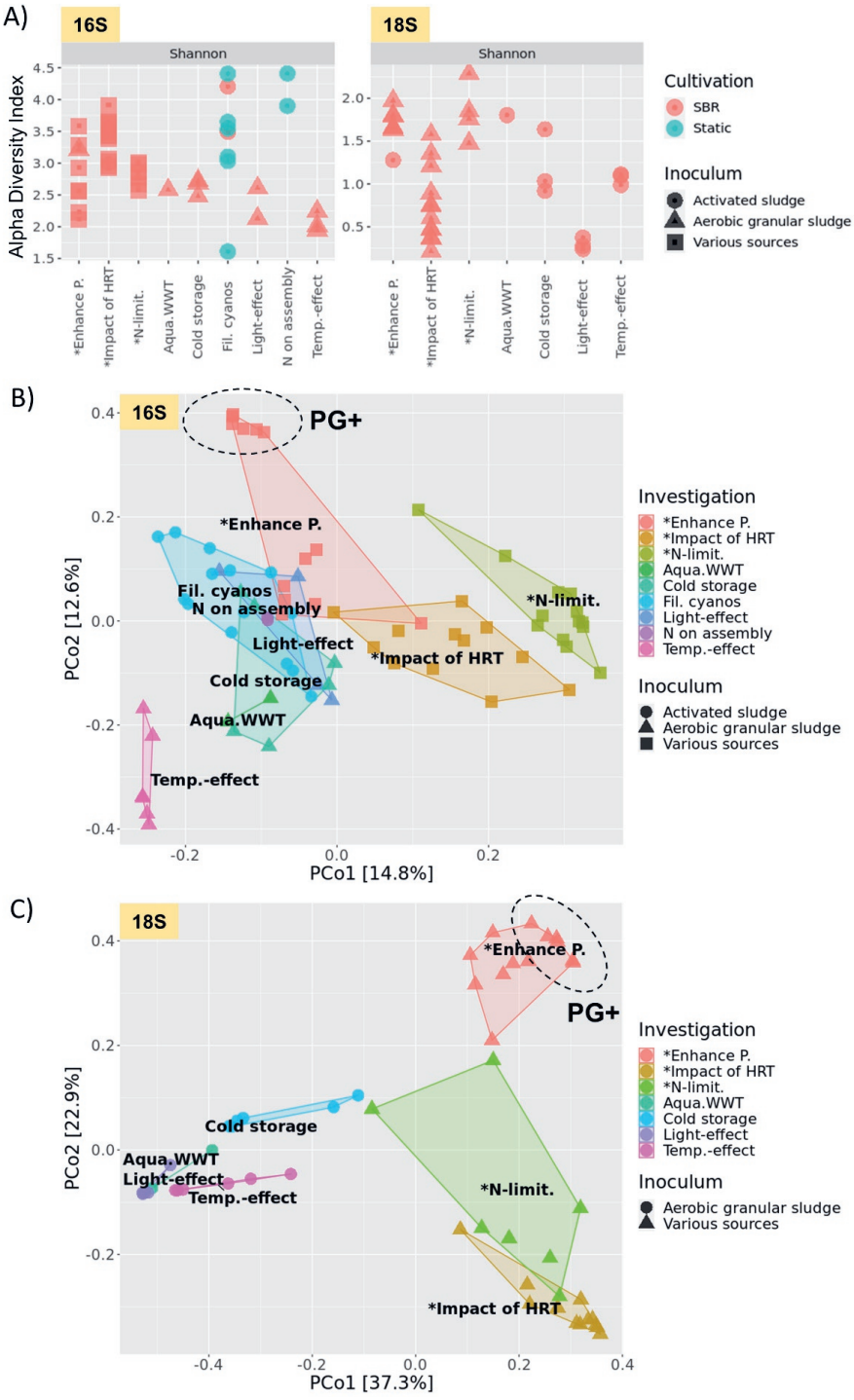

Figure 5: caption see next page

Figure 5: Meta-analysis of the microbial community of photogranules from 9 different studies. (A) Alpha diversity representing the taxonomic diversity within the different studies; **(B)** Principal coordinate analysis (PCoA) of 16S dataset using weighted UniFrac distance. PG+ are highlighted in this plot; **(C)** PCoA of 18S dataset using weighted UniFrac distance including the abundance of observed microorganisms. PG+ are highlighted in this plot.

The same analysis was also performed on the 18S dataset (**figure 4 C**). Not all studies had 18S data available therefore only 4 of the 6 studies were included. The overall results are different to the 16S dataset, showing little similarities between the microbial communities of photogranules. However, as for the 16S dataset, the studies started with activated sludge or aerobic granular sludge as inoculum were more similar than our studies. Besides eukaryotic microalgae, there were also other organisms such as fungi, ciliates, amoeba, and rotifer present. Since these organisms occurred in different proportions among studies, they could drive the dissimilarity between the eukaryotic microbial community of photogranules. These organisms have been under investigated in wastewater treatment and their function in the treatment process is elusive. However, there is evidence that fungi can contribute to aggregation (possibly granule formation) of phototrophs (Muradov et al., 2015; Wrede et al., 2014). Recently, protozoan predation was shown to be an essential component in CAS systems and tightly linked to wastewater treatment efficiency (Burian et al., 2021). Investigating fungi and protozoa in photogranules may reveal key processes in photogranulation overlooked in previous studies.

My meta-analysis revealed a 'core' prokaryotic microbial community for some of the included studies, but also showed that very different communities can form photogranules. It appears that an exact taxonomic composition is of lesser importance for successful photogranulation. As illustrated earlier for the filamentous cyanobacteria, it was not required to have a specific cyanobacterial taxon but rather one (or more) representatives of a specific order (Oscillatoriales, Subsection III). Hence, considering the entire microbial community it might be more vital to have certain functional groups represented that contribute to photogranulation and functioning rather than specific taxa.

1.3 Functional redundancy in photogranules

In complex and diverse microbial assemblages, metabolic functions can be performed by multiple coexisting and taxonomically distinct organisms (Louca et al., 2018). This leads to a functional redundancy that is strongly linked to the stability of functions against environmental perturbation. The specific (long-term) environmental conditions select for the specific metabolic functions exhibited. A consequence is that different microbial assemblages can exhibit similar community gene profiles selected by their environment (Sommer et al., 2017). Photogranulation was shown by a multitude of microbial assemblages so reducing the microbial community to metabolic functions, and investigating functional redundancy with respect to these functions, may improve understanding of photogranule assembly and function (Louca et al., 2018).

Functional annotation on the sequencing dataset used in the previous section revealed that the key metabolic functions and genera representing these functions in photogranules (**table 2**) are: 1) oxygenic photosynthesis; 2) chemoheterotrophy; with optional functions such as 3) nitrification; 4) denitrification; 5) N_2-fixation and 6) polyphosphate accumulation by PAOs. An important taxonomic group is motile filamentous cyanobacteria with their ability to perform locomotive entanglement (Milferstedt et al., 2017b; Trebuch et al., 2020). Oxygenic photosynthesis and chemoheterotrophy are deeply connected by the mutualism of phototrophs and heterotrophs exchanging O_2 and CO_2 and are ubiquitous in all photogranules. Other functions such as nitrification and polyphosphate accumulation are more uncommon and only appear in few studies. Widely distributed functions such as chemoheterotrophy were performed by 43-103 genera and are more resistant to taxonomical change. Other functions such as nitrification were only performed by 4 genera.

Table 2: Functions, functional redundancy, and genera representing the functions found across investigations on photogranules. The different shades of green indicate the number of occurrences of a specific function. The more intense the colour the more genera are representing this function. Please note that for some functions only a few selected genera are listed. Oxygenic photosynthesis might be underrepresented for some studies as eukaryotic phototrophs were not investigated by 18S/23S amplicon sequencing.

Functional redundancy within photogranules

	Aqua. WWT	Light-effect	Temp.-effect	Cold storage	Fil. cyano	N on assembly	*Impact of HRT	*N-limit	*Enhance P.
Oxygenic photosynthesis	8	4	6	4	52	11	14	8	8
Photoheterotrophy	2	2	2	4	5	4	6	1	2
Chemoheterotrophy	43	55	49	88	92	50	103	50	68
Fermentation	13	19	21	35	30	14	27	6	7
Nitrification	0	1	1	1	4	2	2	4	3
Denitrification	1	3	1	6	4	3	5	2	7
N_2-fixation	5	3	3	5	18	4	11	9	5
PAO	0	0	0	1	3	2	3	1	6
GAO	1	0	2	1	2	1	0	0	0
Motile fil. cyanobacteria	5	1	3	1	52	8	11	5	5

Selected genera representing functions

Oxygenic photosynthesis (prokaryotes)	*Cephalothrix*, *Leptolyngbya*, *Limnothrix*, *Oscillatoria*, *Alkalinema*, *Phormidium*, *Pseudanabaena*, *Anabaena*, *Tychonema*, *Pantalinema*
Oxygenic photosynthesis (eukaryotes)	*Chlorella*, *Chlorococcum*, *Botryosphaerella*, *Desmodesmus*, *Scenedesmus*, *Nitzschia*, *Micromonas*
Photoheterotrophy	*Rhodobacter*, *Rhodoplanes*, *Rhodopseudomonas*, *Roseococcus*, *Rhodoferax*
Chemoheterotrophy	*Thauera*, *Zoogloea*, *Candidatus* Accumulibacter, *Tetrasphaera*, *Halomonas*, *Dechloromonas*
Fermentation	*Geothrix*, *Holophaga*, *Bifidobacterium*, *Gardnerella*, *Rothia*, *Cellulosimicrobium*, *Collinsella*, *Bacteroides*, *Petrimonas*
Nitrification	*Nitrosomonas*, *Nitrospira*, *Candidatus* Nitrotoga, *Nitrobacter*
Denitrification	*Corynebacterium*, *Rhodoplanes*, *Paracoccus*, *Thauera*, *Zoogloea*, *Dechloromonas*, *Candidatus* Accumulibacter, *Candidatus* Contendobacter
N_2-fixation	*Calothrix*, *Nostoc*, *Cephalothrix*, *Leptolyngbya*, *Scytolyngbya*, *Azospirillum*, *Azospira*, *Methanospirillum*, *Methylocystis*, *Bradyrhizobium*
PAO	*Candidatus* Accumulibacter, *Tetrasphaera*, *Dechloromonas*, *Halomonas*, *Corynebacterium*, *Candidatus* Obscuribacter
GAO	*Candidatus* Competibacter, *Candidatus* Contendobacter
Motile fil. cyanobacteria	*Cephalothrix*, *Oscillatoria*, *Alkalinema*, *Phormidium*, *Pseudanabaena*, *Anabaena*, *Tychonema*, *Pantalinema*

N_2-fixation was primarily attributed to motile non-heterocyst forming filamentous cyanobacteria that can fix N_2 under dissolved inorganic nitrogen limitation, as observed in **Chapter 2**. Although not reported, these cyanobacteria can be found in most other investigations presented here. Besides cyanobacteria, there are also other N_2-fixing organisms (e.g. *Azospira* spp.) present within most of the photogranules investigated. The presence of N_2-fixation is counterintuitive in the context of wastewater treatment where nutrient removal is preferred. However, as shown in **Chapter 3**, the ability for N_2-fixation can be beneficial for low N:P ratio wastewaters, where nitrogen limitation can be expected.

In previously reported photogranules, PAOs were occasionally present in low abundance. They mostly originated from inocula of activated sludge or aerobic granular sludge but were not particularly favoured during photobioreactor operation nor deliberately added. One study mentions the presence of polyphosphate accumulating cyanobacteria of the genus *Pantanalinema* (Ji et al., 2020). However, polyphosphate accumulation or "luxurious P-uptake" as observed in the study of Ji is often reported in microalgae or bacteria after phosphorus starvation (Solovchenko et al., 2019). The specific PAO metabolism of e.g., *Candidatus* Accumulibacter is induced by alternating anaerobic feast (presence of organic carbon substrate) and aerobic famine (absence of organic carbon substrate) phases (**Chapter 5**). By enriching photogranules with PAOs phosphorus recovery rates were achieved that were 6 times higher than compared to photogranules without PAOs. Therefore, it will be crucial to include PAOs in the microbial community of photogranules and favour the operation conditions for their proper functioning as shown in PG+.

1.4 Ecology of photogranules for wastewater treatment

As illustrated, there are various factors influencing photogranulation in nature and artificial environments (e.g., bioreactors). The question remains if photogranulation can occur with any diverse inoculum that contains the necessary functions. The photogranules obtained within this thesis originated from a diverse inoculum coming from wastewater treatment systems, eutrophic water bodies, aquaria, and microalgal stock cultures (**Chapter 2**). These included all functional groups and traits (motility, filamentous cell arrangement) necessary to successfully assemble the photogranule investigated in **Chapter 2-4**. The first photogranules appeared after one month and the photogranules dominated the systems after 3 months. This was accelerated when the settling time was reduced to 5 min. Later PAOs were introduced to the original photogranules and phosphorus enriched hybrid granule, termed PG+, formed within 4 weeks (**Chapter 5**).

Ultimately, the key for photogranulation (i.e., PG+) is generating a selective environment that promotes the desired microbial functions and traits (**figure 6**). The environment selects a specific microbial community that meets the requirements of the specific niche as Baas Becking already stated in 1934: "Everything is everywhere, but the environment selects" (De Wit and Bouvier, 2006). This implies that from a diverse and species-rich inoculum a microbial consortium performing the desired functions can be assembled by imposing the right cultivation conditions. For this reason, wastewater treatment sludges are well suited as inoculum for the start-up of photogranular systems (Milferstedt et al., 2017) and phototrophic-enhanced biological phosphorus removal (photoEBPR) processes including phototrophs and PAOs (Carvalho et al., 2019). Wastewater treatment sludges hold most of the desired functional groups (chemoheterotrophy, polyphosphate accumulation, nitrification, denitrification) but lack oxygenic photosynthesis. As shown during static incubation of photogranules (Milferstedt et al., 2017) and the start-up of the photoEBPR processes (Carvalho et al., 2019) it is possible to steer the native phototrophic community of wastewater treatment sludges and create a microalgal-bacterial system. This would allow a quick start-up of PG+ using wastewater treatment sludges as well.

The desired metabolic functions in PG+ are: 1) oxygenic photosynthesis; 2) chemoheterotrophy (COD removal); 3) polyphosphate accumulation; with optional functions such as 4) nitrification and 5) denitrification. In a bioreactor these functional groups can be steered by changing operational conditions such as light, cycle length, HRT, SRT pH, temperature, pH, nutrient loading, and alternating between anaerobic, anoxic, and aerobic conditions (**figure 6**). In the PG+ system the key conditions for PG+ assembly were light for oxygenic photosynthesis, anaerobic-feast and aerobic-famine regimes for PAOs, and a strong selection for sedimentation by providing wash-out conditions (**Chapter 5**). Next to these conditions, filamentous cyanobacteria with their locomotive entanglement, and PAOs with their ability to form dense cauliflower-shaped aggregates were crucial for PG+ assembly.

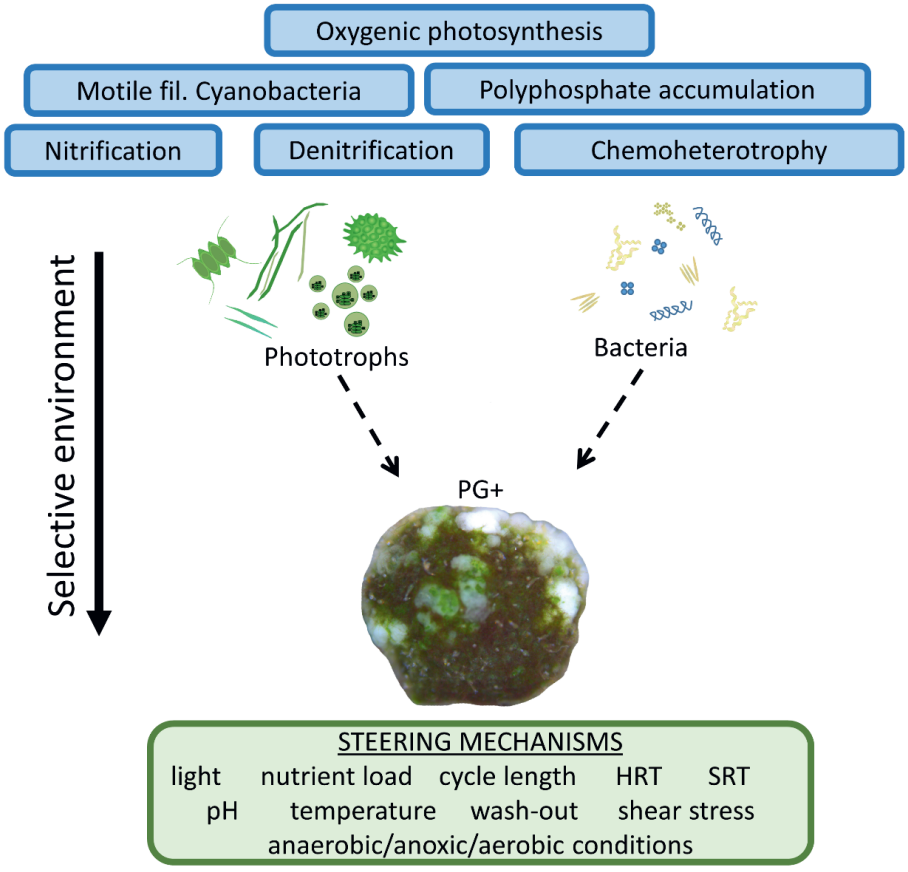

Figure 6: Steering mechanisms for PG+ assembly from desired metabolic functions and traits.

During the process PG+ will experience alternating anaerobic (dark) feast and aerobic (light) famine conditions (**figure 7**). In the anaerobic phase COD is taken up by PAOs and stored intracellularly as polyhydroxyalkanoates (PHA). Simultaneously polyphosphate (polyP) is hydrolysed, and ortho-phosphate (PO_4^{3+}) is released to the bulk liquid. In the aerobic phase phototrophs use light energy to generate O_2 and take up nitrogen and phosphorus for growth. PAOs respire PHA, release CO_2, take up PO_4^{3+} and store it intracellularly as polyP. Simultaneously nitrification and denitrification can occur, while denitrification can be performed by PAOs in the absence of O_2 by using the storage polymers (e.g., PHA, polyP) as electron acceptor (Saad et al., 2016). Concomitantly, nitrogen, and phosphorus is taken up by all organisms for growth. Especially phototrophs will contribute substantially to nitrogen assimilation as shown in **Chapter 5**.

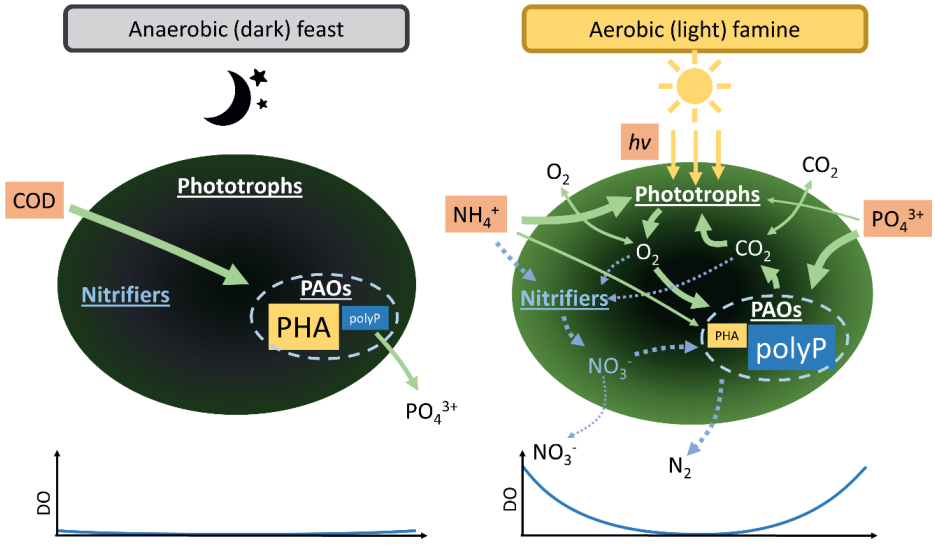

Figure 7: Simplified metabolisms of the key organisms in PG+ occurring during the anaerobic (dark) feast and aerobic (light) famine phase. Polyhydroxyalkanoates (PHA) and polyphosphate (polyP) are important in the metabolisms of polyphosphate accumulating organisms (PAOs). Nitrification (nitrifiers) and denitrification (by PAOs) are represented in blue and with dashed arrows since these processes are optional within PG+. The line thickness of the arrows indicates the magnitude of the conversion rate (the thicker the higher). Below the PG+ the dissolved oxygen (DO) is displayed at the cross section of the granule.

The metabolic activity and stratification of photogranules is largely dependent on light-and nutrient availability, which define the physical and chemical gradient within photogranules. As shown in this thesis, most of the activity within photogranules were confined to the outer layers due to light and substrate gradients (**chapter 4**). Light was rapidly attenuated in the outer 500 μm, which consequently restricted photosynthesis to this area. Organisms coupled to *in-situ* oxygenation, such as chemoheterotrophs and nitrifiers, preferably reside in proximity to phototrophs. Deeper into the centre, oxygen is rapidly consumed, and anoxic conditions occur (**figure 7**). Organisms or processes that need anoxic or anaerobic conditions, such as denitrification, will predominate in this zone. This can facilitate simultaneous nitrification and denitrification in PG+ (>1.5mm diameter) with anoxic zones in the centre (de Kreuk et al., 2005).

Our findings gathered in **Chapter 4** gave a first impression of photogranule structure and functioning without PAOs enrichment. Therefore, it is vital to get further insight into the PG+ and the structural role of PAOs. The relevant functional groups (i.e., phototrophs, PAOs, nitrifiers, denitrifiers) and their activity and metabolites should be mapped within PG+ of different sizes and cultivated under different conditions (e.g., light, nutrient load). Next to microsensor measurement and stable isotope incubations, techniques such as FISH (Weissbrodt et al., 2013), Raman-FISH (Fernando et al., 2019),

FISH-nanoSIMS (Onetto et al., 2017) or MALDI-MSI (Zhang et al., 2019), could give detailed insight into PG+ structure and functioning. This would allow the elucidation of the effect of operation conditions on PG+ morphology, stratification, and metabolic activity.

Additionally, we should investigate the photogranule (i.e., PG+) microbial community in more detail to further unravel photogranulation and microbial functions. Most of the studies on photogranules investigated taxonomy by means of amplicon sequencing and only few recently performed metagenomics to assess the full functional potential of the community (Fan et al., 2021a; Ji and Liu, 2022). It is vital to extend this analysis by metatranscriptomics, metabolomics, and metaproteomics of the PG+ microbial community. This will give us essential information on upregulated genes and metabolites during photogranules assembly (from free suspended cells to photogranules) and the response of PG+ to various cultivation conditions (e.g. wastewater characteristics, light, darkness, pH, temperature, anaerobic, anoxic or anaerobic conditions) or biotic and abiotic stressors (e.g. grazers, organic pollutants). Having this fundamental understanding will facilitate engineering decisions (reactor design and operation mode) on steering the desired microbial functions for wastewater treatment.

Modelling of the PG+ process including granule size and diffusion dependent uptake of nutrients would be valuable to get realistic estimates of photogranule treatment capacity on a large scale. Recently, first modelling attempts were made to establish microscale-level models for individual photogranules (Ouazaite et al., 2020; Tenore et al., 2021). We need to further build kinetic and mass transfer models for photogranules and validate them with past and future lab-scale observations. Ultimately, microscale-level models for individual granules can be extended to whole process models similar to the commonly used activated sludge models (ASM). Having both microscale and process models would be a valuable tool to simulate PG+ structure and functioning, to make projections for future scenarios and aid future research and application.

2 PG+ PROCESS OPERATION AND UPSCALING

2.1 Moving from a reactor operation in-time to in-space

Up until now the photogranule wastewater treatment process was solely carried out under controlled lab conditions in small (1-6L) stirred tank reactors, or bubble columns (Abouhend et al., 2018; Gikonyo et al., 2021; Milferstedt et al., 2017b; Trebuch et al., 2020). The process proved to work well under lab-scale conditions for COD, phosphorus, and nitrogen recovery with minimal to no external oxygen supply. In this thesis we showed that photogranules are effective under various hydraulic retention times (**chapter** 2), nitrogen deficiency (**chapter 3**) and feast-famine regimes (**chapter 5**).

The next steps are to scale up the PG+ treatment system and design a reactor system that provides the right conditions for the process. The main requirements for PG+ with improved phosphorus removal capacity are: 1) an anaerobic and dark feeding phase, 2) an aerobic and illuminated famine phase, 3) a biomass and liquid separation phase. At lab-scale these phases were separated in time and alternated within 2-4 hours. When operating under a natural diurnal cycle the anaerobic dark phase would occur multiple times during the daytime. Consequently, the reactor would need to be shaded and valuable light energy would be lost. In **Chapter 5** we accommodated five anaerobic phases during the daytime and observed a decrease in biomass productivity by 40% and nitrogen removal was impaired. Moreover, shading a large-scale reactor is technically very complex.

The usage of sequencing batch reactors were key in the development of aerobic granular sludge (Morgenroth et al., 1997) and later for photogranules (Abouhend et al., 2018; Tiron Olga, Bumbac Costel, Patroescu I. Viorel, 2015; Trebuch et al., 2020). Recently, the aerobic granular sludge process was investigated in continuous flow systems with the aim to retrofit conventional activated sludge systems (Li et al., 2021; Sun et al., 2019). The principal idea is to operate the system in a plug-flow manner and separate the individual sequencing batch phases in zones within the reactor. Adapting the PG+ system to a continuous flow operation with distinct anaerobic (dark), aerobic (light) and sedimentation phases would allow the maximization of light use during the day and consequently improve treatment performance. Substitution with artificial illumination (e.g., with LED lamps) is not considered here due to their higher environmental impact (Blanken et al., 2013). Mixing of the system can either be achieved mechanically (e.g., impellers) or via (intermittent) aeration.

Here I present a first concept for a continuous flow reactor system for PG+ (**figure 8**). The PG+ treatment process was arranged in space with three distinct phases: 1) An anaerobic feeding phase in a closed dark vessel; 2) An aerobic famine phase in a photobioreactor with an optional on-demand aeration system for addition of O_2 and/or CO_2; 3) Biomass separation in a continuous settling unit. In the beginning of the process incoming wastewater rich in COD, N and P is mixed with recycled biomass. The mixed liquor enters the closed dark vessel where the anaerobic feast phase is taking place. PAOs take up COD anaerobically and store it as PHA intracellularly while releasing ortho-phosphate into the bulk liquid. Nitrogen concentrations remain stable over this period. After the COD is fully taken up the mixed liquor enters a photobioreactor where the aerobic famine phase is taking place. Photosynthesis produces O_2 which is necessary for the PAOs to respire the internally PHA to grow and incorporate ortho-phosphate as polyphosphate intracellularly. In turn PAOs produce the CO_2 that is necessary for photosynthesis. Nitrogen concentrations decrease over this period as phototrophs and, when present, nitrifiers take up ammonia. Phototrophs also contribute to P recovery as they assimilate orthophosphate during this phase.

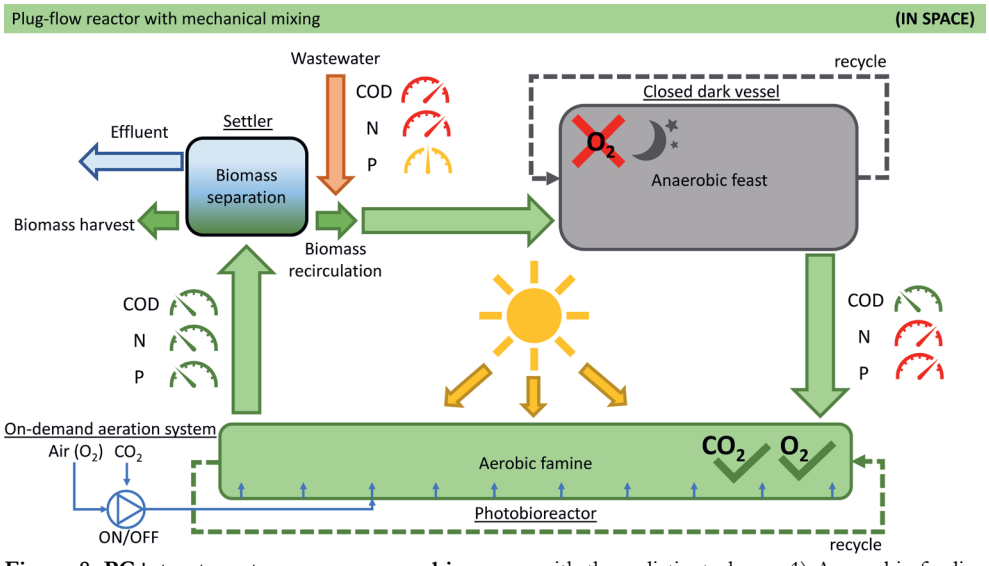

Figure 8: PG+ treatment process arranged in-space with three distinct phases: 1) Anaerobic feeding phase in a closed dark vessel. 2) Aerobic famine phase in a photobioreactor with an optional on-demand aeration system for addition of O_2 and CO_2. 3) Biomass separation in a continuous settling unit. The closed dark vessel and the photobioreactor have the option to recycle the content to change the overall residence time of liquid and biomass in the compartment. In the settler biomass is separated from the treated wastewater. One part of the biomass is returned to the beginning of the process while the other part is harvested and further processed.

The O_2 and CO_2 balance is mainly influenced by the available COD (wastewater characteristics) and light conditions (weather conditions). To have better control over

this balance an on-demand aeration system can be implemented that allows operators to temporarily sparge air (O_2) and/or CO_2 into the photobioreactor when necessary. This allows engineers to operate the PG+ treatment system under optimal conditions and recover nitrogen and phosphorus efficiently. When COD, N and P levels reach the desired discharge limits the mixed liquor enters a settler. Clean effluent is discharged, and one part of the biomass is harvested while the other part is returned to the beginning of the treatment system. Both the closed dark vessel and the photobioreactor have recycling options to increase the residence time of the mixed liquor within the respective zone. This option gives additional control over the overall treatment process.

2.2 Scenario analysis of PG+ wastewater treatment

2.2.1 Potential for different locations and wastewater characteristics

To evaluate possible PG+ treatment scenarios, I mathematically analysed the treatment process, considering two locations and two type of wastewaters. The analysis was performed for spring and summer only (Mar 31st – Sep 30th). The location were the Netherlands (low light = 31 mol photon/m^2/d) and India (high light = 69 mol photon/m^2/d) and the wastewaters were one with low N:P ratio of 4 (N = 40 mg/L; P = 20 mg/L, COD = 600 mg/L) and one with high N:P ratio of 11 (N = 50 mg/L, P = 10 mg/L, COD = 200 mg/L). For each scenario a treatment capacity of 1000 people (130L wastewater per person) was considered and the operational parameters were chosen as such that full N, P and COD removal was achieved. When applicable, nitrification and denitrification was considered. All calculations are based on lab-scale results of photogranules enriched with PAOs (PG+) and parameters obtained for phototrophs and PAOs separately (**Chapter 5**).

In total six scenarios were considered: 1) High N:P ratio and low light (HL); 2) High N:P ratio and high light (HH); 3) High N:P ratio and low light with nitrification and denitrification (HL-ND); 4) High N:P ratio and high light with nitrification and denitrification (HH-ND); 5) Low N:P ratio and low light (LL); 6) Low N:P ratio and high light (LH). These six scenarios gave valuable insight into the footprint (floor area) of the treatment system per person equivalent (PE) and the dominant biological removal mechanisms under different conditions (**figure 9**).

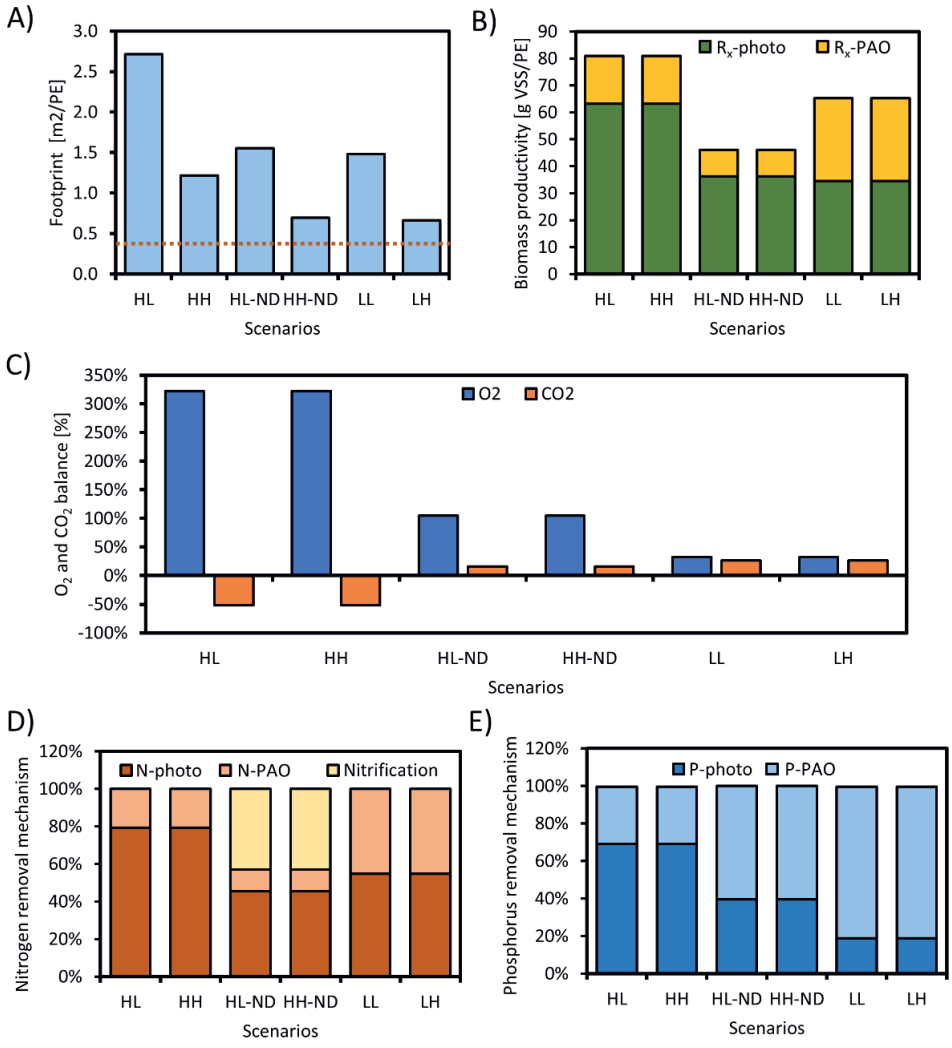

Figure 9: Scenario analysis of PG+ treatment system under different N:P ratio and light conditions and optional nitrification and denitrification. HL: high N:P ratio (11) and low light conditions, HH: high N:P ratio (11) and high light conditions, HL-ND: high N:P ratio (11) and low light conditions with nitrification and denitrification, HH-ND: high N:P ratio (11) and high light conditions with nitrification and denitrification, LL: low N:P ratio (4) and low light conditions, LH: high N:P ratio (4) and hight light conditions. **A)** Footprint of the PG+ treatment per person equivalent (PE). The dashed red line indicates the footprint of a conventional activated sludge treatment system. **B)** Biomass productivity per person equivalent (PE) of the PG+ treatment system. **C)** Oxygen and carbon dioxide balance of the PG+ treatment system. **D)** Nitrogen removal mechanism. **E)** Phosphorus removal mechanism.

In all scenarios full N, P, and COD removal was achieved. An increase in light from low to high resulted in a proportional reduction of treatment plant size across all scenarios (**figure 9A**). The lower COD load in the high N:P ratio wastewater resulted in lower sludge (bacterial) productivity and P removal (**figure 9B**). However, the lower

P removal was compensated for by phototrophic growth, which in turn increases the size of the treatment system. Conventional wastewater treatment systems have footprints of 0.2-0.4 m^2/PE and scaling can be done in volume rather than surface, as needed for phototrophic treatment systems (Chen et al., 2020). The less phototrophic biomass is produced, and the more light is available, the smaller the footprint of the PG+ treatment system. The lower footprint (0.66-0.70 m^2/PE) was found in the HH-ND and LH scenarios. This makes the PG+ treatment system about twice as large as a conventional treatment system, however with the advantage of providing all O_2 and CO_2 internally (without external aeration). The footprint increased to a maximum of 2.72 m^2/PE in the HL scenario when considering low light conditions and higher phototrophic contribution to removal (79% for N and 69% for P taken up by phototrophs) and additionally requires supply of extra CO_2 for photosynthesis (**figure 9A&C**).

One of the major downsides of photobioreactors is the considerably larger footprint needed compared to conventional wastewater treatment, especially at low light conditions. As light is essential for the treatment process the land and illuminated reactor surface needs to be maximized. It is not as simple as increasing the volume of the reactor by increasing the reactor surface horizontally or to some extent vertically. When land is available and cheap the best option is to construct an inexpensive raceway pond occupying a large area. In case land is expensive and scarce, such as in an urban area, the best option is to construct a closed vertical system (e.g., vertically stacked tubular systems) and e.g. place the system along the façade of a building.

2.2.2 Balancing phototrophs, chemoautotrophs and chemoheterotrophs under different conditions

The interplay of phototrophs, chemoautotrophs (nitrifiers), and chemoheterotrophs (PAOs and denitrifiers) is crucial in successful PG+ treatment application and needs to be well balanced especially when an external supply of O_2 and CO_2 is not desired. The organisms compete for the same resources in terms of N and P and the ratio of phototrophs to heterotrophs (nitrifiers) and COD availability determines if the O_2 and CO_2 balance within the system is closed. In lower N:P ratio (<11) wastewaters the contribution of PAOs to phosphorus removal are more important as nitrogen limitation hampers removal by phototrophs (**figure 9E**). In scenario LL and LH at an N:P ratio of 4, removal by PAOs was maximal with 45% for N and 81% for P. It is important that in this scenario sufficient COD is available for P removal by PAOs. Usually there should be a ratio of 1:10 – 1:20 of P:COD to achieve full P removal (Chen et al., 2020). In higher N:P ratio (>11) wastewaters phosphorus limits nitrogen removal by PAOs, making phototrophs more important.

As mentioned previously, the increased ratio of phototrophic removal leads to higher footprints and CO_2 demand. In scenario HL and HH, CO_2 was limiting and needed to be externally supplied. An alternative route I chose was to include nitrification and denitrification to the treatment process. Although, this implies not recovering all N into biomass, it appeared to be a valuable option to achieve a positive CO_2 balance and reduce the footprint by 43% (**figure 9A, C, D**). This was accomplished by decreasing the phototrophic removal and consequently reducing CO_2 demand for photosynthesis. Additionally, denitrification leads to a higher yield of CO_2 per organic carbon substrate, which further benefitted the overall CO_2 balance (Chen et al., 2020).

CO_2 availability was considered as one of the most important parameters in balancing microalgal-bacterial wastewater treatment without external aeration (Casagli et al., 2021). CO_2 is both supplied by respiration of COD by PAOs (or other heterotrophs) and to some extent by the available of alkalinity of the wastewater itself. The right ratio of COD to N and P is crucial to supplying enough CO_2 via respiration for photosynthesis, which in turn provides O_2 for the respiration of COD. It is becoming obvious that there is a delicate balance between phototrophs, PAOs, nitrifiers, and denitrifiers that is very much dependent on wastewater characteristics and light availability.

The presented scenario analysis only dealt with two different wastewater characteristics and light conditions. Since in reality there are a plethora of different combinations of COD, N, P, and light, I propose to implement the option of sparging air (O_2) and CO_2 on demand to support the treatment process under unfavourable conditions (e.g., low light or COD). CO_2 could be obtained from processes emitting CO_2 (e.g., anaerobic digestion, combustion) or directly captured from air, making the PG+ treatment system a carbon capture process (Lackner and Azarabadi, 2021). Aeration will also allow O_2 to be stripped from the liquid as supersaturated dissolved oxygen (DO) concentrations (>100% DO) can impair photosynthesis and PAO activity (Borowitzka et al., 2016; Chen et al., 2020). In all our scenarios excess O_2 production was seen and observed in our experimental setups (**Chapter 5**).

2.2.3 Further considerations for the scenario analysis and future PG+ wastewater treatment

The effect of temperature was not accounted for in the scenario analysis. Light intensity strongly affects temperature and moving to locations with higher light availability also implies higher reactor temperatures (Borowitzka and Moheimani, 2013). Temperature influences metabolic rates and can change the microbial community structure. During this thesis we did not specifically focus on the effect of temperature

on photogranule performance. We operated at 35°C (**chapter 2-4**) and 20°C (**chapter 5**). Unfortunately, a fair comparison between the two conditions cannot be performed as we significantly altered the microbial community (introducing PAOs) and process conditions (feast-famine regime) when moving from 35 to 20°C. Despite these changes we saw similar biomass growth rates and nitrogen removal. Recently, Ji et al. (2021) investigated the performance of photogranules in temperatures ranging from 15 to 30 °C. The authors observed minimal changes in the removal rates of COD, P and N but highlighted that the relative contribution of phototrophs and bacteria to removal altered. While bacteria had a larger contribution at lower temperatures, phototrophs were predominantly active at elevated temperatures. In future studies the effect of temperature must be considered.

The suggested continuous flow system first needs to be vigorously tested under controlled lab conditions and then each sequencing batch phase of the PG+ system should be implemented adequately to ensure proper photogranulation and functioning. It will be essential to ensure that PG+ experience similar condition (i.e., nutrient concentrations, anaerobic/aerobic conditions) to those that they would have during sequencing batch operation. Splitting the batch phases in-space also implies the need to explore new reactor design and means of controlling operational parameters (e.g., dissolved oxygen or dissolved inorganic carbon). In continuous-operated AGS systems the phases were either divided into one compartment per phase (three in total) (Li et al., 2021) or each phase was subdivided into multiple connected compartments (Sun et al., 2019). The latter allowed the accurate simulation of the concentration evolution over the course of the batch (high in the beginning and low at the end) leading to better granulation and functioning compared to the first configuration. The exact reactor configuration suitable for PG+ still needs to be defined and research done on continuous AGS systems can give valuable insight.

Further, the photobioreactor design for the PG+ is crucial as it needs to provide high light exposure and sufficient mixing for PG+ to be optimally exposed to light. PG+ settle easily when not mixed properly. Unfortunately, vigorous mechanical mixing may impair PG+ integrity and can hinder granule formation. It is important to assess different photobioreactor designs (e.g., raceway ponds, tubular, and flat-panel systems) and mixing modes (e.g., impellers, pumps) at small- to pilot-scale to find an optimal photobioreactor design and operation. Maintaining and controlling operation parameters (e.g., DO) is important, especially due to the complex interplay of phototrophs, chemoheterotrophs (including PAOs), nitrifiers and denitrifiers and the varying operation conditions (i.e., light, wastewater characteristics). As previously

suggested, it would be highly advantageous to have microscale and process scale models for the PG+ system that can assist during these engineering decisions.

3 PG+ BIOMASS VALORISATION

Recovery of valuable elements (e.g., N, P, C, K, Mg) from waste streams will be essential in future wastewater treatment applications. Nowadays, conventional systems still have a focus on removal rather than recovery. Recovery of elements is commonly done via biomass assimilation or precipitation of the compound of interest, such as P. Photogranules showed 2-3x higher biomass productivities than conventional activated sludge, due to the combined growth on organic carbon and light energy (**Chapter 2, 3 and 5**). The assimilation of especially nitrogen and carbon was significantly improved over conventional systems. Current wastewater treatment systems recover only about 20% of nitrogen. The remaining fraction is converted to nitrogen gas (75%) or is lost via the effluent (5%) (Chen et al., 2020). In the scenario analysis biomass was produced in the range from 46-81 g/PE/d. Even when considering conversion of dissolved inorganic N to N_2 in scenario HL-ND and HH-ND, the recovery of N was still 2x the amount as in conventional treatment systems.

The generated photogranule biomass can be applied as biofertilizer or bioamendment to nurture and stimulate soil health and plant growth (Suleiman et al., 2020). Biomass constituents of interest are photopigments (e.g., chlorophyll, phycobilin proteins and carotenoids), lipids, proteins, antioxidants (e.g., alkaloids, flavonoids, phenols, tannins, phlorotannin, terpenoids) and storage compounds (e.g., PHA, polyP, cyanophycin) (Borowitzka, 2013; Haq et al., 2019; Kehrein et al., 2020). Extracellular polymeric substances (EPS) excreted by microorganisms recently received wide attention as a possible way to recover and generate biopolymers (Felz et al., 2016). Other research also suggested that EPS of PAOs contains sialic acid that is of interest for medical applications (de Graaff et al., 2019).

So far, only scarce information is available on the exact biomass composition of photogranules, and it is often limited to major elements (i.e., C, N, P) or rudimentary photopigment analysis. It will be vital for biomass valorisation to determine the elemental composition (both macro- and micronutrients), constituents (e.g., photopigments, proteins, lipids, storage polymers) and physical and chemical properties of the biomass. Subsequently, the suitability of photogranule biomass as biofertilizer, soil amendment or biostimulant can be investigated and compared to conventional products. Downstream processing of the biomass must be explored to fractionate certain constituents and fully utilize the biomass in a biorefinery approach. This will

ultimately allow us to recover the valuable elements in wastewater and reuse them for multiple purposes in our economy.

4 CONCLUDING REMARKS

In this thesis we provided a holistic overview on photogranules; from their assembly, the influence of operational parameters (HRT, nitrogen limitation), the optimization of phosphorus removal, to potential upscale scenarios of this technology. Photogranulation was achieved by creating an environment that selected for well-settling biomass and the desired functions suitable for wastewater treatment for carbon and nutrient recovery. The microbial community was shown to be remarkably flexible in their microbial community assembly and functions. This was illustrated by their ability to perform N_2-fixation under nitrogen limitation and the introduction of polyphosphate accumulation under an alternating feast-famine regime to improve phosphorus recovery by 6x. Additionally, we gained valuable insight into the microscale functioning of photogranules, their physical structure and physical, chemical, and biological stratification. Photogranulation was shown to be possible by various taxonomically distinct microbial communities. Bioreactor performance was high in all experiments, showing high efficiency at nutrient removal and recovery. Photogranular technology was also demonstrated to be highly robust, keeping the targeted functions under varying microbial community compositions and operational conditions. Finally, I suggested a continuous flow reactor as a possible configuration for a large-scale natural light-driven photogranular wastewater treatment system.

We made the first steps towards the implementation of photogranular wastewater treatment technology at large scale. Clearly, we need to get a deeper fundamental understanding of the photogranules and must continue researching with an ecological and process engineering mind set. Investigating the metagenome, meta-transcriptome, metabolome, proteome of photogranules will reveal their full functional potential and highlight genes and metabolites that are crucial during photogranulation and the treatment process. Photogranule morphology and microscale functioning must be more closely investigated and connected to the environmental conditions that shape photogranule assembly and metabolic activity. Further, kinetic and mass transfer models should be established for microscale and process scale simulations that aid large-scale process and reactor design. The generated photogranular biomass should be explored for various valorisation options (e.g., biofertilizer, bioplastics). Ultimately, a cost-effective, robust, and easy-to-operate system must be designed that can be applied in low latitude countries around the world to secure water sanitation and the recovery of valuable elements.

5 MATERIALS AND METHODS

5.1 Meta-analysis on 16S and 18S rRNA gene amplicon sequencing data of photogranular microbial communities

Sequencing data from 6 studies on photogranules were obtained from the sequencing read archive (SRA) of NCBI (**table 2**). Primers were removed using *cutadapt* (version 1.18) (Martin, 2013). The obtained sequences were processed with DADA2 (Callahan et al., 2016). Taxonomic alignment of the sequences was done against the SILVA database (release 138) using SINA (https://www.arb-silva.de). The 16S and 18S data set was normalized using the cumulative sums scaling (CSS) function of the R package *metagenomSeq* version 1.24.1 (Paulson et al., 2013). The analysis of the microbiome data was performed with the R-package *phyloseq* (version 1.26.1) (McMurdie and Holmes, 2013) and *ampvis2* (Andersen et al., 2018). The community structure and the change over time of the 16S and 18S dataset were analysed by Principal Coordinate Analysis (PCoA) using weighted UniFrac distance (Lozupone et al., 2011). The 16S dataset was annotated with functions using the tool FAPROTAX (Louca et al., 2016). The default database of FAPROTAX was extended with taxa functionally annotated within the MiDAS database (version 4.8.1) (Nierychlo et al., 2020).

Table 1: Studies considered for the meta-analysis of the microbial community of photogranules. The assession number can be used to access the raw data at the sequencing read archive (SRA) from NCBI. AGS = Aerobic granular sludge; CAS = Conventional activated sludge; FWD = forward primer; REV = reverse primer.

Study	Investigation	Inoculum	Accession Nr.	16SrRNA primer		18SrRNA primer	
				FWD	REV	FWD	REV
Fan et al. 2021	Aqua. WWT	AGS	PRJNA693118	338-F	806-R	528-F	706-R
Fan et al. 2021	Light-effect	AGS	PRJNA723101	338-F	806-R	528-F	706-R
Ji et al. 2021	Temp.-effect	AGS	PRJNA636663	338-F	806-R	528-F	706-R
Shen et al. 2021	Cold storage	AGS	PRJNA715013	338-F	806-R	528-F	706-R
Milferstedt et al. 2017	Fil. cyanos	CAS	PRJNA393678	515-532U	909-928U	NA	NA
Strauch-White et al. 2017	N on assembly	CAS	PRJNA378555	515F	806R	NA	NA

5.2 Scenario analysis on large-scale PG+ wastewater treatment

The empirical data obtained on PG+ from **Chapter 5** was used to extrapolate our findings to different large-scale treatment scenarios. The calculations are based on the biomass yield on light ($Y_{X/ph}$) of 0.74 for phototrophs and biomass yield (Y_{PAO}) on substrate of 0.4 for PAOs. The growth of phototrophs on organic substrate was neglected for simplicity reasons.

The analysis was performed for spring and summer only (Mar 31st – Sep 30th) and the locations the Netherlands (low light = 31 mol photon/m²/d) (Boelee et al., 2012) and India (high light = 69 mol photon/m²/s) (Dalvi et al., 2021). The photon flux is denoted as $I_{ph.}$. Two different types of wastewaters were considered. One with a low N:P ratio of 4 (N = 40 mg/L; P = 20 mg/L, COD = 600 mg/L) and one with a high N:P ratio of 11 (N = 50 mg/L, P = 10 mg/L, COD = 200 mg/L). For each scenario a treatment capacity of 1000 people (130L wastewater per person) was considered, which resulted in a total inflow of $Q = 1000 \times 130 = 130\ 000\ L/d$. The operational parameters were chosen such that full N, P and COD removal was achieved. N and P was assimilated both by phototrophs and PAOs. COD removal was only done by PAOs for growth or denitrification. The growth of nitrifiers or via denitrification was neglected.

$$R_{X,photo} = I_{ph} \times Y_{X/ph} \left[\frac{g}{d}\right] \quad \text{(equation 1)}$$

$$R_{X,PAO} = Q \times (COD_{b,in} - COD_{b,out}) \times Y_{PAO} \left[\frac{g}{d}\right] \quad \text{(equation 2)}$$

An average composition of 7.8% N and 1.4% P for phototrophs and 7.2% N and 7.8% P for PAO was used. These are empirical values obtained from **Chapter 5**. With the amount of biomass produced and the fraction of N and P present in the biomass, the uptake of N (i.e., $R_{N,photo}$, $R_{N,PAO}$) and P from the wastewater was calculated. Calculation are shown here for N:

$$R_{N,photo} = R_{X,photo} \times f_{N,photo} \left[\frac{g}{d}\right] \quad \text{(equation 3)}$$

$$R_{N,PAO} = R_{X,PAO} \times f_{N,PAO} \left[\frac{g}{d}\right] \quad \text{(equation 4)}$$

The contribution of phototrophs and PAOs were chosen as such that full COD, N and P removal was achieved for each scenario. Nitrification and denitrification were considered in case full N removal was not possible by biomass assimilation or to reduce the footprint of the PG+ treatment system.

The footprint of the PG+ treatment system was calculated according to the phototrophic biomass produced:

$$A = \frac{R_{X/ph}}{I_{ph} Y_{X/ph}} [m^2]$$ (equation 5)

To assess the oxygen and carbon dioxide balance the production and consumption of phototrophs, PAOs and nitrifiers was assessed. The following stoichiometric reaction was used for phototrophs with ammonium as the nitrogen source:

$$CO_2 + 0.70H_2O + 0.12NH_4^+ + 0.01H_2PO_4^- \rightarrow CH_{1.78}O_{0.36}N_{0.12}P_{0.01} + 1.18O_2 + 0.11H^+$$ (equation 6)

Per 1 mol of biomass (on C-basis) 1.18 mol O_2 is produced. With this the overall O_2 production was obtained per produced phototrophic biomass. The oxygen consumption of the sludge (*Ro*) consists of the oxygen requirement of the PAOs degrading the COD, and if applicable, nitrifiers converting NH_4^+. The *Ro* is calculated according to:

$$R_O = Q \times (COD_{b,in} - COD_{b,out}) - 1.42 \times P_X + 4.33 \times Q \times (N_{in} - N_{out}) - 2.86 \times (N_{in} - N_{out}) [\frac{g}{d}]$$ (equation 7)

Carbon dioxide production by PAOs was obtained using this stoichiometric reaction:

$$5CH_3COO^- + 1NH_4^+ + 5O_2 \rightarrow C_5H_7O_2N + 3H_2O + 5CO_2 + 5OH^-$$ (equation 8)

Per 1 mol of COD (assuming acetate) 0.5 mol of CO_2 is produced. The CO_2 consumption of nitrification was assumed to be negligible.

Oxygen and carbon dioxide consumption of nitrification:

$$NH_4^+ + 0.0298NH_4^+ + 1.851O_2 + 0.1192CO_2 + 0.0298HCO_3^- \rightarrow 0.0298C_5H_7NO_2 + NO_3^- + 0.9702\,H_2O + H^+$$ (equation 9)

COD consumption and CO_2 production of denitrification:

$$\frac{2.86}{(1 - Y_{OHO})} = 8.6\ mg\ COD/mg\ NO_3 \quad \text{(equation. 10)}$$

The oxygen equivalent of nitrate is 2.86 mgO/mgNO_3-N. For every mg of NO_3, 8.6 mg of COD is necessary.

$$5\ CH_3COOH + 8\ NO_3^- \rightarrow 4\ N_2 + 10\ CO_2 + 6\ H_2O + 8\ OH^- \quad \text{(equation. 11)}$$

For every mol acetate, 2 mol of CO_2 is generated.

References

REFERENCES

Abouhend, A.S., McNair, A., Kuo-Dahab, W.C., Watt, C., Butler, C.S., Milferstedt, K., Hamelin, J., Seo, J., Gikonyo, G.J., El-Moselhy, K.M., Park, C., 2018. The Oxygenic Photogranule Process for Aeration-Free Wastewater Treatment. Environ. Sci. Technol. 52, 3503–3511. https://doi.org/10.1021/acs.est.8b00403

Abouhend, A.S., Milferstedt, K., Hamelin, J., Ansari, A.A., Butler, C., Carbajal-González, B.I., Park, C., 2020. Growth Progression of Oxygenic Photogranules and Its Impact on Bioactivity for Aeration-Free Wastewater Treatment. Environ. Sci. Technol. 54, 486–496. https://doi.org/10.1021/acs.est.9b04745

Adav, S.S., Lee, D.-J., 2008. Extraction of extracellular polymeric substances from aerobic granule with compact interior structure. J. Hazard. Mater. 154, 1120–1126. https://doi.org/10.1016/j.jhazmat.2007.11.058

Adav, S.S., Lee, D.J., Lai, J.Y., 2010. Microbial community of acetate utilizing denitrifiers in aerobic granules. Appl. Microbiol. Biotechnol. 85, 753–762. https://doi.org/10.1007/s00253-009-2263-6

Adav, S.S., Lee, D.J., Tay, J.H., 2008. Extracellular polymeric substances and structural stability of aerobic granule. Water Res. 42, 1644–1650. https://doi.org/10.1016/j.watres.2007.10.013

Ahmad, J.S.M., Cai, W., Zhao, Z., Zhang, Z., Shimizu, K., Lei, Z., Lee, D.J., 2017. Stability of algal-bacterial granules in continuous-flow reactors to treat varying strength domestic wastewater. Bioresour. Technol. 244, 225–233. https://doi.org/10.1016/j.biortech.2017.07.134

Albertsen, M., Karst, S.M., Ziegler, A.S., Kirkegaard, R.H., Nielsen, P.H., 2015. Back to basics - The influence of DNA extraction and primer choice on phylogenetic analysis of activated sludge communities. PLoS One 10, 1–15. https://doi.org/10.1371/journal.pone.0132783

Alpkvist, E., Picioreanu, C., van Loosdrecht, M.C.M., Heyden, A., 2006. Three-dimensional biofilm model with individual cells and continuum EPS matrix. Biotechnol. Bioeng. 94, 961–979. https://doi.org/10.1002/bit.20917

Alzate Marin, J.C., Caravelli, A.H., Zaritzky, N.E., 2016. Nitrification and aerobic denitrification in anoxic-aerobic sequencing batch reactor. Bioresour. Technol. 200, 380–387. https://doi.org/10.1016/j.biortech.2015.10.024

Andersen, K.S., Kirkegaard, R.H., Karst, S.M., Albertsen, M., 2018. ampvis2: An R package to analyse and visualise 16S rRNA amplicon data. bioRxiv 10–11. https://doi.org/10.1101/299537

Ansari, A.A., Abouhend, A.S., Park, C., 2019. Effects of seeding density on photogranulation and the start-up of the oxygenic photogranule process for aeration-free wastewater treatment. Algal Res. 40, 101495. https://doi.org/10.1016/j.algal.2019.101495

APHA/AWWA/WEF, 2012. Standard Methods for the Examination of Water and Wastewater. Stand. Methods 541. https://doi.org/ISBN 9780875532356

Arashiro, L.T., Rada-Ariza, A.M., Wang, M., Van Der Steen, P., Ergas, S.J., 2017. Modelling shortcut nitrogen removal from wastewater using an algal-bacterial consortium. Water Sci. Technol. 75, 782–792. https://doi.org/10.2166/wst.2016.561

Arcila, J.S., Buitrón, G., 2016. Microalgae–bacteria aggregates: effect of the hydraulic retention time on the municipal wastewater treatment, biomass settleability and methane potential. J. Chem. Technol. Biotechnol. 91, 2862–2870. https://doi.org/10.1002/jctb.4901

Ardern, E., Lockett, W.T., 1914. Experiments on the oxidation of sewage without the aid of filters. J. Soc. Chem. Ind. 33, 523–539. https://doi.org/10.1002/jctb.5000331005

Baeten, J.E., van Loosdrecht, M.C.M., Volcke, E.I.P., 2018. Modelling aerobic granular sludge reactors through apparent half-saturation coefficients. Water Res. 146, 134–145. https://doi.org/10.1016/j.watres.2018.09.025

Beeftink, H.H., van den Heuvel, J.C., 1987. Novel anaerobic gas-lift reactor (AGLR) with retention of biomass: Start-up routine and establishment of hold up. Biotechnol. Bioeng. 30, 233–238. https://doi.org/10.1002/bit.260300213

Bergman, B., Gallon, J.., Rai, A.., Stal, L.., 1997. N2 Fixation by non-heterocystous cyanobacteria1. FEMS Microbiol. Rev. 19, 139–185. https://doi.org/10.1111/j.1574-6976.1997.tb00296.x

Berrendero, E., Perona, E., Mateo, P., 2008. Genetic and morphological characterization of Rivularia and Calothrix (Nostocales, Cyanobacteria) from running water. Int. J. Syst. Evol. Microbiol. 58, 447–460. https://doi.org/10.1099/ijs.0.65273-0

Berrendero, E., Valiente, E.F., Perona, E., Gómez, C.L., Loza, V., Munõz-Martín, M.Á., Mateo, P., 2016. Nitrogen

fixation in a non-heterocystous cyanobacterial mat from a mountain river. Sci. Rep. 6, 1–13. https://doi.org/10.1038/srep30920

Beun, J.J., Hendriks, A., Van Loosdrecht, M.C.M., Morgenroth, E., Wilderer, P.A., Heijnen, J.J., 1999. Aerobic granulation in a sequencing batch reactor. Water Res. 33, 2283–2290. https://doi.org/10.1016/S0043-1354(98)00463-1

Blanken, W., Cuaresma, M., Wijffels, R.H., Janssen, M., 2013. Cultivation of microalgae on artificial light comes at a cost. Algal Res. 2, 333–340. https://doi.org/10.1016/j.algal.2013.09.004

Boelee, N.C., Temmink, H., Janssen, M., Buisman, C.J.N., Wijffels, R.H., 2012. Scenario Analysis of Nutrient Removal from Municipal Wastewater by Microalgal Biofilms. Water 4, 460–473. https://doi.org/10.3390/w4020460

Borowitzka, M.A., 2013. High-value products from microalgae-their development and commercialisation. J. Appl. Phycol. 25, 743–756. https://doi.org/10.1007/s10811-013-9983-9

Borowitzka, M.A., Beardall, J., Raven, J.A., 2016. The Physiology of Microalgae, Journal of Applied Phycology. https://doi.org/10.3354/ame01390

Borowitzka, M.A., Moheimani, N.R., 2013. Algae for Biofuels and Energy, Algae for Biofuels and Energy. Springer Netherlands, Dordrecht. https://doi.org/10.1007/978-94-007-5479-9

Bothe, H., Schmitz, O., Yates, M.G., Newton, W.E., 2010. Nitrogen Fixation and Hydrogen Metabolism in Cyanobacteria. Microbiol. Mol. Biol. Rev. 74, 529–551. https://doi.org/10.1128/MMBR.00033-10

Bradley, I.M., Sevillano-Rivera, M.C., Pinto, A.J., Guest, J.S., 2019. Impact of solids residence time on community structure and nutrient dynamics of mixed phototrophic wastewater treatment systems. Water Res. 150, 271–282. https://doi.org/10.1016/j.watres.2018.11.065

Braman, R.S., Hendrix, S.A., 1989. Nanogram nitrite and nitrate determination in environmental and biological materials by vanadium(III) reduction with chemiluminescence detection. Anal. Chem. 61, 2715–2718. https://doi.org/10.1021/ac00199a007

Brehm, U., Krumbein, W.E., Palińska, K.A., 2003. Microbial spheres: a novel cyanobacterial–diatom symbiosis. Naturwissenschaften 90, 136–140. https://doi.org/10.1007/s00114-003-0403-x

Brocke, H.J., Piltz, B., Herz, N., Abed, R.M.M., Palinska, K.A., John, U., Haan, J. den, de Beer, D., Nugues, M.M., 2018. Nitrogen fixation and diversity of benthic cyanobacterial mats on coral reefs in Curaçao. Coral Reefs 37, 861–874. https://doi.org/10.1007/s00338-018-1713-y

Brockmann, D., Gérand, Y., Park, C., Milferstedt, K., Hélias, A., Hamelin, J., 2021. Wastewater treatment using oxygenic photogranule-based process has lower environmental impact than conventional activated sludge process. Bioresour. Technol. 319. https://doi.org/10.1016/j.biortech.2020.124204

Burian, A., Pinn, D., Peralta-Maraver, I., Sweet, M., Mauvisseau, Q., Eyice, O., Bulling, M., Röthig, T., Kratina, P., 2021. Predation increases multiple components of microbial diversity in activated sludge communities. ISME J. 1–9. https://doi.org/10.1038/s41396-021-01145-z

Cai, W., Zhao, Z., Li, D., Lei, Z., Zhang, Z., Lee, D.-J.J., 2019. Algae granulation for nutrients uptake and algae harvesting during wastewater treatment. Chemosphere 214, 55–59. https://doi.org/10.1016/j.chemosphere.2018.09.107

Cakir, F.Y., Stenstrom, M.K., 2005. Greenhouse gas production: A comparison between aerobic and anaerobic wastewater treatment technology. Water Res. 39, 4197–4203. https://doi.org/10.1016/j.watres.2005.07.042

Callahan, B.J., McMurdie, P.J., Rosen, M.J., Han, A.W., Johnson, A.J.A., Holmes, S.P., 2016. DADA2: High-resolution sample inference from Illumina amplicon data. Nat. Methods 13, 581–583. https://doi.org/10.1038/nmeth.3869

Carvalho, V.C.F., Freitas, E.B., Silva, P.J., Fradinho, J.C., Reis, M.A.M., Oehmen, A., 2018. The impact of operational strategies on the performance of a photo-EBPR system. Water Res. 129, 190–198. https://doi.org/10.1016/j.watres.2017.11.010

Carvalho, V.C.F., Kessler, M., Fradinho, J.C., Oehmen, A., Reis, M.A.M., 2021. Achieving nitrogen and phosphorus removal at low C/N ratios without aeration through a novel phototrophic process. Sci. Total Environ. 793, 148501. https://doi.org/10.1016/j.scitotenv.2021.148501

Casagli, F., Rossi, S., Steyer, J.P., Bernard, O., Ficara, E., 2021. Balancing Microalgae and Nitrifiers for Wastewater Treatment: Can Inorganic Carbon Limitation Cause an Environmental Threat? Environ. Sci. Technol. 55, 3940–3955. https://doi.org/10.1021/acs.est.0c05264

Castenholz, R.W., 1968. The behavior of Oscillatoria terebriformis in hot springs. J. Phycol. 4, 132–139. https://doi.org/10.1111/j.1529-8817.1968.tb04687.x

Castenholz, R.W., 1967. Aggregation in a Thermophilic Oscillatoria. Nature 215, 1285–1286. https://doi.org/10.1038/2151285a0

Castenholz, R.W., Rippka, R., Herdman, M., Wilmotte, A., 2015. Subsection III, in: Bergey's Manual of Systematics of Archaea and Bacteria, Major Reference Works. Wiley, pp. 1–4. https://doi.org/10.1002/9781118960608.gbm00432

Chen, G., Ekama, G.A., van Loosdrecht, M.C.M., Brdjanovic, D. (Eds.), 2020. Biological Wastewater Treatment: Principles, Modeling and Design. IWA Publishing. https://doi.org/10.2166/9781789060362

Cieślik, B.M., Namieśnik, J., Konieczka, P., 2015. Review of sewage sludge management: Standards, regulations and analytical methods. J. Clean. Prod. 90, 1–15. https://doi.org/10.1016/j.jclepro.2014.11.031

Cuaresma Franco, M., Buffing, M.F., Janssen, M., Vílchez Lobato, C., Wijffels, R.H., 2012. Performance of Chlorella sorokiniana under simulated extreme winter conditions. J. Appl. Phycol. 24, 693–699. https://doi.org/10.1007/s10811-011-9687-y

Dalvi, V., Chawla, P., Malik, A., 2021. Year-long performance assessment of an on-site pilot scale (100 L) photobioreactor on nutrient recovery and pathogen removal from urban wastewater using native microalgal consortium. Algal Res. 55, 102228. https://doi.org/10.1016/j.algal.2021.102228

de Beer, D., Schramm, A., Santegoeds, C.M., Kuhl, M., 1997. A nitrite microsensor for profiling environmental biofilms. Appl. Environ. Microbiol. 63, 973–977. https://doi.org/10.1128/aem.63.3.973-977.1997

de Beer, D., Weber, M., Chennu, A., Hamilton, T., Lott, C., Macalady, J., M. Klatt, J., 2017. Oxygenic and anoxygenic photosynthesis in a microbial mat from an anoxic and sulfidic spring. Environ. Microbiol. 19, 1251–1265. https://doi.org/10.1111/1462-2920.13654

de Graaff, D.R., Felz, S., Neu, T.R., Pronk, M., van Loosdrecht, M.C.M., Lin, Y., 2019. Sialic acids in the extracellular polymeric substances of seawater-adapted aerobic granular sludge. Water Res. 155, 343–351. https://doi.org/10.1016/j.watres.2019.02.040

de Graaff, D.R., van Loosdrecht, M.C.M., Pronk, M., 2020. Biological phosphorus removal in seawater-adapted aerobic granular sludge. Water Res. 172, 115531. https://doi.org/10.1016/j.watres.2020.115531

de Kreuk, M.K., 2006. Aerobic Granular Sludge: Scaling up a new technology. TU Delft.

de Kreuk, M.K., Heijnen, J.J., Van Loosdrecht, M.C.M., 2005. Simultaneous COD, nitrogen, and phosphate removal by aerobic granular sludge. Biotechnol. Bioeng. 90, 761–769. https://doi.org/10.1002/bit.20470

de Kreuk, M.K., Picioreanu, C., Hosseini, M., Xavier, J.B., van Loosdrecht, M.C.M., 2007. Kinetic model of a granular sludge SBR: Influences on nutrient removal. Biotechnol. Bioeng. 97, 801–815. https://doi.org/10.1002/bit.21196

de Kreuk, M.K., van Loosdrecht, M.C.M., 2004. Selection of slow growing organisms as a means for improving aerobic granular sludge stability. Water Sci. Technol. 49, 9–17. https://doi.org/10.2166/wst.2004.0792

de Sousa Rollemberg, S.L., Mendes Barros, A.R., Milen Firmino, P.I., Bezerra dos Santos, A., 2018. Aerobic granular sludge: Cultivation parameters and removal mechanisms. Bioresour. Technol. 270, 678–688. https://doi.org/10.1016/j.biortech.2018.08.130

Ding, Z., Bourven, I., Guibaud, G., van Hullebusch, E.D., Panico, A., Pirozzi, F., Esposito, G., 2015. Role of extracellular polymeric substances (EPS) production in bioaggregation: application to wastewater treatment. Appl. Microbiol. Biotechnol. 99, 9883–9905. https://doi.org/10.1007/s00253-015-6964-8

DuBois, M., Gilles, K.A., Hamilton, J.K., Rebers, P.A., Smith, F., 1956. Colorimetric Method for Determination of Sugars and Related Substances. Anal. Chem. 28, 350–356. https://doi.org/10.1021/ac60111a017

Fan, S., Ji, B., Abu Hasan, H., Fan, J., Guo, S., Wang, J., Yuan, J., 2021a. Microalgal–bacterial granular sludge process for non-aerated aquaculture wastewater treatment. Bioprocess Biosyst. Eng. 44, 1733–1739. https://doi.org/10.1007/s00449-021-02556-0

Fan, S., Zhu, L., Ji, B., 2021b. Deciphering the effect of light intensity on microalgal-bacterial granular sludge process for non-aerated municipal wastewater treatment. Algal Res. 58, 102437. https://doi.org/10.1016/j.algal.2021.102437

Fang, F., Yang, L., Gan, L., Guo, L., Hu, Z., Yuan, S., Chen, Q., Jiang, L., 2014. DO, pH, and Eh microprofiles in cyanobacterial granules from Lake Taihu under different environmental conditions. J. Appl. Phycol. 26, 1689–1699. https://doi.org/10.1007/s10811-013-0211-4

Fani, R., Gallo, R., Liò, P., 2000. Molecular Evolution of Nitrogen Fixation: The Evolutionary History of the nifD, nifK, nifE, and nifN Genes. J. Mol. Evol. 51, 1–11. https://doi.org/10.1007/s002390010061

Felz, S., Al-Zuhairy, S., Aarstad, O.A., van Loosdrecht, M.C.M., Lin, Y.M., 2016. Extraction of structural extracellular polymeric substances from aerobic granular sludge. J. Vis. Exp. 2016, 1–8. https://doi.org/10.3791/54534

Fernandes, T. V., Shrestha, R., Sui, Y., Papini, G., Zeeman, G., Vet, L.E.M., Wijffels, R.H., Lamers, P., 2015. Closing Domestic Nutrient Cycles Using Microalgae. Environ. Sci. Technol. 49, 12450–12456. https://doi.org/10.1021/acs.est.5b02858

Fernandes, T. V., Suárez-Muñoz, M., Trebuch, L.M., Verbraak, P.J., Van de Waal, D.B., 2017. Toward an Ecologically Optimized N:P Recovery from Wastewater by Microalgae. Front. Microbiol. 8, 1–6. https://doi.org/10.3389/fmicb.2017.01742

Fernando, E.Y., McIlroy, S.J., Nierychlo, M., Herbst, F.-A., Petriglieri, F., Schmid, M.C., Wagner, M., Nielsen, J.L., Nielsen, P.H., 2019. Resolving the individual contribution of key microbial populations to enhanced biological phosphorus removal with Raman–FISH. ISME J. 13, 1933–1946. https://doi.org/10.1038/s41396-019-0399-7

Flemming, H.C., Neu, T.R., Wozniak, D.J., 2007. The EPS Matrix: The "House of Biofilm Cells." J. Bacteriol. 189, 7945–7947. https://doi.org/10.1128/JB.00858-07

Flemming, H.C., Wingender, J., 2010. The biofilm matrix. Nat. Rev. Microbiol. 8, 623–633. https://doi.org/10.1038/nrmicro2415

Flemming, H.C., Wingender, J., Szewzyk, U., Steinberg, P., Rice, S.A., Kjelleberg, S., 2016. Biofilms: An emergent form of bacterial life. Nat. Rev. Microbiol. 14, 563–575. https://doi.org/10.1038/nrmicro.2016.94

Flores, E., López-Lozano, A., Herrero, A., 2015. Nitrogen Fixation in the Oxygenic Phototrophic Prokaryotes (Cyanobacteria): The Fight Against Oxygen, in: Biological Nitrogen Fixation. John Wiley & Sons, Inc, Hoboken, NJ, USA, pp. 879–890. https://doi.org/10.1002/9781119053095.ch86

Garcia-Pichel, F., Castenholz, R.W., 2001. Chapter 14 Photomovement of microorganisms in benthic and soil microenvironments, in: Häder, D.-P., Breure, A.M.B.T.-C.S. in P. (Eds.), Photomovement. Elsevier, pp. 403–420. https://doi.org/https://doi.org/10.1016/S1568-461X(01)80018-1

George, D.M., Vincent, A.S., Mackey, H.R., 2020. An overview of anoxygenic phototrophic bacteria and their applications in environmental biotechnology for sustainable Resource recovery. Biotechnol. Reports 28, e00563. https://doi.org/10.1016/j.btre.2020.e00563

Gikonyo, J.G., Ansari, A.A., Abouhend, A.S., Tobiason, J.E., Park, C., 2021. Hydrodynamic granulation of oxygenic photogranules. Environ. Sci. Water Res. Technol. 7, 427–440. https://doi.org/10.1039/D0EW00957A

Gonzalez-Gil, G., Holliger, C., 2014. Aerobic granules: Microbial landscape and architecture, stages, and practical implications. Appl. Environ. Microbiol. 80, 3433–3441. https://doi.org/10.1128/AEM.00250-14

Grewe, C.B., Pulz, O., 2012. The Biotechnology of Cyanobacteria, in: Ecology of Cyanobacteria II. Springer Netherlands, Dordrecht, pp. 707–739. https://doi.org/10.1007/978-94-007-3855-3_26

Grigoryeva, N.Y., Liss, A.A., 2020. Prospects of fluorescence methods application for monitoring of cyanobacterial cultures in biotechnology, in: Abstract Book of the 2nd International Scientific Conference "Plants and Microbes: The Future of Biotechnology" PLAMIC2020. PLAMIC2020 Organizing committee. https://doi.org/10.28983/PLAMIC2020.095

Guerrero, M.A., Jones, R.D., 1996. Photoinhibition of marine nitrifying bacteria. I. Wavelength-dependent response. Mar. Ecol. Prog. Ser. 141, 183–192. https://doi.org/10.3354/meps141183

Gutzeit, G., Lorch, D., Weber, A., Engels, M., Neis, U., 2005. Bioflocculent algal-bacterial biomass improves low-cost wastewater treatment . Water Sci Technol. Water Sci Technol 52, 9–18.

Häder, D.-P., 1984. Wie orientieren sich Cyanobakterien im Licht. Biol. unserer Zeit 14, 78–83. https://doi.org/https://doi.org/10.1002/biuz.19840140304

Häder, D.P., 1987. Photosensory behavior in procaryotes. Microbiol. Rev. 51, 1–21. https://doi.org/10.1128/MMBR.51.1.1-21.1987

Hagemann, M., Eisenhut, M., Hackenberg, C., Bauwe, H., 2010. Recent Advances in Phototrophic Prokaryotes, Advances in experimental medicine and biology, Advances in Experimental Medicine and Biology. Springer New York, New York, NY. https://doi.org/10.1007/978-1-4419-1528-3

Hanada, S., Hiraishi, A., Shimada, K., Matsuura, K., 1995. Chloroflexus aggregans sp. nov., a filamentous phototrophic bacterium which forms dense cell aggregates by active gliding movement. Int. J. Syst. Bacteriol. 45, 676–681. https://doi.org/10.1099/00207713-45-4-676

Haq, S.H., Al-Ruwaished, G., Al-Mutlaq, M.A., Naji, S.A., Al-Mogren, M., Al-Rashed, S., Ain, Q.T., Al-Amro, A.A., Al-Mussallam, A., 2019. Antioxidant, Anticancer Activity and Phytochemical Analysis of Green Algae, Chaetomorpha Collected from the Arabian Gulf. Sci. Rep. 9, 18906. https://doi.org/10.1038/s41598-019-55309-1

Henze, M., 2008. Biological wastewater treatment : principles, modelling and design LK - https://wur.on.worldcat.org/oclc/236186544, TA - TT -. IWA Pub., London SE - 511 pages : illustrations (some color) ; 29 cm.

Herlemann, D.P.R., Labrenz, M., Jürgens, K., Bertilsson, S., Waniek, J.J., Andersson, A.F., 2011. Transitions in bacterial communities along the 2000 km salinity gradient of the Baltic Sea. ISME J. 5, 1571–1579. https://doi.org/10.1038/ismej.2011.41

Hollander, M. de, 2018. nioo-knaw/hydra: 1.3.6. https://doi.org/10.5281/ZENODO.1434147

Holtappels, M., Lavik, G., Jensen, M.M., Kuypers, M.M.M., 2011. 15N-Labeling Experiments to Dissect the Contributions of Heterotrophic Denitrification and Anammox to Nitrogen Removal in the OMZ Waters of the Ocean, in: Methods in Enzymology. Elsevier Inc., pp. 223–251. https://doi.org/10.1016/B978-0-12-381294-0.00010-9

Huang, W., Li, B., Zhang, C., Zhang, Z., Lei, Z., Lu, B., Zhou, B., 2015. Effect of algae growth on aerobic granulation and nutrients removal from synthetic wastewater by using sequencing batch reactors. Bioresour. Technol. 179, 187–192. https://doi.org/10.1016/j.biortech.2014.12.024

Huber, M., Knutti, R., 2012. Anthropogenic and natural warming inferred from changes in Earth's energy balance. Nat. Geosci. 5, 31–36. https://doi.org/10.1038/ngeo1327

Hugerth, L.W., Muller, E.E.L., Hu, Y.O.O., Lebrun, L.A.M., Roume, H., Lundin, D., Wilmes, P., Andersson, A.F., 2014. Systematic design of 18S rRNA gene primers for determining eukaryotic diversity in microbial consortia. PLoS One 9. https://doi.org/10.1371/journal.pone.0095567

Irvine-Fynn, T.D.L., Bridge, J.W., Hodson, A.J., 2010. Rapid quantification of cryoconite: granule geometry and in situ supraglacial extents, using examples from Svalbard and Greenland. J. Glaciol. 56, 297–308. https://doi.org/10.3189/002214310791968421

Janssen, M., 2016. Microalgal Photosynthesis and Growth in Mass Culture, 1st ed, Advances in Chemical Engineering. Elsevier Inc. https://doi.org/10.1016/bs.ache.2015.11.001

Ji, B., Liu, C., 2022. CO2 improves the microalgal-bacterial granular sludge towards carbon-negative wastewater treatment. Water Res. 208, 117865. https://doi.org/10.1016/j.watres.2021.117865

Ji, B., Liu, Y., 2021. Assessment of Microalgal-Bacterial Granular Sludge Process for Environmentally Sustainable Municipal Wastewater Treatment. ACS ES&T Water 1, 2459–2469. https://doi.org/10.1021/acsestwater.1c00303

Ji, B., Zhang, M., Wang, L., Wang, S., Liu, Y., 2020. Removal mechanisms of phosphorus in non-aerated microalgal-bacterial granular sludge process. Bioresour. Technol. 312, 123531. https://doi.org/10.1016/j.biortech.2020.123531

Ji, B., Zhu, L., Wang, S., Liu, Y., 2021. Temperature-effect on the performance of non-aerated microalgal-bacterial granular sludge process in municipal wastewater treatment. J. Environ. Manage. 282, 111955. https://doi.org/10.1016/j.jenvman.2021.111955

Karya, N.G.A.I., van der Steen, N.P., Lens, P.N.L., 2013. Photo-oxygenation to support nitrification in an algal-bacterial consortium treating artificial wastewater. Bioresour. Technol. 134, 244–250. https://doi.org/10.1016/j.biortech.2013.02.005

Kehrein, P., Van Loosdrecht, M., Osseweijer, P., Garfí, M., Dewulf, J., Posada, J., 2020. A critical review of resource recovery from municipal wastewater treatment plants-market supply potentials, technologies and bottlenecks. Environ. Sci. Water Res. Technol. 6, 877–910. https://doi.org/10.1039/c9ew00905a

Kleikamp, H.B.C., Pronk, M., Tugui, C., Guedes da Silva, L., Abbas, B., Lin, Y.M., van Loosdrecht, M.C.M., Pabst, M., 2021. Database-independent de novo metaproteomics of complex microbial communities. Cell Syst. 12, 375-383.e5. https://doi.org/10.1016/j.cels.2021.04.003

Klipp, W., Masepohl, B., Gallon, J.R., Newton, W.E., 2005. Genetics and Regulation of Nitrogen Fixation in Free-Living Bacteria, Genetics and Regulation of Nitrogen Fixation in Free-Living Bacteria, Nitrogen Fixation: Origins, Applications, and Research Progress. Kluwer Academic Publishers, Dordrecht. https://doi.org/10.1007/1-4020-2179-8

Konopka, A., 2009. What is microbial community ecology. ISME J. 3, 1223–1230. https://doi.org/10.1038/ismej.2009.88

Köster, J., Rahmann, S., 2012. Snakemake-a scalable bioinformatics workflow engine. Bioinformatics 28, 2520–2522. https://doi.org/10.1093/bioinformatics/bts480

Kruschel, C., Castenholz, R.W., 1998. The effect of solar UV and visible irradiance on the vertical movements of cyanobacteria in microbial mats of hypersaline waters. FEMS Microbiol. Ecol. 27, 53–72. https://doi.org/10.1016/S0168-6496(98)00056-7

Kühl, M., Fenchel, T., 2000. Bio-optical characteristics and the vertical distribution of photosynthetic pigments and photosynthesis in an artificial cyanobacterial mat. Microb. Ecol. 40, 94–103. https://doi.org/10.1007/s002480000061

Kumar, R., Venugopalan, V.P., 2015. Development of self-sustaining phototrophic granular biomass for bioremediation applications. Curr. Sci. 108, 1653–1661.

Kuo-Dahab, W.C., Stauch-White, K., Butler, C.S., Gikonyo, G.J., Carbajal-González, B., Ivanova, A., Dolan, S., Park, C., 2018. Investigation of the Fate and Dynamics of Extracellular Polymeric Substances (EPS) during Sludge-Based Photogranulation under Hydrostatic Conditions. Environ. Sci. Technol. 52, 10462–10471. https://doi.org/10.1021/acs.est.8b03033

Lackner, K.S., Azarabadi, H., 2021. Buying down the Cost of Direct Air Capture. Ind. Eng. Chem. Res. 60, 8196–8208. https://doi.org/10.1021/acs.iecr.0c04839

Langford, H., Hodson, A., Banwart, S., Bøggild, C., 2010. The microstructure and biogeochemistry of Arctic cryoconite granules. Ann. Glaciol. 51, 87–94. https://doi.org/10.3189/172756411795932083

Lemaire, R., Yuan, Z., Blackall, L.L., Crocetti, G.R., 2008. Microbial distribution of Accumulibacter spp. and Competibacter spp. in aerobic granules from a lab-scale biological nutrient removal system. Environ. Microbiol. 10, 354–363. https://doi.org/10.1111/j.1462-2920.2007.01456.x

Lettinga, G., van Velsen, A.F.M., Hobma, S.W., de Zeeuw, W., Klapwijk, A., 1980. Use of the upflow sludge blanket (USB) reactor concept for biological wastewater treatment, especially for anaerobic treatment. Biotechnol. Bioeng. 22, 699–734. https://doi.org/10.1002/bit.260220402

Li, D., Yang, J., Li, Y., Zhang, J., 2021. Research on rapid cultivation of aerobic granular sludge (AGS) with different feast-famine strategies in continuous flow reactor and achieving high-level denitrification via utilization of soluble microbial product (SMP). Sci. Total Environ. 786, 147237. https://doi.org/10.1016/j.scitotenv.2021.147237

Li, H., Sherman, D.M., Bao, S., Sherman, L.A., 2001. Pattern of cyanophycin accumulation in nitrogen-fixing and non-nitrogen-fixing cyanobacteria. Arch. Microbiol. 176, 9–18. https://doi.org/10.1007/s002030100281

Li, P., Harding, S.E., Liu, Z., 2001. Cyanobacterial exopolysaccharides: Their nature and potential biotechnological applications. Biotechnol. Genet. Eng. Rev. 18, 375–404. https://doi.org/10.1080/02648725.2001.10648020

Lichtenthaler, H.K., 1987. Chlorophylls and Carotenoids: Pigments of Photosynthetic Biomembranes. Methods Enzymol. 148, 350–382. https://doi.org/10.1016/0076-6879(87)48036-1

Liu, G., Wang, J., 2012. Probing the stoichiometry of the nitrification process using the respirometric approach. Water Res. 46, 5954–5962. https://doi.org/10.1016/j.watres.2012.08.006

Liu, L., Fan, H., Liu, Y., Liu, C., Huang, X., 2017. Development of algae-bacteria granular consortia in photo-sequencing batch reactor. Bioresour. Technol. 232, 64–71. https://doi.org/10.1016/j.biortech.2017.02.025

Liu, L., Zeng, Z., Bee, M., Gibson, V., Wei, L., Huang, X., Liu, C., 2018. Characteristics and performance of aerobic algae-bacteria granular consortia in a photo-sequencing batch reactor. J. Hazard. Mater. 349, 135–142. https://doi.org/10.1016/j.jhazmat.2018.01.059

Liu, X.W., Sheng, G.P., Yu, H.Q., 2009. Physicochemical characteristics of microbial granules. Biotechnol. Adv. 27,

1061–1070. https://doi.org/10.1016/j.biotechadv.2009.05.020

Liu, Y.J., Gu, J., Liu, Y., 2018. Energy self-sufficient biological municipal wastewater reclamation: Present status, challenges and solutions forward. Bioresour. Technol. 269, 513–519. https://doi.org/10.1016/j.biortech.2018.08.104

Loosdrecht, M.C.., Picioreanu, C., Heijnen, J.J., 1997. A more unifying hypothesis for biofilm structures. FEMS Microbiol. Ecol. 24, 181–183. https://doi.org/10.1111/j.1574-6941.1997.tb00434.x

Lopez-Vazquez, C.M., Oehmen, A., Hooijmans, C.M., Brdjanovic, D., Gijzen, H.J., Yuan, Z., van Loosdrecht, M.C.M., 2009. Modeling the PAO-GAO competition: Effects of carbon source, pH and temperature. Water Res. 43, 450–462. https://doi.org/10.1016/j.watres.2008.10.032

Louca, S., Parfrey, L.W., Doebeli, M., 2016. Decoupling function and taxonomy in the global ocean microbiome. Science (80-.). 353, 1272–1277. https://doi.org/10.1126/science.aaf4507

Louca, S., Polz, M.F., Mazel, F., Albright, M.B.N., Huber, J.A., O'Connor, M.I., Ackermann, M., Hahn, A.S., Srivastava, D.S., Crowe, S.A., Doebeli, M., Parfrey, L.W., 2018. Function and functional redundancy in microbial systems. Nat. Ecol. Evol. 2, 936–943. https://doi.org/10.1038/s41559-018-0519-1

Lowry, O.H., Rosebrough, N.J., Farr, A.L., Randall, R.J., 1951. Protein measurement with the Folin phenol reagent. J. Biol. Chem. 193, 265–75. https://doi.org/10.1016/0304-3894(92)87011-4

Lozupone, C., Lladser, M.E., Knights, D., Stombaugh, J., Knight, R., 2011. UniFrac: An effective distance metric for microbial community comparison. ISME J. 5, 169–172. https://doi.org/10.1038/ismej.2010.133

Lyimo, T., Hamisi, M., 2009. Cyanobacteria Occurrence and Nitrogen Fixation Rates in the Seagrass Meadows of the East Coast of Zanzibar: Comparisons of Sites With and Without Seaweed Farms. West. Indian Ocean J. Mar. Sci. 7. https://doi.org/10.4314/wiojms.v7i1.48253

Mahowald, N., Jickells, T.D., Baker, A.R., Artaxo, P., Benitez-Nelson, C.R., Bergametti, G., Bond, T.C., Chen, Y., Cohen, D.D., Herut, B., Kubilay, N., Losno, R., Luo, C., Maenhaut, W., McGee, K.A., Okin, G.S., Siefert, R.L., Tsukuda, S., 2008. Global distribution of atmospheric phosphorus sources, concentrations and deposition rates, and anthropogenic impacts. Global Biogeochem. Cycles 22. https://doi.org/10.1029/2008GB003240

Malin, G., Walsby, A.E., 1985. Chemotaxis of a cyanobacterium on concentration gradients of carbon dioxide, bicarbonate and oxygen. J. Gen. Microbiol. 131, 2643–2652. https://doi.org/10.1099/00221287-131-10-2643

Martin, M., 2013. Cutadapt removes adapter sequences from high-throughput sequencing reads. EMBnet.journal 17, 10–12. https://doi.org/10.14806/ej.17.1.200

McCarty, P.L., Bae, J., Kim, J., 2011. Domestic wastewater treatment as a net energy producer-can this be achieved? Environ. Sci. Technol. 45, 7100–7106. https://doi.org/10.1021/es2014264

McIlroy, S.J., Kirkegaard, R.H., McIlroy, B., Nierychlo, M., Kristensen, J.M., Karst, S.M., Albertsen, M., Nielsen, P.H., 2017. MiDAS 2.0: An ecosystem-specific taxonomy and online database for the organisms of wastewater treatment systems expanded for anaerobic digester groups. Database 2017, 1–9. https://doi.org/10.1093/database/bax016

McIlroy, S.J., Saunders, A.M., Albertsen, M., Nierychlo, M., McIlroy, B., Hansen, A.A., Karst, S.M., Nielsen, J.L., Nielsen, P.H., 2015. MiDAS: The field guide to the microbes of activated sludge. Database 2015. https://doi.org/10.1093/database/bav062

McMurdie, P.J., Holmes, S., 2013. phyloseq: An R Package for Reproducible Interactive Analysis and Graphics of Microbiome Census Data. PLoS One 8, e61217. https://doi.org/10.1371/journal.pone.0061217

McSwain, B.S., Irvine, R.L., Hausner, M., Wilderer, P.A., 2005. Composition and distribution of extracellular polymeric substances in aerobic flocs and granular sludge. Appl. Environ. Microbiol. 71, 1051–1057. https://doi.org/10.1128/AEM.71.2.1051-1057.2005

Meng, F., Liu, D., Huang, W., Lei, Z., Zhang, Z., 2019a. Effect of salinity on granulation, performance and lipid accumulation of algal-bacterial granular sludge. Bioresour. Technol. Reports 7, 100228. https://doi.org/10.1016/j.biteb.2019.100228

Meng, F., Xi, L., Liu, D., Huang, Weiwei, Lei, Z., Zhang, Z., Huang, Wenli, 2019b. Effects of light intensity on oxygen distribution, lipid production and biological community of algal-bacterial granules in photo-sequencing batch reactors. Bioresour. Technol. 272, 473–481. https://doi.org/10.1016/j.biortech.2018.10.059

Meyer, R.L., Zeng, R.J., Giugliano, V., Blackall, L.L., 2005. Challenges for simultaneous nitrification, denitrification, and

phosphorus removal in microbial aggregates: Mass transfer limitation and nitrous oxide production. FEMS Microbiol. Ecol. 52, 329–338. https://doi.org/10.1016/j.femsec.2004.11.011

Middelhoven, W.J., 2004. Trichosporon wieringae sp.nov., an anamorphic basidiomycetous yeast from soil, and assimilation of some phenolic compounds, polysaccharides and other non-conventional carbon sources by saprophytic Trichosporon species. Antonie Van Leeuwenhoek 86, 329–337. https://doi.org/10.1007/s10482-004-0226-6

Milferstedt, K., Hamelin, J., Park, C., Jung, J., Hwang, Y., Cho, S.-K., Jung, K.-W., Kim, D.-H., 2017a. Biogranules applied in environmental engineering. Int. J. Hydrogen Energy 42, 27801–27811. https://doi.org/10.1016/j.ijhydene.2017.07.176

Milferstedt, K., Kuo-Dahab, W.C., Butler, C.S., Hamelin, J., Abouhend, A.S., Stauch-White, K., McNair, A., Watt, C., Carbajal-González, B.I., Dolan, S., Park, C., 2017b. The importance of filamentous cyanobacteria in the development of oxygenic photogranules. Sci. Rep. 7, 1–15. https://doi.org/10.1038/s41598-017-16614-9

Mohamed, A.Y.A., Welles, L., Siggins, A., Healy, M.G., Brdjanovic, D., Rada-Ariza, A.M., Lopez-Vazquez, C.M., 2021. Effects of substrate stress and light intensity on enhanced biological phosphorus removal in a photo-activated sludge system. Water Res. 189, 116606. https://doi.org/10.1016/j.watres.2020.116606

Morgenroth, E., Sherden, T., Van Loosdrecht, M.C.M., Heijnen, J.J., Wilderer, P.A., 1997. Aerobic granular sludge in a sequencing batch reactor. Water Res. 31, 3191–3194. https://doi.org/10.1016/S0043-1354(97)00216-9

Morton, J.T., Toran, L., Edlund, A., Metcalf, J.L., Lauber, C., Knight, R., 2017. Uncovering the Horseshoe Effect in Microbial Analyses. mSystems 2, 1–8. https://doi.org/10.1128/mSystems.00166-16

Muradov, N., Taha, M., Miranda, A.F., Wrede, D., Kadali, K., Gujar, A., Stevenson, T., Ball, A.S., Mouradov, A., 2015. Fungal-assisted algal flocculation: application in wastewater treatment and biofuel production. Biotechnol. Biofuels 8, 24. https://doi.org/10.1186/s13068-015-0210-6

Nancharaiah, Y.V., Kiran Kumar Reddy, G., 2018. Aerobic granular sludge technology: Mechanisms of granulation and biotechnological applications. Bioresour. Technol. 247, 1128–1143. https://doi.org/10.1016/j.biortech.2017.09.131

Neu, T.R., Kuhlicke, U., 2017. Fluorescence Lectin bar-coding of glycoconjugates in the extracellular matrix of biofilm and Bioaggregate forming microorganisms. Microorganisms 5, 1–13. https://doi.org/10.3390/microorganisms5010005

Neu, T.R., Lawrence, J.R., 2017. The extracellular matrix - an intractable part of biofilm systems, in: Flemming, H.-C., Neu, T.R., Wingender, J. (Eds.), The Perfect Slime: Microbial Extracellular Polymeric Substances (EPS). IWA Publishing.

Nicolaus, B., Panico, A., Lama, L., Romano, I., Manca, M.C., De Giulio, A., Gambacorta, A., 1999. Chemical composition and production of exopolysaccharides from representative members of heterocystous and non-heterocystous cyanobacteria. Phytochemistry 52, 639–647. https://doi.org/10.1016/S0031-9422(99)00202-2

Nielsen, L.P., Sloth, N.P., 1994. Denitrification, nitrification and nitrogen assimilation in photosynthetic microbial mats, in: Microbial Mats. Springer Berlin Heidelberg, Berlin, Heidelberg, pp. 319–324. https://doi.org/10.1007/978-3-642-78991-5_34

Nierychlo, M., Andersen, K.S., Xu, Y., Green, N., Jiang, C., Albertsen, M., Dueholm, M.S., Nielsen, P.H., 2020. MiDAS 3: An ecosystem-specific reference database, taxonomy and knowledge platform for activated sludge and anaerobic digesters reveals species-level microbiome composition of activated sludge. Water Res. 182, 115955. https://doi.org/10.1016/j.watres.2020.115955

Onetto, C.A., Eales, K.L., Guagliardo, P., Kilburn, M.R., Gambetta, J.M., Grbin, P.R., 2017. Managing the excessive proliferation of glycogen accumulating organisms in industrial activated sludge by nitrogen supplementation: A FISH-NanoSIMS approach. Syst. Appl. Microbiol. 40, 500–507. https://doi.org/10.1016/j.syapm.2017.07.006

Oswald, W., Gotaas, H., Golueke, W., E., G., Hermann, E., 1957. Algae in Waste Water Treatment. Sew. Ind. Waters 29, 437–457.

Ouazaite, H., Milferstedt, K., Hamelin, J., Desmond-Le Quéméner, E., 2020. Mapping the biological activities of filamentous oxygenic photogranules. Biotechnol. Bioeng. 1–11. https://doi.org/10.1002/bit.27585

Oyserman, B.O., Martirano, J.M., Wipperfurth, S., Owen, B.R., Noguera, D.R., McMahon, K.D., 2017. Community Assembly and Ecology of Activated Sludge under Photosynthetic Feast–Famine Conditions. Environ. Sci. Technol. 51, 3165–3175. https://doi.org/10.1021/acs.est.6b03976

Oyserman, B.O., Noguera, D.R., del Rio, T.G., Tringe, S.G., McMahon, K.D., 2016. Metatranscriptomic insights on gene expression and regulatory controls in Candidatus Accumulibacter phosphatis. ISME J. 10, 810–822. https://doi.org/10.1038/ismej.2015.155

Paerl, H.W., Pinckney, J.L., Kucera, S.A., 1995. Clarification of the Structural and Functional Roles of Heterocysts and Anoxic Microzones in the Control of Pelagic Nitrogen Fixation. Limnol. Oceanogr. 40, 634–638.

Paerl, H.W., Priscu, J.C., 1998. Microbial Phototrophic, Heterotrophic, and Diazotrophic Activities Associated with Aggregates in the Permanent Ice Cover of Lake Bonney, Antarctica. Microb. Ecol. 36, 221–230.

Paerl, H.W., Prufert, L.E., Ambrose, W.W., 1991. Contemporaneous N2 Fixation and Oxygenic Photosynthesis in the Nonheterocystous Mat-Forming Cyanobacterium Lyngbya aestuarii. Appl. Environ. Microbiol. 57, 3086–3092. https://doi.org/10.1128/AEM.57.11.3086-3092.1991

Park, C., Dolan, S., 2019. Algal-sludge granule for wastewater treatment and bioenergy feedstock generation. US10189732B2.

Park, C., Takeuchi, N., 2021. Unmasking photogranulation in decreasing glacial albedo and net autotrophic wastewater treatment. Environ. Microbiol. 23, 6391–6404. https://doi.org/10.1111/1462-2920.15780

Park, J.B.K., Craggs, R.J., Shilton, A.N., 2015. Algal recycling enhances algal productivity and settleability in Pediastrum boryanum pure cultures. Water Res. 87, 97–104. https://doi.org/10.1016/j.watres.2015.09.013

Park, J.B.K., Craggs, R.J., Shilton, A.N., 2011. Recycling algae to improve species control and harvest efficiency from a high rate algal pond. Water Res. 45, 6637–6649. https://doi.org/10.1016/j.watres.2011.09.042

Paulson, J.N., Pop, M., Bravo, H.C., 2013. metagenomeSeq: Statistical analysis for sparse high-throughput sequncing. http://www.cbcb.umd.edu/software/metagenomeSeq.

Pentecost, A., 1984. Effects of Sedimentation and Light Intensity on Mat-forming Oscillatoriaceae with Particular Reference to Microcoleus lyngbyaceus Gomont. Microbiology 130, 983–990. https://doi.org/10.1099/00221287-130-4-983

Peñuelas, J., Poulter, B., Sardans, J., Ciais, P., Van Der Velde, M., Bopp, L., Boucher, O., Godderis, Y., Hinsinger, P., Llusia, J., Nardin, E., Vicca, S., Obersteiner, M., Janssens, I.A., 2013. Human-induced nitrogen-phosphorus imbalances alter natural and managed ecosystems across the globe. Nat. Commun. 4. https://doi.org/10.1038/ncomms3934

Peñuelas, J., Sardans, J., Rivas-ubach, A., Janssens, I.A., 2012. The human-induced imbalance between C, N and P in Earth's life system. Glob. Chang. Biol. 18, 3–6. https://doi.org/10.1111/j.1365-2486.2011.02568.x

Picioreanu, C., van Loosdrecht, M.C.M., Heijnen, J.J., 1998. Mathematical modeling of biofilm structure with a hybrid differential-discrete cellular automaton approach. Biotechnol. Bioeng. 58, 101–116. https://doi.org/10.1002/(SICI)1097-0290(19980405)58:1<101::AID-BIT11>3.0.CO;2-M

Pijuan, M., Ye, L., Yuan, Z., 2010. Free nitrous acid inhibition on the aerobic metabolism of poly-phosphate accumulating organisms. Water Res. 44, 6063–6072. https://doi.org/10.1016/j.watres.2010.07.075

Princic, Mahne, Megusar, Paul, Tiedje, 1998. Effects of pH and oxygen and ammonium concentrations on the community structure of nitrifying bacteria from wastewater. Appl. Environ. Microbiol. 64, 3584–90.

Pronk, M, Abbas, B., Al-zuhairy, S.H.K., Kraan, R., Kleerebezem, R., van Loosdrecht, M.C.M., 2015. Effect and behaviour of different substrates in relation to the formation of aerobic granular sludge. Appl. Microbiol. Biotechnol. 99, 5257–5268. https://doi.org/10.1007/s00253-014-6358-3

Pronk, M., de Kreuk, M.K., de Bruin, B., Kamminga, P., Kleerebezem, R., van Loosdrecht, M.C.M., 2015. Full scale performance of the aerobic granular sludge process for sewage treatment. Water Res. 84, 207–217. https://doi.org/10.1016/j.watres.2015.07.011

Pronk, M., Neu, T.R., van Loosdrecht, M.C.M., Lin, Y.M., 2017. The acid soluble extracellular polymeric substance of aerobic granular sludge dominated by Defluviicoccus sp. Water Res. 122, 148–158. https://doi.org/10.1016/j.watres.2017.05.068

Rada-Ariza, María, A., Lopez-Vazquez, C.M., Van der Steen, N.P., Lens, P.N.L., 2017. Nitrification by microalgal-bacterial consortia for ammonium removal in flat panel sequencing batch photo-bioreactors. Bioresour. Technol. https://doi.org/10.1016/j.biortech.2017.08.019

Revsbech, N.P., 1989. An Oxygen Microsensor with a Guard Cathode. Limnol. Oceanogr. 34, 474–478.

Rippka, R., Waterbury, J.B., 1977. The synthesis of nitrogenase by non-heterocystous cyanobacteria. FEMS Microbiol. Lett. 2, 83–86. https://doi.org/10.1111/j.1574-6968.1977.tb00913.x

Risgaard-Petersen, N., Nicolaisen, M.H., Revsbech, N.P., Lomstein, B.A., 2004. Competition between Ammonia-Oxidizing Bacteria and Benthic Microalgae. Appl. Environ. Microbiol. 70, 5528–5537. https://doi.org/10.1128/AEM.70.9.5528-5537.2004

Rossi, F., De Philippis, R., 2015. Role of cyanobacterial exopolysaccharides in phototrophic biofilms and in complex microbial mats. Life 5, 1218–1238. https://doi.org/10.3390/life5021218

Sand-Jensen, K., 2014. Ecophysiology of gelatinous Nostoc colonies: Unprecedented slow growth and survival in resource-poor and harsh environments. Ann. Bot. 114, 17–33. https://doi.org/10.1093/aob/mcu085

Schindelin, J., Arganda-Carreras, I., Frise, E., Kaynig, V., Longair, M., Pietzsch, T., Preibisch, S., Rueden, C., Saalfeld, S., Schmid, B., Tinevez, J.-Y., White, D.J., Hartenstein, V., Eliceiri, K., Tomancak, P., Cardona, A., 2012. Fiji: an open-source platform for biological-image analysis. Nat. Methods 9, 676–682. https://doi.org/10.1038/nmeth.2019

Severin, I., Acinas, S.G., Stal, L.J., 2010. Diversity of nitrogen-fixing bacteria in cyanobacterial mats. FEMS Microbiol. Ecol. 73, no-no. https://doi.org/10.1111/j.1574-6941.2010.00925.x

Seviour, T., Pijuan, M., Nicholson, T., Keller, J., Yuan, Z., 2009. Gel-forming exopolysaccharides explain basic differences between structures of aerobic sludge granules and floccular sludges. Water Res. 43, 4469–4478. https://doi.org/10.1016/j.watres.2009.07.018

Seviour, T., Yuan, Z., van Loosdrecht, M.C.M., Lin, Y., 2012. Aerobic sludge granulation: A tale of two polysaccharides? Water Res. 46, 4803–4813. https://doi.org/10.1016/j.watres.2012.06.018

Shen, Y., Zhu, L., Ji, B., Fan, S., Xiao, Y., Ma, Y., 2021. Reactivation of Frozen Stored Microalgal-Bacterial Granular Sludge under Aeration and Non-Aeration Conditions. Water 13, 1974. https://doi.org/10.3390/w13141974

Sihvonen, L.M., Lyra, C., Fewer, D.P., Rajaniemi-Wacklin, P., Lehtimäki, J.M., Wahlsten, M., Sivonen, K., 2007. Strains of the cyanobacterial genera Calothrix and Rivularia isolated from the Baltic Sea display cryptic diversity and are distantly related to Gloeotrichia and Tolypothrix. FEMS Microbiol. Ecol. 61, 74–84. https://doi.org/10.1111/j.1574-6941.2007.00321.x

Silva, G.H.R., Sueitt, A.P.E., Haimes, S., Tripidaki, A., van Zwieten, R., Fernandes, T. V., 2019. Feasibility of closing nutrient cycles from black water by microalgae-based technology. Algal Res. 44, 101715. https://doi.org/10.1016/j.algal.2019.101715

Singh, D.D., Saikrishnan, K., Kumar, P., Surolia, A., Sekar, K., Vijayan, M., 2005. Unusual sugar specificity of banana lectin from Musa paradisiaca and its probable evolutionary origin. Crystallographic and modelling studies. Glycobiology 15, 1025–1032. https://doi.org/10.1093/glycob/cwi087

Slegers, P.M., Lösing, M.B., Wijffels, R.H., van Straten, G., van Boxtel, A.J.B., 2013. Scenario evaluation of open pond microalgae production. Algal Res. 2, 358–368. https://doi.org/10.1016/j.algal.2013.05.001

Smith, V.H., Sturm, B.S.M., deNoyelles, F.J., Billings, S.A., 2010. The ecology of algal biodiesel production. Trends Ecol. Evol. 25, 301–309. https://doi.org/10.1016/j.tree.2009.11.007

Soejima, A., Yamazaki, N., Nishino, T., Wakana, I., 2009. Genetic variation and structure of the endangered freshwater benthic alga Marimo, Aegagropila linnaei (Ulvophyceae) in Japanese lakes. Aquat. Ecol. 43, 359–370. https://doi.org/10.1007/s10452-008-9204-9

Solovchenko, A.E., Ismagulova, T.T., Lukyanov, A.A., Vasilieva, S.G., Konyukhov, I. V, Pogosyan, S.I., Lobakova, E.S., Gorelova, O.A., 2019. Luxury phosphorus uptake in microalgae. J. Appl. Phycol. 31, 2755–2770. https://doi.org/10.1007/s10811-019-01831-8

Sommer, F., Anderson, J.M., Bharti, R., Raes, J., Rosenstiel, P., 2017. The resilience of the intestinal microbiota influences health and disease. Nat. Rev. Microbiol. 15, 630–638. https://doi.org/10.1038/nrmicro.2017.58

Stal, L., 1997. Fermentation in cyanobacteria. FEMS Microbiol. Rev. 21, 179–211. https://doi.org/10.1016/S0168-6445(97)00056-9

Stal, L.J., 1995. Physiological ecology of cyanobacteria in microbial mats and other communities. New Phytol. 131, 1–32. https://doi.org/10.1111/j.1469-8137.1995.tb03051.x

Stanier, R.Y., Deruelles, J., Rippka, R., Herdman, M., Waterbury, J.B., 1979. Generic Assignments, Strain Histories and Properties of Pure Cultures of Cyanobacteria. Microbiology 111, 1–61. https://doi.org/10.1099/00221287-111-

1-1

Stauch-White, K., Srinivasan, V.N., Camilla Kuo-Dahab, W., Park, C., Butler, C.S., 2017. The role of inorganic nitrogen in successful formation of granular biofilms for wastewater treatment that support cyanobacteria and bacteria. AMB Express 7, 146. https://doi.org/10.1186/s13568-017-0444-8

Staudt, C., Horn, H., Hempel, D.C., Neu, T.R., 2004. Volumetric measurements of bacterial cells and extracellular polymeric substance glycoconjugates in biofilms. Biotechnol. Bioeng. 88, 585–592. https://doi.org/10.1002/bit.20241

Stewart, W.D.P., Lex, M., 1970. Nitrogenase activity in the blue-green alga Plectonema boryanum strain 594. Arch. Mikrobiol. 73, 250–260. https://doi.org/10.1007/BF00410626

Stokholm-Bjerregaard, M., McIlroy, S.J., Nierychlo, M., Karst, S.M., Albertsen, M., Nielsen, P.H., 2017. A Critical Assessment of the Microorganisms Proposed to be Important to Enhanced Biological Phosphorus Removal in Full-Scale Wastewater Treatment Systems. Front. Microbiol. 8, 1–18. https://doi.org/10.3389/fmicb.2017.00718

Su, G., Morris, J.H., Demchak, B., Bader, G.D., 2014. Biological Network Exploration with Cytoscape 3. Curr. Protoc. Bioinforma. 47, 8.13.1-8.13.24. https://doi.org/10.1002/0471250953.bi0813s47

Suleiman, A.K.A., Lourenço, K.S., Clark, C., Luz, R.L., da Silva, G.H.R., Vet, L.E.M., Cantarella, H., Fernandes, T. V., Kuramae, E.E., 2020. From toilet to agriculture: Fertilization with microalgal biomass from wastewater impacts the soil and rhizosphere active microbiomes, greenhouse gas emissions and plant growth. Resour. Conserv. Recycl. 161, 104924. https://doi.org/10.1016/j.resconrec.2020.104924

Sun, Y., Angelotti, B., Wang, Z.W., 2019. Continuous-flow aerobic granulation in plug-flow bioreactors fed with real domestic wastewater. Sci. Total Environ. 688, 762–770. https://doi.org/10.1016/j.scitotenv.2019.06.291

Takeuchi, N., Kohshima, S., Seko, K., 2001. Structure, Formation, and Darkening Process of Albedo-Reducing Material (Cryoconite) on a Himalayan Glacier: A Granular Algal Mat Growing on the Glacier. Arctic, Antarct. Alp. Res. 33, 115. https://doi.org/10.2307/1552211

Tamulonis, C., Kaandorp, J., 2014. A Model of Filamentous Cyanobacteria Leading to Reticulate Pattern Formation. Life 4, 433–456. https://doi.org/10.3390/life4030433

Tamulonis, C., Postma, M., Kaandorp, J., 2011. Modeling filamentous cyanobacteria reveals the advantages of long and fast trichomes for optimizing light exposure. PLoS One 6. https://doi.org/10.1371/journal.pone.0022084

Tay, J.-H., Tay, S.T.-L., Liu, Y., Show, K.Y., Ivanov, V., 2006. Biogranulation technologies for wastewater treatment: Microbial granules. Elsevier.

Tenore, A., Mattei, M.R., Frunzo, L., 2021. Multiscale modelling of oxygenic photogranules.

Tiron, O., Bumbac, C., Manea, E., Stefanescu, M., Lazar, M.N., 2017. Overcoming Microalgae Harvesting Barrier by Activated Algae Granules. Sci. Rep. 7, 1–11. https://doi.org/10.1038/s41598-017-05027-3

Tiron, O., Bumbac, C., Patroescu, I. V., Badescu, V.R., Postolache, C., 2015. Granular activated algae for wastewater treatment. Water Sci. Technol. 71, 832–839. https://doi.org/10.2166/wst.2015.010

Tiron Olga, Bumbac Costel, Patroescu I. Viorel, S.M., 2015. Activated algae granulation: a biological solution for efficient microalgae harvesting. J. Biotechnol. 208, S19. https://doi.org/doi:10.1016/j.jbiotec.2015.06.046

Togashi, T., Sasaki, H., Yoshimura, J., 2015. A geometrical approach explains Lake Ball (Marimo) formations in the green alga, Aegagropila linnaei. Sci. Rep. 4, 3761. https://doi.org/10.1038/srep03761

Trebuch, L.M., Oyserman, B.O., Janssen, M., Wijffels, R.H., Vet, L.E.M., Fernandes, T.V., 2020. Impact of hydraulic retention time on community assembly and function of photogranules for wastewater treatment. Water Res. 173, 115506. https://doi.org/10.1016/j.watres.2020.115506

UNICEF, 2020. State of the world's sanitation: an urgent call to transform sanitation for better health, environments, economies and societies. World Health Organization, Geneva PP - Geneva.

van den Hende, S., 2014. Microalgal bacterial flocs for wastewater treatment: from concept to pilot scale.

Van Den Hende, S., Carré, E., Cocaud, E., Beelen, V., Boon, N., Vervaeren, H., 2014. Treatment of industrial wastewaters by microalgal bacterial flocs in sequencing batch reactors. Bioresour. Technol. 161, 245–254. https://doi.org/10.1016/j.biortech.2014.03.057

Van Den Hende, S., Vervaeren, H., Desmet, S., Boon, N., 2011a. Bioflocculation of microalgae and bacteria combined

with flue gas to improve sewage treatment. N. Biotechnol. 29, 23–31. https://doi.org/10.1016/j.nbt.2011.04.009

Van Den Hende, S., Vervaeren, H., Saveyn, H., Maes, G., Boon, N., 2011b. Microalgal bacterial floc properties are improved by a balanced inorganic/organic carbon ratio. Biotechnol. Bioeng. 108, 549–558. https://doi.org/10.1002/bit.22985

Van Der Steen, P., Rahsilawati, K., Rada-Ariza, A.M., Lopez-Vazquez, C.M., Lens, P.N.L., 2015. A new photo-activated sludge system for nitrification by an algal-bacterial consortium in a photo-bioreactor with biomass recycle. Water Sci. Technol. 72, 443–450. https://doi.org/10.2166/wst.2015.205

Vishniac, W., Santer, M., 1957. The *thiobacilli*. Bacteriol. Rev. 21, 195–213.

Vitousek, P.M., Cassman, K., Cleveland, C., Crews, T., Field, C.B., Grimm, N.B., Howarth, R.W., Marino, R., Martinelli, L., Rastetter, E.B., Sprent, J.I., 2002. Towards an ecological understanding of biological nitrogen fixation. Biogeochemistry 57–58, 1–45. https://doi.org/10.1023/A:1015798428743

Volkova, E., Sorokovikova, E., Belykh, O., Tikhonova, I., Bondarenko, N., 2020. Photogranules Formed by Filamentous Cyanobacteria and Algae of the Genus Spirogyra Link in the Coastal Zone of Lake Baikal. Bull. Baikal State Univ. 30, 14–22. https://doi.org/10.17150/2500-2759.2020.30(1).14-22

Wang, M., Yang, H., Ergas, S.J., van der Steen, P., 2015. A novel shortcut nitrogen removal process using an algal-bacterial consortium in a photo-sequencing batch reactor (PSBR). Water Res. 87, 38–48. https://doi.org/10.1016/j.watres.2015.09.016

Wang, Q., He, J., 2020. Complete nitrogen removal via simultaneous nitrification and denitrification by a novel phosphate accumulating Thauera sp. strain SND5. Water Res. 185, 116300. https://doi.org/10.1016/j.watres.2020.116300

Wang, X., Wen, X., Yan, H., Ding, K., Zhao, F., Hu, M., 2011. Bacterial community dynamics in a functionally stable pilot-scale wastewater treatment plant. Bioresour. Technol. 102, 2352–2357. https://doi.org/10.1016/j.biortech.2010.10.095

Weissbrodt, D.G., Neu, T.R., Kuhlicke, U., Rappaz, Y., Holliger, C., 2013. Assessment of bacterial and structural dynamics in aerobic granular biofilms. Front. Microbiol. 4, 1–18. https://doi.org/10.3389/fmicb.2013.00175

Whale, G.F., Walsby, A.E., 1984. Motility of the cyanobacterium microcoleus chthonoplastes in mud. Br. Phycol. J. 19, 117–123. https://doi.org/10.1080/00071618400650121

Wiegant, W.M., 1988. The "spaghetti theory" on anaerobic sludge formation, or the inevitability of granulation. Granul. Anaerob. Sludge Microbiol. Technol. 146–152.

Wilbanks, E.G., Jaekel, U., Salman, V., Humphrey, P.T., Eisen, J.A., Facciotti, M.T., Buckley, D.H., Zinder, S.H., Druschel, G.K., Fike, D.A., Orphan, V.J., 2014. Microscale sulfur cycling in the phototrophic pink berry consortia of the Sippewissett Salt Marsh. Environ. Microbiol. 16, 3398–3415. https://doi.org/10.1111/1462-2920.12388

Wilbanks, E.G., Salman-Carvalho, V., Jaekel, U., Humphrey, P.T., Eisen, J.A., Buckley, D.H., Zinder, S.H., 2017. The Green Berry Consortia of the Sippewissett Salt Marsh: Millimeter-Sized Aggregates of Diazotrophic Unicellular Cyanobacteria. Front. Microbiol. 8, 1–12. https://doi.org/10.3389/fmicb.2017.01623

Wilén, B.-M., Liébana, R., Persson, F., Modin, O., Hermansson, M., 2018. The mechanisms of granulation of activated sludge in wastewater treatment, its optimization, and impact on effluent quality. Appl. Microbiol. Biotechnol. 102, 5005–5020. https://doi.org/10.1007/s00253-018-8990-9

Wingender, J., Neu, T.R., Flemming, H.-C., 1999. Microbial Extracellular Polymeric Substances. Springer Berlin Heidelberg, Berlin, Heidelberg. https://doi.org/10.1007/978-3-642-60147-7

Wolf, G., Picioreanu, C., van Loosdrecht, M.C.M., 2007. Kinetic modeling of phototrophic biofilms: The PHOBIA model. Biotechnol. Bioeng. 97, 1064–1079. https://doi.org/10.1002/bit.21306

Wrede, D., Taha, M., Miranda, A.F., Kadali, K., Stevenson, T., Ball, A.S., Mouradov, A., 2014. Co-cultivation of fungal and microalgal cells as an efficient system for harvesting microalgal cells, lipid production and wastewater treatment. PLoS One 9. https://doi.org/10.1371/journal.pone.0113497

Xia, Y., Wang, Yubo, Wang, Yi, Chin, F.Y.L., Zhang, T., 2016. Cellular adhesiveness and cellulolytic capacity in Anaerolineae revealed by omics-based genome interpretation. Biotechnol. Biofuels 9, 1–13. https://doi.org/10.1186/s13068-016-0524-z

Yamada, T., Sekiguchi, Y., Hanada, S., Imachi, H., Ohashi, A., Harada, H., Kamagata, Y., 2006. Anaerolinea

thermolimosa sp. nov., Levilinea saccharolytica gen. nov., sp. nov. and Leptolinea tardivitalis gen. nov., sp. nov., novel filamentous anaerobes, and description of the new classes Anaerolineae classis nov. and Caldilineae classis nov. in the . Int. J. Syst. Evol. Microbiol. 56, 1331–1340. https://doi.org/10.1099/ijs.0.64169-0

Yin, Y., Sun, J., Liu, F., Wang, L., 2019. Effect of nitrogen deficiency on the stability of aerobic granular sludge. Bioresour. Technol. 275, 307–313. https://doi.org/10.1016/j.biortech.2018.12.069

Zhang, B., Lens, P.N.L., Shi, W., Zhang, R., Zhang, Z., Guo, Y., Bao, X., Cui, F., 2018a. Enhancement of aerobic granulation and nutrient removal by an algal–bacterial consortium in a lab-scale photobioreactor. Chem. Eng. J. 334, 2373–2382. https://doi.org/10.1016/j.cej.2017.11.151

Zhang, B., Lens, P.N.L., Shi, W., Zhang, R., Zhang, Z., Guo, Y., Bao, X., Cui, F., 2018b. The attachment potential and N-acyl-homoserine lactone-based quorum sensing in aerobic granular sludge and algal-bacterial granular sludge. Appl. Microbiol. Biotechnol. 102, 5343–5353. https://doi.org/10.1007/s00253-018-9002-9

Zhang, B., Xu, X., Zhu, L., 2017. Structure and function of the microbial consortia of activated sludge in typical municipal wastewater treatment plants in winter. Sci. Rep. 7, 17930. https://doi.org/10.1038/s41598-017-17743-x

Zhang, M., Ji, B., Liu, Y., 2021. Microalgal-bacterial granular sludge process: A game changer of future municipal wastewater treatment? Sci. Total Environ. 752, 141957. https://doi.org/10.1016/j.scitotenv.2020.141957

Zhang, P., Chen, Y.P., Qiu, J.H., Dai, Y.Z., Feng, B., 2019. Imaging the Microprocesses in Biofilm Matrices. Trends Biotechnol. 37, 214–226. https://doi.org/10.1016/j.tibtech.2018.07.006

Zippel, B., Neu, T.R., 2011. Characterization of Glycoconjugates of Extracellular Polymeric Substances in Tufa-Associated Biofilms by Using Fluorescence Lectin-Binding Analysis. Appl. Environ. Microbiol. 77, 505–516. https://doi.org/10.1128/AEM.01660-10

Thesis Summary

THESIS SUMMARY

In the Anthropocene human activities drastically shape natural ecosystems on land and sea due to a growing population and demand for water, food, and energy. This disturbs the biosphere and has an influence on global climate. A major issue is that many human activities often inefficiently use resources and are carried out in a linear fashion. Especially the highly industrialized and globalized agricultural practices contribute to an ecologically devastating global redistribution of major nutrients such as carbon, nitrogen, and phosphorus. Due to human activities, the stoichiometry of carbon and nitrogen relative to phosphorus have started to change, which is altering natural and managed ecosystems around the globe. Mitigating these anthropogenic consequences on the environment is one of the most urgent challenges we face today.

Most carbon, nitrogen, and phosphorus used in agriculture is converted into our food and ultimately ends up in our wastewater. Improper treatment and discharge of wastewater into surface waters is causing eutrophication all over the world. This results in algal blooms in freshwater and coastal ecosystems and impairs biological diversity and ecosystem functioning. Conventional wastewater treatment plants are designed as end-of-pipe solutions that focus on removing pollutants rather than recovering valuable elements from wastewater. With this linear practice, we are continuing to deposit massive amounts of nutrients around the world and concentrating them where they are not needed, ultimately causing harm to ecosystems. Therefore, it is crucial to develop techniques that can "mine" these waste streams and reintroduce their resources to our economy. Similar to the sun fuelling global nutrient cycles, light-driven biological resource recovery processes could effectively mine waste streams.

Photogranules are a novel wastewater treatment technology that can utilize the sun's energy to treat (waste)water and at the same time generate valuable biomass. The microbial community consists of phototrophs (e.g.., microalgae, cyanobacteria) and non-phototrophic microorganisms (e.g., nitrifiers, denitrifiers, PAOs) that form dark-green spheroid agglomerates. Photogranules have excellent settling properties and are easy to harvest. Introducing photosynthesis to the treatment process has the advantage of *in-situ* oxygenation. Oxygen produced by phototrophs is directly available for heterotrophs (and nitrifiers). In turn, carbon dioxide produced by respiration is sequestered via photosynthesis. This reduces (or eliminates) the need for energy intensive external aeration and simultaneously minimizes greenhouse gas emissions. Additionally, photogranules can use both light and organic carbon for metabolic energy and consequently can have 2-3x higher biomass productivity compared to conventional

treatment systems. This makes them especially suitable for nutrient recovery application.

Photogranulation was observed by various taxonomically distinct phototrophic microbial communities but the key principles for photogranulation are still elusive. Photogranules have been shown to work under various conditions and have proven to efficiently recover nitrogen, and carbon. However, photogranules exhibit lower conversion rates for phosphorus compared to established wastewater treatment technologies, such as aerobic granular sludge. In the wastewater treatment process photogranules experience highly fluctuating physical and chemical conditions. To date there is poor understanding of the effect of these conditions on photogranulation, microbial community assembly, photogranule morphology, microscale functioning, and finally on the efficacy of nutrient recovery processes.

The aim or this thesis was to advance the field of phototrophic wastewater treatment by systematically exploring the microbial community assembly and functions of photogranules. To achieve this, we designed bioreactors that allowed photogranulation and subsequently explored the functional potential of photogranules for wastewater treatment by changing operation conditions. We integrated various approaches and techniques to investigate the microbial community composition and function, physical structure, and microscale functionality of photogranules. Ultimately, we provided a holistic overview on the microbial ecology and process engineering of photogranular technology to pave the way for more sustainable wastewater treatment.

In **chapter 2** we generated photogranules under hydrodynamic conditions in lab-scale bioreactors operated in sequencing batch mode. We used a diverse and species-rich inoculum from various sources and followed the microbial community assembly, from free-suspended cells to floccular aggregates and finally to photogranules. The main drivers for photogranulation were identified to be motile filamentous cyanobacteria and the excretion of extracellular polymeric substances (EPS). Operating the lab-scale bioreactors at low hydraulic retention time increased the selection pressure for well-settling biomass, which promoted photogranulation and decreased photogranule assembly time. Additionally, at low hydraulic retention times removal rates were increased due to higher nutrient loading.

Wastewater can have various elemental compositions. In low N:P ratio wastewaters the microorganisms can face insufficient amounts of nitrogen for growth, which consequently hinders the biological treatment process. Therefore, in **chapter 3** we investigated the effect of nitrogen limitation on the treatment performance and morphology of photogranules. We showed that part of the microbial community of

photogranules can perform N_2-fixation and can maintain treatment performance despite nitrogen limitation. N_2-fixation was mainly attributed to the non-heterocyst forming motile filamentous cyanobacteria that was found to be important for the structural integrity of the photogranule. Long-term exposure to nitrogen-limiting conditions showed an effect on photogranule morphology. Photogranules exhibited a loose and open structure with occasional voids and crevices under these conditions. As a consequence, photogranules had an increased surface area, which could have facilitated nitrogen uptake under low concentrations, and which could also have favoured N_2-fixation.

In **chapter 4** we investigated the physical, chemical, and biological structure of photogranules and their metabolic functions on a microscale. This was achieved by applying microscopic and microsensor techniques and conducting incubations with isotopically labelled carbon or nitrogen substrates. We confirmed the structural role of gliding motile filamentous cyanobacteria by visualizing their complex interwoven network spanning through the entire photogranule. Additionally, we localized EPS excreted by cyanobacterial filaments and bacteria, which seemed to act like a glue holding the photogranule together and providing additional structural support. Due to light and substrate gradients most of the biological activity of microorganisms was confined to the outer 500 μm of the photogranule, while denitrification potentially extended further into the centre. Furthermore, we showed that processes for oxygen, carbon and nitrogen are internally coupled. This accounted especially for photosynthesis, nitrification, and heterotrophic activities.

Photogranules showed high removal rates for carbon and nitrogen, but lower rates for phosphorus compared to other biological treatment systems. In **chapter 5** we addressed this challenge by enhancing phosphorus removal with the introduction of polyphosphate accumulating organisms (PAOs). We accomplished this by mixing photogranules with aerobic granular sludge and operating the bioreactors under a feast-famine regime with an anaerobic (dark) and aerobic (light) phase. PAOs successfully integrated into photogranules and thereby increased phosphorus removal by 6x compared to photogranules without PAOs. The developed process was termed PG+. Further, we investigated the suitability of the PG+ process under a natural diurnal cycle introducing a 12h dark anaerobic phase. Neither phototrophs nor PAOs were adversely affected by this anaerobic phase and therefore are suitable for operation under a natural diurnal cycle.

Last, I summarized all our findings in **chapter 6** and discussed them in detail. To support the discussion, I performed a meta-analysis on publicly available microbial community data of photogranules and used our lab-scale findings to perform a scenario

analysis. The meta-analysis supported our findings on the importance of the microbial community compositions and functions, but also showed that photogranulation can be achieved by taxonomically different microbial communities. The main functions found in photogranules were 1) oxygenic photosynthesis and 2) chemoheterotrophy. Motile filamentous cyanobacteria were present in all investigated photogranules, which confirms their importance for photogranulation due to their locomotive entanglement. I pointed out that a deeper understanding of the microbial community and its metabolic capability is still necessary to fully understand photogranule assembly.

Further, I revealed design principles for photogranular bioreactor configuration and modes of operation at large-scale. A sequencing batch reactor was regarded as not optimal for large scale application due to suboptimal use of sunlight during the day. Therefore, I proposed a continuous flow system, which allows the full use of all light available during the day. Additionally, I suggested an on-demand aeration system for the aerobic phase to compensate for possible low light conditions (O_2 addition) or low COD input (CO_2 addition). The scenario analysis illustrated the potential for large-scale application of photogranular technology and provided estimates for treatment performance and areal requirements. The locations chosen for analysis were the Netherlands and India. Under "low" light conditions the footprint of a photogranule treatment plant was almost 4x higher compared to conventional treatment systems. Under "high" light conditions the footprint was reduced to less than twice. This would make photogranular technology especially suitable for low latitude countries where sanitation is often still lacking and urgently needed.

Finally, I propose the investigation of the microbial community of photogranules in more detail, by means of metagenomics, metatranscriptomic, metabolomics and proteomics. This will reveal key genes and metabolites crucial during photogranulation and the treatment process. A better understanding of photogranule morphology and microscale functioning will be key to understanding the effect of environmental conditions on photogranule assembly and metabolic activity. Further, kinetic and mass transfer models should be established for microscale and process scale simulation. These will aid large-scale process and reactor design. The generated photogranular biomass should be explored for various valorisation options (e.g. biofertilizer, bioplastics). Ultimately, a cost-effective, robust, and easy-to-operate system must be designed that can be applied to secure water sanitation and the recovery of valuable elements.

Acknowledgements

ACKNOWLEDGEMENTS

A wonderful journey comes to an end. Everything that was accomplished wouldn't have been possible without the help and support of numerous persons. In this section I would like to thank all the people that I met along the way and that helped substantially during my time professionally, mentally, and socially. I feel I could fill another booklet only with these acknowledgements and would like to apologize for the ones that I don't mention specifically in person.

First of all, I want to convey my deepest gratitude to **Tania**. I first met her as a MSc student during my thesis at NIOO from 2015-2016. There was an immediate "click". Both with the research topic she was (and still is) working on, but also on a personal level. One reason we are sticking together for so long is that we share a lot of the same values and beliefs. We are both eager to understand and harness the potential of nature for an ecological sustainable future. These ambitions unite us at work and led so far to a wonderful professional journey from MSc thesis, over the PhD to a Postdoc. Probably it is destiny?! Over the years we became friends and I look back at uncountable wonderful moments with her. From drinks and dinners at her house over trips to New Delhi and visiting her in Portugal. I always felt welcome at her home with her lovely family and know that I can count on her when in need. She and her family are in my heart of hearts. Wherever the journey will lead, I do hope that Tania and I continue working together towards our dreams of a better world. I deeply belief that the vision behind Tania's well know phrase "Bem-vindo ao mundo de amanhã!" will become reality.

One of the major reasons why I came to Wageningen to study was the subject of microalgal biotechnology. In fact, the first course I took was taught by **Marcel** and I was immediately fascinated by his knowledge and skills on microalgal biotechnology. Having him later as a supervisor was a blessing. I could not image a person more knowledgeable about microalgae ranging from the most fundamental understanding of photosynthesis to large scale application of microalgal production systems. I value the critical mind that he brought into our discussions. Often, Marcel laid down the basic principle in physics, chemistry or biology and conveyed a certain idea or argument with a "simple" back-of-the-envelope calculation. Additionally, he is not easy to convince and easily impressed by aesthetic visionary concepts on algal production systems integrated in buildings or with artificial illumination. Exactly, this honesty and critical thinking is what I admire in him and was learning along the way from him.

Louise is a wonderful person. I admire her drive and I am astonished in how many million things she is involved at the same time. It was an honour to have her as a

promotor during my PhD. Meeting and discussing with her always left me with a feeling that I am on the right path and part of a bigger plan to work towards an ecological sustainable future. She is a true visionary and a person of public interest. I remember how people were astound when I said that I am working with her. Not only in these moments I realized how privileged I was to work so closely with her - the "David Attenborough of the Netherlands". Although Louise is involved in high-level decisions and mixes with the upper-class, she is down to earth and stays true to her core values. I especially enjoyed our trip to New Delhi, where we had time to interact more closely and get to know each other better. A lot of the visionary ideas I have, were shaped by her.

Rene the "algae guru". I know his name and work ever since I got interesting in microalgal biotechnology back in Vienna. He and his work were certainly one of the major reasons why I was coming to Wageningen. I immediately followed courses of his department of Bioprocess Engineering (BPE) and did my Master theses in projects related to BPE. Although I heard a lot about Rene during my Master, I never had the chance to talk to him. When I started as a PhD, I was quite intimidated at first by his wisdom and thought he would disapprove my research and ideas. Over the years I got to know him better and realized how wrong my perception was in the beginning. Rene is a caring, calm, but also critical person. I appreciate the meetings and discussions we had over the years. In some meetings or discussions, he would be quiet for the most part and only speak at the end or in crucial moments. But what he said was always true, honest, and caring and often was giving the right direction for the next steps that I should take.

Next, I would like to thank my paranymphs **Hui, Philip** and **Narcis** that were at my side during the PhD journey. Hui started almost at the same time as me at NIOO and became dear colleagues, friends, and office mates from the beginning. He always had kind words to calm me down when I was stressed ("How bad could it be") or working too hard ("It is time to go home"). Additionally, he would always have a little salty or sweet treat to share to regain energy. Philip and I started our master studies in Wageningen at the same time. I know him since the beginning of my days in this little town, became close friends and share uncountable great experiences. He started his PhD before I did. Seeing how happily he was doing it, I certainly wanted to start one as well. Unfortunately, in the policy of WUR there are only two paranymphs allowed on stage, but Narcis is no less of a paranymph for me. I met him during the master studies as well and we became later PhD colleagues at BPE and friends. He is such a cheerful and caring person. I enjoyed every second that we had together at work or meeting him in private going out for food and drinks.

The BSc. and MSc. students I had during my PhD substantially contributed to the outcome of this thesis. I would like to thank **Mauk**, **Egbert**, **Carlos**, **Kobe**, **Stijn**, **Robert**, **Quirine**, and **Jasper**. Additionally, I would like to thank **Sido**, who was hired in a 5-month research project alongside the PhD project. As much as I taught them, I was also learning from them. I am grateful to have been able to work with you so closely together and explore the wonderful world of photogranules. Generally, I would like to thank the wonderful group of the **Pooper Troopers** for their support in the lab but also for generating such a great working atmosphere. I always enjoyed our meetings and discussion but also having drinks and dinner outside work. I am very much looking forward to the next Pooper Trooper alumni event.

Next, I would like to thank the excellent research assistance at aquatic ecology, NIOO and WUR. Without their help most of the experimental work and the results I based this thesis on would not have been possible. **Nico** was essential and is certainly in the "Pooper Trooper Hall of fame". He helped setting up the experimental setups and measured thousands and thousands of samples, no matter if gaseous, liquid, or solid. Besides his professional skills I value all the fun and sincere conversations we had during the last years. Further, I am grateful for **Suzanne** introducing me to the wonderful world of algal cultivation and especially showing me how to microscope phytoplankton. Additionally, I would like to thank **Erik**, **Dennis** and **Michaela** for their assistance and relentless effort in helping things moving forward. Next, I would like to thank **Ciska**, **Iris** and **Hans** for their support in doing chemical analysis and **Agata** and **Tanja** for their support in the molecular lab. Further, **Mattias** and **Fleur** from the bioinformatic support were essential and helped me to get familiar with bioinformatic tools to explore the microbial community of photogranules. Next, I would like to thank **Gilles**, **Jeroen**, **Rene** and **Gerben-Jan** from TD at NIOO. They were always there to realise and translate my craziest ideas for new experimental setups into practice. Additionally, I would like to thank **Gregor** and **Eke** for their support in the greenhouse experiments and with the "Poep is Goud" installation. Eke was the first person I met on my first day when I started the PhD at NIOO. I will never forget how nervous I was and how talking to him made me confident and calm. Every time, I met him at work I left with a happy feeling. He is such a great spirit. Next, I would like to thank the research assistants from BPE **Fred**, **Rick**, **Sebastiaan**, **Snezana**, and **Wendy** for their advice when I needed it. Additionally, I would like to thank **Hans** from the workshop at WUR for the uncountable times he was fabricating and assisting with specific electronic equipment.

I am very grateful to have worked with such wonderful people during my time in the LotusHR project. **Vivek** was my direct PhD buddy in New Delhi and together we

experienced a lot professionally but also during our spiritual journey to Kedarnath in the Himalayan mountains. Many thanks for these great experiences and looking forward to continuing working with you and preparing the next journey. "Perrrrrfect". I also would like to thank **Antonella**, **Bruno**, **Elackiya**, **Sumit**, **Steef**, **Ralph**, **Merle**, **Huub**, **Nora**, **Kasia**, **Doris**, **Theo**, **Cor**, **Maartje**, **Gert-Jan**, **Paul** and many more from the Lotus crew that made my PhD to such a rich and lively experience.

During my PhD project I had the opportunity to collaborate with wonderful people and share the excitement about photogranules. First, I would like to thank **Dirk** and **Olivia** from MPI Bremen and their expertise in microsensor measurements. On several occasions we had the chance to do experiments together - first at NIOO and later at MPI. When I came to Bremen, Dirk was so kind to offer his house for me to stay while he was on holidays. Olivia and I had a great time poking the photogranules and exploring the city of Bremen. That was just one or two weeks before whole Europe would go into the first lockdown and all our plans to continue this research had to change. I was not able to come to Bremen a second time, but we continued the collaboration remotely with the help of our friends at FedEx and managed to write up our results in a great scientific article. Later we finally reunited at a scientific cruise in the Waddenzee in the Netherlands. These were wonderful moments I will never forget. Further, I would like to thank **Thomas** and **Ute** from UFZ Magdeburg for the opportunity to visit them and learn and utilize the confocal laser scanning microscope. I was so lucky to manage to be there just before they retired and were amazed by their knowledge and skills on investigating biofilm systems. Finally, I would like to thank **Mario** from TU Delft for his advice on PAOs.

Next, I would like to thank my office mates from the "Best Office". The office changed over time as people come and go but I couldn't be happier with the persons I could experience so close. Starting with **Kim**, **Casper**, and Tania. Later Hui and **Kaiyi**. Thanks to all for the fun moments during work and the support you gave. Kim was the first PhD I met at NIOO during my master thesis, and I remember her advice: "Never do a PhD!". Apologies, I didn't follow your advice, but I know exactly what you meant back then – the ups and downs of the PhD journey. Casper and I were very synchronized with our contracts and I am looking forward to be Postdoc colleagues with him in the future. Kaiyi is very special to me. When he started with his PhD under the supervision of Tania, I was very happy to have a direct lab buddy. Together we would manage the "Blackwater" lab and had a lot of fun.

All the time at NIOO would only be half as fun if it wouldn't have been about the NIOO colleagues. During my years I met so many different generations of PhDs and postdocs, and I would like to thank **Antonella, Thijs, Libin, Wei, Zhipeng, Peiyu,**

Manqi, Alena, Mandy, Sven, Karen, Aleksandra, Cleo, Ana Paula, Marta, Paolo, Marika, Maggie, Nandini, Shuwen, Qing, Berte, Nandini, Kerstin, Lilith, **Asmita**, **Dianneke**, **Nacho**, **Adam**, **Kyle**, **Lara**, **Raul**, **Christina**, **German**, **Ben**, **Ana**, **Morgan**, **Sytske**, **Haymanti**, **Mariana**, **Kay**, and many more for the great time at NIOO and outside. Having fun in the lab, having coffee, having scientific, political, or societal discussions, or going for dinner or having drinks. Especially, I loved the NIOO climbing group that was established with **Adam**, **Kyle**, **Lara**, **Alex**, **Sytske**, **Jose** and **Iris**. That gave me so much joy and energy especially in the beginning of my PhD. Further I would like to thank **Dedmer**, **Steven**, **Liesbeth**, **Wolf**, **Lisette**, **Ellen** and **Suzanne** for the inspiring discussions and interactions over the years. Additionally, I would like to thank **Elly**, **Gerrie**, **David** and **Froukje** for their support along the way.

Although I didn't spend so much time at BPE, I still feel connected to the department and the people. I cherish the moments when I came over to for a scientific meeting, borrels or going for drinks after work. I would like to thank **Narcis**, **Anna**, **Christian**, **Robin**, **Fabian**, **Jort**, **Iris**, **August**, **Pieter**, **Calvin**, **Camillo**, **Edgar**, **Barbara**, **Rocca**, **Renske**, **Kylie**, **Enrico**, **Marta**, **Sebastian**, **Marta**, **Sabine**, **Pauline**, **Chunzhe**, **Pedro, Iago, Iulian, Dirk, Giuseppe, Sarah, Antoinette, Rafael, Carlos,** and **Maria** for the wonderful time we had. A great moment was to go on conferences together on two occasions. The YoungAlgeaneers symposium in Oban, Scotland, with **Pieter** and **Marta** or the AlgaeEurope 2018 conference in Amsterdam, the Netherlands, with all the algae people from BPE. What great memories!

Music is a very important part of my life, and I had the great chance to meet people in Wageningen that I share this with. In my master studies I started playing in the band The Colour of Leaves with **David**, **Mario**, **Anton** and **Chema**. Before we split up, we recorded a wonderful album in an old monastery in Austria. Finishing the works on our album during lockdown was just giving me the right energy to go through the pandemic. "Hummus and cheese forever". At the last stretch of my PhD, I am very grateful to have met other wonderful musicians and started to play in the band 'Chila Collective' with **Angelo**, **Desu**, **Erik Wim**, **Erik D.**, **Arno,** and **Finn**. To be able to play with other like-minded people gives me great joy and lifts my spirit. Also, I would like to thank **Guus** (Daan) for the wonderful time playing guitar together.

At the end of my PhD, I am looking back at 8 years being in Wageningen. In this time, I met so many people of which many I can call friends. Without this social network my life in the Netherlands would be a lot more difficult and boring. I would like to thank **Philip**, **Tommy** & **Titta**, **Guido** & **Janne** & **Amelie**, **Sarah** & **Emma**, **Martin** & **Amilcar**, **Niccolo** & **Donna**, **Carlotte**, **Matthijs**, **Marloes**, **Yann**, **Piz Estrada Jesus Daniel**, **Cam**, **Paolo**, **Sui**, **Cynthia** & **Bas de Baas**, **Gijs** & **Maud**, **Sylvia**,

Lorenz, **Vincent**, **Peicheng**, **Dimitrios**, **Weiwei**, **Krishna**, **Hristo**, **Serko**, and many more.

Additionally, I would like to convey my deepest gratitude to my friends back home. They are a huge part of my life and all of them shaped me to the person I am today. Thanks a lot, to **Maxi** & **Manon**, **Berndti** & **Katrin**, **Berti** & **Geanina** & **Luisa**, **Wolfi** & **Nina**, **Markus** & **Vicky**, **Thomas** & **Anni**, **Fabian** & **Anna**, **Paul** & **Leni**, **Kathi**, **Aline**, **Iti**, **Gilbert**, **Kasper**, **Jonny**, and many more.

I also want to thank my family for all their support and the wonderful time we shared. Thank you, **Fra** & **Mama**, my sister **Nina,** and my grandparents **Francesco** & **Fliedale**, **Erwin** & **Helga**. Especially, I would like to thank my Opale (Francesco) that sadly passed away halfway my PhD. He was always supportive of my endeavours and very proud of what I was doing. The whole town he was living in knew that I was working on supplying fresh water to the entire sub-continent of India – a very easy task! Although he could not attend the defence physically, he is always there in my heart. Additionally, I would like to thank my parent in-law **Mark** & **Helga**, my sister in-law **Alina**, **Mutti** and the extended family in the USA, **Louis**, **Mary** and many more.

Last but not least I want to thank my wonderful wife and soulmate **Ina**. We know each other for such a long time and went through thick and thin. We met the beginning of our bachelor studies in Vienna and my love to her is ever-growing in an endless exponential curve. Together we came to Wageningen to do our master studies and later a PhD. She was supporting me in every kind of way in my life and especially along the last stretch of the PhD journey. Now I am done, and I will do the same for her.

About the author

ABOUT THE AUTHOR

Lukas Matthias Trebuch was born on the 22nd of August 1989 in Friesach in Carinthia, Austria. He grew up in the city of Vienna but spent a lot of his time in the rural and mountainous region where he was born. Through his upbringing he got a great sense for nature and appreciated the astounding landscape of the Alps. Especially he got interested in geology and water.

After finishing high school (GWIKU Haizingergasse, Wien) in 2008 he did his civil service in schools for mentally and physically challenged children. In 2009 he started his bachelor studies in Food- and Biotechnology at the University for Natural Resources and Life Science Vienna (BOKU). During his bachelor thesis at the department of Nanobiotechnology at BOKU he was researching a novel drug carrying vehicle using liposomes with a functionalized surface of S-layers derived from bacteria. In 2012 he did an internship at the biopharmaceutical company Polymun Scientific in Vienna where he worked in the upstream and R&D lab of the company. After obtaining his bachelor's degree in 2013 he continued his master studies in Biotechnology at BOKU. During an Erasmus exchange at Wageningen University (WUR) in 2014 he got fascinated by the vast potential of microalgal biotechnology and decided to continue his Master studies at WUR. During his Master studies he performed two theses. The first thesis he performed at Biobased Chemistry and Technology (BCT) on validating agal productivity models for various cultivation systems from open raceway pond to tubular bioreactors with data obtained at AlgaePARC, Wageningen. The second thesis was performed at the Netherlands Institute of Ecology (NIOO-KNAW) where he investigated *Chlorella sorokiniana* as a microalga for wastewater treatment. He specifically focused on the micronutrient limitation that can occur during the treatment of anaerobically digested blackwater. In 2016 he obtained his master's degree.

In 2017, Lukas started his PhD study within the Local treatment of urban sewage and streams for healthy reuse (LotusHR) research program. This program was a Dutch-Indian collaboration with the aim to establish a holistic wastewater treatment approach to generate water for reuse, energy and products. There he explored the potential of photogranular technology, and the results are described in this thesis. Currently, Lukas is employed as a postdoctoral researcher at NIOO-KNAW in the department of Aquatic Ecology where he continues investigating photogranular technology.

List of publications

Fernandes, T. V., Suárez-Muñoz, M., Trebuch, L.M., Verbraak, P.J., Van de Waal, D.B., 2017. Toward an Ecologically Optimized N:P Recovery from Wastewater by Microalgae. Front. Microbiol. 8, 1–6. https://doi.org/10.3389/fmicb.2017.01742

Trebuch, L.M., Oyserman, B.O., Janssen, M., Wijffels, R.H., Vet, L.E.M., Fernandes, T. V, 2020. Impact of hydraulic retention time on community assembly and function of photogranules for wastewater treatment. Water Res. 115506. https://doi.org/10.1016/j.watres.2020.115506

Trebuch, L.M., Schoofs, K., Vaessen, S., Neu, T.R., Janssen, M., Wijffels, R.H., Vet, L.E.M., Fernandes, T. V, 2022. How N_2-fixation can sustain wastewater treatment performance of photogranules under nitrogen limiting conditions. *Submitted for publication.*

Trebuch, L.M., Bourceau, O., Vaessen, S., Neu, T.R., de Beer, D., Janssen, M., Wijffels, R.H., Vet, L.E.M., Fernandes, T. V, 2022. High resolution functional analyses and community structure of photogranules. *Submitted for publication.*

Trebuch, L.M., Sohier, J., Pronk, M., Janssen, M., Wijffels, R.H., Vet, L.E.M., Fernandes, T. V, 2022. Enhancing phosphorus removal of photogranules by incorporating polyphosphate accumulating organisms. *Manuscript in preparation.*

Fernandes, T. V., Trebuch, L.M., Wijffels, R.H, 2022. Chapter 4: Microalgae-based technologies for circular wastewater treatment, Integrated Wastewater Management and Valorization using Algal Cultures, Elsevier Publications. *Under review.*

Fernandes, T. V., Trebuch, L.M. (2021) Microalgae bacteria photogranules, Dutch patent application No. NL2028485

PE&RC training and education statement

With the training and education activities listed below the PhD candidate has complied with the requirements set by the C.T. de Wit Graduate School for Production Ecology and Resource Conservation (PE&RC) which comprises of a minimum total of 32 ECTS (= 22 weeks of activities)

Review of literature (4.5 ECTS)

- Self-sedimenting algal-bacterial communities for wastewater treatment

Post-graduate courses (8.8 ECTS)

- Microalgal process design; WUR (2017)
- Environmental biotechnology; TU Delft (2018)
- Advanced biofilm course; TU Delft (2019)
- Using Python for research; Harvard University via EdX (2021)

Laboratory training and working visits (5.1 ECTS)

- Confocal laser scanning microscopy (CLSM) of photogranules; Microbiology of Interfaces, Department River Ecology, Helmholtz Centre for Environmental Research (2020)
- Microsensor measurements of photogranules; Max-Plank-Institute for Marine Microbiology, Microsensor Research group (2020)

Invited review of journal manuscripts (3 ECTS)

- Biotechnology and Bioengineering: photogranules: microsensor measurements and modelling (2020)
- Algal Research: operation of an algal photobioreactor at pilot-scale (2021)
- Water Research: photogranules enriched with methanotrophs (2021)

Competence strengthening / skills courses (3.04 ECTS)

- Supervising students; WUR (2018)
- Scientific writing; WUR (2019)
- Successful grant writing; KNAW (2021)

Scientific integrity/ethics in science activities (0.3 ECTS)

- Science integrity workshop; NIOO-KNAW (2019)

PE&RC Annual meetings, seminars and the PE&RC weekend (1.8 ects)

- PE&RC First year weekend (2017)
- PE&RC Midterm weekend (2019)
- PE&RC Last year afternoon (2020)

Discussion groups / local seminars or scientific meetings (7.5 ects)

- Chemical communication; NIOO-KNAW (2018)
- Metagenomics study group; NIOO-KNAW (2020-2021)
- Microalgal theme meetings; WUR (2018-2021)

International symposia, workshops and conferences (12.2 ects)

- Young algaeneers; Oban, Scotland (2018)
- AlgaEurope; Amsterdam, NL (2018)
- NERN Days; Lunteren, NL (2018)
- IWalgae; Valladolid, Spain (2019)
- EEFLisbon; Lisbon, PT (2019)
- IWA MEWE, Delft, NL (2021)
- IWA Biofilm; Notre Dame, USA (2021)

Committee work

- PE&RC PhD council (2017-2018)

BSc/MSc thesis supervision (24 ects)

- Microbial community assembly of microorganism in suspension to photogranule
- Extraction of extracellular polymeric substances from photogranules
- Respirometric analysis of photogranules
- Effect of nitrogen limitation on photogranules
- Visualizing the physical, chemical, and biological structure of photogranules
- Scaling up the photogranular technology
- Modelling the photogranular wastewater treatment process
- Optimizing phosphorus recovery by photogranules

COLOPHON

The research presented in this thesis was conducted at the department of Aquatic Ecology at the Netherlands Institute of Ecology (NIOO-KNAW), Wageningen, the Netherlands.

The research described in this thesis was financially supported by the LOcal Treatment of Urban sewage and Streams for Healthy Reuse (LOTUS^{HR}) research programme with project number 15424-3b, which is (partly) financed by the Dutch Research Council (NWO).

This is NIOO Thesis Number 191

Cover design: Katharina Duran-Trebuch

Design: Lukas M. Trebuch

Printed by: Digiforce || Proefschriftmaken